Development of Novel *N*-Heterocyclic Carbene Gold(I) Complexes as Chemotherapeutics

Danielle Curran

12350476

This thesis is submitted to University College Dublin in fulfilment of the requirements for the degree of Doctor of Philosophy

School of Chemistry, University College Dublin

Head of School: Dr Michael Casey

Principal Supervisor: Dr Matthias Tacke

Doctoral Studies Panel: Dr Xiangming Zhu and Dr Tony Keene

November 2020

Contents

Chapter 3

NHC*-Gold(I) Complexes of Cyanides and Acetylides

Chapter 4

NHC*-Gold(I) Dithiocarbamates

Chapter 5

Synthesis of NHC*-Gold(I) Amino Acid and Peptide Conjugates

Preface

The work presented in this thesis was performed between the months of September 2016 to November 2020 in the UCD School of Chemistry, University College Dublin, Ireland. It was carried out in the research group of Dr Matthias Tacke, and is, to the best of my knowledge, original except where due reference is made to other authors.

X-Ray crystallography and structure elucidation was carried out by Dr Helge Müller-Bunz at University College Dublin. *In vitro* biological evaluation was carried out by Prof. Rainer Schobert, Matthias Rothemund and Sofia I. Bär at the University of Bayreuth, Germany. Inhibition experiments were conducted by Prof. Ingo Ott and Dr Uttara Basu at the Technical University of Braunschweig, Germany. *In vivo* biological experiments were carried out by Prof. Dr Wolfgang Walther, Prof. Dr Anja Sterner-Kock and Britta Büttner at Experimental Pharmacology & Oncology Berlin-Buch GmbH (EPO), Germany.

I hereby certify that the submitted work is my own work, was completed while registered as a candidate for the degree stated on the Title Page, and I have not obtained a degree elsewhere on the basis of the research presented in this submitted work.

_____

Danielle Curran

Abstract

We present herein, a series of *N*-heterocyclic carbene (NHC) gold(I) complexes derived from (1,3-dibenzyl-4,5-diphenylimidazol-2-ylidene)gold(I) chloride. Ligand substitution of this NHC-gold(I) chloride complex allowed the coordination of a variety of ligands to the gold(I) centre. These complexes were designed to create a structure-activity-relationship for NHC-gold(I) complexes. Chapter 1 introduces *N*-heterocyclic carbenes and highlights the importance of metal-based drug design. Chapter 2 describes the synthesis of NHC-gold(I) complexes with halide, carbene and phosphine ligands. *In vitro* MTT-based proliferation assays against the human colon carcinoma call line HCT-116 and the multidrug-resistant breast cancer cell line MCF-7 show the effect that ligand modification has on the antiproliferative properties of these gold(I) complexes. We found the cationic gold(I) complexes to be promising anticancer drug candidates. Chapter 3 discusses NHC-gold(I) acetylides which did not exhibit great cytotoxicity but presented interesting aurophilic interactions in the solid state. Chapter 4 presents optimised NHC-gold(I) complexes with the introduction of dithiocarbamate ligands. *In vitro* cell tests reported the highest activity observed with an IC_{50} value of 0.28 μM against the breast cancer cell line MCF-7. An *in vivo* xenograft mouse model experiment was carried out with the dimethyldithiocarbamate complex against the human prostate cancer PC-3 which showed the NHC-gold(I) complex had strong chemotherapeutic properties. Chapter 5 describes the synthesis of NHC-gold(I) cysteine derivatives. Solid-phase peptide synthesis is used to prepare a series of cysteine-based dipeptides which were coordinated to the NHC-gold(I) complex.

Abbreviations

br	Broad
calcd.	Calculated
$CDCl_3$	Deuterated chloroform
d	Doublet (NMR)
d	Day
DAPTA	3,7-Diacetyl-1,3,7-triaza-5-phosphabicyclo[3.3.1]nonane
dd	Doublet of doublets (NMR)
dt	Doublet of triplets (NMR)
DIC	*N,N'*-Diisopropylcarbodiimide
DIPEA	*N-N'*-Diisopropylethylamine
DMF	Dimethylformamide
DMSO	Dimethylsulfoxide
ESI	Electronspray ionisation mode
Fmoc	Fluorenylmethoxycarbonyl
GI_{50}	50% cell growth inhibition
h	Hours
HCT-116^{wt}	Colon cancer cell line (wild type)
HCT-116 $p53^{-/-}$	Colon cancer cell line with a p53 knockout gene
HOMO	Highest occupied molecular orbital
HRMS	High resolution mass spectrometry
Hz	Hertz
IC_{50}	50% inhibition concentration
IR	Infrared
i.p.	Intraperitoneally
J	Coupling constant
LUMO	Lowest unoccupied molecular orbital
m	Multiplet (NMR)
MCF-7^{topo}	Breast cancer cell line with Topotecan treatment
mdr	Multidrug-resistant

min	Minutes
MTD	Maximum tolerated dose
MTT	3-(4,5-dimethyl-thiazol-2-yl)-2,5-diphenyltetrazolium bromide)
NCI	National Cancer Institute
NHC	*N*-heterocyclic carbene
NMR	Nuclear Magnetic Resonance
NMRI:nu/nu mice	Naval Medical Research Institute immunodeficient "nude" mice
p	Pentet (NMR)
PC-3	Prostate cancer cell line
ppm	Parts per million
PTA	1,3,5-Triaza-7-phosphaadamantane
q	Quartet (NMR)
ROS	Reactive oxygen species
rt	Room temperature
s	Singlet (NMR)
s.c.	Subcutaneously
t	Triplet (NMR)
TBAF	Tetra-*n*-butylammonium fluoride
TFA	Trifluoroacetic acid
TLC	Thin layer chromatography
TMS	Tetramethylsilane
Trx	Thioredoxin
TrxR	Thioredoxin Reductase
δ	Chemical shift in parts per million

Note: Cell lines not listed here are described preceding their abbreviated names.

Acknowledgements

First, I would like to thank my supervisor Dr Matthias Tacke for giving me the opportunity to do this PhD. Also, I'd like to thank Dr Xiangming Zhu who was as good as a supervisor to me.

Many thanks to the technical staff who provided much needed services, advice and help throughout my PhD: Dr Yannick Ortin, Dr Guanghua Jin, Dr Jimmy Muldoon and Dr Rónán Crowley. A special thanks to Dr Helge Müller-Bunz for sharing his expertise on X-ray crystallography. I would also like to extend a thank you to Dr Marina Rubini for her help and expertise on peptide chemistry.

I am very grateful to Prof. Garreth Redmond for arranging funding to allow me to continue my studies. I would like to extend a massive thank you to Susan Wilson who always had time for me, her help and check-ins are greatly appreciated.

To my co-workers, most significantly Dr Cillian O'Beirne who always looked out for me and helped me greatly over the years. Past members Dhiyaa Althagafi, Hessah Althani, Nada Hamad and current members Cian McCarthy, Shane Donnelly and Zoe Beato who have made the lab such a happy and supportive environment. Many thanks to Cillian, Cian and the Evans' group members Niall Collins and Lorna Conway who gave me a reason to leave the lab and have been fantastic friends I was lucky to come upon.

A huge thank you to all my wonderful housemates (and guests) over the years at Bellevue Copse and now at Dale Road. You guys kept me smiling and laughing after long hard days.

Cian McCarthy you deserve the biggest thank you. Thank you for all the time, support, rant listening, dinners, column help, laughs and love which without I would have been lost. Your kindness in every moment of my PhD got me through all the tough days. Thank you so much.

To my Dublin parents Christina and Antu who kept me sane and well fed; me and my stretchy pants are forever grateful for everything you have done for me over the years.

Most importantly, my wonderful family. Momma-bear, daddy, Emmerdale, Matt, Josh and Lily who believed in me even when they didn't understand what I was doing. Who supported me even if that meant they avoided texting me all week. For all the endless love, support and hugs (especially off my brothers!), thank you. I love you all so dearly x

Chapter One

Introduction

1.1 *N*-Heterocyclic Carbenes

1.1.1 A Brief History of *N*-Heterocyclic Carbenes

N-Heterocyclic carbenes (NHCs) have recently gained significant attraction for their pivotal role in applications such as catalysis, ionic liquids and metallodrugs. Modification of the NHC structure can influence the stability, structure and reactivity of their associated compounds. NHCs consist of a divalent carbene and at least one nitrogen atom.

Most notable in the discovery of NHCs is the seminal work of Arduengo in isolating the first "bottle-able" NHC.[1] However, the pursuit of carbenes started as early as 1835 when Dumas attempted to synthesise the methylene carbene by dehydration of methanol.[2] However, at this point the reactivity of a free carbene was not yet understood. It was Breslow and Wanzlick that contributed the nitrogen atoms to the NHC structures we are familiar with today.[3,4] They noticed the presence of a nitrogen atom led to a dramatically more stable carbene. However, the monomeric carbene was still unattainable. Wanzlick managed to prepare the dimeric compound **1.1**[4] and also recognised its potential as a ligand and formed a NHC-mercury complex **1.2** (**Figure 1.1**).[5] It wasn't until 1988 that the first (phosphino)(silyl)carbene **1.3** was isolated by Bertrand.[6] Three years later Arduengo reported the successful isolable NHC **1.5**.[1] It is worth noting that the metal-carbene complexes designed by Öfele[7] (**1.**4) and Wanzlick inspired Arduengo to use the bulky adamantyl substituents on the nitrogen atoms which led to the successful isolation of the NHC. This synthetic discovery allowed access to NHCs which advanced the vast number of complexes reported in the literature today.

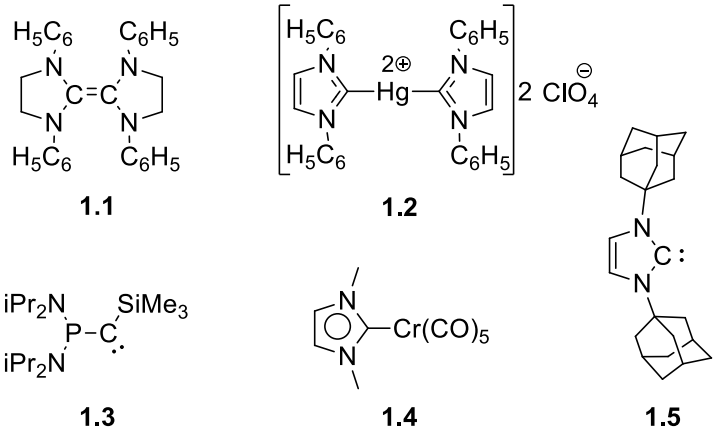

Figure 1.1 Early carbene and NHC compounds.

1.1.2 Structural Properties of *N*-Heterocyclic Carbenes

Achieving the free carbene proved difficult due to the reactive nature of the carbene. The carbene is a divalent species with six valent electrons, thus disregarding the octet rule. There are two types of carbenes: Fischer and Schrock. Carbenes have two non-bonding electrons which reside in a singlet state for Fischer carbenes and a triplet state for Schrock carbenes (**Figure 1.2a**). Fischer carbenes are typically bound to low oxidation state, late transition metals. These Fischer carbenes generally carry a partial positive charge, creating an electrophilic carbene carbon. Whereas, Schrock carbenes are found with high oxidation state, early transition metals that present a nucleophilic carbon. NHCs act as Fischer carbenes, without the positive charge.[8,9] The NHC carbene resides in a singlet ground state. The nitrogen atoms play a key role in stabilising the carbene (**Figure 1.2b**, carbene carbon is marked as pink). The HOMO is the sp^2-hybridised lone pair and the LUMO is the unoccupied p-orbital. The nitrogen atoms inductively lower the energy of the occupied σ-orbital by drawing electrons away from the carbene (**Figure 1.2c**, marked in blue arrows). Meanwhile, the nitrogen lone pairs mesomerically donate electron density into the empty p-orbital of the carbene (**Figure 1.2c**, marked with red arrows). This results in a larger energy gap between the σ and p orbital which further stabilises the singlet ground state.[10] Furthermore, the cyclic NHC structure favours the singlet state as the N-C-N angle of the carbene is in a bent sp^2 arrangement. The lone pair of the carbene sits in the plane of the carbene which aids its nucleophilicity.[11] NHCs are strong σ-donor ligands for transition metals.[12] The sp^2-hybridised lone pair at the carbene donates

electrons into an empty metal σ-orbital. Additionally, the π-back donation of electrons from the metal into the carbene p-orbital has been considered important to the metal-ligand bond.[13,14]

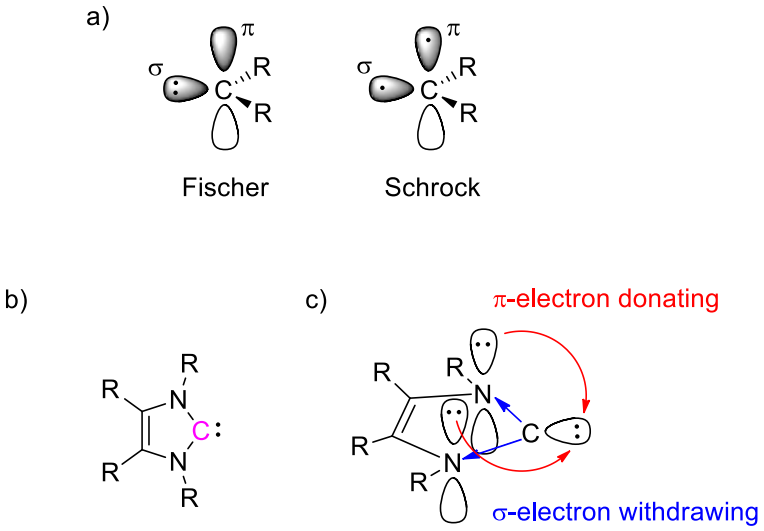

Figure 1.2 a) Singlet and triplet state electrons in Fischer and Schrock carbenes, b) NHC structure with carbene carbon marked in pink, c) Ground state electronic structure of imidazol-2-ylidenes.

Factors such as ring size, heteroatoms and the choice of substituents on each heteroatom can impact the stability, electronic and nucleophilic characteristics of the carbenes.[15] Five-membered rings are the most abundant class of NHCs, however NHCs can be formed in four to seven-membered rings.[16,17] Larger ring sizes result in a wider N-C-N carbene bond angle which can affect the carbene stabilisation. Although the NHC shown in **Figure 1.2** involves two nitrogen atoms, stable carbenes can be formed with other heteroatoms such as sulfur (thiazolylidenes), oxygen (oxazolylidenes) or carbon, the latter forming cyclic(alkyl)(amino)carbenes (CAACs). Other variations such as triazolylidenes, featuring a third nitrogen atom, or *N*,*N*′-diamidocarbenes (DACs) have also been reported.[8] The substituents on the heteroatoms also play an important role in stabilising the carbene, both electronically and sterically. Bulky nitrogen substituents can kinetically stabilise the carbene by disfavouring dimerization to form the olefin.[14,18]

1.1.3 Synthesis of Imidazoliums

Imidazolium salts of the type **1.7** can be prepared by nucleophilic substitution at the nitrogen atoms of the imidazole or via multicomponent reactions. The former route is the most common approach as the nitrogens on the imidazole can be readily deprotonated with a suitable base and subsequently alkylated with alkyl halides. The second alkylation is performed with a second equivalent of an alkyl halide. This allows the synthesis of unsymmetrically alkyl-substituted imidazoliums. For symmetrically substituted imidazolium salts a one-pot approach can be employed with two equivalents of the same alkylating agent.[10] The synthesis of the imidazolium salt used in this work adopts this method and was previously published by Patil et al. (**Scheme 1.1**).[19] Commercially available 4,5-diphenyl-1*H*-imidazole **1.6** was deprotonated with potassium carbonate and reacted with two equivalents of benzyl bromide affording 1,3-dibenzyl-4,5-diphenylimidazolium bromide (**1.7**) in a 68% yield.

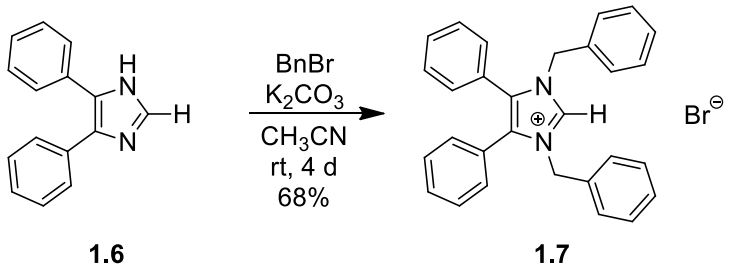

1.6 **1.7**

Scheme 1.1 Synthesis of imidazolium bromide **1.7**.

The multicomponent generation of imidazolium salts involves the reaction of primary amines, glyoxal and formaldehyde in the presence of a Brønsted acid (**Scheme 1.2**).[20] This method is advantageous as it allows access to symmetrically substituted imidazolium salts that are sterically demanding. The unsymmetrical imidazolium salts can be achieved by combining the multicomponent reaction with an *N*-alkylation step.[10]

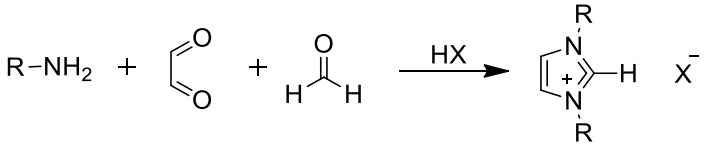

Scheme 1.2 Multicomponent synthesis of imidazolium salts.

NHCs can be incorporated into metal complexes directly from the imidazolium salts thus it is not necessary to further deprotonate the azolium cations into the free carbene.[21] However, this

can be achieved by deprotonation with a base such as NaH or KO^{t}Bu. In addition, the deprotonation can be conducted by Herrmann's ammonia method, where the deprotonation occurs with the addition of NaH to a solution of the imidazolium salt dissolved in liquid ammonia and an aprotic solvent like THF.[22] Alternatively, desulfurization of imidazole-2-thiones can form the free carbene without first generating the imidazolium salt.[23]

1.1.4 Biological Activity

An interesting class of natural product imidazoliums are lepidilines A-D (**Figure 1.3**). The naturally occurring alkaloids are isolated from *Lepidium meyenii*, the Peruvian maca root. Traditionally it has been used to enhance fertility, for anti-inflammation and as an anti-oxidant.[24,25] Lepidilines A-D consist of a 1,3-dibenzyl-4,5-dimethylimidazolium structure with variations on the benzyl substituents and at the imidazolium 1-position. Studies conducted on lepidiline A (1,3-dibenzyl-4,5-dimethylimidazolium chloride) and lepidiline B (1,3-dibenzyl-2,4,5-trimethylimidazolium chloride) reported higher activity for the methyl derivative lepidiline B. Lepidiline A exhibited antiproliferative properties against the human ovarian cancer cell line FDIGROV, reporting an ED_{50} value of 7.39 μg/ mL.[26] Lepidiline B exhibited activity against the human bladder (UMUC3), pancreatic (PACA2), breast (MDA231) and ovarian (FDIGROV) carcinoma cell lines.

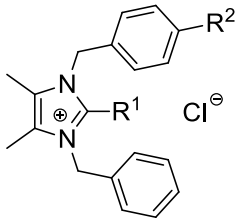

lepidiline A: R^1 = H; R^2 = H
lepidiline B: R^1 = CH_3; R^2 = H
lepidiline C: R^1 = H; R^2 = OCH_3
lepidiline D: R^1 = CH_3; R^2 = OCH_3

Figure 1.3 Naturally occurring lepidilines A-D.

Structurally analogous imidazolium compounds have been developed and assessed for their biological properties.[27,28] A library of phenylacylimidazolium bromides (**1.8**, **Figure 1.4**) were developed and biological assessment revealed that the presence of *tert*-butyl groups at the 1 or 3-position decreased the activity, while the presence of aromatic groups increased the cytotoxicity.[29] The most potent derivative featured an imidazol-2-ylidene structure (R^2 = H) with 2,4,6-trimethylbenzene at the 1-position (R^1) and 4-methoxyphenylacyl at the 3-position

(R^3). This compound presented IC_{50} values of 1.5-5.0 μM across eight human cancer cell lines. Furthermore, a collection of alkoxyimidazolium salts (**1.9)** displayed strong antiproliferative properties against the human leukaemia and breast cancer cell lines HL-60 and MCF-7.[30] The most active complexes had a methyl substituted backbone and an adamantyloxy group at the 3-position. The choice of counterion did not appear to effect the cytotoxicity. Imidazolium-based ionic liquids **1.10** with long aliphatic chains showed increased cancer cell inhibitory effects with longer chain lengths.[31] Imidazoliums present great potential in biological applications as ionic liquids or as coordinated NHC ligands in metal-based complexes.[32–34]

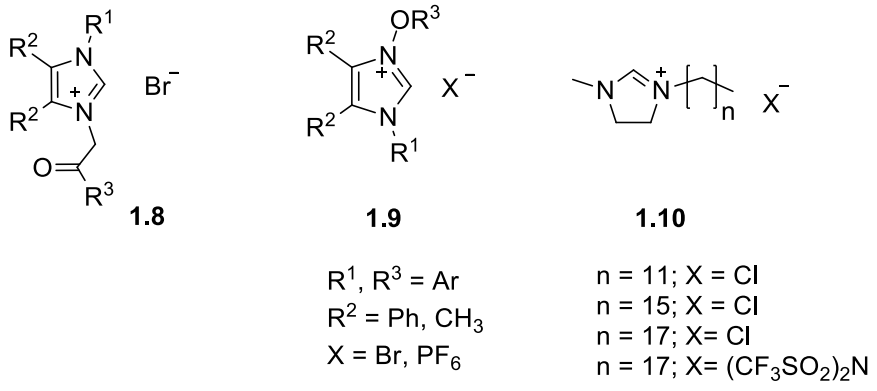

Figure 1.4 Biologically active imidazolium salts.

1.2 Gold

1.2.1 Gold in Medicinal Chemistry

"Gold has great remedial virtues, the place of which no other drug can supply"-Samuel Hahneman

Gold has a long history in medicine and is often seen as a substance of wealth and power, even referred to as *rex metallorum*, or the King of Metals. Quite deserving of this title, gold's use in medicine has extended to many ailments over the centuries. As early as 2500 BC, Chinese records use gold in medicine, while gold powder, Swarma bhasma, was used by Ayurvedic physicians in India.[35,36] Gold has appeared in treatments of leprosy, epilepsy, lupus, alcoholism, tuberculosis and most notably rheumatoid arthritis.[37,38] Robert Koch is associated with the foundation of modern gold therapeutics. In 1890, it was noted that gold cyanide was bacteriostatic against tubercle bacillus. A connection was drawn between tuberculosis and the suspected infectious disease rheumatoid arthritis, which resulted in trials with gold formulations.[39] These early trials with gold thiopropanol sodium sulphonate (Allocrysin, **Figure 1.5**) injections proved successful which encouraged further research into gold compounds for the treatment of rheumatoid arthritis. Although early gold formulations were successful, they were not without side effects. As a result the drugs were administered via intramuscular injection on a weekly basis. Forestier reported that the use of gold sodium thiomalate and gold thioglucose were the most promising candidates. Gold sodium thiomalate (Myocrisin) and gold thioglucose (Solganol) were both on the market for the treatment of rheumatoid arthritis for over 70 years (**Figure 1.5**). Phosphine ligands were introduced to gold complexes to create orally administered drugs. In 1980, triethylphosphine-gold peracetylated thioglucose (Auranofin; Ridaura) was developed as an oral anti-arthritic drug (**Figure 1.5**). The oral administration of auranofin was advantageous, however the drug was less efficacious. The use of gold drugs for the treatment of rheumatoid arthritis, also known as chrysotherapy, is still conducted today.

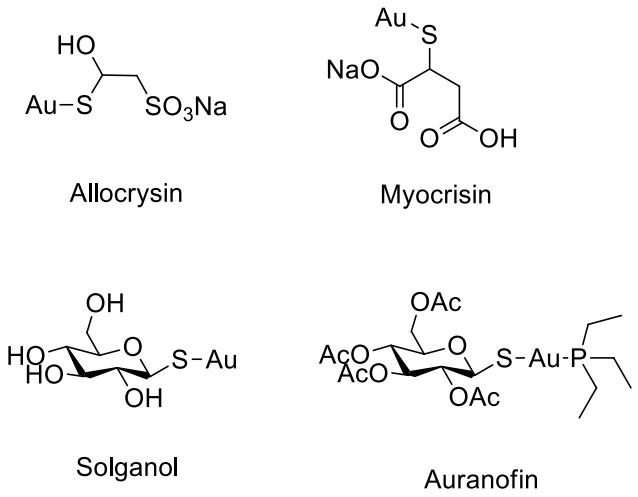

Figure 1.5 Gold complexes used in chrysotherapy.

Meanwhile, in 1969 a series of platinum compounds were found to inhibit the cancer cell lines sarcoma 180 and leukaemia L1210 in mice.[40] This discovery founded the concept of metal-based inorganic compounds as antitumour agents. The most potent compound developed was *cis*-Pt(II)$(NH_3)_2Cl_2$, or cisplatin as it is known today (**Figure 1.6**). Cisplatin is a highly active chemotherapeutic agent used in the treatment of testicular, ovarian, bladder and lung cancers.[41] However, cisplatin and other platinum-based drugs, such as carboplatin or oxaliplatin, carried severe side effects.[42] Also, cancer cell lines became cisplatin or platinum-resistant which posed a huge issue for their treatment.[43]

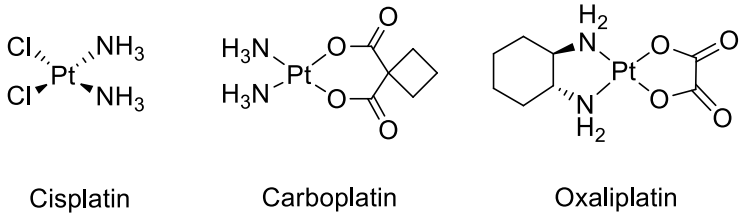

Figure 1.6 Platinum-based chemotherapeutic drugs.

As a result, efforts were focussed on alternative treatments with other late transition metal complexes. The aim was to overcome the side effects of cisplatin whilst maintaining its high anticancer activity. A considerable amount of metal-based complexes have been developed over the years with metals such as ruthenium,[44,45] palladium,[46] titanium,[47] copper,[48,49] tin[50] and gold.[51] Immediately, gold was recognised as a potential anticancer agent. Gold is most commonly found in the +1 and +3 oxidation states. Gold(I) has a d^{10} closed-shell configuration

and generally forms linear two-coordinate complexes. On the other hand, gold(III) has a d^8 closed-shell configuration and is isoelectronic and isostructural to square planar Pt(II) complexes. Both gold(I) and gold(III) complexes have been found to be highly active potential anticancer agents. However, gold(III) complexes are more readily reduced to gold(I) or gold(0) which has been associated with a loss in activity. Significant efforts have been carried out to design stable biologically active gold(III) complexes.[52–54] The discovery of the gold(I) drug auranofin drew more attention to gold(I), thus resulted in more research carried out on gold(I) complexes.

In order to establish new metal-based anticancer drugs, previously developed compounds were reassessed. This led to the repurposing of auranofin. Recently, auranofin has been investigated for potential therapeutic applications against cancer, HIV/AIDS,[55] bacterial infections[56] and most recently SARS-COV-2.[57] Auranofin first showed chemotherapeutic properties in 1985 when Mirabelli et al. tested the complex against several cancer cell lines.[58] Finding cytotoxic activity, auranofin was subsequently tested i*n vivo* against the P388 leukaemia mouse model. Since, numerous studies have demonstrated the high anticancer potential of auranofin. Interestingly, the effect of auranofin and other gold-based drugs has been observed in cisplatin-resistant cancer cells.[59] Auranofin is currently undergoing clinical trials for the treatment of chronic lymphocytic leukaemia (CLL), small lymphocytic lymphoma (SLL) and prolymphocytic lymphoma (PLL) (ClinicalTrials.gov Identifier: NCT01419691) and for the treatment of recurrent epithelial ovarian, primary peritoneal and fallopian tube cancer (NCT01747798; NCT03456700).

1.2.2 Chemotherapy

To date cisplatin remains one of the most successful anticancer drugs which is still in use in several cancer treatments. As a result the cytostatic drug is generally used as a standard to compare novel compounds against. Auranofin is also commonly used as a representative of gold(I) drugs. As shown in **Table 1.1**, auranofin has been found to be more active than cisplatin on both the breast cancer cell line MCF-7 and the colon cancer cell line HCT-116.[60]

Table 1.1 IC_{50} values (μM) reported for cisplatin and auranofin after 72 h of incubation.[60]

Compound	MCF-7	HCT-116
Cisplatin	18.21 ± 0.10	5.42 ± 0.12
Auranofin	2.89 ± 0.05	3.78 ± 0.10

As different types of cancer require different treatments, often a combination chemotherapeutic approach is used to incorporate several mechanisms of action with one regimen. Platinum-based drugs cisplatin (CPT) and oxaliplatin are often used in conjunction with non-metal drugs. **Table 1.2** details the ID_{50} values of commonly used non-metal drugs: doxorubicin (DOX), 5-fluorouracil (5-FU), methotrexate (MTX), etopoxide (ETO) and taxol (TAX);[61] although these are only a small selection of available drugs. Combination therapies often provide a greater response through additive or synergistic effects. As it is a multi-targeting approach an outcome is often achieved sooner and with less side effects. Combination chemotherapy can also avoid the induction of platinum-resistance in cancer cells. Although these non-metal drugs exhibit strong antiproliferative properties they are not without side effects. Thus, the demand to design novel potent metal-based drugs is still present.

Table 1.2 ID_{50} values (μM) of some established anticancer drugs reported by Miranda et al.[61] against human cancer cell lines: A498 (renal), EVSA-T (breast), H226 (non-small-cell lung), IGROV (ovarian), M19 MEL (melanoma), MCF-7 (breast), WIDR (colon).

Drug	A498	EVSA-T	H226	IGROV	M19 MEL	MCF-7	WIDR
DOX	0.90	0.08	1.99	0.60	0.16	0.10	0.11
CPT	22.53	4.22	32.69	1.69	5.58	6.99	9.67
5-FU	1.43	4.75	3.40	2.97	4.42	7.50	2.25
MTX	0.37	0.05	22.87	0.07	0.23	0.18	<0.003
ETO	13.14	3.17	39.34	5.8	5.05	25.94	1.50
TAX	0.003	<0.003	<0.003	<0.003	<0.003	<0.003	<0.003

1.2.3 Mechanism of Action

It is conceded that gold-based drugs elicit cell death through a multifaceted mechanism of action. However, it is agreed that the mitochondrial Thioredoxin reductase enzyme is the primary target for gold(I) drugs.[62] The thioredoxin system includes thioredoxin (Trx), thioredoxin reductase (TrxR) and NADPH; the Trx system is responsible for the intracellular redox and homeostasis system. The enzymes interact in a redox process which results in the formation of disulphide bonds in Trx and a sulphide-selenide bond in TrxR. While there are cytosolic and mitochondrial isoforms of the enzyme the mitochondrial TrxR appears to be the main target. The enzyme features a selenocysteine-cysteine moiety at the redox active site.[63] Gold(I) species in particular, as soft Lewis acids, have a high affinity for the soft selenol and thiol groups. Gold complexes are known to bind to other thiol-based enzymes such as glutathione reductase (GR) and human serum albumin, which reduces its bioavailability. The importance of the selenium atom was noted as binding to TrxR is significantly greater than to GR which lacks the selenium atom.[64] As the selenocysteine is the penultimate amino acid in the protein sequence it is quite accessible to incoming gold drugs.

Normally, NADPH interacts with TrxR and begins a chain of reduction, resulting in the reduced-Trx reducing proteins in the cell (**A**, **Figure 1.7**). However, when a gold drug, such as auranofin, binds to TrxR this process is halted. Once the gold binds to the selenoprotein it strongly inhibits the enzyme. When TrxR is inhibited Trx remains oxidised (Trx-S_2) and cannot carry out essential reduction in the cell. This leads to cell oxidative stress, which increases the reactive oxygen species (ROS) and causes apoptosis. As ROS production accompanies cell death, cancer cells often over-express TrxR to handle the increased levels of ROS.[65,66] This poses an opportunity to develop cancer drugs that express selecectivity to TrxR. In addition, peroxiredoxin (Prx) enzymes can also become oxidised as a result of TrxR inhibition. Prx enzymes normally protect the cell from H_2O_2, however when oxidised the ROS is left unregulated.[47]

Furthermore, it was observed that the gold drug can alter the redox state of the TrxR enzyme which can induce mitochondrial membrane permeability transition.[67] This leads to swelling and the release of pro-apoptotic proteins such as cytochrome *c*.[66,68] Although the mechanism of action of gold-based drugs remains under question, it is clear the inhibition of TrxR by gold(I) results in apoptosis through a multitude of attacks.

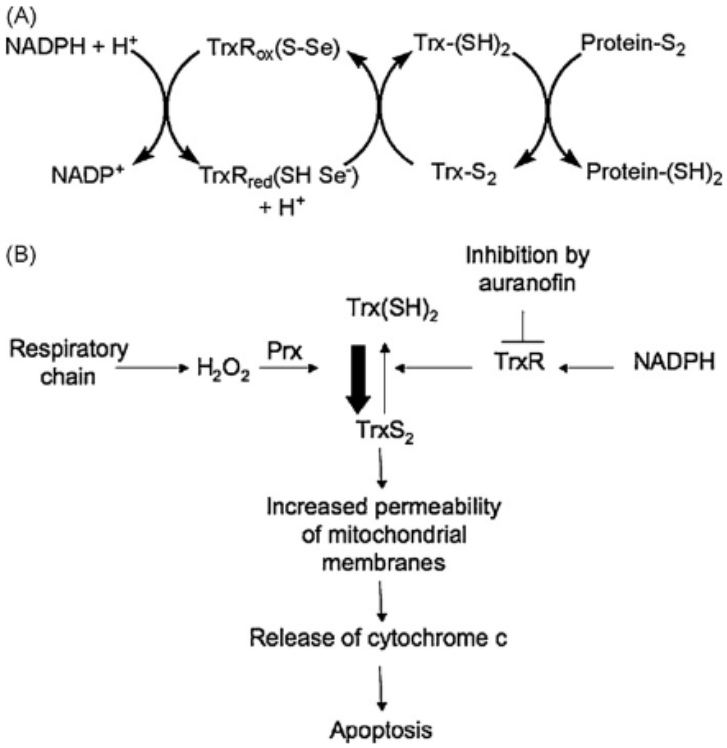

Figure 1.7 A: The thioredoxin system as depicted by Barnard and Berners-Price[69], B: a mechanism of auranofin alteration of the thiol redox balance resulting in apoptosis as depicted by Bindoli et al.[68] $Trx(SH)_2$: reduced, $Trx\text{-}S_2$: oxidised.

The inhibitory effect of gold thioglucose on rat liver TrxR was first reported by Hill et al..[70] Since, auranofin and other gold(I)-based drugs have been found to be potent TrxR inhibitors.[64,67,71,72] Ott et al. confirmed the inhibitory effect of gold(I) drugs by comparing the imidazolium salt **1.11** to both the gold(I) chloro derivative **1.12** and the cationic biscarbene complex $[NHC_2Au]^+$ (**1.13**).[73] The imidazolium salt which lacks gold exhibited negligible inhibition (above 200 μM), while all the gold complexes tested presented sub-micromolar activity. As shown in **Figure 1.8**, the neutral chloride complex exhibited the highest response with an IC_{50} value of 0.320 μM against the mammalian rat liver mitochondrial TrxR. However, auranofin reported a much higher activity with an IC_{50} value of 0.114 μM.

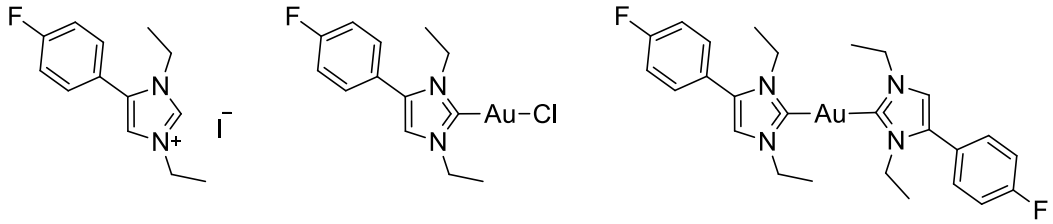

1.11 >200 μM

1.12 0.320 μM

1.13 0.823 μM

Figure 1.8 NHC-gold(I) complexes with reported IC_{50} values against mammalian TrxR.

1.2.4 Synthesis

Raubenheimer et al. synthesised bis(1-methylimidazolyl)aurate compounds **1.15** in high yields with several gold(I) source compounds.[74] First, the use of chloro(tetrahydrothiophene)gold(I) was demonstrated with imidazol-2-yllithium **1.14** affording the biscarbene complexes in high yields after protonation or alkylation (**Scheme 1.3**). Next, [AuCl(PPh_3)] was used to prepare the [Au(PPh_3)(NHC]$^+$ complexes which underwent homoleptic rearrangement according to **Equation 1.1** to form the biscarbene complexes.

$$2[AuL^1(L^2)] \longrightarrow [AuL^1{}_2] + [AuL^2{}_2] \qquad (1.1)$$

However, the use of [Au(C_6F_5)(THT)] or AuCN resulted in the monocarbenegold(I) compounds **1.16** and **1.17**. Raubenheimer also investigated the synthesis of monocarbene gold(I) complexes via oxidation of gold(III) halide complexes.[75]

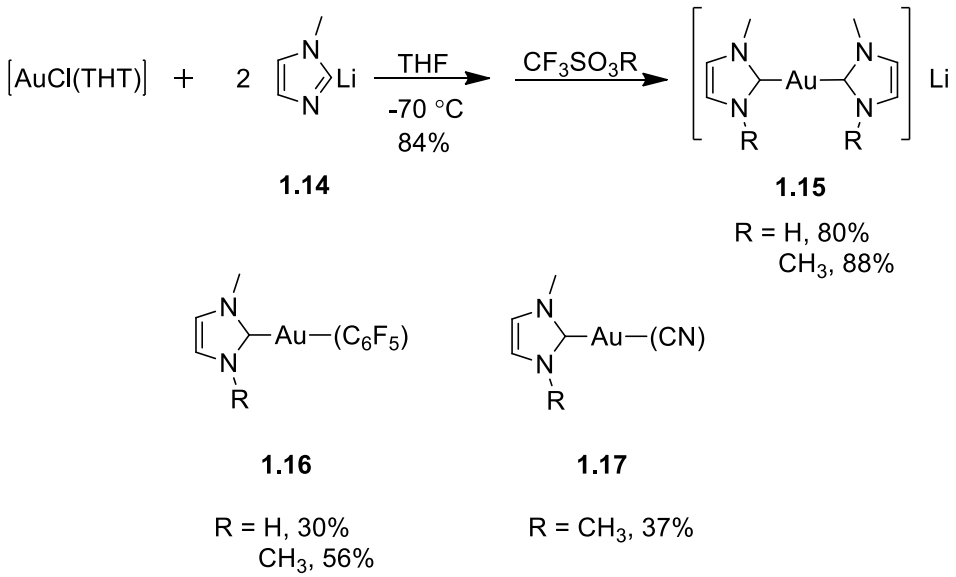

Scheme 1.3 Raubenheimer's synthesis of gold(I) biscarbene and monocarbene complexes.

Wang and Lin developed the most frequently used method of carbene transfer agents (**Scheme 1.4**).[76] The synthesis of NHC-gold(I) complexes was demonstrated by reacting 1,3-diethylbenzimidazolium bromide **1.18** with silver oxide to form the silver(I) complex **1.19**. This was then treated with chloro(dimethylsulfide)gold(I) to give the NHC gold(I) complex **1.20**. In addition, they produced the biscarbene gold(I) complex with a PF_6^- counterion via the same route. This method has been proven reliable by the numerous examples of its replication to generate new NHC gold(I) complexes.[77,78]

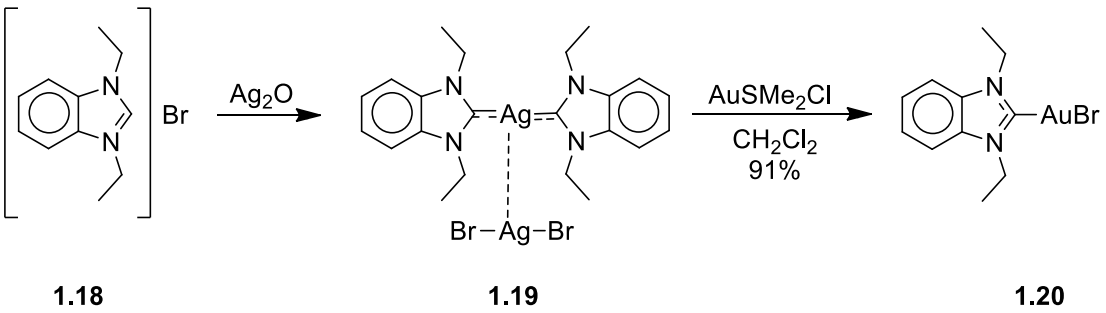

1.18 **1.19** **1.20**

Scheme 1.4 Carbene transfer route to NHC-gold(I) complexes.

This carbene transfer approach has been adopted in the Tacke group (**Scheme 1.5**). Imidazolium bromide **1.7** was reacted with silver oxide to form the NHC-silver(I) bromide complex *in situ* which was further reacted with chloro(dimethylsulfide)gold(I) to generate the NHC-gold(I) chloride **1.21** in a 49% yield.

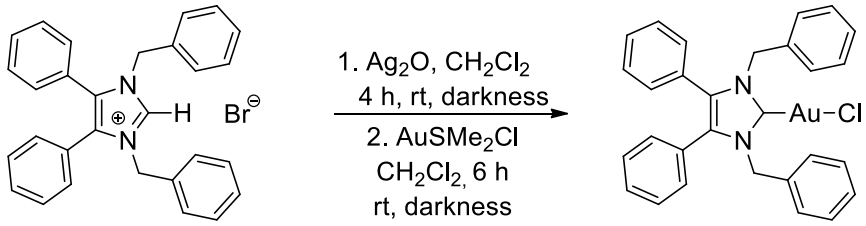

1.7 **1.21**

Scheme 1.5 Synthesis of NHC-gold(I) chloride **1.21**.

The direct reaction of AuCl with a free carbene has proven unsuccessful. The reaction of Au(SMe2)Cl with free carbene compounds **1.22** has produced NHC-gold(I) complexes **1.23** with a variety of ligand substituents in high yields (**Scheme 1.6**).[79] However, the preparation of the 2,4,6-trimethylphenyl (IMes) derivatives proved problematic. The IMes-gold(I) complex was prepared successfully using the silver carbene transfer route discussed above.

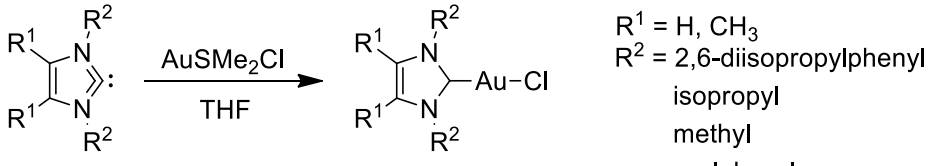

1.22 **1.23**

Scheme 1.6 Direct reaction of the free carbene and chloro(dimethylsulfide)gold(I).

A series of gold(I) complexes featuring 4,5-diarylimidazoles (**1.25**) with various substituents were prepared by first deprotonating the imidazolium salts **1.24** with lithium bis(trimethylsilyl)amide (LiHMDS) and then reacting with the chloro (dimethylsulfide)gold(I).[80] The products were also prepared via the silver transmetallation method to allow a comparison of the two established methods. Higher yields were achieved with the former method employing LiHMDS. The presence of LiBr was essential in both procedures to ensure the sole isolation of the gold(I) bromide complex.

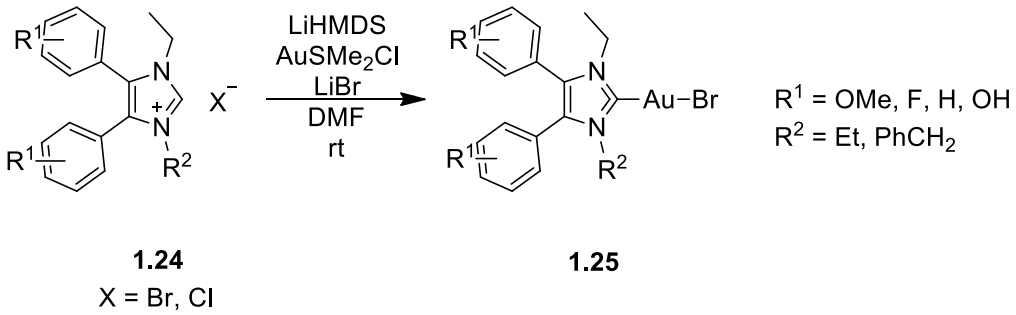

1.24
X = Br, Cl

1.25

Scheme 1.7 Synthesis of NHC gold(I) bromide with LiHMDS.

More recently, a method applicable to both saturated and unsaturated imidazoliums was developed, which avoided the generation of a free carbene and achieved the synthesis of previously challenging compounds.[81] The versatile approach was demonstrated on the synthesis of NHC gold(I) halide complexes. A selection of thirteen NHC salts were coordinated to the gold to produce the NHC-gold(I) chloride complexes in high yields of 60-97%. The procedure also afforded the bromo and iodido derivatives (**Scheme 1.8**).

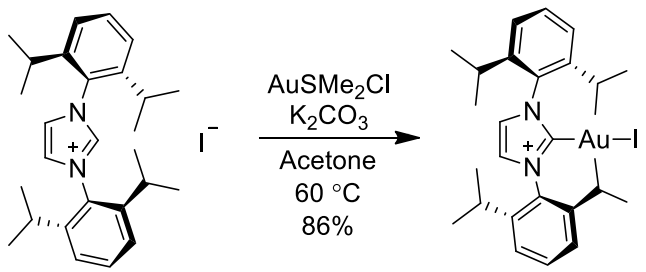

1.26

1.27

Scheme 1.8 One-step procedure with K_2CO_3 to generate NHC gold(I) halides.

1.2.5 Aurophilicity

A common feature in gold(I) complexes is the presence of aurophilic interactions. These Au···Au interactions are often weak, with energies of 29-60 kJ/mol.[77] Intermolecular or intramolecular aurophilic interactions occur between two linear two-coordinate gold(I) atoms. The distance between the two gold centres is within the range of 2.50-3.50 Å.[82] This phenomena occurs due to the relativistic effects of the closed-shell gold(I) atom. These metallophilic interactions are also observed in similar heavy atoms like Cu, Ag, Ir, Pt, Hg and Tl. It's been shown that mononuclear gold(I) compounds can interact with more than one gold atom which may result in the formation of dimers or oligomers along one or two-dimensions in the solid state.[83] These aurophilic interactions can result in luminescent compounds which has encouraged research into designing gold(I) compounds directly for that application.[84]

1.3 Gold(I) Complexes

1.3.1 Phosphine-Gold(I) Complexes

The success of auranofin led to a rise in phosphine-gold(I) analogues.[85] The replacement of the thioglucose with iodide resulted in heightened cytotoxic activity as the IC_{50} decreased from 0.754 μM for auranofin to 0.394 μM on the ovarian cancer cell line A2780 (**1.28**, **Figure 1.9**).[86] This study also included cisplatin which reported a higher IC_{50} value of 1.53 μM. However, the replacement of the thioglucose with chloride and bromide was less successful. Marzano et al. synthesised the triethylphosphinegold(I) complexes and assessed them for their antiproliferative properties against several cancer cell lines.[87] While both complexes exhibited higher activities than cisplatin they proved only comparable to the phosphine gold(I) drug auranofin. The same study reported high cytotoxic activity with phosphine gold(I) thiolate compounds [Au(xant)(PEt_3)] and [Au(SCN)(PEt_3)] and cyanate compound [Au(CN)(PEt_3)] (**1.29**). Considering their average IC_{50} values an 80- and 2-fold increase in activity was observed in comparison to cisplatin and auranofin, respectively. This study correlated the soft nature of these thiolate ligands to the heightened biological response, while the chloride and bromide displayed less of an affinity for the soft gold(I) species and resulted in less active compounds.

The choice of phosphine ligand was also examined in [AuCl(PR_3)] complexes which were tested for their antiproliferative effects against the human breast cancer cell line MCF-7 and the colon carcinoma cell line HCT-29 (**1.30**).[88] The complexes exhibited comparable activity to both cisplatin (IC_{50} 7.0 μM on HT-29; 2.0 μM on MCF-7) and auranofin (IC_{50} 2.6 μM on HT-29; 1.1 μM on MCF-7) and found the triphenylphosphine derivative to be the most active with IC_{50} values of 4.2 and 2.6 μM on the HT-29 and MCF-7 cell lines respectively. More water soluble phosphanes such as 1,3,5-triaza-7-phosphaadamantane (PTA) and 3,7-diacetyl-1,3,7-triaza-5-phosphabicyclo[3.3.1]nonane (DAPTA) were also assessed in gold(I) complexes. PTA ligands featuring *para*-substituted benzylic groups reported much higher activity than cisplatin on the colon cancer Caco-2/PD7 and Caco-2/TC7 cell lines.[89] The best complex [AuCl(PTA-CH_2-Ph-*p*-NO_2)]Br (**1.31**) presented an IC_{50} value of 3.27 μM on the Caco-2/TC7 which is comparable to the highly active auranofin (2.1 μM) on the same cell line. Gold(I) thiolate complexes with PTA and DAPTA ligands (**1.32**) presented activity greater than cisplatin on the renal cancer cell line A498 and the colon cancer cell line WIDR.[61] However, on a range of other cell lines they were

less effective than cisplatin, it was also noted that the PTA ligand produced more active compounds than the DAPTA ligand. It was established that the Au(PR_3) moiety was crucial to the high activity of these compounds, hence efforts were concentrated on the ligands trans to the phosphine gold(I) species. It became quite clear that S-donor ligands were important for cytotoxic activity which led to an abundance of research carried out on thiolate ligands. Excellent activity has been found with carbonimidothioates,[90] dithiocarbamates[91] and oxadiazole[92] ligands to name but a few.[93] Alkynyl ligands in the place of thiols led to equally promising complexes as a series of phosphine gold(I) complexes with 4-ethynylanisole (**1.33**) displayed IC_{50} values of 2.6-5.0 μM on the colon cancer cell line HT-29 and 1.1-3.8 μM on the breast adenocarcinoma cell line MDA-MB-231.[94] Alkynyl gold(I) complexes with PTA, DAPTA and PPh_3 have demonstrated strong antiproliferative properties.[95–97]

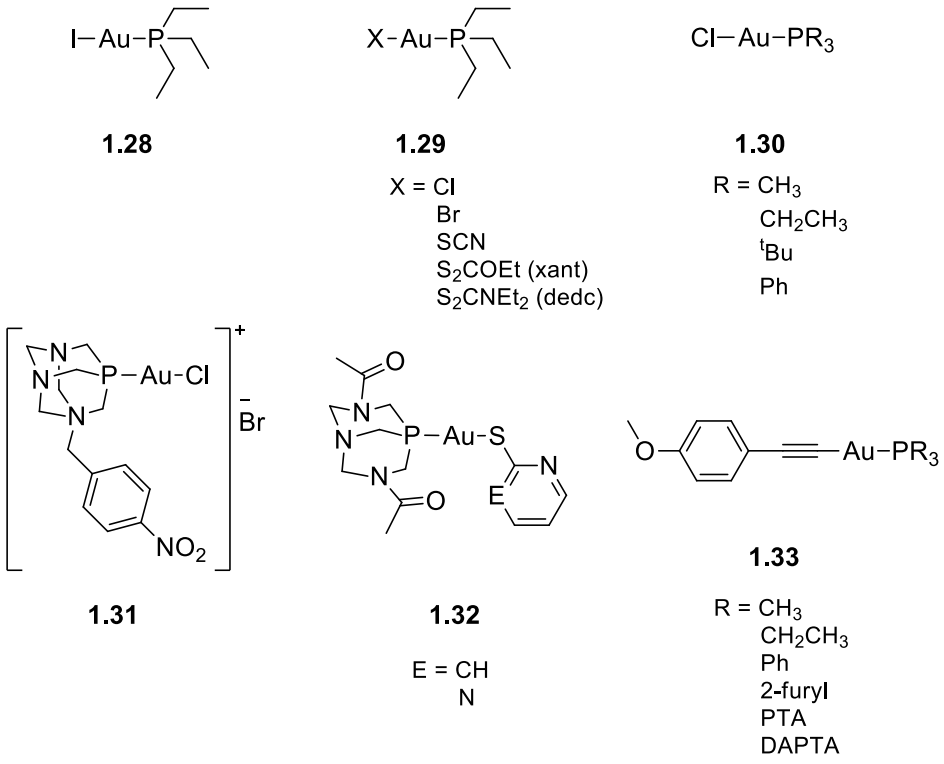

Figure 1.9 Selected phosphine gold(I) complexes.

1.3.2 NHC-Gold(I) Complexes

As seen in section 1.1.1, metal-NHC complexes such as Wanzlick's mercury carbene **1.2** and Öfele's chromium carbene **1.4** were synthesised prior to the isolation of the first free carbene. In fact, the first metal carbene was synthesised unknowingly in 1925 by Chugaev, Chugaev's salt, $[Pt(C_4H_9N_4)(MeNC)_2]Cl$ (**1.34**), was later recognised as a carbene (**Figure 1.10**).[98] Lappert and co-workers carried out extensive early research on transition-metal NHC complexes.[99,100] After the isolation of the free carbene there was a surge of metal-based NHC complexes. Metal-NHC complexes initially found application in catalysis.[101] Most notable is the case of Grubbs second generation catalyst **1.35** where the tricyclohexylphosphine ligand was replaced with an NHC resulting in enhanced activity.[102] A trend of replacing phosphine ligands with NHCs began as it was apparent that NHCs were a more desirable ligand. NHC ligands are more readily synthesised, more stable and possess increased σ-donating properties.[8]

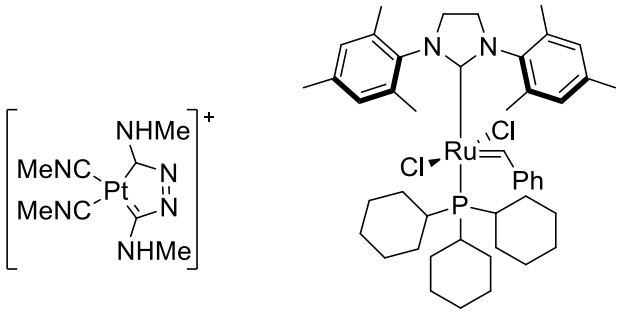

1.34 **1.35**

Figure 1.10 Chugaev's salt and Grubbs' 2nd generation catalyst.

Baker and Berners-Price first established the biological applications of gold(I) NHC complexes in 2005. Antitumoural properties were initially found in a series of dinuclear gold(I) complexes with bridging NHC ligands.[103] The group proceeded to synthesise cationic mononuclear biscarbene complexes **1.36** of the form $[(R_2Im)_2Au]^+$ and neutral complexes of the form (NHC)AuX with varying substituents on the NHC nitrogen atoms to modify the lipophilicities of the complexes (**Figure 1.11**).[78,104] Included in the complexes designed were auranofin analogues **1.37** with the PEt_3 ligand replaced by NHC ligands. All of these complexes reported the induction of mitochondrial membrane permeabilisation which confirmed their potential as antitumoural agents. This encouraged the switch to NHC-based complexes for the development of chemotherapeutics.

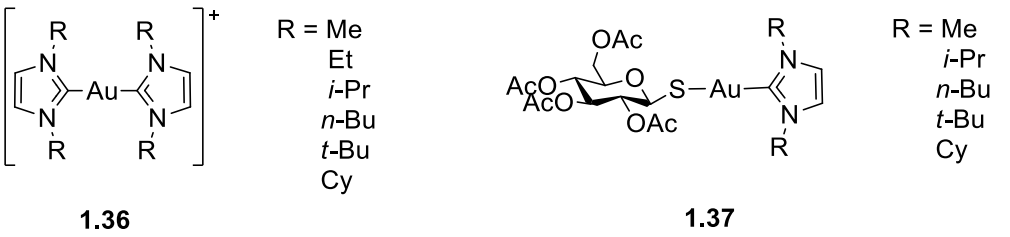

Figure 1.11 NHC gold(I) complexes developed by Baker and Berners-Price et al.

A desirable trait of NHCs is the ability to fine-tune the properties by structural alterations. Possible areas to modify the NHC complexes include the wingtips or nitrogen substituents at the 1,3-positions; the carbene backbone at the 4,5-positions; or the adjacent ligand coordinated to the gold atom.

As shown earlier in Section 1.1.4, the nitrogen substituents play a key role in the antiproliferative properties of these NHC complexes. Generally, bulky alkyl moieties decrease the activity of the compounds while aryl compounds tend to increase the activity. NHC gold(I) complexes **1.38** with alkyl chains of various lengths were synthesised from octadecylimidazole and evaluated for their cytotoxic properties against the colon cancer cell line HT-29 and the breast cancer cell line MDA-MB 231 (**Figure 1.12**).[105] Interestingly, the metal-free imidazolium salts proved more active than their gold counterparts, this proved especially true for the longer chained gold derivatives. Furthermore, a series of NHC gold(I) complexes with varying nitrogen substituents demonstrated that smaller less-bulky groups had higher cytotoxicity on the renal cancer cell line Caki-1.[106]

The effect of the carbene backbone on biological activity was observed by Liu et al. by changing methoxy and fluoro substituent positions on the phenyl groups in a series of 4,5-diarylimidazole complexes.[80] The 2-fluoro derivative **1.39** displayed the highest activity on the breast cancer cell line MCF-7, presenting a higher IC_{50} value (0.80 ± 0.06 μM) than both cisplatin (1.6 ± 0.5 μM) and auranofin (1.1 μM)(**Figure 1.12**). Interestingly, when the 4,5-diaryl groups were removed the activity decreased. Placing a benzene at the 4,5-positions, creating a benzimidazol-2-ylidene structure, has resulted in low IC_{50} values on breast and colon cancer cell lines, with 1,3-diethyl substituted complex **1.40** reporting an IC_{50} value of 4.6 μM on the breast cancer cell line MCF-7.[107] Variations to the phenyl substituents in 1,3-diaryl-4,5-diarylimidazol-2-ylidene gold(I) complexes (**1.41)**, displayed the highest cytotoxicity in the

derivatives without any phenyl substitution.[108] Although, it is worth noting the 4-methoxybenzyl substitution at the 1,3-position and 4-isopropylphenyl substitution at the 4,5-position reported a moderate IC_{50} value of 12 μM on the breast cancer cell line MCF-7. Symmetrical substitution at the 1,3-positions has also proven more effective than unsymmetrical complexes.[109]

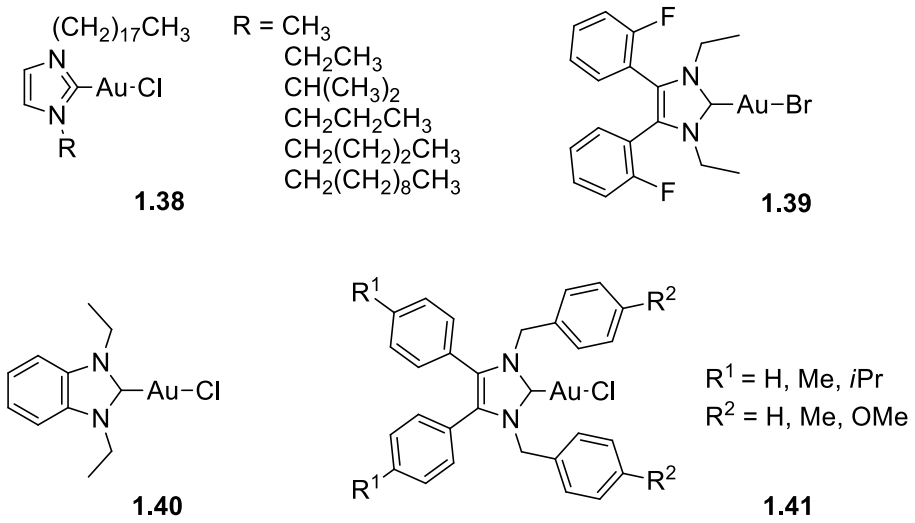

Figure 1.12 Gold(I) complexes with modifications to the NHC ligand.

The nitrogen substituents on a benzimidazol-2-ylidene structure have been designed with alkyne moieties to allow azide-alkyne click reactions to generate more interesting complexes with biomolecules. The azide-alkyne click reaction was tested with alkynyl derivative **1.42** and benzyl azide to successfully form the triazole derivative **1.43** (**Scheme 1.13**). Although the triazole complex has not yet been biologically evaluated, the alkynyl complex **1.42** exhibited good cytotoxicity on the leukaemia cell line CCRF-CEM (IC_{50} 16.19 μM) which provides a good starting point for future complexes.[110]

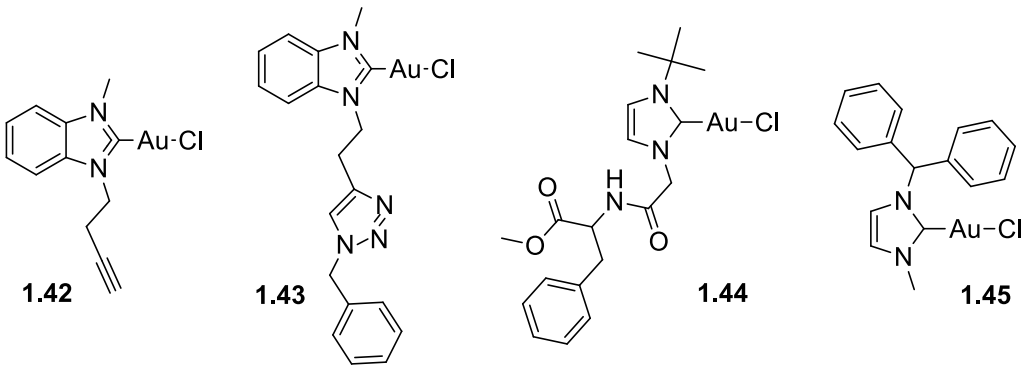

Figure 1.13 NHC gold(I) complexes designed with accessible functionalities on the NHC ligand.

Interestingly, Lemke et al. took the approach of adding an amino acid moiety to the nitrogen wingtips of the NHC ligand. The *N*-phenylalanine derived NHC gold(I) chloride complex **1.44** presented significantly lower cytotoxicity than a diphenyl derivative **1.45** tested in the same study.[111] On the colon cancer cell line HT-29, the amino acid derived complex exhibited an IC_{50} value of 63.8 ± 6.7 μM, while the diphenyl derivative reported higher activity than cisplatin (7.9 ± 1.2 μM) with an IC_{50} of 2.8 ± 1.7 μM. These findings suggest a simpler NHC substituent system generally produces more active gold(I) complexes.

Alternatively, the ligand trans to the NHC gold(I) complex can be replaced. Several auranofin analogues have been synthesised with NHC ligands replacing the triethylphosphine (**Figure 1.14**). Using the same approach as Baker et al. an auranofin analogue was developed with a bis(2,6-diisopropylphenyl)-imidazole structure (**1.46**).[79] The Tacke group designed an auranofin analogue featuring the 1,3-dibenzyl-4,5-diphenylimidazol-2-ylidene ligand (**1.47**) and evaluated its biological activity. In comparison to cisplatin (IC_{50} on MCF-7: 14, Caki-1: 3.3), higher activity was observed for the NHC gold(I) thiosugar on the breast cancer cell line MCF-7 with an IC_{50} value of 6.1 ± 1.5 μM, while less activity was seen on the renal cancer CAKI-1 cell line with an IC_{50} value of 14 ± 2 μM.[108] Later work, developed NHC gold(I) complexes with a range of thiosugars which revealed the α-thioglucose derivative was more active than its β-counterpart.[112]

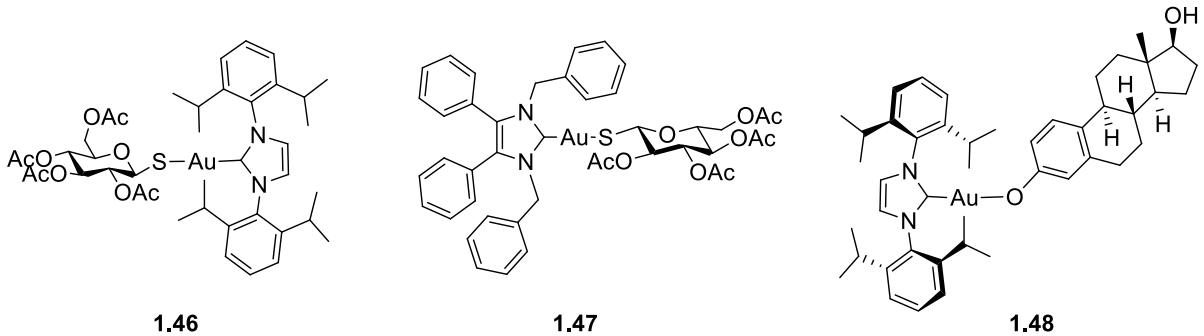

1.46 **1.47** **1.48**

Figure 1.14 NHC gold(I) complexes with biocompatible ligands.

NHC-gold(I) hydroxide was hailed as a golden synthon for its ability to perform straightforward synthesis which previously proved challenging.[113] Starting from the versatile

synthon NHC-Au-OH, several gold(I) complexes were synthesised with biocompatible ligands, including amino acids, thiosugars and steroids such as β-estradiol.[114] The auranofin analogue which featured a Au-S bond presented comparable activity to the hydroxide and chloride derivatives against human prostate and breast cancer cell lines. The gold(I) thiosugar reported an IC_{50} value of 0.82 μM on the breast cancer cell line MDA MB231, while the β-estradiol derivative **1.48** exhibited an IC_{50} value of >3.0 μM. With the exception of the thioglucose derivative, the biocompatible ligands formed an Au-O bond which exhibited 3-fold reduction in activity compared to their precursor. This indicated the type of bond formed at the gold(I) centre played a key role.

Since, considerable work has been carried out to change the ligand adjacent to the NHC-gold(I) complex in an attempt to increase the biological activity. A series of 4,5-diarylimidazol-2-ylidene gold(I) chloro complexes demonstrated the potential of halides and pseudohalides (**1.49**, **Figure 1.15**).[115] The iodido and acetato derivatives were found the most promising with lower IC_{50} values than cisplatin and auranofin reported on the human liver carcinoma and hepatoma cell lines HEPG2 and Hep3B. It was noted that for all complexes, the fluoro substituted phenyl complexes exhibited lower cytotoxicity than the methoxy derived analogues. Similar cytotoxicity was observed with a series of pseudohalide and thiolate gold(I) complexes developed in the Tacke group.[116] The azide and thiocyanate derivatives (**1.50**) presented the best activity with GI_{50} values of 0.29-1.95 μM and 1.38-4.57 μM respectively, reported against human breast, renal, leukaemia, ovarian and colon cancer cell lines.

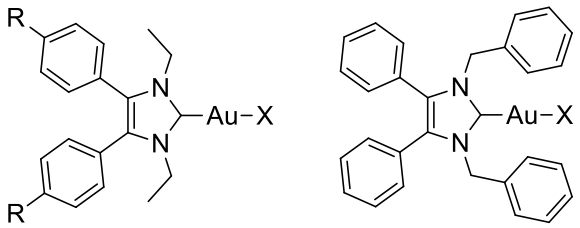

1.49
X = Br, I, NCO, OAc
R = F, OMe

1.50
X = SCN, N_3,

Figure 1.15 NHC-gold(I) complexes with halides and pseudohalides.

The use of thiols in phosphine gold(I) complexes proved extremely effective which indicated the combination of NHC gold(I) complexes and thiolates could result in potent anticancer

agents. Indeed, a collection of NHC gold(I) thiophenolate derivatives **1.51** presented low sub-micromolar inhibition of TrxR and low single-digit IC_{50} values against the human colon cancer cell line HT-29 (**Figure 1.16**).[117] Recently, the use of selenone ligands in NHC gold(I) complexes have been evaluated. The unsubstituted 1,3-imidazolidine-2-selenone reported higher cytotoxicity than the *N,N'*-substituted derivatives (**1.52**).[118] The NHC gold(I) selenone displayed an IC_{50} value of 33 ± 1 μM on the human colon cancer cell line HCT15, which is comparable to cisplatin with an IC_{50} of 32 ± 2 μM. They proposed the poor activity was due to the bulky substituents on the nitrogen and supported this theory by evaluating the NHC-gold(I) chloride derivative which displayed much lower activity than the selenone complexes.[119] As inhibition of the selenium based TrxR enzyme is responsible for the anticancer properties of gold-based drugs, the coordination of selenols to NHC gold(I) complexes is very promising. Work carried out on optimising the gold-ligand bond has led to NHC gold(I) complexes with an azide functionality to allow azide-alkyne click reactions to afford more relevant ligands. Robilotto et al. demonstrated the addition of 7-(propargyloxy)coumarin to a NHC-gold(I) azide forming a gold-carbon bond to the newly established triazole (**1.53**).[120]

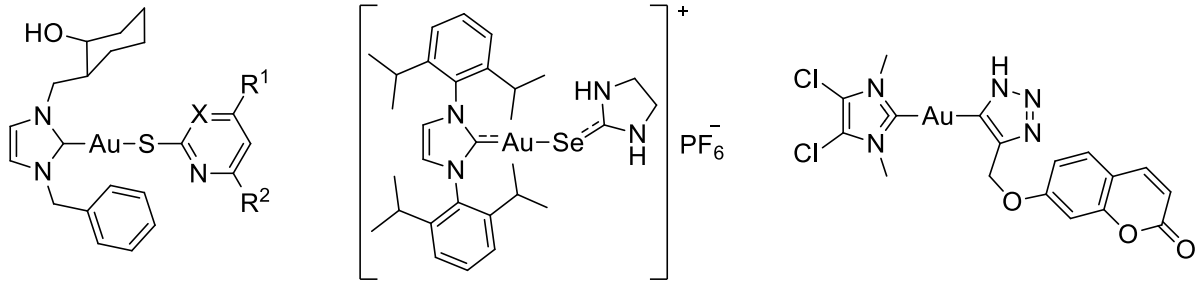

1.51 **1.52** **1.53**

X = CH, N
R^1 = H, CH_3
R^2 = H, CH_3, OH

Figure 1.16 NHC gold(I) complexes with thiol, selenone and triazole ligands.

NHCs have proven to be useful ligands for both stabilising compounds and increasing the cytotoxicity through structural modifications. Thus the addition of a second NHC ligand to the gold(I) centre poses great potential for enhanced biological activity. Cationic complexes bearing two NHC ligands, or biscarbene complexes, have reported excellent cytotoxicity. Caffeine-based gold(I) biscarbene complexes were synthesised and biologically assessed in comparison to a simpler benzimidazol-2-ylidene derivative.[121] The gold(I) caffeine complexes

featured different substituents at the 1-position of the NHC which showed the *N*-ethyl complex **1.54** was the most biologically active substituent (**Figure 1.17**). Interestingly, the caffeine derivatives exhibited significantly less activity than the benzimidazol-based complex. The best activity for the benzimidazol-2-ylidene compound was found on the ovarian cancer cell line A2780 with an IC_{50} value of 0.54 ± 0.12 μM, however this compound did not show any selectivity and reported equally high activity on the non-cancerous HEK-293T cell line. The conclusion yet again is that more simple NHC structures result in higher cytotoxicity.

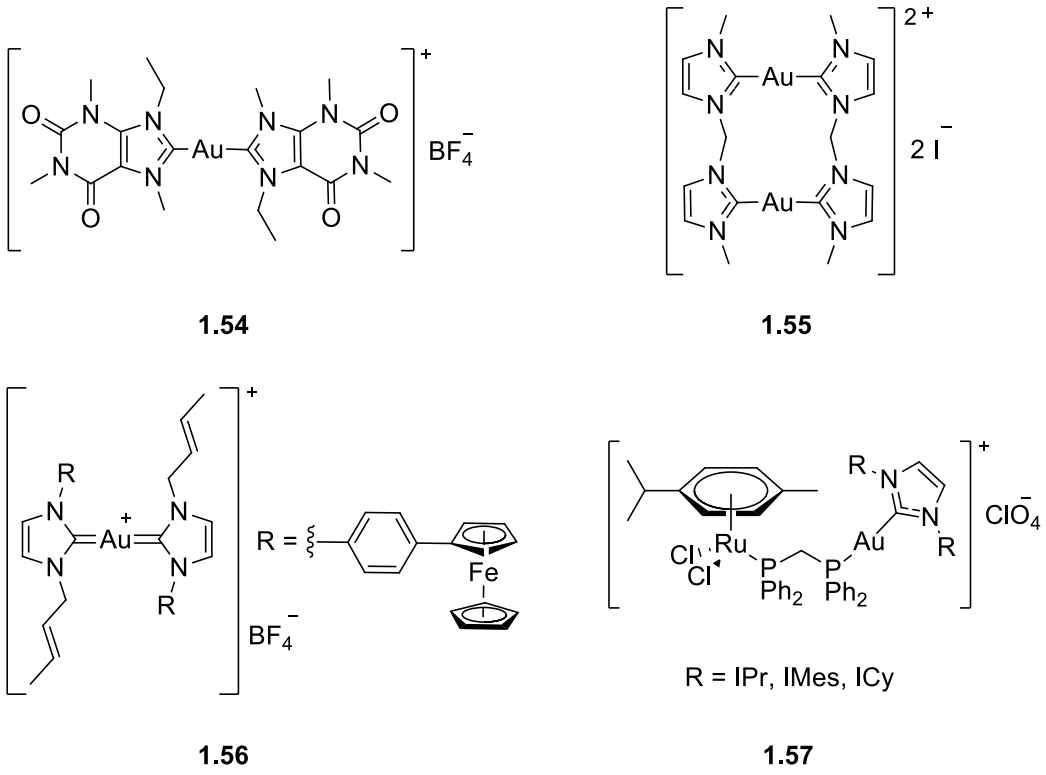

Figure 1.17 Cationic gold(I) complexes bearing NHCs and phosphines.

The ability to influence the biological activity of these complexes with simple structural modifications provides countless possibilities for designing NHC gold(I) complexes as anticancer agents. Additional measures can be taken into account to further enhance the activity such as creating dinuclear complexes with more than one gold atom or heterobimetallic complexes. This is evident as the seminal work of Berners-Price and Baker et al. reported the antitumoural effects of dinuclear gold(I) complexes with bridging NHC ligands (**1.55**).[122] A bimetallic biscarbene gold(I) complex with a ferrocenyl moiety exhibited greater cytotoxicity than cisplatin against the cervical epithelioid carcinoma and leukaemia cell lines HeLa and

Jurcat (**1.56**).[123] The highest activity was found on the Jurcat cell line with an IC_{50} value of 0.253 ± 0.031 μM compared to the 0.783 ± 0.054 μM value for cisplatin. The incorporation of a ruthenium complex to a NHC gold(I) fragment showed the hetetometallic complexes were more potent and more cell selective than their monometallic gold(I) precursors.[106]

The examples provided herein represent only a selection from the library of gold complexes that have been developed for biological application. Many exploratory reviews have delved into this topic.[51,124,125]

1.4 Project Aim

The aim of this project is to create a structure-activity-relationship for NHC-gold(I) complexes, with the wider objective to develop potent anticancer drug candidates. While there are an abundance of NHC gold(I) complexes reported in the literature there is a lack of consistency which prevents a clear approach to the synthesis of biologically active gold(I) complexes. Generally, the effect of ligand substitution and NHC modifications are assessed through *in vitro* cell testing. However, most research groups alter both the NHC and the coordinated ligand thus preventing an accurate trend to be determined. As discussed above, the 1,3-dibenzyl-4,5-diphenylimidazol-2-ylidene gold(I) chloride (**1.21**) reported a higher cytotoxic response than the phenyl substituted analogues. In fact, when evaluated against the National Cancer Institute (NCI) 60 cancer cell line panel the NHC-gold(I) chloride complex exhibited an average GI_{50} value of 1.78 μM, while the NHC-gold(I) auranofin analogue displayed an average GI_{50} value of 1.95 μM.[126] Thus, to synthesise more potent anticancer complexes the NHC-gold(I) chloride derivative **1.21** will be taken as the starting point in this thesis. The 1,3-dibenzyl-4,5-diphenyl-imidazol-2-ylidene structure will remain the same throughout this work to ensure the monitored effect on cytotoxicity can be associated solely with the alteration of the ligand trans to the NHC-gold(I). Ligand classes that have demonstrated potential in previously reported gold(I) complexes will be coordinated to the NHC-gold(I) complex in an attempt to improve the biological activity.

References

(1) Arduengo III, A. J.; Harlow, R. L.; Kline, M. A Stable Crystalline Carbene. *J. Am. Chem. Soc.* **1991**, *113*, 361–363.

(2) Dumas, J. B.; Peligot, E. Mémoire Sur l'esprit-de-Bois et Les Divers Composés Éthéres Qui En Proviennent. *Ann. Chim. Phys.* **1835**, *58*, 5–74.

(3) Breslow, R. On the Mechanism of Thiamine Action. IV. Evidence from Studies on Model Systems. *J. Am. Chem. Soc.* **1958**, *80*, 3719–3726.

(4) Wanzlick, H.-W. Nucleophile Carben-Chemie. *Angew. Chemie* **1962**, *74*, 129–134.

(5) Wanzlick, H. -W; Schönherr, H. -J. Direct Synthesis of a Mercury Salt-Carbene Complex. *Angew. Chem. Int. Ed.* **1968**, *7*, 141–142.

(6) Igau, A.; Grutzmacher, H.; Baceiredo, A.; Bertrand, G. Analogous α,α'-Bis-Carbenoid Triply Bonded Species: Synthesis of a Stable λ5-Phospaacetylene. *J. Am. Chem. Soc.* **1988**, *110*, 6463–6466.

(7) Öfele, K. 1,3-Dimethyl-4-Imidazolinyliden-(2)-Pentacarbonylchrom Ein Neuer Übergangsmetall-Carben-Komplex. *J. Organomet. Chem.* **1968**, *12*, 42–43.

(8) Patil, S. A.; Patil, S. A.; Patil, R.; Keri, R. S.; Balakrishna, G. R.; Tacke, M. N-Heterocylic Carbene Metal Complexes as Bio-Organometallic Antimicrobial and Anticancer Drugs. *Future Med. Chem.* **2015**, *7*, 1305–1333.

(9) Brothers, P. J.; Roper, W. R. Transition-Metal Dihalocarbene Complexes. *Chem. Rev.* **1988**, *88*, 1293–1326.

(10) Hahn, F. E.; Jahnke, M. C. Heterocyclic Carbenes: Synthesis and Coordination Chemistry. *Angew. Chem. Int. Ed.* **2008**, *47*, 3122–3172.

(11) Marinelli, M.; Santini, C.; Pellei, M. Recent Advances in Medicinal Applications of Coinage-Metal (Cu and Ag) N-Heterocyclic Carbene Complexes. *Curr. Top. Med. Chem.* **2016**, *16*, 2995–3017.

(12) Meng, G.; Kakalis, L.; Nolan, S. P.; Szostak, M. A Simple ^{1}H NMR Method for Determining the σ-Donor Properties of N-Heterocyclic Carbenes. *Tetrahedron Lett.* **2019**,

60, 378–381.

(13) Azofra, L. M.; Veenboer, R. M. P.; Falivene, L.; Vummaleti, S. V. C.; Poater, A.; Nolan, S. P.; Cavallo, L. Quantifying Electronic Similarities between NHC-Gold(I) Complexes and Their Isolobal Imidazolium Precursors. *Phys. Chem. Chem. Phys.* **2019**, *21*, 15615–15622.

(14) Díez-González, S.; Nolan, S. P. Stereoelectronic Parameters Associated with N-Heterocyclic Carbene (NHC) Ligands: A Quest for Understanding. *Coord. Chem. Rev.* **2007**, *251*, 874–883.

(15) Hopkinson, M. N.; Richter, C.; Schedler, M.; Glorius, F. An Overview of N-Heterocyclic Carbenes. *Nature* **2014**, *510*, 485–496.

(16) Despagnet-Ayoub; Grubbs, R. H. A Stable Four-Membered N-Heterocyclic Carbene. *J. Am. Chem. Soc.* **2004**, *126*, 10198–10199.

(17) Scarborough, C. C.; Grady, M. J. W.; Guzei, I. A.; Gandhi, B. A.; Bunel, E. E.; Stahl, S. S. Pd(II) Complexes Possessing a Seven-Membered N-Heterocyclic Carbene Ligand. *Angew. Chem. Int. Ed.* **2005**, *44*, 5269–5272.

(18) Böhm, V. P. W.; Herrmann, W. A. The "Wanzlick Equilibrium." *Angew. Chem. Int. Ed.* **2000**, *39*, 4036–4038.

(19) Patil, S.; Deally, A.; Gleeson, B.; Müller-Bunz, H.; Paradisi, F.; Tacke, M. Novel Benzyl-Substituted N-Heterocyclic Carbene-Silver Acetate Complexes: Synthesis, Cytotoxicity and Antibacterial Studies. *Metallomics* **2011**, *3*, 74–88.

(20) Böhm, V. P. W.; Weskamp, T.; Gstöttmayr, C. W. K.; Herrmann, W. A. Eine Nickel-Katalysierte Kreuzkuppling von Arylchloriden Mit Aryl-Grignard-Reagentien. *Angew. Chemie* **2000**, *112*, 1672–1674.

(21) Benhamou, L.; Chardon, E.; Lavigne, G.; Bellemin-Laponnaz, S.; César, V. Synthetic Routes to N-Heterocyclic Carbene Precursors. *Chem. Rev.* **2011**, *111*, 2705–2733.

(22) Herrmann, W. A.; Köcher, C.; Gooßen, L. J.; Artus, G. R. Heterocyclic Carbenes: A High Yielding Synthesis of Novel Functionalized N-Heterocyclic Carbenes in Liquid Ammonia. *Chem. Eur. J.* **1996**, *2*, 1627–1636.

(23) Wolfe, D. M.; Schreiner, P. R. Facile Conversion of Amino Acids into 1-Alkyl Imidazol-2-Thiones, and Their Oxidative Desulfurization to Imidazoles with Benzoyl Peroxide. *Synthesis* **2007**, *13*, 2002–2008.

(24) Jin, W.; Chen, X.; Dai, P.; Yu, L. Lepidiline C and D: Two New Imidazole Alkaloids from Lepidium Meyenii Walpers (Brassicaceae) Roots. *Phytochem. Lett.* **2016**, *17*, 158–161.

(25) Cheng, C.; Shen, F.; Ding, G.; Liu, A.; Chu, S.; Ma, Y.; Hou, X.; Hao, E.; Wang, X.; Hou, Y.; Bai, G. Lepidiline A Improves the Balance of Endogenous Sex Hormones and Increase Fecundity by Targeting HSD17B1. *Mol. Nutr. Food Res.* **2020**, *64*, 1900706–1900715.

(26) Cui, B.; Zheng, B. L.; He, K.; Zheng, Q. Y. Imidazole Alkaloids from Lepidium Meyenii. *J. Nat. Prod.* **2003**, *66*, 1101–1103.

(27) Riduan, S. N.; Zhang, Y. Imidazolium Salts and Their Polymeric Materials for Biological Applications. *Chem. Soc. Rev.* **2013**, *42*, 9055–9070.

(28) Stromyer, M. L.; Southerland, M. R.; Satyal, U.; Sikder, R. K.; Weader, D. J.; Baughman, J. A.; Youngs, W. J.; Abbosh, P. H. Synthesis, Characterization, and Biological Activity of a Triphenylphosphonium-Containing Imidazolium Salt against Select Bladder Cancer Cell Lines. *Eur. J. Med. Chem.* **2020**, *185*, 111832–111854.

(29) Yang, X.-D.; Zeng, X.-H.; Zhang, Y.-L.; Qing, C.; Song, W.-J.; Li, L.; Zhang, H.-B. Synthesis and Cytotoxic Activities of Novel Phenacylimidazolium Bromides. *Bioorg. Med. Chem. Lett.* **2009**, *19*, 1892–1895.

(30) Mlostoń, G.; Celeda, M.; Poper, W.; Kowalczyk, M.; Gach-Janczak, K.; Janecka, A.; Jasiński, M. Synthesis, Selected Transformations, and Biological Activity of Alkoxy Analogues of Lepidilines A and C. *Materials* **2020**, *13*, 4190.

(31) Malhotra, S. V.; Kumar, V.; Velez, C.; Zayas, B. Imidazolium-Derived Ionic Salts Induce Inhibition of Cancerous Cell Growth through Apoptosis. *MedChemComm* **2014**, *5*, 1404–1409.

(32) Egorova, K. S.; Gordeev, E. G.; Ananikov, V. P. Biological Activity of Ionic Liquids and Their Application in Pharmaceuticals and Medicine. *Chem. Rev.* **2017**, *117*, 7132–7189.

(33) Cochrane, A. R.; Kennedy, A. R.; Kerr, W. J.; Lindsay, D. M.; Reid, M.; Tuttle, T. The

Natural Product Lepidiline A as an N-Heterocyclic Carbene Ligand Precursor in Complexes of the Type [Ir(Cod)(NHC)(PPh_3)]X: Synthesis, Characterisation, and Application in Hydrogen Isotope Exchange Catalysis. *Catalysts* **2020**, *10*, 161.

(34) Hindi, K. M.; Panzner, M. J.; Tessier, C. A.; Cannon, C. L.; Youngs, W. J. The Medicinal Applications of Imidazolium Carbene Metal Complexes. *Chem. Rev.* **2009**, *109*, 3859–3884.

(35) Huaizhi, Z.; Yuantao, N. China's Ancient Gold Drugs. *Gold Bull.* **2001**, *34*, 24–29.

(36) Paul, W.; Sharma, C. P. Blood Compatibility Studies of Swarna Bhasma (Gold Bhasma), an Ayurvedic Drug. *Int. J. Ayurveda Res.* **2011**, *2*, 14–22.

(37) Whitehouse, M. W. Therapeutic Gold. Is It Due for a Come-Back? *Inflammopharmacology* **2008**, *16*, 107–109.

(38) Eisler, R. Chrysotherapy: A Synoptic Review. *Inflamm. Res.* **2003**, *52*, 487–501.

(39) Kean, W. F.; Forestier, F.; Kassam, Y.; Buchanan, W. W.; Rooney, P. J. The History of Gold Therapy in Rheumatoid Disease. *Semin. Arthritis Rheum.* **1985**, *14*, 180–186.

(40) Rosenberg, B.; Vancamp, L.; Trosko, J. E.; Mansour, V. H. Platinum Compounds: A New Class of Potent Antitumour Agents. *Nature* **1969**, *222*, 385–386.

(41) Dasari, S.; Tchounwou, P. B. Ciplatin in Cancer Therapy: Molecular Mechanisms of Action. *Eur. J. Pharmacol.* **2014**, *740*, 364–378.

(42) Astolfi, L.; Ghiselli, S.; Guaran, V.; Chicca, M.; Simoni, E.; Olivetto, E.; Lelli, G.; Martini, A. Correlation of Adverse Effects of Cisplatin Administration in Patients Affected by Solid Tumours: A Retrospective Evaluation. *Oncol. Rep.* **2013**, *29*, 1285–1292.

(43) Kelland, L. R.; Sharp, S. Y.; O'Neill, C. F.; Raynaud, F. I.; Beale, P. J.; Judson, I. R. Mini-Review: Discovery and Development of Platinum Complexes Designed to Circumvent Cisplatin Resistance. *J. Inorg. Biochem.* **1999**, *77*, 111–115.

(44) Bergamo, A.; Gaiddon, C.; Schellens, J. H. M.; Beijnen, J. H.; Sava, G. Approaching Tumour Therapy beyond Platinum Drugs: Status of the Art and Perspectives of Ruthenium Drug Candidates. *J. Inorg. Biochem.* **2012**, *106*, 90–99.

(45) Herman, A.; Tanski, J. M.; Tibbetts, M. F.; Anderson, C. M. Synthesis, Characterization, and in Vitro Evaluation of a Potentially Selective Anticancer, Mixed-Metal [Ruthenium(III)-Platinum(II)] Trinuclear Complex. *Inorg. Chem.* **2008**, *47*, 274–280.

(46) Puthraya, K. H.; Srivastava, T. S.; Amonkar, A. J.; Adwankar, M. K.; Chitnis, M. P. Some Mixed-Ligand Palladium(II) Complexes of 2,2′-Bipyridine and Amino Acids as Potential Anticancer Agents. *J. Inorg. Biochem.* **1985**, *25*, 207–215.

(47) Fernández-Vega, L.; Silva, V. A. R.; Domínguez-González, T. M.; Claudio-Betancourt, S.; Toro-Maldonado, R. E.; Maso, L. C. C.; Ortiz, K. S.; Pérez-Verdejo, J. A.; González, J. R.; Rosado-Fraticelli, G. T.; Meléndez, F. P.; Santiago, F. M. B.; Rivera-Rivera, D. A.; Navarro, C. M.; Chardón, A. C. B.; Vera, A. O.; Tinoco, A. D. Evaluating Ligand Modifications of the Titanocene and Auranofin Moieties for the Development of More Potent Anticancer Drugs. *Inorganics* **2020**, *8*, 10.

(48) Teyssot, M.-L.; Jarrousse, A.-S.; Chevry, A.; De Haze, A.; Beaudoin, C.; Manin, M.; Nolan, S. P.; Díez-González, S.; Morel, L.; Gautier, A. Toxicity of Copper(I)-NHC Complexes against Human Tumor Cells: Induction of Cell Cycle Arrest, Apoptosis, and DNA Cleavage. *Chem. Eur. J.* **2009**, *15*, 314–318.

(49) Streciwilk, W.; Hackenberg, F.; Müller-Bunz, H.; Tacke, M. Synthesis and Cytotoxicity Studies of *P*-Benzyl Substituted NHC-Copper(I) Bromide Derivatives. *Polyhedron* **2014**, *80*, 3–9.

(50) Esmail, S. A. A.; Shamsi, M.; Chen, T.; Al-asbahy, W. M. Design, Synthesis and Characterization of Tin-Based Cancer Chemotherapy Drug Entity: In Vitro DNA Binding, Cleavage, Induction of Cancer Cell Apoptosis by Triggering DNA Damage-Mediated P53 Phosphorylation and Molecular Docking. *Appl. Organomet. Chem.* **2018**, *33*, 4651–4665.

(51) Mármol, I.; Quero, J.; Rodríguez-Yoldi, M. J.; Cerrada, E. Gold as a Possible Alternative to Platinum-Based Chemotherapy for Colon Cancer Treatment. *Cancers* **2019**, *11*, 780.

(52) Bortoluzzi, M.; Scrivanti, A.; Reolon, A.; Amadio, E.; Bertolasi, V. Synthesis and Characterization of Novel Gold(III) Complexes with Polydentate N-Donor Ligands Based on the Pyridine and Triazole Heterocycles. *Inorg. Chem. Commun.* **2013**, *33*, 82–85.

(53) Casini, A.; Hartinger, C.; Gabbiani, C.; Mini, E.; Dyson, P. J.; Keppler, B. K.; Messori, L. Gold(III) Compounds as Anticancer Agents: Relevance of Gold-Protein Interactions for Their Mechanism of Action. *J. Inorg. Biochem.* **2008**, *102*, 564–575.

(54) Marzano, C.; Ronconi, L.; Chiara, F.; Giron, M. C.; Faustinelli, I.; Cristofori, P.; Trevisan, A.; Fregona, D. Gold(III)-Dithiocarbamato Anticancer Agents: Activity, Toxicology and Histopathological Studies in Rodents. *Int. J. Cancer* **2011**, *129*, 487–496.

(55) Roder, C.; Thomson, M. J. Auranofin: Repurposing an Old Drug for a Golden New Age. *Drugs R. D.* **2015**, *15*, 13–20.

(56) Thangamani, S.; Mohammad, H.; Abushahba, M. F. N.; Sobreira, T. J. P.; Hedrick, V. E.; Paul, L. N.; Seleem, M. N. Antibacterial Activity and Mechanism of Action of Auranofin against Multi-Drug Resistant Bacterial Pathogens. *Sci. Rep.* **2016**, *6*, 22571–22584.

(57) Rothan, H. A.; Stone, S.; Natekar, J.; Kumari, P.; Arora, K.; Kumar, M. The FDA-Approved Gold Drug Auranofin Inhibits Novel Coronavirus (SARS-COV-2) Replication and Attenuates Inflammation in Human Cells. *Virology* **2020**, *547*, 7–11.

(58) Mirabelli, C. K.; Johnson, R. K.; Sung, C. M.; Faucette, L.; Muirhead, K.; Crooke, S. T. Evaluation of the in Vivo Antitumor Activity and in Vitro Cytotoxic Properties of Auranofin, a Coordinated Gold Compound, in Murine Tumor Models. *Cancer Res.* **1985**, *45*, 32–39.

(59) Marzano, C.; Gandin, V.; Folda, A.; Scutari, G.; Bindoli, A.; Rigobello, M. P. Inhibition of Thioredoxin Reductase by Auranofin Induces Apoptosis in Cisplatin-Resistant Human Ovarian Cancer Cells. *Free Radic. Biol. Med.* **2007**, *42*, 872–881.

(60) Tabrizi, L.; Abyar, F. Conjugation of Gold(III) Complex with Vitamin B1 and Chlorambucil Derivatives: Anticancer Evaluation and Mechanistic Insights. *Metallomics* **2020**, *12*, 721–731.

(61) Miranda, S.; Vergara, E.; Mohr, F.; de Vos, D.; Cerrada, E.; Mendía, A.; Laguna, M. Synthesis, Characterization, and in Vitro Cytotoxicity of Some Gold(I) and Trans Platinum(II) Thionate Complexes Containing Water-Soluble PTA and DAPTA Ligands. X-Ray Crystal Structures of [Au($SC_4H_3N_2$)(PTA)], Trans-[Pt($SC_4H_3N_2$)$_2$(PTA)$_2$], Trans-

[Pt(SC$_5$H$_4$N)$_2$. *Inorg. Chem.* **2008**, *47*, 5641–5648.

(62) Zhang, X.; Selvaraju, K.; Saei, A. A.; D'Arcy, P.; Zubarev, R. A.; Arnér, E. S.; Linder, S. Repurposing of Auranofin: Thioredoxin Reductase Remains a Primary Target of the Drug. *Biochimie* **2019**, *162*, 46–54.

(63) Ott, I. On the Medicinal Chemistry of Gold Complexes as Anticancer Drugs. *Coord. Chem. Rev.* **2009**, *253*, 1670–1681.

(64) Gromer, S.; Arscott, L. D.; Williams, C. H.; Schirmer, R. H.; Becker, K. Human Placenta Thioredoxin Reductase. *J. Biol. Chem.* **1998**, *273*, 20096–20101.

(65) Nobili, S.; Mini, E.; Landini, I.; Gabbiani, C.; Casini, A.; Messori, L. Gold Compounds as Anticancer Agents: Chemistry, Cellular Pharmacology, and Preclinical Studies. *Med. Res. Rev.* **2010**, *30*, 550–580.

(66) Bindoli, A.; Rigobello, M. P.; Scutari, G.; Gabbiani, C.; Casini, A.; Messori, L. Thioredoxin Reductase: A Target for Gold Compounds Acting as Potential Anticancer Drugs. *Coord. Chem. Rev.* **2009**, *253*, 1692–1707.

(67) Rigobello, M. P.; Scutari, G.; Boscolo, R.; Bindoli, A. Induction of Mitochondrial Permeability Transition by Auranofin, a Gold(I)-Phosphine Derivative. *Br. J. Pharmacol.* **2002**, *136*, 1162–1168.

(68) Rigobello, M. P.; Folda, A.; Baldoin, M. C.; Scutari, G.; Bindoli, A. Effect of Auranofin on the Mitochrondrial Generation of Hydrogen Peroxide. Role of Thioredoxin Reductase. *Free Radic. Res.* **2005**, *39*, 687–695.

(69) Barnard, P. J.; Berners-Price, S. J. Targeting the Mitochondrial Cell Death Pathway with Gold Compounds. *Coord. Chem. Rev.* **2007**, *251*, 1889–1902.

(70) Hill, K. E.; McCollum, G. W.; Boeglin, M. E.; Burk, R. F. Thioredoxin Reductase Activity Is Decreases by Selenium Deficiency. *Biochem. Biophys. Res. Commun.* **1997**, *234*, 293–295.

(71) Urig, S.; Fritz-Wolf, K.; Réau, R.; Herold-Mende, C.; Tóth, K.; Davioud-Charvet, E.; Becker, K. Undressing of Phosphine Gold(I) Complexes as Irreversible Inhibitors of Human Disulfide Reductases. *Angew. Chem. Int. Ed.* **2006**, *45*, 1881–1886.

(72) Hickey, J. L.; Ruhayel, R. A.; Barnard, P. J.; Baker, M. V; Berners-Price, S. J.; Filipovska, A. Mitochondria-Targeted Chemotherapeutics: The Rational Design of Gold (I) N-Heterocyclic Carbene Complexes That Are Selectively Toxic to Cancer Cells and Target Protein Selenols in Preference to Thiols. *J. Am. Chem. Soc.* **2008**, *130*, 12570–12571.

(73) Schmidt, C.; Albrecht, L.; Balasupramaniam, S.; Misgeld, R.; Karge, B.; Brönstrup, M.; Prokop, A.; Baumann, K.; Reichl, S.; Ott, I. A Gold(I) Biscarbene Complex with Improved Activity as a TrxR Inhibitor and Cytotoxic Drug: Comparative Studies with Different Gold Metallodrugs. *Metallomics* **2019**, *11*, 533–545.

(74) Raubenheimer, H. G.; Lindeque, L.; Cronje, S. Synthesis and Characterisation of Neutral and Cationic Diamino Carbene Complexes of Gold(I). *J. Organomet. Chem.* **1996**, *511*, 177–184.

(75) Raubenheimer, H. G.; Olivier, P. J.; Lindeque, L.; Desmet, M.; Hrušak, J.; Kruger, G. J. Oxidative Addition of Mono and Bis(Carbene) Complexes Derived from Imidazolyl and Thiazolyl Gold(I) Compounds. *J. Organomet. Chem.* **1997**, *544*, 91–100.

(76) Wang, H. M. J.; Lin, I. J. B. Facile Synthesis of Silver(I)-Carbene Complexes. Useful Carbene Transfer Agents. *Organometallics* **1998**, *17*, 972–975.

(77) Wang, H. M. J.; Chen, C. Y. L.; Lin, I. J. B. Synthesis, Structure, and Spectroscopic Properties of Gold(I) Carbene Complexes. *Organometallics* **1999**, *18*, 1216–1223.

(78) Baker, M. V.; Barnard, P. J.; Berners-Price, S. J.; Brayshaw, S. K.; Hickey, J. L.; Skelton, B. W.; White, A. H. Synthesis and Structural Characterisation of Linear Au(I) N-Heterocyclic Carbene Complexes: New Analogues of the Au(I) Phosphine Drug Auranofin. *J. Organomet. Chem.* **2005**, *690*, 5625–5635.

(79) de Frémont, P.; Stevens, E. D.; Eelman, M. D.; Fogg, D. E.; Nolan, S. P. Synthesis and Characterisation of Gold(I) N-Heterocyclic Carbene Complexes Bearing Biologically Compatible Moieties. *Organometallics* **2006**, *25*, 5824–5828.

(80) Liu, W.; Bensdorf, K.; Proetto, M.; Abram, U.; Hagenbach, A.; Gust, R. NHC Gold Halide Complexes Derived from 4,5-Diarylimidazoles: Synthesis, Structural Analysis, and Pharmacological Investigations as Potential Antitumor Agents. *J. Med. Chem.* **2011**, *54*,

8605–8615.

(81) Collado, A.; Gómez-Suárez, A.; Martin, A. R.; Slawin, A. M. Z.; Nolan, S. P. Straightforward Synthesis of [Au(NHC)X] (NHC = N-Heterocyclic Carbene, X = Cl, Br, I) Complexes. *Chem. Commun.* **2013**, *49*, 5541–5543.

(82) Schmidbaur, H.; Schier, A. Aurophilic Interactions as a Subject of Current Research: An up-Date. *Chem. Soc. Rev.* **2012**, *41*, 370–412.

(83) Andris, E.; Andrikopoulos, P.; Schulz, J.; Turek, J.; Růžička, A.; Roithová, J.; Rulíšek, L. Aurophilic Interactions in [(L)AuCl]...[(L')AuCl] Dimers: Calibration by Experiment and Theory. *J. Am. Chem. Soc.* **2018**, *140*, 2316–2325.

(84) Głodek, M.; Pawlędzio, S.; Makal, A.; Plażuk, D. The Impact of Crystal Packing and Aurophilic Interactions on the Luminescence Properties in Polymorphs and Solvate of Aroylacetylide–Gold(I) Complexes. *Chem. Eur. J.* **2019**, *25*, 13131–13145.

(85) Lima, C. J.; Rodríguez, L. Phosphine-Gold(I) Compounds as Anticancer Agents: General Description and Mechanisms of Action. *Anticancer Agents Med. Chem.* **2011**, *11*, 921–928.

(86) Marzo, T.; Massai, L.; Pratesi, A.; Stefanini, M.; Cirri, D.; Magherini, F.; Becatti, M.; Landini, I.; Nobili, S.; Mini, E.; Crociani, O.; Arcangeli, A.; Pillozzi, S.; Gamberi, T.; Messori, L. Replacement of the Thiosugar of Auranofin with Iodide Enhances the Anticancer Potency in a Mouse Model of Ovarian Cancer. *ACS Med. Chem. Lett.* **2019**, *10*, 656–660.

(87) Gandin, V.; Fernandes, A. P.; Rigobello, M. P.; Dani, B.; Sorrentino, F.; Tisato, F.; Björnstedt, M.; Bindoli, A.; Sturaro, A.; Rella, R.; Marzano, C. Cancer Cell Death Induced by Phosphine Gold(I) Compounds Targeting Thioredoxin Reductase. *Biochem. Pharmacol.* **2010**, *79*, 90–101.

(88) Scheffler, H.; You, Y.; Ott, I. Comparative Studies on the Cytotoxicity, Cellular and Nuclear Uptake of a Series of Chloro Gold(I) Phosphine Complexes. *Polyhedron* **2010**, *29*, 66–69.

(89) Atrián-Blasco, E.; Gascón, S.; Rodríguez-Yoldi, M. J.; Laguna, M.; Cerrada, E. Synthesis of Gold(I) Derivatives Bearing Alkylated 1,3,5-Triaza-7-Phosphaadamantane as

Selective Anticancer Metallodrugs. *Eur. J. Inorg. Chem.* **2016**, 2791–2803.

(90) Yeo, C. I.; Ooi, K. K.; Akim, A. M.; Ang, K. P.; Fairuz, Z. A.; Binti, S. N.; Halim, A.; Ng, S. W.; Seng, H.-L.; Tiekink, E. R. T. The Influence of R Substituents in Triphenylphosphinegold(I) Carbonimidothioates, $Ph_3PAu[SC(OR)=NPh]$(R=Me, Et and IPr), upon in Vitro Cytotoxicity against the HT-29 Colon Cancer Cell Line and upon Apoptotic Pathways. *J. Inorg. Biochem.* **2013**, *127*, 24–38.

(91) Altaf, M.; Monim-ul-Mehboob, M.; Isab, A. A.; Dhuna, V.; Bhatia, G.; Dhuna, K.; Altuwaijri, S. The Synthesis, Spectroscopic Characterization and Anticancer Activity of New Mono and Binuclear Phosphanegold(I) Dithiocarbamate Complexes. *New J. Chem.* **2015**, *39*, 377–385.

(92) de Almeida, A. M.; de Oliveira, B. A.; de Castro, P. P.; de Mendonça, C. C.; Furtado, R. A.; Nicolella, H. D.; da Silva, V. L.; Diniz, C. G.; Tavares, D. C.; Silva, H.; de Almeida, M. V. Lipophilic Gold(I) Complexes with 1,3,4-Oxadiazol-2-Thione or 1,3-Thiazolidine-2-Thione Moieties: Synthesis and Their Cytotoxic and Antimicrobial Activites. *BioMetals* **2017**, *30*, 841–857.

(93) Tiekink, E. R. T. Phosphinegold(I) Thiolates- Pharmacological Use and Potential. *Bioinorg. Chem. Appl.* **2003**, *1*, 53–67.

(94) Andermark, V.; Göke, K.; Kokoschka, M.; Abu el Maaty, M. A.; Lum, C. T.; Zou, T.; Sun, R. W.; Aguiló, E.; Oehninger, L.; Rodríguez, L.; Bunjes, H.; Wöl, S.; Che, C.; Ott, I. Alkynyl Gold (I) Phosphane Complexes : Evaluation of Structure–Activity-Relationships for the Phosphane Ligands, Effects on Key Signaling Proteins and Preliminary in-Vivo Studies with a Nanoformulated Complex. *J. Inorg. Biochem.* **2016**, *160*, 140–148.

(95) Vergara, E.; Cerrada, E.; Casini, A.; Zava, O.; Laguna, M.; Dyson, P. J. Antiproliferative Activity of Gold (I) Alkyne Complexes Containing Water-Soluble Phosphane Ligands. *Organometallics* **2010**, *29*, 2596–2603.

(96) Meyer, A.; Bagowski, C. P.; Kokoschka, M.; Stefanopoulou, M.; Alborzinia, H.; Can, S.; Vlecken, D. H.; Sheldrick, W. S.; Wölfl, S.; Ott, I. On the Biological Properties of Alkynyl Phosphine Gold (I) Complexes. *Angew. Chem. Int. Ed.* **2012**, *51*, 8895–8899.

(97) García-Moreno, E.; Tomás, A.; Atrián-Blasco, E.; Gascón, S.; Romanos, E.; Rodriguez-Yoldi, M. J.; Cerrada, E.; Laguna, M. In Vitro and in Vivo Evaluation of Organometallic Gold(I) Derivatives as Anticancer Agents. *Dalton Trans.* **2016**, *45*, 2462–2475.

(98) Rouschias, G.; Shaw, B, L. A Revised Structure for Chugaev's Salt $[PtC_8H_{15}N_6]_xCl_x$. *Chem. Commun.* **1970**, 183.

(99) Coleman, A. W.; Hitchcock, P. B.; Lappert, M. F.; Maskell, R. K.; Müller, J. H. Carbene Complexes: XIX. Optically Active Electron-Rich Olefin-Derived Carbene-Transition-Metal Complexes. Crystal Structures of $[RhCl(COD)(C_7H_{12}N_2)]$, $[RhCl(COD)(C_9H_{16}N_2)]$, $[RhCl(PPh_3)_2(C_9H_{18}N_2)]$ and $[Co(CO)(NO)(PPh_3)(C_6H_{12}N_2)]$. *J. Organomet. Chem.* **1985**, *296*, 173–196.

(100) Lappert, M. F. The Coordination Chemistry of Electron-Rich Alkenes (Enetetramines). *J. Organomet. Chem.* **1988**, *358*, 185–214.

(101) Díez-González, S.; Marion, N.; Nolan, S. P. N-Heterocyclic Carbenes in Late Transition Metal Catalysis. *Chem. Rev.* **2009**, *109*, 3612–3676.

(102) Scholl, M.; Ding, S.; Lee, C. W.; Grubbs, R. H. Synthesis and Activity of a New Generation of Ruthenium-Based Olefin Metathesis Catalysts Coordinated with 1,3-Dimesityl-4,5-Dihydroimidazol-2-Ylidene Ligands. *Org. Lett.* **1999**, *1*, 953–956.

(103) Barnard, P. J.; Baker, M. V.; Berners-Price, S. J.; Day, D. A. Mitochondrial Permeability Transition Induced by Dinuclear Gold(I)-Carbene Complexes: Potential New Antimitochondrial Antitumour Agents. *J. Inorg. Biochem.* **2004**, *98*, 1642–1647.

(104) Baker, M. V.; Barnard, P. J.; Berners-Price, S. J.; Brayshaw, S. K.; Hickey, J. L.; Skelton, B. W.; White, A. H. Cationic, Linear Au(I) N-Heterocyclic Carbene Complexes: Synthesis, Structure and Anti-Mitochondrial Activity. *Dalton Trans.* **2006**, 3708–3715.

(105) Arcau, J.; Andermark, V.; Rodrigues, M.; Giannicchi, I.; Pérez-Garcia, L.; Ott, I.; Rodríguez, L. Synthesis and Biological Activity of Gold(I) N-Heterocyclic Carbene Complexes with Long Aliphatic Side Chains. *Eur. J. Inorg. Chem.* **2014**, 6117–6125.

(106) Fernández-Gallardo, J.; Elie, B. T.; Sanaú, M.; Contel, M. Versatile Synthesis of Cationic N-Heterocyclic Carbene-Gold(I) Complexes Containing a Second Ancillary Ligand.

Design of Heterobimetallic Ruthenium-Gold Anticancer Agents. *Chem. Commun.* **2016**, *52*, 3155–3158.

(107) Rubbiani, R.; Kitanovic, I.; Alborzinia, H.; Can, S.; Kitanovic, A.; Onambele, L. A.; Stefanopoulou, M.; Geldmacher, Y.; Sheldrick, W. S.; Wolber, G.; Prokop, A.; Wölfl, S.; Ott, I. Benzimidazol-2-Ylidene Gold(I) Complexes Are Thioredoxin Reductase Inhibitors with Multiple Antitumor Properties. *J. Med. Chem.* **2010**, *53*, 8608–8618.

(108) Hackenberg, F.; Müller-Bunz, H.; Smith, R.; Streciwilk, W.; Zhu, X.; Tacke, M. Novel Ruthenium(II) and Gold(I) NHC Complexes: Synthesis, Characterization, and Evaluation of Their Anticancer Properties. *Organometallics* **2013**, *32*, 5551–5560.

(109) Patil, S.; Deally, A.; Hackenberg, F.; Kaps, L.; Müller-Bunz, H.; Schobert, R.; Tacke, M. Novel Benzyl- or 4-Cyanobenzyl-Substituted N-Heterocyclic (Bromo)(Carbene)Silver(I) and (Carbene)(Chloro)Gold(I) Complexes: Synthesis and Preliminary Cytotoxicity Studies. *Helv. Chim. Acta* **2011**, *94*, 1551–1562.

(110) Garner, M. E.; Niu, W.; Chen, X.; Ghiviriga, I.; Tan, W.; Veige, A. S. N-Heterocyclic Carbene Gold(I) and Silver(I) Complexes Bearing Functional Groups for Bio-Conjugation. *Dalton Trans.* **2015**, *44*, 1914–1923.

(111) Lemke, J.; Pinto, A.; Niehoff, P.; Vasylyeva, V.; Metzler-Nolte, N. Synthesis, Structural Characterisation and Anti-Proliferative Activity of NHC Gold Amino Acid and Peptide Conjugates. *Dalton Trans.* **2009**, *35*, 7063–7070.

(112) Dada, O.; Sánchez-Sanz, G.; Tacke, M.; Zhu, X. Synthesis and Anticancer Activity of Novel NHC-Gold(I)-Sugar Complexes. *Tetrahedron Lett.* **2018**, *59*, 2904–2908.

(113) Gaillard, S.; Slawin, A. M. Z.; Nolan, S. P. A N-Heterocyclic Carbene Gold Hydroxide Complex: A Golden Synthon. *Chem. Commun.* **2010**, *46*, 2742–2744.

(114) Weaver, J.; Gaillard, S.; Toye, C.; Macpherson, S.; Nolan, S. P.; Riches, A. Cytotoxicity of Gold(I) N-Heterocyclic Carbene Complexes Assessed by Using Human Tumor Cell Lines. *Chem. Eur. J.* **2011**, *17*, 6620–6624.

(115) Bian, M.; Fan, R.; Jiang, G.; Wang, Y.; Lu, Y.; Liu, W. Halo and Pseudohalo Gold(I)-NHC Complexes Derived from 4,5-Diarylimidazoles with Excellent In Vitro and In Vivo

Anticancer Activities Against HCC. *J. Med. Chem.* **2020**, *63*, 9197–9211.

(116) Dada, O.; Curran, D.; O'Beirne, C.; Müller-Bunz, H.; Zhu, X.; Tacke, M. Synthesis and Cytotoxicity Studies of Novel NHC–Gold(I) Pseudohalides and Thiolates. *J. Organomet. Chem.* **2017**, *840*, 30–37.

(117) Rubbiani, R.; Schuh, E.; Meyer, A.; Lemke, J.; Wimberg, J.; Metzler-Nolte, N.; Meyer, F.; Mohr, F.; Ott, I. TrxR Inhibition and Antiproliferative Activities of Structurally Diverse Gold N-Heterocyclic Carbene Complexes. *MedChemComm* **2013**, *4*, 942–948.

(118) Seliman, A. A. A.; Altaf, M.; Onawole, A. T.; Ahmad, S.; Ahmed, M. Y.; Al-Saadi, A. A.; Altuwaijri, S.; Bhatia, G.; Singh, J.; Isab, A. A. Synthesis, X-Ray Structures and Anticancer Activity of Gold(I)- Carbene Complexes with Selenones as Co-Ligands and Their Molecular Docking Studies with Thioredoxin Reductase. *J. Organomet. Chem.* **2017**, *848*, 175–183.

(119) Seliman, A. A. A.; Altaf, M.; Odewunmi, N. A.; Kawde, A.-N.; Zierkiewicz, W.; Ahmad, S.; Altuwaijri, S.; Isab, A. A. Synthesis, X-Ray Structure, DFT Calculations and Anticancer Activity of a Selenourea Coordinated Gold(I)-Carbene Complex. *Polyhedron* **2017**, *137*, 197–206.

(120) Robilotto, T. J.; Deligonul, N.; Updegraff, J. B.; Gray, T. G. Azido, Triazolyl, and Alkynyl Complexes of Gold(I): Syntheses, Structures, and Ligand Effects. *Inorg. Chem.* **2013**, *52*, 9659–9668.

(121) Bertrand, B.; Stefan, L.; Pirrotta, M.; Monchaud, D.; Bodio, E.; Richard, P.; Le Gendre, P.; Warmerdam, E.; De Jager, M. H.; Groothuis, G. M. M.; Picquet, M.; Casini, A. Caffeine-Based Gold(I) N-Heterocyclic Carbenes as Possible Anticancer Agents: Synthesis and Biological Properties. *Inorg. Chem.* **2014**, *53*, 2296–2303.

(122) Barnard, P. J.; Baker, M. V.; Berners-Price, S. J.; Skelton, B. W.; White, A. H. Dinuclear Gold(I) Complexes of Bridging Bidentate Carbene Ligands: Synthesis, Structure and Spectroscopic Characterisation. *Dalton Trans.* **2004**, *7*, 1038–1047.

(123) Horvath, U. E. I.; Bentivoglio, G.; Hummel, M.; Schottenberger, H.; Wurst, K.; Nell, M. J.; van Rensburg, C. E. J.; Cronje, S.; Raubenheimer, H. G. A Cytotoxic

Bic(Carbene)Gold(I) Complex of Ferrocenyl Complexes: Synthesis and Structural Characterisation. *New J. Chem.* **2008**, *32*, 533–539.

(124) Lin, I. J. B.; Vasam, C. S. Review of Gold(I) N-Heterocyclic Carbenes. *Can. J. Chem.* **2005**, *83*, 812–825.

(125) Porchia, M.; Pellei, M.; Marinelli, M.; Tisato, F.; Del Bello, F.; Santini, C. New Insights in Au-NHCs Complexes as Anticancer Agents. *Eur. J. Med. Chem.* **2018**, *146*, 709–746.

(126) Walther, W.; Dada, O.; O'Beirne, C.; Ott, I.; Sánchez-Sanz, G.; Schmidt, C.; Werner, C.; Zhu, X.; Tacke, M. In Vitro and In Vivo Investigations into the Carbene Gold Chloride and Thioglucoside Anticancer Drug Candidates NHC-AuCl and NHC-AuSR. *Lett. Drug Des. Discov.* **2017**, *14*, 125–134.

Chapter Two

NHC*-Gold(I) Halide, Carbene and Phosphine Complexes

Work published as:

Novel Anticancer NHC*-Gold(I) Complexes Inspired by Lepidiline A

D. Curran, H. Müller-Bunz, S. I. Bär, R. Schobert, X. Zhu, M. Tacke

Molecules, **2020**, *25*, 3474-3491

2.1 Introduction

Globally, cancer is the second leading cause of death, reporting an estimated 9.6 million deaths in 2018.[1] In particular, breast cancer is the most frequently diagnosed cancer for women and also responsible for the highest mortality.[1,2] Men are most frequently diagnosed with prostate cancer, however lung cancer is the most common cause of cancer death.[3] Tackling the burden of cancer has proven inconceivably challenging and new-age strategies are required to develop treatments and preventative medicines. Metal-based chemotherapeutics have demonstrated their effectiveness with the ongoing use of cisplatin. However, the repurposing of anti-arthritic gold(I) drug auranofin has attracted attention to the potential of gold-based anticancer agents. NHC-gold(I) complexes have emerged as a promising class of anticancer drugs. The possibility to modulate their biological activity by performing structural modifications makes them highly useful for drug design.

Exploring structural variations on the NHC ligand was demonstrated in Chapter 1, while fewer examples are reported of substituting the ligand coordinated to the NHC-gold(I) centre. Ligand substitution proved an effective tool for drug development in the case of the triethylphosphine gold(I) iodide (**1.28**, **Figure 1.9**) which displayed a 2-fold increase in activity compared to the thioglucose derivative.[4] This behaviour was also observed in a series of halo and pseudohalo gold(I) complexes developed from 4,5-diarylimidazol-2-ylidenes.[5] It was noted the antiproliferative properties of the halo derivatives increased with the larger halide, potentially due to the increased lipophilicity. The iodido derivative **2.1** displayed the highest activity with an IC_{50} value of 0.50 ± 0.02 μM on the human liver carcinoma cell line HepG2 (**Figure 2.1**).

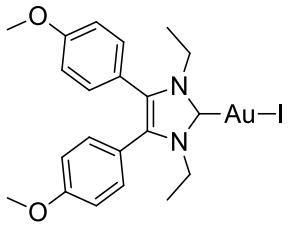

2.1

Figure 2.1 NHC-gold(I) iodide complex **2.1**.

High cytotoxicity has also been observed with the addition of second stabilising ligand such as an NHC or phosphine. Berners-Price and Baker at al. first reported the biological applications

of gold(I) complexes in a series of cationic linear biscarbene complexes **1.36** (**Figure 1.11**) that showed anti-mitochondrial activity (**Figure 2.2**).[6] It was noted that the induction of cell permeability was increased with the lipophilicity of the complexes. Later on, Rubbiani et al. demonstrated that higher activity can be achieved against TrxR and the colon cancer cell line HT-29 by replacing the bromide with a second NHC.[7] The cationic biscarbene **2.3** reported an IC_{50} value of 5.1 ± 1.1 μM on the HT-29 cell line and remarkably a 2.5-fold increase in TrxR inhibition compared to the bromo analogue with an IC_{50} value of 0.47 ± 0.14 μM.

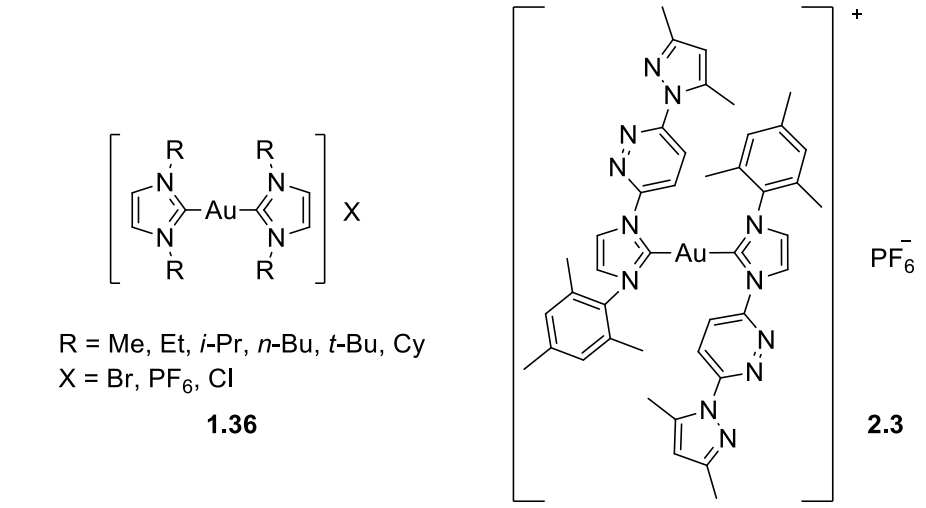

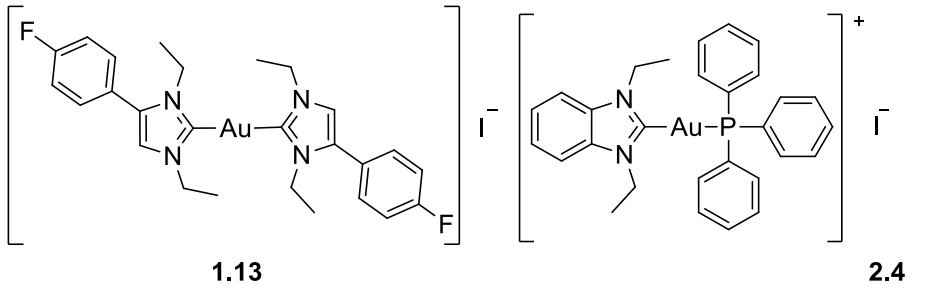

Figure 2.2 Cationic gold(I) biscarbene complexes (**1.36**, **2.23** and **1.13**) and [NHC-Au-PPh_3]I complex **2.4**.

Extensive biological studies on the 4-(4′-fluorophenyl)-1,3-diethylimidazol-2-ylidene derived mono- and biscarbene gold(I) complexes revealed that in relation to protein binding studies, a significantly greater percentage of the monocarbene complex tightly bound to fetal calf serum and bovine serum albumin in contrast to the biscarbene complex **1.13**.[8] The data also reported that the biscarbene complex had a quicker cellular uptake than the neutral auranofin complex (1 h versus 4 h).

Complexes featuring both an NHC and a phosphine ligand have also displayed promising cytotoxic activity. The use of triphenylphosphine in a benzimidazol-2-ylidene gold(I) complex reported the highest cytotoxicity against the colon and breast cancer cell lines HT-29 and MCF-7, out of a selection of phosphine ligands.[9] However, the isopropyl, ethyl and methyl derivatives exhibited significantly higher TrxR inhibition than the phenyl derivative; complex **2.4** reported an IC_{50} of 0.66 ± 0.02 μM against TrxR (**Figure 2.2**). The addition of a methoxy group to the 5-position on the benzimidazol-2-ylidene reduced both the cancer cell cytotoxicity and the TrxR inhibition.[10] However, the NHC-Au-PPh_3 complex still presented low single-digit micromolar activity against human colon, breast and pancreatic cancer cell lines. A comparison was drawn between cationic gold(I) complexes of the type $[(NHC_2)Au]^+$ and $[(NHC)Au(PPh_3)]^+$, and the neutral NHC-gold chloride. Both cationic complexes displayed significantly higher antiproliferative properties against the human breast and colon cancer cell lines MCF-7 and HT-29, than the neutral complex. It is worth noting that the biscarbene complex presented an IC_{50} value of 3.13 ± 0.54 μM on the non-tumorigenic human embryonic kidney cell line HEK-293 compared to an IC_{50} value of 0.41 ± 0.18 μM for the NHC-Au-PPh_3 complex, indicating the biscarbene complex showed bioselectivity while the phosphine derived complex did not.[11]

Chapter Proposal

Drawing inspiration from the proposition that NHC ligands are more favourable than phosphines, we decided to synthesise complexes with halide, carbene and phosphine ligands. We seek to find a greater understanding of these complexes by evaluating the complexes with *in vitro* biological testing and through computational analysis. Furthermore, the use of halide ligands allowed us to create monocarbene complexes which can be compared to the biscarbene complexes which present an additional NHC ligand.

2.2 Synthesis

2.2.1 Synthesis of NHC*-Gold(I) Halides

The imidazolium bromide salt **1.7** was synthesised with modified conditions (**Scheme 1.1**).[12] The commercially available 4,5-diphenyl-1*H*-imidazole was deprotonated with K_2CO_3 and reacted with two equivalents of benzyl bromide as reported, however the reaction was heated at 35° C for 48 h which afforded 1,3-dibenzyl-4,5-diphenylimidazolium bromide (**1.7**) in a higher yield of 90%. NHC*-gold(I) chloride (**1.21**) was prepared as reported in a higher yield of 84% (**Scheme 1.5**).[13] From here on the complexes developed with this 1,3-dibenzyl-4,5-diphenylimidazol-2-ylidene system will be noted as NHC*. NHC*-gold(I) bromide was synthesised via an established method,[14] by reacting the imidazolium salt **1.7** directly with chloro(dimethylsulfide)gold(I) affording **2.5** in a high yield (**Scheme 2.1**). Whereas the iodide analogue was formed from the already coordinated NHC*-gold(I) chloride, **1.21**, affording **2.6** after a halide exchange with an excess of potassium iodide. Compound **2.6** was formed in a good yield, however the product exhibited minor instability in solution when exposed to light.

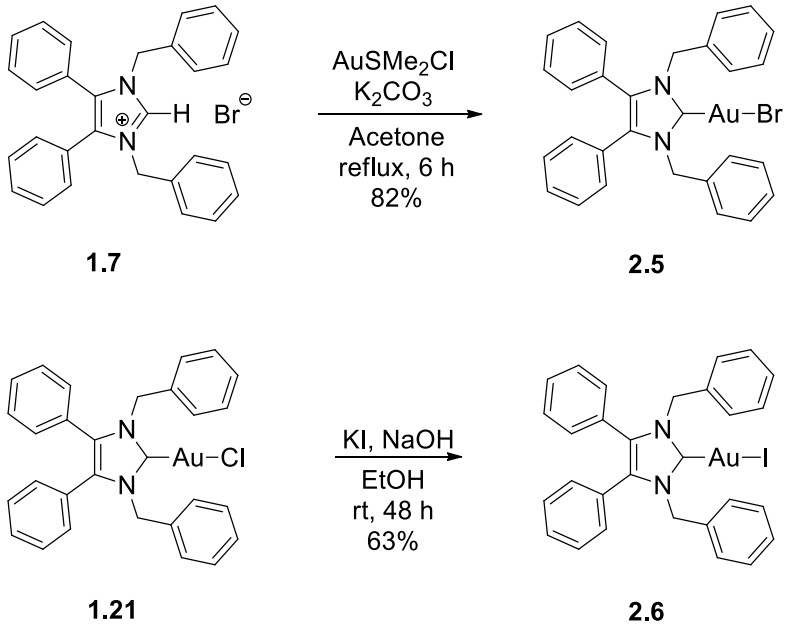

1.7 **2.5**

1.21 **2.6**

Scheme 2.1 Synthesis of NHC*-gold(I)-halides **2.5** and **2.6**.

The ^{1}H-NMR spectra of **2.5** and **2.6** are identical to the chloride analogue **1.21** (**Figure 2.3**). However, in the ^{13}C-NMR spectrum the carbene carbon of **2.6** appears at δ = 181.5 ppm, more downfield than both the bromide or chloride species (δ = 174.9 and 171.6 ppm, respectively).

Chemical shifts are increasingly shielded as electronegativity increases, thus **1.21** is the furthest upfield due to its high electronegativity and **2.6** is downfield due to its lower electronegativity.

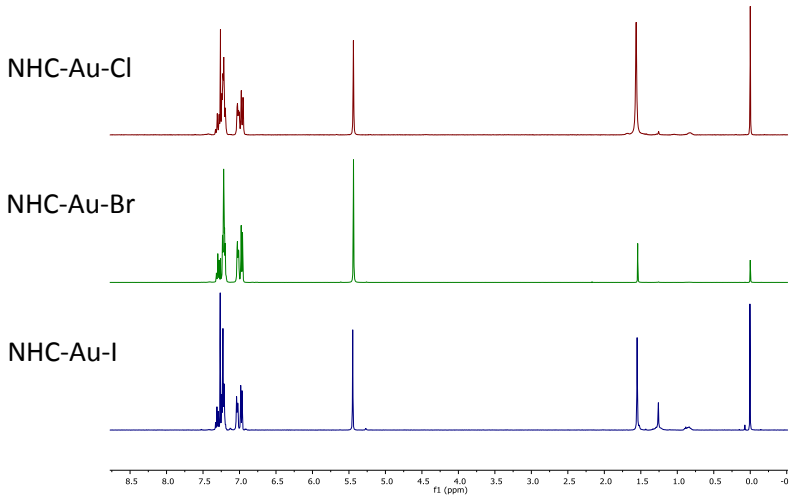

Figure 2.3 Stacked ^{1}H-NMR spectra of NHC*-Au-X complexes **1.21**, **2.5** and **2.6** showing the CH_2 peak at 5.44 ppm.

2.2.2 Synthesis of Bis(NHC*)-Gold(I) Complexes

A series of biscarbenes were synthesised with varying anions, according to literature conditions (**Scheme 2.3**).[15] Initially, the imidazolium salts **2.7, 2.8** and **2.9** were formed through anion exchange, replacing the bromide anion with hexafluorophosphate, tetrafluoroborate and iodide, in high yields of 87-91% (**Scheme 2.2**).

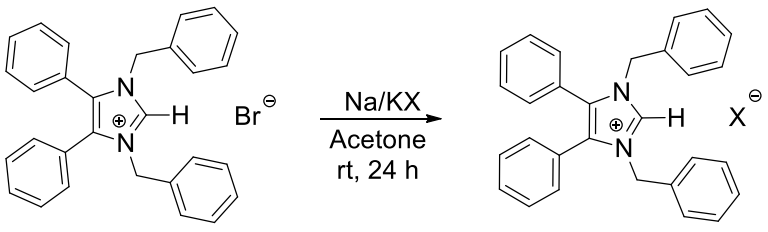

1.7

2.7: X = PF_6; 91%
2.8: X = BF_4; 88%
2.9: X = I; 87%

Scheme 2.2 Synthesis of imidazolium salts **2.7**, **2.8** and **2.9**.

These imidazolium salts were subsequently treated with silver oxide and later transmetallated *in situ* with half an equivalent of chloro(dimethylsulfide)gold(I) to afford biscarbenes **2.10**-**2.13**

in high yields. Interestingly, the time was quite variable in these reactions. Biscarbenes **2.10** and **2.13** had reaction times of 20 h, whereas the reaction time of **2.11** was extended to 48 h to ensure full conversion. This was due to the size of the anion and thus the bromide complex **2.12** unsurprisingly had the longest reaction time of 72 h. This reaction was monitored by both TLC and ^{1}H-NMR spectroscopy.

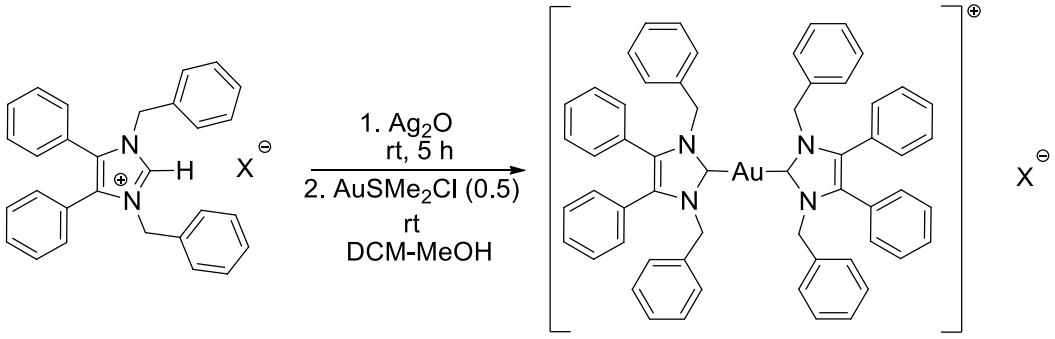

2.7
2.8
1.7
2.9

2.10: X = PF_6; 86%
2.11: X = BF_4; 87%
2.12: X = Br; 50%
2.13: X = I; 52%

Scheme 2.3 Synthesis of [NHC*$_2$Au]X complexes **2.10**-**2.13**.

The CH_2 moiety of the NHC ligand is a convenient spectroscopic handle to monitor the conjugation of new ligands. The monocarbene complexes **1.21**, **2.5** and **2.6** all show a characteristic CH_2 peak at δ = 5.44 ppm in their respective ^{1}H-NMR spectra (**Figure 2.3**). The CH_2 peaks appear at δ = 5.23, 5.39 and 5.43 ppm for the imidazolium salts **2.7**, **2.8** and **2.9**, whereas upon coordination to the gold the CH_2 peaks shift to δ = 5.19, 5.21 and 5.22 ppm for biscarbenes **2.10**, **2.11** and **2.13**, respectively (**Figure 2.4**).

Monitoring the region of δ = 5-6 ppm using ^{1}H-NMR spectroscopy during the reaction enabled full conversion of these complexes to be achieved. The inserted ^{1}H-NMR spectra in **Figure 2.4** was taken before reaction completion and shows two CH_2 peaks at δ = 5.44 and 5.22 which correspond to the formation of the NHC*-Au-X species and the $[NHC^*_2Au]^+$ species. This suggests that the monocarbene is made first which undergoes a homoleptic rearrangement to form the biscarbene complex.

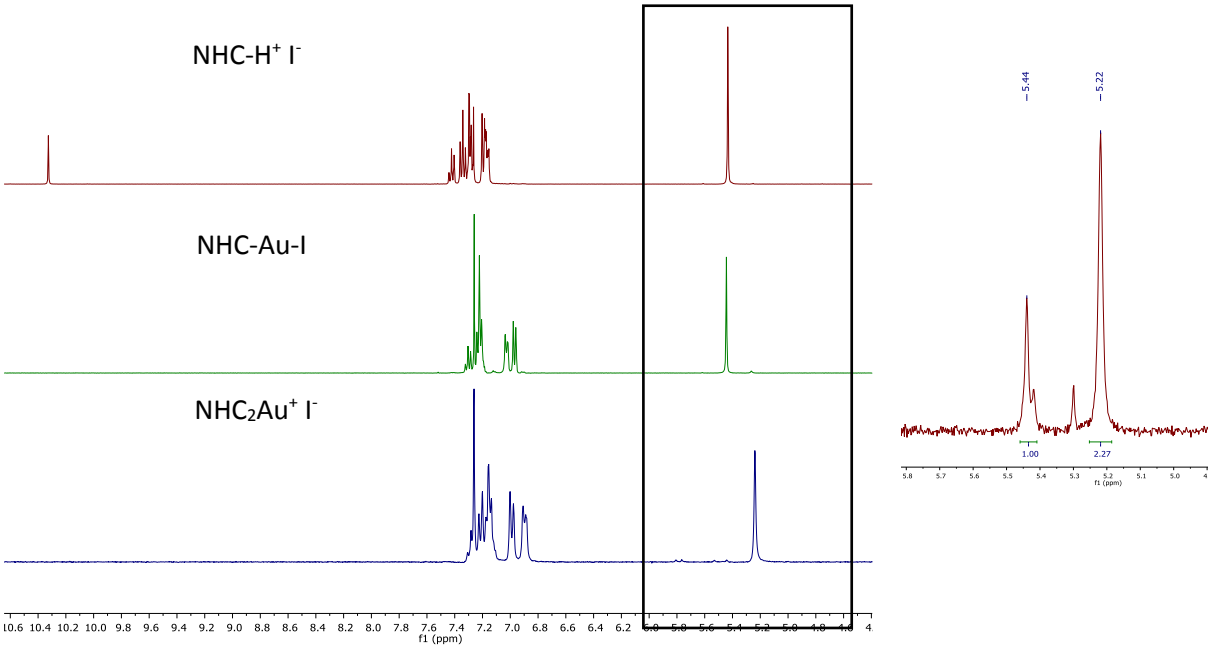

Figure 2.4 Stacked ^{1}H-NMR spectra of **2.9**, **2.6** and **2.13** displaying the imidazolium proton in **2.9** and the CH_2 shift from δ = 5.43 (**2.9**) to 5.44 (**2.6**) and 5.22 (**2.13**) ppm. The inserted ^{1}H-NMR spectra of half made **2.13** shows two CH_2 peaks at δ = 5.44 and 5.22 ppm.

In addition, the imidazolium salts **2.7**, **2.8** and **2.9** have a distinctive imidazolium proton peak at δ = 8.56, 9.94 and 10.33 ppm. The disappearance of this C^2 imidazolium proton from each ^{1}H-NMR spectra further indicated coordination to the gold.[9] ^{19}F-NMR and ^{31}P-NMR spectroscopy confirmed the presence of the anion in both the imidazolium and the conjugated biscarbene complexes.

2.2.3 Synthesis of NHC*-Gold(I)-Phosphine Complexes

Mixed NHC*-gold(I)-phosphine complexes **2.14** and **2.15** were synthesised following an established method (**Scheme 2.4**).[16] Complex **1.21** was reacted with triphenylphosphine and either $NaPF_6$ or $NaBF_4$. The short reaction time enabled the formation of complexes **2.14** and **2.15** which were isolated via recrystallisation. Ligand scrambling was observed, particularly with longer reaction times, and degradation to $[NHC^*_2Au]^+$ and PPh_3-Au-Cl was noted. This is unsurprising as PPh_3 is more labile than the NHC ligand, thus the rearrangement to the biscarbene $[NHC^*_2Au]^+$ complex was favourable.[11]

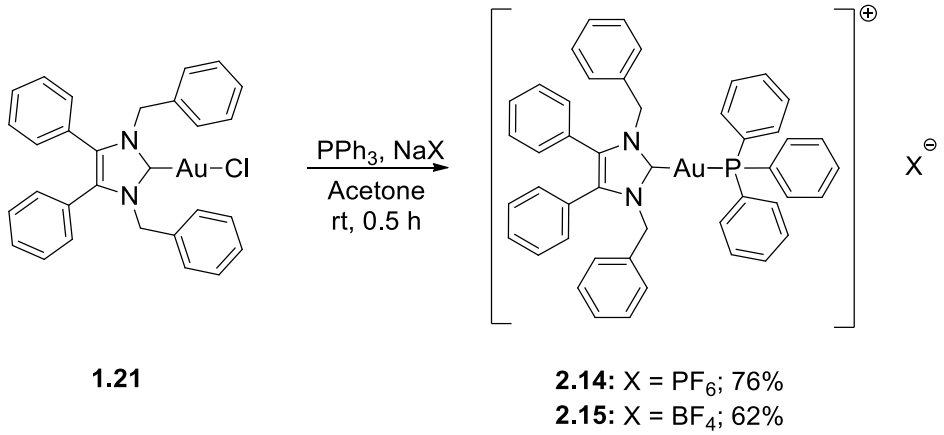

Scheme 2.4 Synthesis of [NHC*-Au-PPh_3]X complexes **2.14** and **2.15**.

^{1}H-NMR spectroscopy confirmed conjugation of the triphenylphosphine ligand as additional peaks were reported in the aromatic region. The appearance of a new peak in the ^{31}P-NMR spectra further confirmed the presence of the triphenylphosphine ligand.[17] The ^{19}F-NMR spectra of **2.14** and **2.15** remained the same as biscarbenes **2.10** and **2.11** despite the change of ligand.

The coordination of 1,3,5-triaza-7-phosphaadamantane (PTA) to the NHC*-gold(I) complex was attempted. The above method afforded the $[NHC^*\text{-Au-PTA}]^+$ complexes in mixtures with the biscarbene complexes. The formation of the desired $[NHC^*\text{-Au-PTA}]^+$ complex was confirmed through ESI^+ mass spectrometry as the $[M]^+$ peak for $C_{35}H_{36}N_5PAu$ was detected at 754.6 *m*/z. It was apparent these complexes were not very stable as in solution they readily underwent homoleptic rearrangement forming the biscarbene complexes. As a result these complexes were not isolated and characterised.

2.3 Structural Discussion

The molecular structures of **2.9**-**2.12**, **2.14** and **2.15** were determined by single crystal X-ray diffraction, with selected bond lengths and angles displayed in **Tables 2.1** and **2.2**. The X-ray crystal data and structure refinement are found in **Tables 2.3**-**2.5**.

Complexes **2.7** and **2.8** crystallised in the monoclinic space group $P2_1/c$ (#14) with one molecule of the complex and one solvate CH_2Cl_2 molecule contained in the independent unit (**Figure 2.5**). Complex **2.9** crystallised in the triclinic space group $P\bar{1}$ (#2) with one molecule of the complex and one solvate C_2H_5OH molecule contained in the independent unit (**Figure 2.5**). Compounds **2.5** and **2.6** crystallised in the triclinic space group $P\bar{1}$ (#2) with one molecule of the complex and one solvate CH_2Cl_2 molecule contained in the independent unit. Compound **2.10** crystallised in the monoclinic space group $P2_1/c$ (#14) in the absence of solvate molecules. Compounds **2.11, 2.12**, **2.14** and **2.15** were crystallised in the triclinic space group $P\bar{1}$ (#2) in the absence of solvate molecules. Crystals of **2.9**-**2.11** and **2.15** were obtained from the slow evaporation of a hot saturated ethanol solution at room temperature. Crystals of **2.5**-**2.8** and **2.14** were grown by the slow infusion of pentane into a saturated CH_2Cl_2 solution at -18 °C.

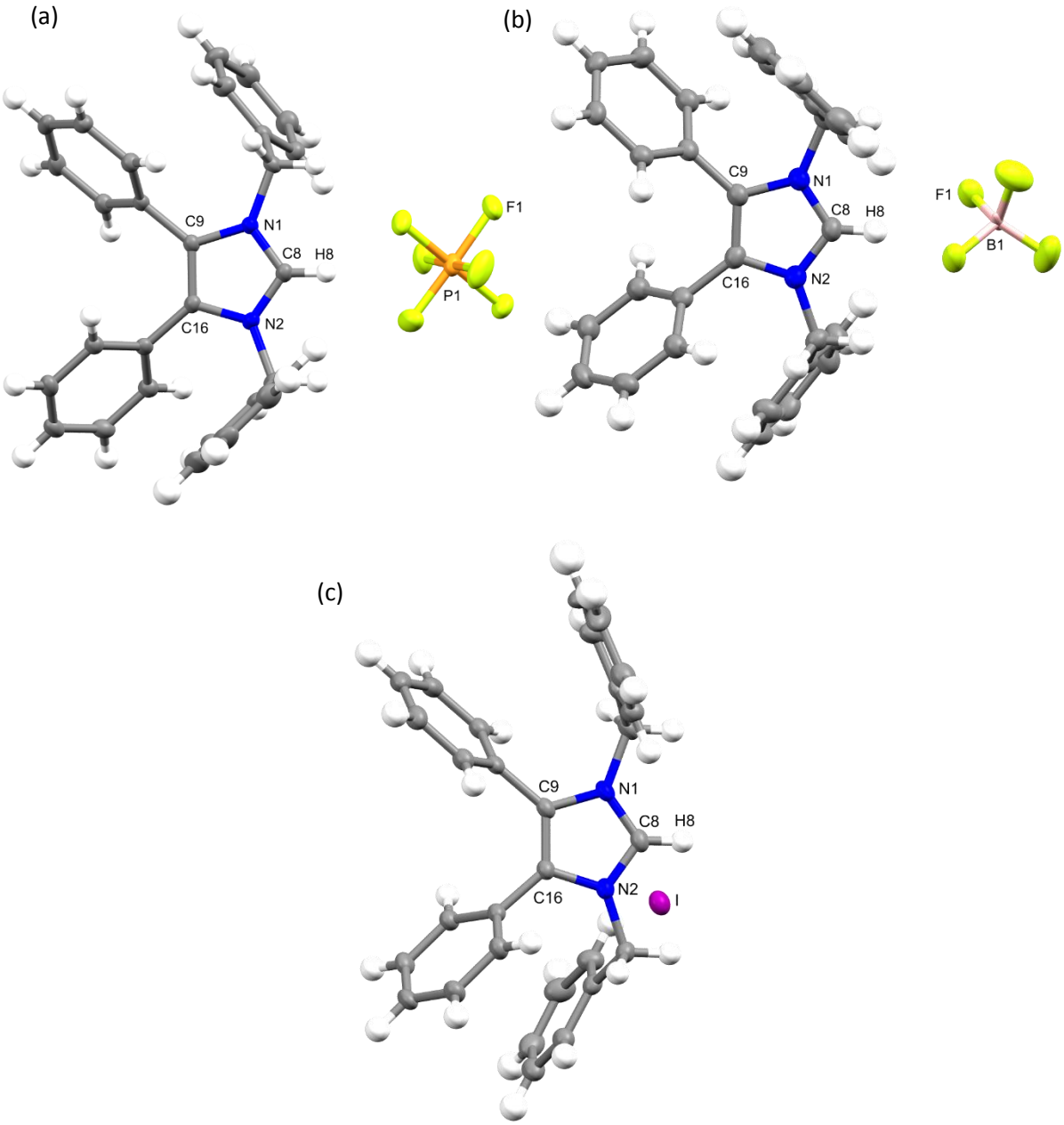

Figure 2.5 X-ray diffraction structure of imidazolium salts (a) **2.7,** (b) **2.8** and (c) **2.9**; thermal ellipsoids are drawn on the 50% probability level. Solvent molecules have been omitted for clarity.

In the case of imidazolium salts **2.7** and **2.8**, the anions PF_6^- and BF_4^- are positioned opposite the imidazolium proton. Short H···F contacts of 2.458 Å and 2.273 Å were measured between the imidazolium hydrogen atom and the fluorine atoms of **2.7** and **2.8**, respectively.[18] However, the anion I^- is positioned off-centre in complex **2.9**, to accommodate the solvate C_2H_5OH molecule present in the crystal lattice. As shown in **Figure 2.6** it appears that the ethanol

molecule is adjacent to the imidazolium proton, with contact between the imidazolium hydrogen atom and the oxygen atom of the ethanol (H···O 2.343 Å). The I^- anion presented contacts with both the hydrogen atom of the ethanol (H···I 2.6543 Å) and the hydrogen atom of the CH_2 group of the NHC ligand (H···I 3.0647 Å).

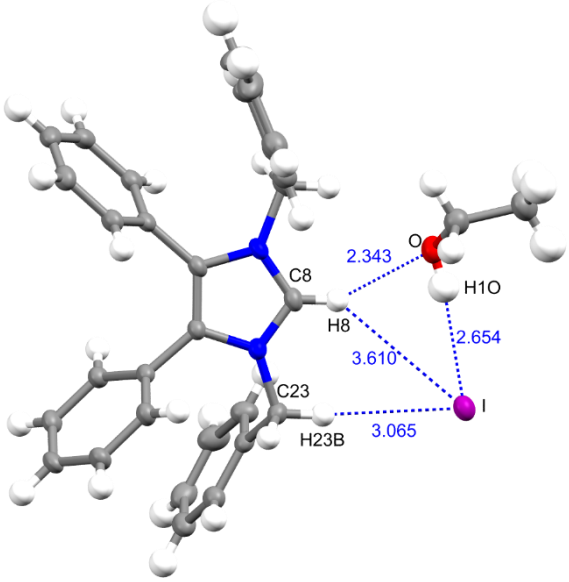

Figure 2.6 X-ray diffraction structure of NHC-H^+ I^- (**2.9**) and C_2H_5OH, with measured intermolecular distances marked in blue.

Table 2.1 Selected bond lengths (Å) of imidazolium salts **2.7**, **2.8** and **2.9**.

	N(1)-C(8)	**N(2)-C(8)**	**C(9)-N(1)**	**C(16)-N(2)**	**C(9)-C(16)**
2.7	1.329(19)	1.325(2)	1.393(18)	1.392(18)	1.369(2)
2.8	1.320(4)	1.322(4)	1.396(4)	1.393(4)	1.368(4)
2.9	1.331(2)	1.326(2)	1.391(2)	1.393(2)	1.361(3)

Considering the bonding in the imidazolium structures of **2.7**, **2.8** and **2.9**, it was noted that the N-C bonds are all shorter than single bonds (1.47 Å) and correspond to the range accepted for aromatic bonds (1.34 Å).[19] The observed shorter carbene C-N bond can be explained by the π-donation of the nitrogen into the carbene carbon. Additionally, the C-C bond in the backbone of the imidazole is indicative of a double bond. In fact, the C-C bonds of 1.361(3)-1.369(2) Å are

in between the values commonly accepted as an aromatic bond and a double bond. The complexes do not exhibit significant variations despite the choice of anion.

Upon coordination to gold the C-N bonds at the carbene elongated slightly from ~1.32 Å to ~1.35 Å, hence exhibiting more single-bond character (**Table 2.2**). The auxiliary C-N and C-C backbone bond lengths remained the same as those present in the imidazolium precursors. These structural changes are contributed to the increased electron density donation from the carbene to the gold(I) centre.[18]

Table 2.2 Selected bond lengths (Å) and angles (°) of the NHC*-gold(I) complexes.

	N(1)-C(8)	N(2)-C(8)	C(8)-Au	Au-X	C(8)-Au-X
2.5[a]	1.350(3)	1.349(3)	2.000(3)	2.404(3)	177.38(8)
2.6[b]	1.352(2)	1.353(2)	2.005(18)	2.555(15)	174.66(5)
2.10[c]	1.347(3)	1.344(3)	2.022(2)	2.021(2)	176.14(8)
2.11[c]	1.338(4)	1.353(3)	2.022(3)	2.019(3)	173.92(10)
2.12[c]	1.352(5)	1.344(5)	2.026(4)	2.026(4)	172.79(15)
2.14[d]	1.345(3)	1.346(3)	2.038(2)	2.280(5)	177.84(6)
2.15[d]	1.342(3)	1.355(3)	2.035(2)	2.283(6)	179.40(6)

[a] X= Br. [b] X= I. [c] X= C(37). [d] X= P(1).

All complexes exhibited similar Au-C bond lengths (2.000(3)-2.038(2) Å), within the expected range for these NHC-gold(I) complexes. All complexes exhibited a distorted linear geometry at the gold(I) centre, with the C(8)-Au-X bond angle in the range of 173.92(10)-179.40(6) °. First considering the halide derivatives, **2.5** and **2.6**, the Au-X bond lengths increased as the halide descended the periodic table due to the trans effect. The Au-I bond was the longest, which directly reflects the strong trans effect of the carbene onto the weaker halide bond. This trend is maintained with the chloro derivative **1.21** which reported a Au-Cl bond length of 2.3013(6) Å.[20] Biscarbenes **2.10** and **2.11** have almost identical Au-C bond lengths to both carbenes. Lastly, compounds **2.14** and **2.15** displayed Au-P bond lengths similar to those seen previously in other phosphine-gold(I) complexes.[21,22] The strong trans effect of the carbene is shown throughout the complexes which results in the following trend in bond lengths: carbene< phosphine< bromide< iodide.

The solid state structures of halides **2.5** and **2.6** showed columns of molecules in a head-to-tail fashion. This orientation allows for intermolecular Au···Au contacts of 3.5850(3) Å and 3.5449(3) Å, respectively. This distance is characteristic of a very weak aurophilic interaction, at the limit of the accepted range (2.50-3.50 Å)[23]. The two molecules featuring an aurophilic interaction are further distanced (~6 Å) from the next neighbouring molecule.

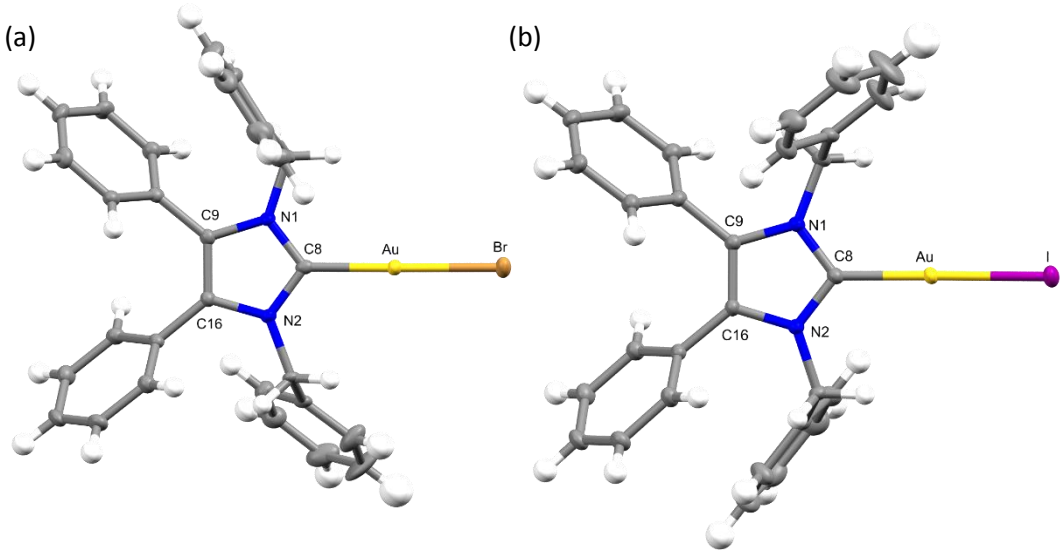

Figure 2.7 X-ray diffraction structure of (a) **2.5** and (b) **2.6**; thermal ellipsoids are drawn on the 50% probability level. Solvate molecules have been omitted for clarity.

Cationic complexes **2.10, 2.11, 2.14** and **2.15** do not display aurophilic bonding, however they feature interesting arrays with their corresponding anions. The solid state structures of **2.10** and **2.11** showed the PF_6^- and BF_4^- counterions positioned on the opposite side of the complex to the phenyl rings, i.e. the phenyl rings are directed away from the anion. In the case of biscarbene **2.10** this happens in pairs of molecules where the two sets of phenyl rings face each other resulting in a larger distance of 8.0913(4) Å between two gold(I) centres. Additionally, the carbene backbones are positioned almost perpendicularly to each other (**Figure 2.8**). This may be to accommodate the large counterion PF_6^-. Short H···F contacts of 2.405 and 2.474 Å were measured between the PF_6^- fluorine atoms and the hydrogen atoms of both CH_2 moieties on the NHC ligand. The distance between the gold atom and the closest fluorine atom is 3.457(2) Å.

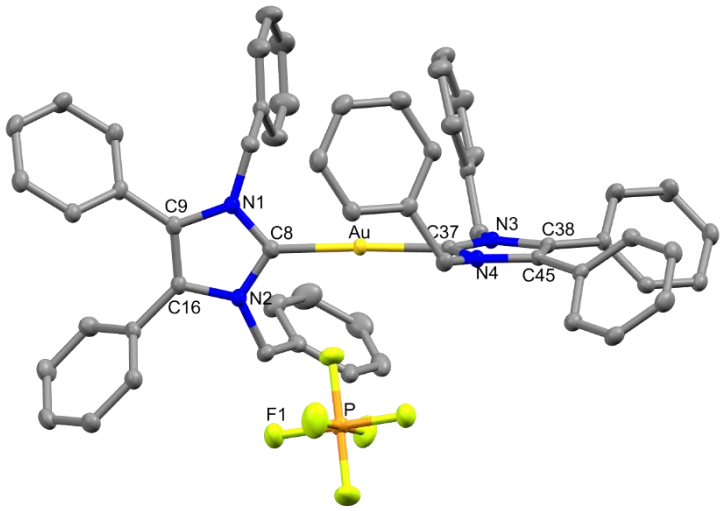

Figure 2.8 X-ray diffraction structure of **2.10**; thermal ellipsoids are drawn on the 50% probability level. Hydrogen atoms have been omitted for clarity.

Conversely, complex **2.11** presented both carbene backbones in the same plane. This allows for two BF_4^- anions to be present between two of the biscarbenes, as shown in **Figure 2.9b**. As observed in complex **2.10**, the phenyl rings are oriented away from the anion resulting in an overlap with neighbouring NHC phenyl rings. The gold atom is now positioned between the two anions with similar distances to both (Au···F 3.721(2) Å and 3.667(2) Å). Intermolecular interactions between the BF_4^- anion and both CH_2 moieties of the NHC ligand were noted with H···F distances of 2.550 and 2.559 Å.

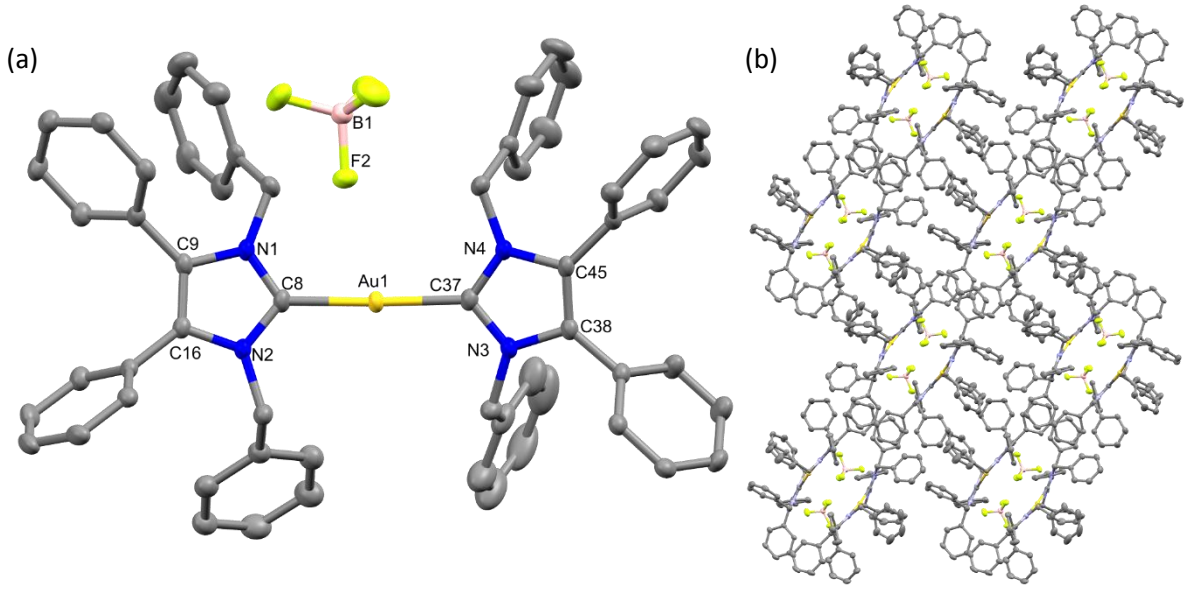

Figure 2.9 (a) X-ray diffraction structure of **2.11**; thermal ellipsoids are drawn on the 50% probability level. Hydrogen atoms have been omitted for clarity. (b) Crystal packing of **2.11** along *a*-axis.

X-ray diffraction of a **2.12** crystal revealed a mixture of 3[(NHC*$_2$Au)(AgBr$_2$)] and (NHC*$_2$Au)Br (**Figure 2.10**). The minor component was the desired **2.12**, whereas the major component of the lattice was the biscarbene with the $AgBr_2^-$ anion, due to the residual silver bromide formed as a by-product in the synthesis of these biscarbene complexes. The crystal data and structure refinement of **2.12** can be found in **Table S1** in the Appendix. Both the silver and bromide atoms are distanced 3.0219(3) Å from the gold centre. The $AgBr_2^-$ anion displayed bond lengths of 2.4366(6) and 2.4578(7) Å and a Br-Ag-Br angle of 156.16(3) °.

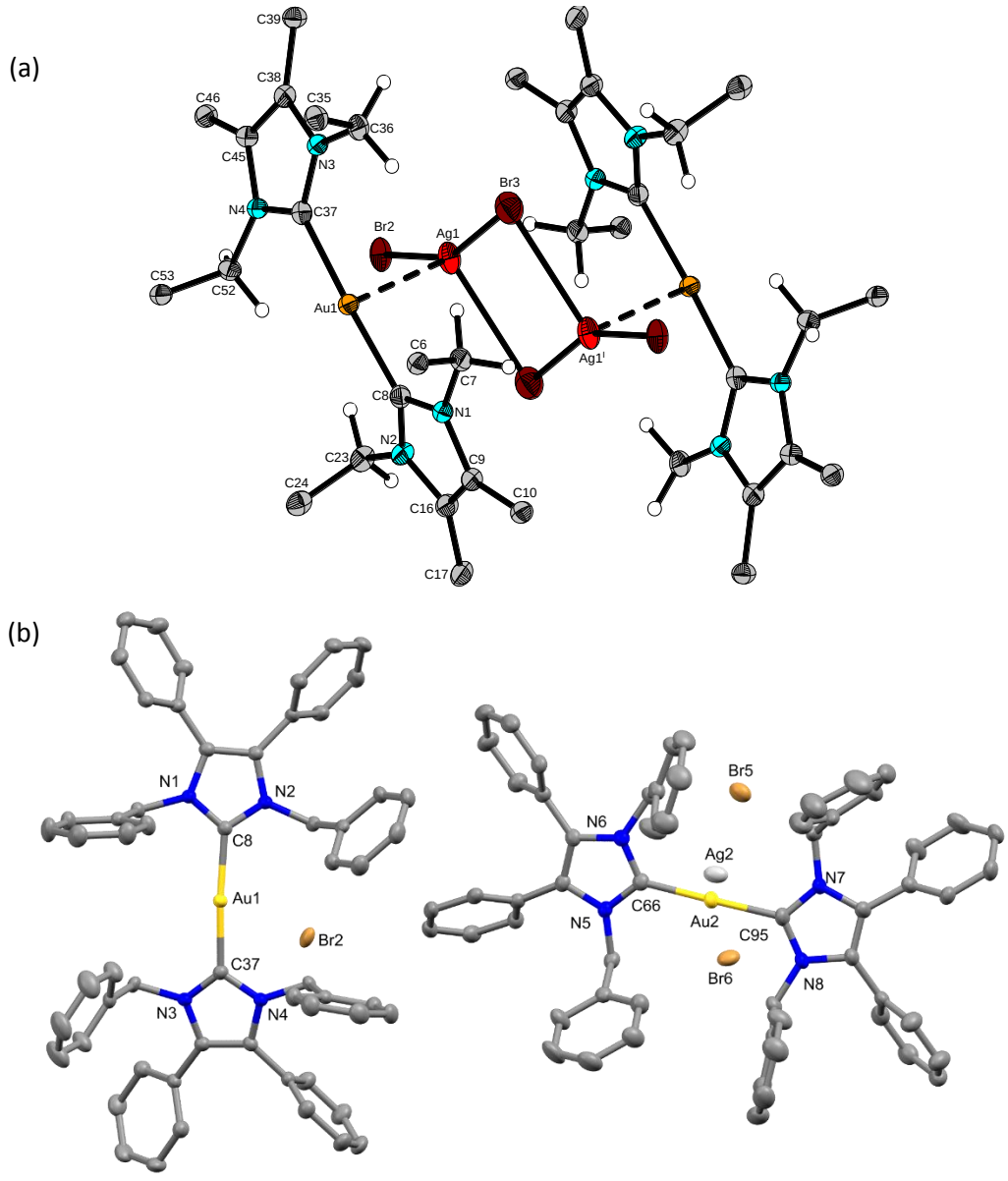

Figure 2.10 X-ray diffraction structure of **2.12**; thermal ellipsoids are drawn on the 50% probability level. a) The major component (NHC*$_2$Au)AgBr$_2$, with phenyl groups represented by their *ipso* carbons only. Structures are generally drawn on Mercury, however to present the Au···Ag interaction to the AgBr$_2$ anion this was drawn on Olex2. b) The minor component (NHC*$_2$Au)Br and the major component (NHC*$_2$Au)AgBr$_2$ are drawn on Mercury with the hydrogen atoms omitted for clarity.

The solid state structures of the NHC*-Au-PPh_3 complexes **2.14** and **2.15** (**Figure 2.11**) feature molecules in a staggered head-to-tail manner, where the PPh_3 moiety neighbours another PPh_3 and the NHC neighbours another NHC. As seen with the biscarbene complexes, there are interactions between the fluorine atoms of the anions and the CH_2 hydrogen atoms of the NHC ligand (H···F: **2.14**, 2.452 Å; **2.15**, 2.529 and 2.610 Å). Additionally, contacts of ~2.5 Å were noted between the fluorine atoms and the hydrogen atoms of the phenyl rings of both the NHC and the PPh_3 ligand. The distances between the gold atom and the closest fluorine atoms are 3.646(2) and 4.179(2) Å for **2.14** and **2.15**, respectively.

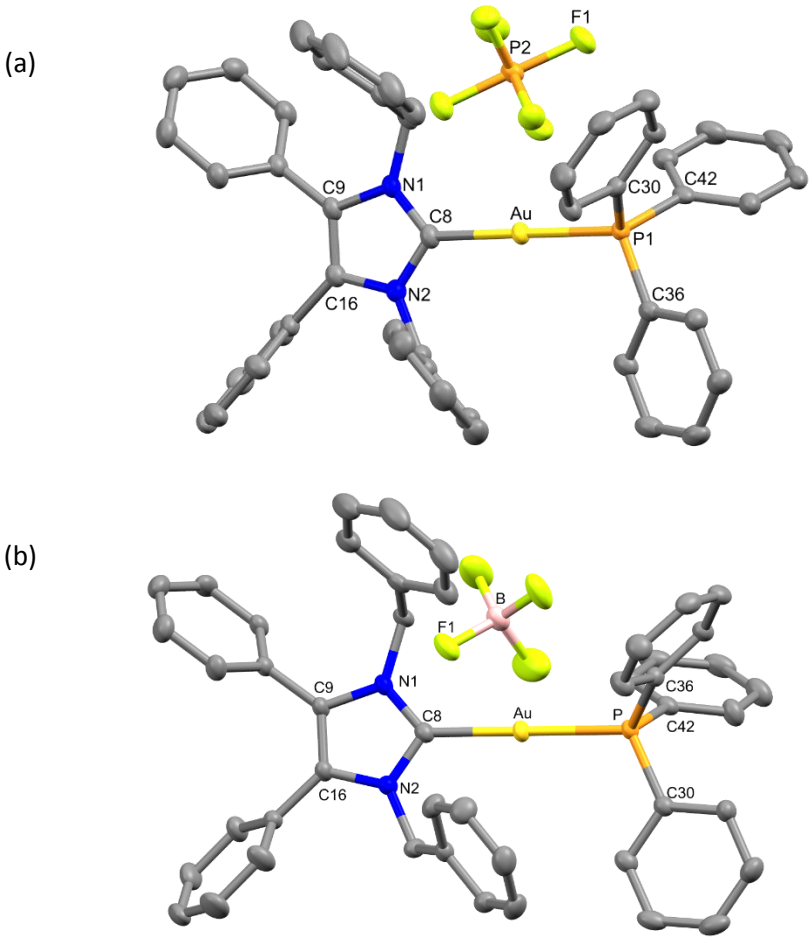

Figure 2.11 X-ray diffraction structure of (a) **2.14** and (b) **2.15**; thermal ellipsoids are drawn on the 50% probability level. Hydrogen atoms have been omitted for clarity.

Table 2.3 Crystal data and structure refinement for complexes **2.7**, **2.8** and **2.9**.

	2.7	**2.8**	**2.9**
Empirical Formula	$C_{30}H_{27}N_2F_6PCl_2$	$C_{30}H_{27}BN_2F_4Cl_2$	$C_{31}H_{31}N_2OI$
Formula Weight ($g \cdot mol^{-1}$)	631.40	573.24	574.48
Temperature (K)	100(2)	100(2)	100(2)
Crystal system	Monoclinic	Monoclinic	Triclinic
Space group	P21/c (#14)	P21/c (#14)	$P\bar{1}$ (#2)
Unit cell dimensions			
a (Å)	27.2461(2)	26.9824(8)	9.5674(2)
b (Å)	9.29252(5)	8.9655(2)	11.1445(1)
c (Å)	25.0932(2)	25.2783(7)	14.2490(2)
α (°)	90	90	74.338(1)
β (°)	113.1558(7)	114.445(4)	70.584(2)
γ (°)	90	90	77.557(1)
Volume ($Å^3$)	5841.40(8)	5566.9(3)	1366.39(4)
Z	8	8	2
Density (calcd) (mg/m^3)	1.436	1.368	1.396
Absorption coefficient (mm^{-1})	3.069	2.526	9.391
F (000)	2592	2368	584
Crystal size (mm^3)	0.309 x 0.134 x 0.053	0.175 x 0.044 x 0.031	0.277 x 0.157 x 0.110
θ (°)	3.529 to 76.827	3.503 to 62.423	3.368 to 76.944
Index ranges	$-32 \le h \le 34$	$-28 \le h \le 31$	$-12 \le h \le 12$
	$-11 \le k \le 11$	$-9 \le k \le 10$	$-13 \le k \le 12$
	$-31 \le l \le 31$	$-29 \le l \le 29$	$-17 \le l \le 17$
Reflections collected	78264	27221	30823
Independent reflections R_{int}	12283 (0.0349)	8869 (0.0686)	5712 (0.0375)
Completeness to θ_{max} (%)	100.0	99.9	100.0
Absorption correction	Gaussian	Gaussian	Gaussian
Max and min transmission	0.861 and 0.547	0.936 and 0.795	0.687 and 0.450
Refinement method	Full–matrix Least–squares on F^2	Full–matrix Least–squares on F^2	Full–matrix Least–squares on F^2
Data/ restraints/ parameters	12283 / 1 / 754 [a]	8869 / 0 / 703	5712 / 0 / 318
Goodness-of-fit on F2	1.051	1.011	1.059
Final R indices [$I > 2\sigma(I)$]	R1 = 0.0382	R1 = 0.0519	R1 = 0.0236
	wR2 = 0.0958	wR2 = 0.1245	wR2 = 0.0624
R indices (all data)	R1 = 0.0435	R1 = 0.0751	R1 = 0.0243
	wR2 = 0.1003	wR2 = 0.1404	wR2 = 0.0628
Largest diff. peak and hole	1.012 and –0.829	0.583 and –0.348	0.533 and –0.732

[a] The sum of the three disorder parts was restrained to be 1 using SUMP.

Table 2.4 Crystal data and structure refinement for complexes **2.5** and **2.6**.

	2.5	**2.6**
Empirical Formula	C_{30} H_{26} N_2 Cl_2 Br Au	C_{30} H_{26} N_2 Cl_2 I Au
Formula Weight ($g \cdot mol^{-1}$)	762.30	809.29
Temperature (K)	100(2)	100(2)
Crystal system	Triclinic	Triclinic
Space group	$P\bar{1}$ (#2)	$P\bar{1}$ (#2)
Unit cell dimensions		
a (Å)	8.9019(2)	9.0569(2)
b (Å)	13.1121(3)	13.0587(2)
c (Å)	13.7953(3)	14.0021(3)
α (°)	112.593(2)	112.936(2)
β (°)	102.638(2)	102.247(2)
γ (°)	101.910(2)	102.555(2)
Volume ($Å^3$)	1373.18(6)	1405.14(5)
Z	2	2
Density (calcd) (mg/m^3)	1.844	1.913
Absorption coefficient (mm^{-1})	7.028	6.545
F (000)	736	772
Crystal size (mm^3)	0.263 x 0.151 x 0.093	0.256 x 0.161 x 0.062
θ (°)	2.956 to 30.508	2.989 to 32.858
Index ranges	$-12 \le h \le 12$	$-13 \le h \le 13$
	$-18 \le k \le 18$	$-19 \le k \le 19$
	$-19 \le l \le 19$	$-21 \le l \le 20$
Reflections collected	29326	44345
Independent reflections R_{int}	8375 (0.0421)	9743 (0.0278)
Completeness to θ_{max} (%)	99.8	99.8
Absorption correction	Gaussian	Gaussian
Max and min transmission	0.618 and 0.316	0.716 and 0.318
Refinement method	Full–matrix Least–squares on F^2	Full–matrix Least–squares on F^2
Data/ restraints/ parameters	8375 / 0 / 325	9743 / 0 / 325
Goodness-of-fit on F2	1.040	1.063
Final R indices [$I > 2\sigma(I)$]	R1 = 0.0258	R1 = 0.0189
	wR2 = 0.0524	wR2 = 0.0449
R indices (all data)	R1 = 0.0321	R1 = 0.0203
	wR2 = 0.0550	wR2 = 0.0458
Largest diff. peak and hole	1.307 and –0.759	1.132 and –0.699

Table 2.5 Crystal data and structure refinement for complexes **2.10**, **2.11**, **2.14** and **2.15**.

	2.10	**2.11**	**2.14**	**2.15**
Empirical Formula	$C_{58}H_{48}N_4F_6PAu$	$C_{58}H_{48}BF_4N_4Au$	$C_{47}H_{39}N_2F_6P_2Au$	$C_{47}H_{39}BN_2F_4PAu$
Formula Weight ($g \cdot mol^{-1}$)	1142.94	1084.78	1004.71	946.55
Temperature (K)	100(2)	100(2)	100(2)	100(2)
Crystal system	Monoclinic	Triclinic	Triclinic	Triclinic
Space group	$P2_1/c$ (#14)	$P\bar{1}$ (#2)	$P\bar{1}$ (#2)	$P\bar{1}$ (#2)
Unit cell dimensions				
a (Å)	16.9459(1)	14.5025(1)	11.73747(8)	11.1534(2)
b (Å)	19.0314(1)	15.1574(1)	13.92645(7)	13.8188(2)
c (Å)	15.31484(8)	22.0115(2)	14.41601(7)	14.7889(2)
α (°)	90	90.4807(6)	80.3519(4)	81.470(1)
β (°)	93.7614(5)	91.3160(6)	66.5068(5)	68.978(2)
γ (°)	90	91.5461(5)	69.5446(5)	69.069(2)
Volume ($Å^3$)	4928.46(5)	4835.34(6)	2023.76(2)	1986.72(6)
Z	4	4	2	2
Density (calcd) (mg/m^3)	1.540	1.490	1.649	1.582
Absorption coefficient (mm^{-1})	6.469	6.194	8.128	3.798
F (000)	2288	2176	996	940
Crystal size (mm^3)	0.261 x 0.061 x 0.043	0.129 x 0.101 x 0.078	0.280 x 0.181 x 0.094	0.401 x 0.293 x 0.278
θ (°)	3.496 to 77.108	3.527 to 76.829	3.345 to 76.837	2.990 to 32.745
Index ranges	$-21 \le h \le 21$ $-23 \le k \le 23$ $-14 \le l \le 19$	$-18 \le h \le 18$ $-18 \le k \le 19$ $-27 \le l \le 27$	$-12 \le h \le 14$ $-17 \le k \le 17$ $-18 \le l \le 18$	$-16 \le h \le 16$ $-20 \le k \le 20$ $-21 \le l \le 22$
Reflections collected	100377	131179	78827	46327
Independent reflections R_{int}	10384 (0.0504)	20239 (0.0405)	8487 (0.0318)	13629 (0.0444)
Completeness to θ_{max} (%)	100.0	100.0	100.0	99.8
Absorption correction	Gaussian	Gaussian	Gaussian	Gaussian
Max and min transmission	0.793 and 0.388	0.709 and 0.568	0.539 and 0.245	0.457 and 0.380
Refinement method	Full–matrix Least–squares on F^2	Full–matrix Least–squares on F^2	Full–matrix Least–squares on F^2	Full–matrix Least–squares on F^2
Data/ restraints/ parameters	10384 / 0 / 631	20239 / 0 / 1225	8487 / 0 / 524	13629 / 0 / 505
Goodness-of-fit on F2	1.037	1.051	1.081	1.053
Final R indices [$I > 2\sigma(I)$]	R1 = 0.0222 wR2 = 0.0546	R1 = 0.0254 wR2 = 0.0555	R1 = 0.0192 wR2 = 0.0491	R1 = 0.0312 wR2 = 0.0683
R indices (all data)	R1 = 0.0273 wR2 = 0.0581	R1 = 0.0322 wR2 = 0.0585	R1 = 0.0197 wR2 = 0.0492	R1 = 0.0359 wR2 = 0.0709
Largest diff. peak and hole	0.693 and –1.292	0.915 and –1.276	1.202 and –0.714	3.089 and –0.932

2.4 Biological Evaluation

The *in vitro* biological evaluation of the compounds synthesised in this chapter was carried out by Prof. Rainer Schobert and Sofia Bär in the University of Bayreuth, Germany. The anticancer activity of the gold(I) compounds **2.5, 2.6, 2.10, 2.11, 2.14** and **2.15** were tested via MTT-based proliferation assays against the human colon carcinoma cell line HCT-116^{wt} and the multidrug-resistant (*mdr*) human breast carcinoma cell line MCF-7^{topo} (**Table 2.6**). The activity of these complexes has been compared to two well-known drugs cisplatin and auranofin and NHC*-gold(I) chloride (**1.21**) as an internal comparison.[24]

Table 2.6 IC_{50} values (μM) of compounds **2.5**, **2.6**, **2.10**, **2.11**, **2.14** and **2.15** against HCT-116^{wt} and MCF-7^{topo} cells after 72 h of incubation.

	HCT-116^{wt}	**MCF-7^{topo}**
Cisplatin[a]	5.42 ± 0.12	18.21 ± 0.10
Auranofin[a]	3.78 ± 0.10	2.89 ± 0.05
1.21	22.7 ± 1.2	20.8 ± 1.9
2.5	16.7 ± 2.5	12.8 ± 2.4
2.6	0.64 ± 0.01	1.1 ± 0.2
2.10	0.41 ± 0.01	0.7 ± 0.1
2.11	0.29 ± 0.01	0.80 ± 0.04
2.14	1.3 ± 0.1	1.5 ± 0.2
2.15	2.3 ± 0.2	2.4 ± 0.2

[a] Cisplatin and auranofin IC_{50} values against HCT-116 and MCF-7 cell lines have been included for comparative purposes.[24]

All complexes tested displayed excellent cytotoxicity with low micromolar activity, with the exception of complex **2.5**. Excluding **2.5**, all complexes were more active against the colon carcinoma cell line HCT-116^{wt} than the breast cancer cell line. Complexes **2.6, 2.10, 2.11, 2.14** and **2.15** were found to be more active than cisplatin and auranofin on both cell lines.

Considering the series of halides, **2.5** exhibited similar activity to the chloride analogue **1.21**, while **2.6** was significantly more active than both compounds. Compound **2.6** reached sub-micromolar activity on the colon cancer cell line HCT-116^{wt} with an IC_{50} value of 0.64 ± 0.01

μM. Biscarbenes **2.10** and **2.11** exhibited similar IC_{50} values, both having sub-micromolar activity against both cell lines. Comparing these two biscarbene complexes to the phosphine derivatives **2.14** and **2.15**, it is evident that the presence of a second NHC ligand contributes to a more active complex than the addition of a phosphine ligand. This supports the argument that NHCs are a superior ligand than phosphines. Interestingly, the choice of counterion did not impact the activity of complexes **2.10**-**2.11** or **2.14**-**2.15**.

Moreover, biscarbenes **2.10** and **2.11** can be compared to the monocarbene complexes **1.21**, **2.5** and **2.6**. These NHC-Au-X type complexes will dissociate under physiological conditions into $[NHC\text{-}Au]^+$. Hence, it is useful to compare these monocarbenes and biscarbenes to assess the importance of a second carbene ligand. It was noted that although the NHC*-Au-I complex was very active, the monocarbenes in general had significantly lower cytotoxicity than the biscarbenes.

It is worth noting that the trend seen with the bond lengths (carbene< phosphine< bromide< iodide) also represents the trend in cytotoxicity, with the exception of the highly active iodido complex. Hence, the biscarbene complexes with the shortest Au-X bond lengths displayed the highest activity and the bromo derivative **2.5** exhibited the second longest Au-X bond and the lowest activity.

In summary, excellent cytotoxicity was found against both the colon carcinoma cell line HCT-116^{wt} and the breast carcinoma cell line MCF-7^{topo}. When compared to cisplatin and auranofin higher activity was observed for all the complexes, except the bromide derivative, against both cell lines. Gratifyingly, the iodide complex **2.6** and the biscarbene complexes **2.10** and **2.11** achieved sub-micromolar activity. Overall, **2.11** had the highest anticancer activity with an IC_{50} value of 0.29 ± 0.01 μM on the colon cancer cell line HCT-116^{wt}. These three complexes show high potential as chemotherapeutics.

2.5 Computational Analysis

The computational analysis presented in this chapter was carried out by Dr Goar Sánchez-Sans at the Irish Centre for High-End Computing (ICHEC), Dublin.

The enthalpy of formation has been obtained at the MN15/6-311++G(2df,p)/LANL2TZ(f) level for both NHC*-Au-Cl (**1.21**) and Ph_3P-Au-Cl compounds (**Figure 2.12**). The results showed that **1.21** presents a more negative enthalpy (−315.0 kJ/mol) than Ph_3P-Au-Cl (−274.3 kJ/mol), which indicated that the formation of **1.21** was more favourable. Natural bond orbital (NBO) analysis showed that the Au-Cl unit in **1.21** is slightly less negative ($-0.32e^-$) than in Ph_3P-Au-Cl ($-0.35e^-$), and displayed slightly shorter Au–Cl distances in **1.21** (2.291 Å) than in Ph_3P-AuCl (2.299 Å). This is indicative of a stronger bond between the gold and the carbene due to the higher σ-donating effect of the nucleophilic NHC* ligand.

Also, for **1.21**, two backbonding donations from the gold into the π* C–N antibonding orbitals are observed, E(2) = 15.9 and 16.1 kJ/mol; while in Ph_3P-Au-Cl, three backbonding donations are observed from the Au atom into the π* P–C antibonding orbitals with E(2) = 16.2, 16.0, and 14.9 kJ/mol. The additional backbonding in the Ph_3P-Au-Cl molecule reduces its bond strength, resulting in a weaker donating ligand. Conclusively, these results give credence to NHCs being a more favourable ligand than phosphines.

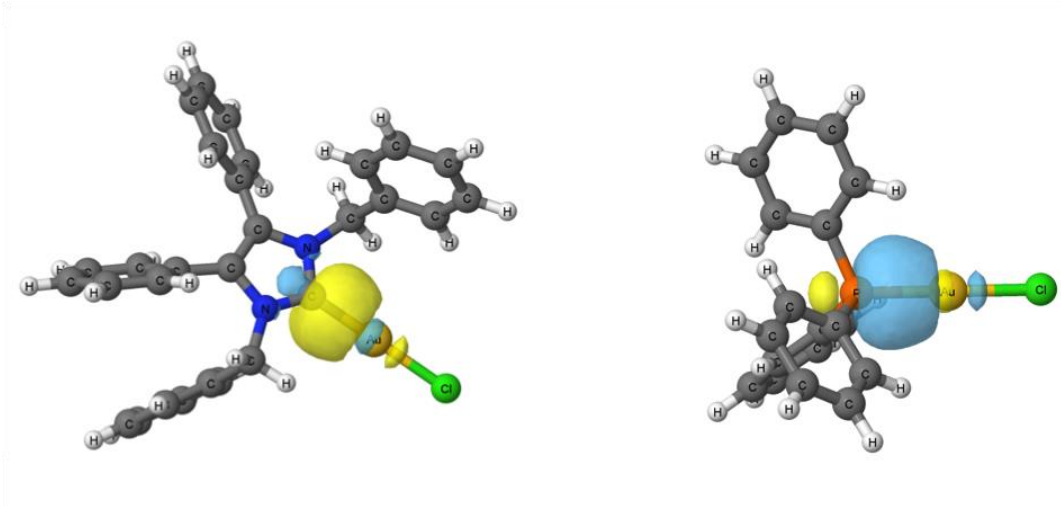

Figure 2.12 Molecular orbital corresponding to the σ-C–Au and σ-P–Au bonds of NHC*-Au-Cl (**1.21**) and Ph_3P-Au-Cl respectively.

2.6 Conclusion and Outlook

NHC*-gold(I) complexes were synthesised and tested for their antiproliferative properties in order to develop potential chemotherapeutics. Complexes of the type NHC-Au-L and [NHC-Au-L]$^+$ were synthesised with halide, carbene and phosphine ligands. All complexes (bar **2.13**) were characterised with X-ray crystallography. Weak aurophilic interactions were observed in complexes **2.5** and **2.6**, with Au···Au distances of 3.5850(3) and 3.5449(3) Å, respectively. A correlation was drawn between the bond length of the complexes and their respective cytotoxicity. The *in vitro* anticancer activities of these gold(I)-based complexes were tested against the human colon cancer cell line HCT-116^{wt} and the multidrug-resistant human breast cancer cell line MCF-7^{topo}. Good cytotoxicity was observed by all complexes tested. The iodide derivative **2.6** showed excellent cytotoxicity against both cell lines, reaching sub-micromolar activity against HCT-116^{wt}. Biscarbenes **2.10** and **2.11** presented sub-micromolar activity against both cell lines, with **2.11** reaching an IC_{50} value of 0.29 ± 0.01 μM on the colon cancer cell line HCT-116^{wt}. The highest cytotoxic response was found with the biscarbene complexes suggesting that not only are NHC ligands more favourable than phosphines but also that two NHC ligands render highly active complexes. Furthermore, calculated formation enthalpies of **1.21** and PPh_3-Au-Cl, supports this argument as the formation of **1.21** proved energetically more favourable. Additionally, natural bond orbital analysis of both compounds confirmed higher σ-donating properties with **1.21**.

The results in this Chapter are very promising. Thus, further biological studies for the most active complexes is essential to progress this project. A xenograft mouse model study would be ideal to properly assess their capabilities as anticancer agents *in vivo*. Additionally, a mechanistic study would allow us to investigate the cellular uptake of the cationic complexes in comparison to the neutral monocarbene complexes.

2.7 Experimental Section

2.7.1 General Experimental Conditions for all Chapters

All chemicals were purchased and used as received, unless otherwise stated. Solvents were dried according to the standard procedures, when necessary. ^{1}H, ^{13}C, ^{19}F and ^{31}P spectra were recorded on either a 300, 400 or 500 MHz Varian spectrometer at room temperature (rt). Chloroform ($CDCl_3$), dimethyl sulfoxide (DMSO) and water (D_2O) were used as deuterated solvents. The residual solvent peak or tetramethylsilane (TMS) were used as the internal standard. All chemical shifts are reported as δ values in parts per million (ppm). Infrared spectra were recorded on a Bruker ALPHA PLATINUM ATR spectrometer (Millerica, MA, USA). High resolution accurate mass data were obtained on either a Waters/Micromass LCT TOF spectrometer (Milford, MA, USA) or Agilent 6546 LC/Q-TOF spectrometer (Santa Clara, CA, USA) under electrospray ionisation technique. Melting points were measured on a Stuart™ (Stone, UK) melting point apparatus SMP10. Elemental analysis was conducted on an Exeter Analytical CE-440 elemental analyser (Coventy, UK). X-Ray crystallography data was collected on a Rigaku Oxford Diffraction (Chalgrove, Oxfordshire, UK) SuperNova A diffractometer. Absorbance measurements were done with a TECAN (Männedorf, Zurich, Switzerland) Infinite F200 plate reader.

Structure Determination

X-ray crystallography data was collected on a Rigaku Oxford Diffraction SuperNova A diffractometer by Dr Helge Müller-Bunz at University College Dublin, Ireland. A complete dataset was collected, assuming that the Friedel pairs are not equivalent. An analytical absorption correction based on the shape of the crystal was performed.[25] The structures were solved by direct methods using SHELXS and refined by full matrix least-squares on F2 for all data using SHELXL.[26] Hydrogen atoms were added at calculated positions and refined using a riding model. Their isotropic temperature factors were fixed to 1.2 times (1.5 times for methyl and OH groups) the equivalent isotropic displacement parameters of the parent atom. Anisotropic thermal displacement parameters were used for all non-hydrogen atoms. CCDC 2012886 (**2.5**), CCDC 2012885 (**2.6**), CCDC 2012887 (**2.10**), CCDC 2012888 (**2.11**), CCDC 2013114 (**2.14**) and CCDC 2013115 (**2.15**) contain the supplementary crystallographic data for this

Chapter, available free of charge from the Cambridge Crystallographic Data Centre via www.ccdc.cam.ac.uk/structures.

MTT-Based Proliferation Assay

MTT-based proliferation assays were carried out at the University of Bayreuth, Germany. The cytotoxic activity of all complexes were determined via MTT-based proliferation assays for the colon carcinoma cell line HCT-116^{wt} (DSMZ ACC-581) and the multidrug-resistant breast cancer cell line MCF-7^{topo} (DMSZ ACC-115). The cells, kept in Dulbecco's Modified Eagle Medium (1% Antibiotic-Antimycotic, 10% Fetal Bovine Serum), were seeded into the wells of a clear 96 well plate (5×10^4 cells/mL) and incubated for 24 h at standard cell culture conditions (37 °C, 5% CO_2, 95% humidity). Freshly made stock solutions (10 mM in DMF) of the gold complexes were diluted with sterile Milli-Q water. Any precipitation was treated with 4.44 µL/mL tween80 to produce soluble solutions of the complexes. Appropriate pre-diluted solutions and DMF (negative control), were added into the wells and further incubated for 72 h. The plates were centrifuged (300 g, 5 min, 4 °C) and the back medium was exchanged for a MTT solution (0.05% in PBS) and the cells were further incubated for 2 h. Thereupon, the MTT solution was again discarded, and the cells and violet water-insoluble formazan were dissolved in an SDS/DMSO solution (25 µL; 10% SDS, 0.6% AcOH). After another incubation time of 1 h at 37 °C, the absorbance of formazan at 570 nm and the background at 630 nm were measured. The absorbance of the wells treated with the solvent was set to 100% viable cells, and the percentage of viable cells in the wells treated with the gold complexes was calculated accordingly. IC_{50} values were determined using Graphpad Prism, means and SD were calculated from four independent experiments.

2.7.2 Synthesis

1,3-Dibenzyl-4,5-diphenylimidazolium bromide (1.7)

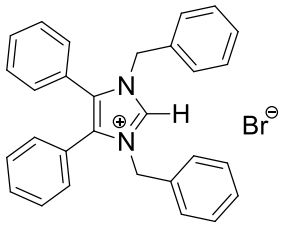

Using modified literature conditions,[12] 4,5-diphenyl-1-imidazole (4.41 g, 0.020 mol, 1.0 equiv.) and K_2CO_3 (4.15 g, 0.030 mol, 1.5 equiv.) were stirred in CH_3CN (30 mL) at rt for 15 mins. Benzyl bromide (5.23 mL, 0.044 mol, 2.2 equiv.) was added and the reaction stirred for 2 d at 35 °C. The reaction was filtered and the solvent reduced to approximately 5 mL. Et_2O (50 mL) was added to precipitate a solid. The product was filtered, washed with Et_2O (15 mL) and dried *in vacuo* to give a white solid (8.68 g, 90%). ^{1}H-NMR (400 MHz, $CDCl_3$, δ ppm): 11.22 (s, 1H, $CH_{imidazole}$), 7.41 (m, 2H, ArCH), 7.32 (m, 4H, ArCH), 7.27 (m, 3H, ArCH), 7.25 (m, 4H, ArCH), 7.11 (tt, *J* = 8.6, 1.6 Hz, 8H, ArCH), 5.51 (s, 4H, CH_2). ^{13}C-NMR (101 MHz, $CDCl_3$, δ ppm):. 137.9 (C), 133.7 (CH), 132.6 (C), 131.8 (CH), 130.9 (CH), 129.5 (CH), 129.4 (CH), 128.9 (CH), 125.1 (C), 51.9 (CH_2).

(1,3-Dibenzyl-4,5-diphenylimidazol-2-ylidene)gold(I) chloride (1.21)

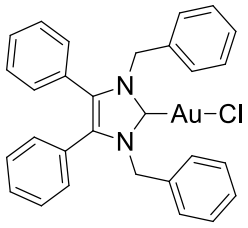

Using literature conditions,[13] imidazolium bromide **1.7** (0.96 mg, 2.00 mmol, 1.0 equiv.) and Ag_2O (0.26 g, 1.12 mmol, 0.55 equiv.) were stirred in CH_2Cl_2 (40 mL) overnight at rt in darkness. $AuSMe_2Cl$ (0.59 g, 2.00 mmol, 1.0 equiv.) was added and the reaction stirred for a further 6 h. The reaction was filtered through a short silica plug. The solvent was reduced to approximately 2 mL under reduced pressure. Pentane (40 mL) was added to precipitate a solid. The product was filtered, washed with pentane (15 mL), and dried *in vacuo* to give a white solid (1.12 g,

87%). ^{1}H-NMR (400 MHz, $CDCl_3$, δ ppm): 7.30 (t, *J* = 7.4 Hz, 2H, ArCH), 7.25–7.16 (m, 10H, ArCH), 7.06–6.92 (m, 8H, ArCH), 5.44 (s, 4H, CH_2). ^{13}C-NMR (101 MHz, $CDCl_3$, δ ppm): 171.6 (NCN), 135.6 (C), 132.2 (C), 130.9 (CH), 129.5 (CH), 128.8 (CH), 128.7 (CH), 128.2 (CH), 127.6 (C), 127.4 (CH), 53.2 (CH_2).

(1,3-Dibenzyl-4,5-diphenylimidazol-2-ylidene)gold(I) bromide (2.5)

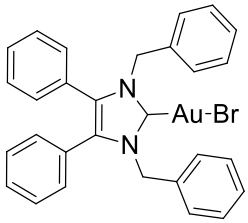

Using literature conditions,[14] imidazolium bromide **1.7** (50 mg, 0.104 mmol), $AuSMe_2Cl$ (31 mg, 0.104 mmol) and K_2CO_3 (14 mg, 0.104 mmol) were stirred in acetone (5 mL) at reflux (60 °C) for 6 h. Reaction was monitored by TLC (CH_2Cl_2-MeOH; 7:1). The solvent was removed under reduced pressure and the crude dissolved in CH_2Cl_2 (15 mL). This was filtered through Celite and the solvent reduced to approximately 2 mL and pentane (40 mL) added to precipitate a white solid. This was filtered, washed with pentane (15 mL) and dried *in vacuo* to give a white solid (58 mg, 82%). ^{1}H-NMR (400 MHz, $CDCl_3$, δ ppm): 7.30 (t, *J* = 7.4 Hz, 3H, ArCH), 7.24-7.19 (m, 9H, ArCH), 7.02 (dd, *J* = 7.1, 2.1 Hz, 7H, ArCH), 6.96 (d, *J* = 7.1 Hz, 4H, ArCH), 5.44 (s, 4H, CH_2). ^{13}C-NMR (101 MHz, $CDCl_3$, δ ppm): 174.9 (NCN), 135.8 (C), 132.2 (C), 130.9 (CH), 129.5 (CH), 128.8 (CH), 128.7 (CH), 128.2 (CH), 127.7 (C), 127.4 (CH), 53.1 (CH_2). HRMS (ESI$^+$) *m*/*z*: $[M + H]^+$ calcd. 677.0867; found 677.0847. IR (ATR, cm^{-1}): 3056 (w), 3028 (w), 1604 (w), 1487 (m), 1446 (s), 1025 (m). Melting point range: 218-220 °C. Anal. calcd. for $C_{29}H_{24}N_2AuBr$ (677.38) in %: C, 51.42; H, 3.57; N, 4.14; Br, 11.80. Found: C, 51.59; H, 3.51; N, 4.05; Br, 11.85.

(1,3-Dibenzyl-4,5-diphenylimidazol-2-ylidene)gold(I) iodide (2.6)

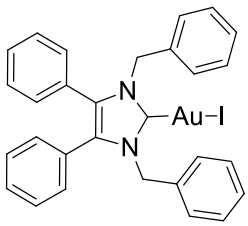

NHC*-Au(I)-Cl (**1.21**) (50 mg, 0.079 mmol, 1.0 equiv.) and NaOH (4 mg, 0.079 mmol, 1.0 equiv.) were stirred with an excess of KI (65 mg, 0.395 mmol, 5.0 equiv.) in EtOH (15 mL) at rt for 48 h. The solvent was removed under reduced pressure, the crude was dissolved in CH_2Cl_2 (15 mL) and dried over anhydrous $MgSO_4$. This was filtered and reduced to approximately 2 mL under reduced pressure. Pentane (40 mL) was added to precipitate a solid. The product was filtered, washed with pentane (15 mL), and dried *in vacuo* to give an off white solid (36 mg, 63%). ^{1}H-NMR (500 MHz, $CDCl_3$, δ ppm): 7.30 (t, *J* = 7.5 Hz, 2H, ArCH), 7.24-7.19 (m, 9H, ArCH), 7.04-7.01 (m, 4H, ArCH), 6.97 (d, *J* = 7.2 Hz, 4H, ArCH), 5.44 (s, 4H, CH_2). ^{13}C-NMR (101 MHz, $CDCl_3$, δ ppm): 181.5 (NCN), 135.6 (C), 131.9 (C), 130.8 (CH), 130.7 (CH), 129.4 (CH), 128.6 (CH), 128.1 (CH), 127.6 (C), 127.3 (CH), 52.7 (CH_2). HRMS (ESI$^+$) *m*/*z*: $[M + Na]^+$ calcd. 747.0548; found 747.0541. IR (ATR, cm^{-1}): 3062 (w), 3028 (w), 1603 (w), 1494 (m), 1447 (s), 1023 (m). Melting point range: 192-195 °C. Anal. calcd. for $C_{29}H_{24}N_2AuI$ (724.38) in %: C, 48.09; H, 3.34; N, 3.87. Found: C, 47.80; H, 3.18; N, 3.74.

1,3-Dibenzyl-4,5-diphenylimidazolium hexafluorophosphate (2.7)

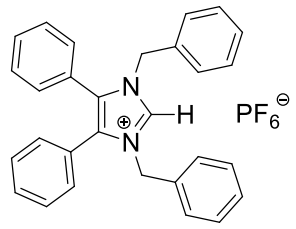

Using literature conditions,[16] imidazolium bromide **1.7** (250 mg, 0.520 mmol, 1.0 equiv.) and $NaPF_6$ (135 mg, 0.800 mmol, 1.5 equiv.) were stirred in acetone (30 mL) at rt for 24 h. The solvent was removed under reduced pressure and the crude dissolved in CH_2Cl_2 (15 mL). This was filtered and the solvent reduced to approximately 2 mL and pentane (40 mL) added to precipitate a white solid. This was filtered, washed with pentane (15 mL) and dried *in vacuo* to give a white solid (258 mg, 91%). ^{1}H-NMR (400 MHz, $CDCl_3$, δ ppm): 8.56 (s, 1H, $CH_{imidazole}$), 7.43-7.38 (m, 3H, ArCH), 7.36-7.31 (m, 5H, ArCH), 7.29 (dd, *J* = 4.9, 1.8 Hz, 5H, ArCH), 7.19 (d, *J* = 7.0 Hz, 4H, ArCH), 7.07-7.02 (m, 4H, ArCH), 5.23 (s, 4H, CH_2). ^{19}F-NMR (376 MHz, $CDCl_3$, δ ppm): -71.76, -73.65. ^{31}P-NMR (162 MHz, $CDCl_3$, δ ppm): 62.90, -135.44, -139.84, -144.25, -148.65, -153.06. ^{13}C-NMR (101 MHz, $CDCl_3$, δ ppm): 135.3 (C), 133.0 (CH), 132.7 (C), 130.9 (CH), 130.6 (CH), 129.4 (CH), 129.3 (CH), 129.2 (CH), 128.6 (CH), 124.7 (C), 51.9 (CH_2). HRMS (ESI$^+$)

m/*z*: [M – PF_6]$^+$ calcd. 401.2012; found 401.2012. HRMS (ESI^-) *m*/*z*: [PF_6]$^-$ calcd. 144.9642; found 144.9647. IR (ATR, cm^{-1}): 3077 (w), 2923 (m), 1603 (w), 1497 (m), 1451 (m), 1022 (s). Anal. calcd. for $C_{29}H_{25}N_2PF_6$ (546.49) in %: C, 63.74; H, 4.61; N, 5.13; F, 20.86. Found: C, 63.72; H, 4.59; N, 5.09; F, 20.52.

1,3-Dibenzyl-4,5-diphenylimidazolium tetrafluoroborate (2.8)

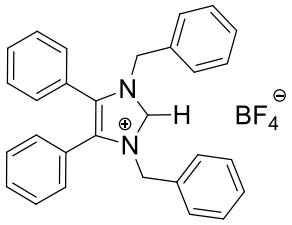

In a procedure identical to above reaction: Imidazolium bromide **1.7** (250 mg, 0.520 mmol), $NaBF_4$ (88 mg, 0.800 mmol, 1.5 equiv.) and acetone (30 mL). After workup and precipitation a white solid was formed (224 mg, 88%). ^{1}H-NMR (400 MHz, $CDCl_3$, δ ppm): 9.94 (s, 1H, $CH_{imidazole}$), 7.43-7.38 (m, 2H, ArCH), 7.32 (t, *J* = 7.5 Hz, 4H, ArCH), 7.26-7.22 (m, 4H, ArCH), 7.14 (dd, *J* = 8.3, 1.2 Hz, 4H, ArCH), 7.12-7.04 (m, 6H, ArCH), 5.39 (s, 4H, CH_2). ^{19}F-NMR (376 MHz, $CDCl_3$, δ ppm): -151.89, -151.95. ^{13}C-NMR (101 MHz, $CDCl_3$, δ ppm): 136.8 (C), 133.2 (CH), 132.6 (C), 130.9 (CH), 130.5 (CH), 129.3 (CH), 129.2 (CH), 129.1 (CH), 128.6 (CH), 124.9 (C), 51.7 (CH_2). HRMS (ESI^+) *m*/*z*: [M – BF_4]$^+$ calcd. 401.2012; found 401.2012. HRMS (ESI^-) *m*/*z*: [BF_4]$^-$ calcd. 86.0065; found 86.0070. IR (ATR, cm^{-1}): 3069 (w), 2913 (w), 1605 (w), 1497 (w), 1452 (m), 1020 (s). Anal. calcd. for $C_{29}H_{25}N_2BF_4$ (488.34) in %: C, 71.33; H, 5.16; N, 5.74; F, 15.56. Found: C, 71.22; H, 5.11; N, 5.97; F, 10.27.

1,3-Dibenzyl-4,5-diphenylimidazolium iodide (2.9)

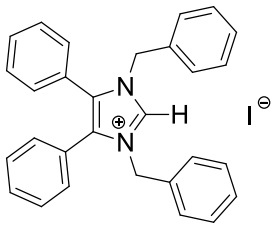

In a procedure identical to above reaction: Imidazolium bromide **1.7** (125 mg, 0.260 mmol), KI (66 mg, 0.400 mmol, 1.5 equiv.) and acetone (30 mL). After workup and precipitation a pale yellow solid was formed (120 mg, 87%). ^{1}H-NMR (400 MHz, $CDCl_3$, δ ppm): 10.33 (s, 1H, $CH_{imidazole}$), 7.42 (t, *J* = 7.4 Hz, 2H, ArCH), 7.34 (t, *J* = 7.5 Hz, 5H, ArCH), 7.29 (dd, *J* = 5.0, 1.9 Hz, 5H, ArCH), 7.22-7.14 (m, 8H, ArCH), 5.43 (s, 4H, CH_2). ^{13}C-NMR (101 MHz, $CDCl_3$, δ ppm): 136.4 (C), 133.0 (CH), 132.6 (C), 131.1 (CH), 130.7 (CH), 129.4 (CH), 129.3 (CH), 129.2 (CH), 128.8 (CH), 124.75 (C), 51.7 (CH_2). HRMS (ESI$^+$) *m*/*z*: $[M - I]^+$ calcd. 401.2012; found 401.2018. HRMS (ESI$^-$) *m*/*z*: X $[I]^-$ calcd. 126.9045; found 126.9050. IR (ATR, cm^{-1}): 2940 (m), 1604 (w), 1495 (w), 1448 (m), 1020 (m). Anal. calcd. for $C_{29}H_{25}N_2I$ (528.437) in %: C, 65.91; H, 4.77; N, 5.30. Found: C, 65.39; H, 4.66; N, 5.21.

Bis-[1,3-dibenzyl-4,5-diphenylimidazol-2-ylidene]gold(I) hexafluorophosphate (2.10)

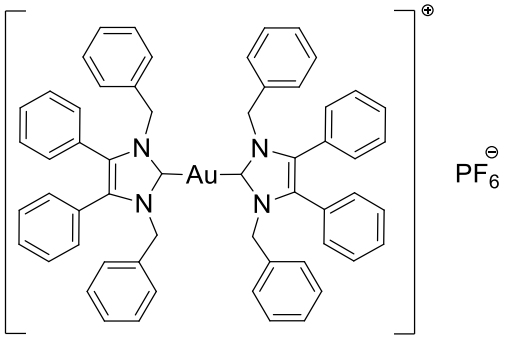

Using literature conditions,[16] imidazolium salt **2.7** (50 mg, 0.092 mmol, 1.0 equiv.) and Ag_2O (23 mg, 0.101 mmol, 1.1 equiv.) were stirred in CH_2Cl_2-MeOH (1:1, 30 mL) in darkness for 5 h. $AuSMe_2Cl$ (13 mg, 0.046 mmol, 0.5 equiv.) was added and the reaction stirred for a further 20 h. The solvent was removed under reduced pressure. The residue was dissolved in CH_2Cl_2 (15 mL) and filtered through Celite. The solvent was reduced to approximately 2 mL and pentane (40 mL) was added to precipitate the product. This was filtered, washed with pentane (15 mL) and dried *in vacuo* to give a white solid (45 mg, 86%). ^{1}H-NMR (400 MHz, $CDCl_3$, δ ppm): 7.28 (d, *J* = 7.4 Hz, 2H, ArCH), 7.20 (t, *J* = 7.5 Hz, 11H, ArCH), 7.16-7.10 (m, 11H, ArCH), 7.03-6.96 (m, 8H, ArCH), 6.88 (dd, *J* = 7.0, 2.1 Hz, 8H, ArCH), 5.19 (s, 8H, CH_2). ^{13}C-NMR (101 MHz, $CDCl_3$, δ ppm): 184.8 (NCN), 136.6 (C), 132.9 (C), 130.8 (CH), 129.5 (CH), 128.8 (CH), 127.9 (CH), 127.1 (CH), 126.8 (CH), 52.4 (CH_2). ^{19}F-NMR (376 MHz, $CDCl_3$, δ ppm): -72.31, -74.20. ^{31}P-NMR (162 MHz, $CDCl_3$, δ ppm): 62.90, -135.39, -139.79, -144.20, -148.61, -153.01. HRMS (ESI$^+$) *m*/*z*: [M

- PF_6 + H]$^+$ calcd. 997.3545; found 997.3557. LRMS (ESI$^-$) *m*/*z*: 145.0 [PF_6]$^-$. IR (ATR, cm^{-1}): 3029 (w), 2920 (w), 1602 (w), 1496 (w), 1486 (w), 1025 (m). Melting point range: 208-211 °C. Anal. calcd. for $C_{58}H_{48}N_4AuPF_6$ (1142.96) in %: C, 60.95; H, 4.23; N, 4.90; F, 9.97. Found: C, 60.95; H, 4.17; N, 4.85; F, 9.56.

Bis-[1,3-dibenzyl-4,5-diphenylimidazol-2-ylidene]gold(I) tetrafluoroborate (2.11)

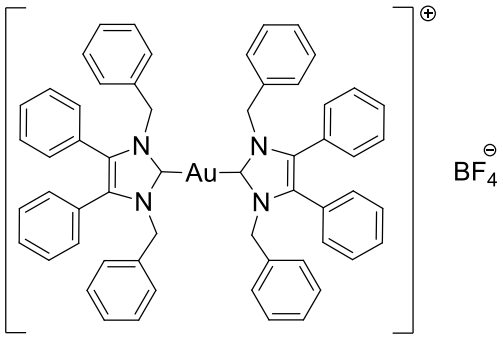

In a procedure identical to the above reaction: Imidazolium salt **2.8** (45 mg, 0.093 mmol, 1.0 equiv.), Ag_2O (23.6 mg, 0.102 mmol, 1.1 equiv.) and CH_2Cl_2-MeOH (1:1, 30 mL) for 5 h. $AuSMe_2Cl$ (14 mg, 0.046 mmol, 0.5 equiv.) was added and the reaction stirred for a further 48 h. After workup and precipitation a white solid was formed (44 mg, 87%). ^{1}H-NMR (400 MHz, $CDCl_3$, δ ppm): 7.28 (d, *J* = 7.4 Hz, 2H, ArCH), 7.20 (t, *J* = 7.6 Hz, 8H, ArCH), 7.17-7.10 (m, 12H, ArCH), 7.00 (d, *J* = 7.3 Hz, 8H, ArCH), 6.88 (d, *J* = 6.0 Hz, 8H, ArCH), 5.21 (s, 8H, CH_2). ^{13}C-NMR (101 MHz, $CDCl_3$, δ ppm): 184.7 (NCN), 136.6 (C), 132.9 (C), 130.8 (CH), 129.6 (CH), 128.8 (CH), 127.9 (CH), 127.1 (CH), 126.8 (CH), 52.4 (CH_2). ^{19}F-NMR (376 MHz, $CDCl_3$, δ ppm): -153.77, -153.82. HRMS (ESI$^+$) *m*/*z*: [M – BF_4]$^+$ calcd. 997.3545; found 97.3514. LRMS (ESI$^-$) *m*/*z*: 87.0 [BF_4]$^-$. IR (ATR, cm^{-1}): 3061 (w), 3031 (w), 1604 (w), 1496 (m), 1449 (m), 1051 (s). Melting point range: 205-208 °C. Anal. calcd. for $C_{58}H_{48}N_4AuBF_4$ (1084.80) in %: C, 64.22; H, 4.46; N, 5.16; F, 7.01. Found: C, 63.92; H, 4.26; N, 5.12; F, 6.76.

Bis-[1,3-dibenzyl-4,5-diphenylimidazol-2-ylidene]gold(I) iodide (2.13)

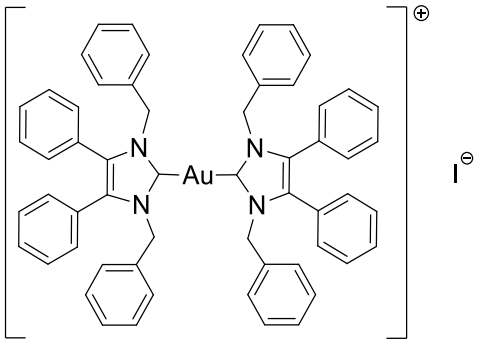

In a procedure identical to the above reaction: Imidazolium salt **2.9** (45 mg, 0.093 mmol, 1.0 equiv.), Ag_2O (23.6 mg, 0.102 mmol, 1.1 equiv.) and CH_2Cl_2-MeOH (1:1, 30 mL) for 5 h. $AuSMe_2Cl$ (14 mg, 0.046 mmol, 0.5 equiv.) was added and the reaction stirred for a further 20 h. After workup and precipitation a white solid was formed (27.3 mg, 52%). ^{1}H-NMR (600 MHz, $CDCl_3$, δ ppm): 7.29 (d, *J* = 7.5 Hz, 2H, ArCH), 7.20 (t, *J* = 7.7 Hz, 12H, ArCH), 7.18-7.13 (m, 12H, ArCH), 6.99 (d, *J* = 7.5 Hz, 8H, ArCH), 6.89 (d, *J* = 7.0 Hz, 8H, ArCH), 5.22 (s, 8H, CH_2). ^{13}C-NMR (101 MHz, $CDCl_3$, δ ppm): 184.6 (NCN), 136.5 (C), 132.9 (C), 130.7 (CH), 129.6 (CH), 128.8 (CH), 128.0 (CH), 126.9 (CH), 126.7 (CH), 52.5 (CH_2). HRMS (ESI$^+$) *m*/*z*: $[M - I]^+$ calcd. 997.3539; found 997.3545. LRMS (ESI$^-$) *m*/*z*: 126.9 $[I]^-$. IR (ATR, cm^{-1}): 3059 (w), 3030 (w), 1603 (w), 1496 (m), 1449 (s), 1022 (m). Anal. calcd. for $C_{58}H_{48}N_4AuI$ (1124.90) in %: C, 61.93; H, 4.30; N, 4.98. Found: C, 62.78; H, 4.47; N, 4.91.

Triphenylphosphino-(1,3-dibenzyl-4,5-diphenylimidazol-2-ylidene)gold(I) hexafluorophosphate (2.14)

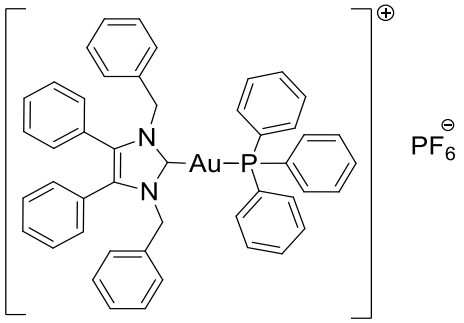

1.21 (63.3 mg, 0.10 mmol, 1.0 equiv.), PPh_3 (34.1 mg, 0.13 mmol, 1.3 equiv.) and $NaPF_6$ (20.2 mg, 0.12 mmol, 1.2 equiv.) were stirred in acetone (10 mL) at rt for 30 min. The solvent was removed

under reduced pressure. The residue was dissolved in CH_2Cl_2 (15 mL) and filtered. The solvent was removed under reduced pressure to form a white solid. Hot ethanol (40 mL) was added to the solid and filtered *in vacuo* to give a white crystalline solid (77 mg, 76%). ^{1}H-NMR (400 MHz, $CDCl_3$, δ ppm): 7.56-7.50 (m, 3H, ArCH), 7.44 (td, *J* = 7.6, 1.9 Hz, 6H, ArCH), 7.35-7.27 (m, 12H, ArCH), 7.25-7.17 (m, 11H, ArCH), 7.05 (dd, *J* = 6.2, 3.1 Hz, 4H, ArCH), 5.41 (s, 4H, CH_2). ^{13}C-NMR (101 MHz, $CDCl_3$, δ ppm): 187.6 (NCN), 136.8 (C), 134.3 (CH), 134.2 (CH), 133.1 (C), 132.2 (C), 130.9 (CH), 129.7 (CH), 129.6 (CH), 129.5 (CH), 129.0 (CH), 128.1 (CH), 127.1 (CH), 126.9 (C), 52.5 (CH_2). ^{19}F-NMR (376 MHz, $CDCl_3$, δ ppm): -72.38, -74.28. ^{31}P-NMR (162 MHz, $CDCl_3$, δ ppm): 62.90, 39.86, -131.02, -135.43, -139.83, -144.24, -148.64, -153.05. HRMS (ESI^+) *m*/*z*: [M-PF_6]$^+$ calcd. 859.2516; found 859.2479. LRMS (ESI^-) *m*/*z*: 144.9 [PF_6]$^-$. IR (ATR, cm^{-1}): 3053, 1585, 1496, 1434, 1025, 832. Anal. calcd. for $C_{47}H_{39}N_2AuP_2F_6$ (1004.73) in %: C, 56.18; H, 3.91; N, 2.79; F, 11.35. Found: C, 55.95; H, 3.79; N, 2.68; F, 11.02.

Triphenylphosphino-(1,3-dibenzyl-4,5-diphenylimidazol-2-ylidene)gold(I) tetrafluoroborate (2.15)

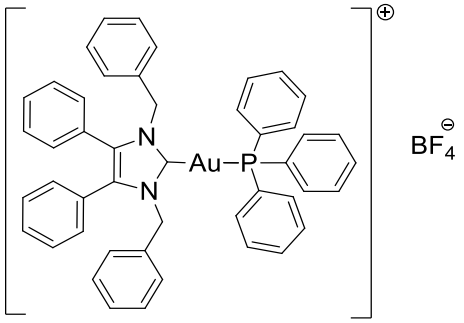

1.21 (94.9 mg, 0.15 mmol, 1.0 equiv.), PPh_3 (51.1 mg, 0.19 mmol, 1.3 equiv.) and $NaBF_4$ (19.8 mg, 0.18 mmol, 1.2 equiv.) were stirred in acetone (10 mL) at rt for 30 min. The solvent was removed under reduced pressure. The residue was dissolved in CH_2Cl_2 (15 mL) and filtered. The solvent was removed under reduced pressure to form an oily residue. The residue was dissolved in hot ethanol (20 mL) and left to cool to form colourless crystals (100.4 mg, 62%). ^{1}H-NMR (400 MHz, $CDCl_3$, δ ppm): 7.52 (td, *J* = 7.2, 1.7 Hz, 3H, ArCH), 7.44 (td, *J* = 7.5, 2.4 Hz, 6H, ArCH), 7.34-7.27 (m, 9H, ArCH), 7.24-7.15 (m, 11H, ArCH), 7.06 (dd, *J* = 6.4, 3.0 Hz, 4H, ArCH), 5.44 (s, 4H, CH_2). ^{13}C-NMR (101 MHz, $CDCl_3$, δ ppm): 187.6 (NCN), 136.9 (C), 134.3 (CH), 134.2 (CH), 133.2 (C), 132.1 (C), 130.9 (CH), 129.8 (CH), 129.7 (CH), 129.6 (CH), 129.0 (CH), 128.1 (CH), 127.1

(CH), 126.9 (C), 52.6 (CH_2). ^{19}F-NMR (376 MHz, $CDCl_3$, δ ppm): -153.73, -153.78. ^{31}P-NMR (162 MHz, $CDCl_3$, δ ppm): 25.21, -139.86. HRMS (ESI^+) *m*/*z*: $[M - BF_4]^+$ calcd. 859.2511; found 859.2519. LRMS (ESI^-) *m*/*z*: 87.1 $[BF_4]^-$. IR (ATR, cm^{-1}): 3062, 1591, 1496, 1437, 1052, 692. Anal. calcd. for $C_{47}H_{39}N_2AuPBF_4$ (946.57) in %: C, 59.64; H, 4.15; N, 2.96; F, 8.03. Found: C, 59.52; H, 3.97; N, 2.90; F, 8.48.

2.7.3 Computational Details

The computational analysis was carried out by Dr Goar Sánchez-Sans at the Irish Centre for High-End Computing (ICHEC), Dublin. Compounds have been optimized at the MN15[27] computational level with the 6–311++G(2df,p) basis set[28] applied to the lighter elements inclusive of chlorine. The LANL2TZ(f) basis set[29] is used throughout for the gold atoms. Frequency calculations have been performed at the same level in order to confirm that the structures obtained correspond to energetic minima. The effect of water solvation was then accounted for using the SMD approach implemented in the Gaussian16 package[30] including dispersing, repulsing, and cavitation energy terms of the solvent in the optimisation. Orbitals have been calculated using NBO 6.0[31] and plotted using Jmol software[32].

References

(1) Ferlay, J.; Colombet, M.; Soerjomataram, I.; Mathers, C.; Parkin, D. M.; Piñeros, M.; Znaor, A.; Bray, F. Estimating the Global Cancer Incidence and Mortality in 2018: GLOBOCAN Sources and Methods. *Int. J. Cancer* **2019**, *144*, 1941–1953.

(2) Clèries, R.; Rooney, R. M.; Vilardell, M.; Espinàs, J. A.; Borras, J. M. Assessing Predicted Age-Specific Breast Cancer Mortality Rates in 27 European Countries by 2020. *Clin. Transl. Oncol.* **2018**, *20*, 313–321.

(3) Culp, M. B.; Soerjomataram, I.; Efstathiou, J. A.; Bray, F.; Jemel, A. Recent Global Patterns in Prostate Cancer Incidence and Mortality Rates. *Eur. Urol.* **2020**, *77*, 38–52.

(4) Marzo, T.; Massai, L.; Pratesi, A.; Stefanini, M.; Cirri, D.; Magherini, F.; Becatti, M.; Landini, I.; Nobili, S.; Mini, E.; Crociani, O.; Arcangeli, A.; Pillozzi, S.; Gamberi, T.;

Messori, L. Replacement of the Thiosugar of Auranofin with Iodide Enhances the Anticancer Potency in a Mouse Model of Ovarian Cancer. *ACS Med. Chem. Lett.* **2019**, *10*, 656–660.

(5) Bian, M.; Fan, R.; Jiang, G.; Wang, Y.; Lu, Y.; Liu, W. Halo and Pseudohalo Gold(I)-NHC Complexes Derived from 4,5-Diarylimidazoles with Excellent In Vitro and In Vivo Anticancer Activities Against HCC. *J. Med. Chem.* **2020**, *63*, 9197–9211.

(6) Baker, M. V.; Barnard, P. J.; Berners-Price, S. J.; Brayshaw, S. K.; Hickey, J. L.; Skelton, B. W.; White, A. H. Cationic, Linear Au(I) N-Heterocyclic Carbene Complexes: Synthesis, Structure and Anti-Mitochondrial Activity. *Dalton Trans.* **2006**, 3708–3715.

(7) Rubbiani, R.; Schuh, E.; Meyer, A.; Lemke, J.; Wimberg, J.; Metzler-Nolte, N.; Meyer, F.; Mohr, F.; Ott, I. TrxR Inhibition and Antiproliferative Activities of Structurally Diverse Gold N-Heterocyclic Carbene Complexes. *MedChemComm* **2013**, *4*, 942–948.

(8) Schmidt, C.; Albrecht, L.; Balasupramaniam, S.; Misgeld, R.; Karge, B.; Brönstrup, M.; Prokop, A.; Baumann, K.; Reichl, S.; Ott, I. A Gold(I) Biscarbene Complex with Improved Activity as a TrxR Inhibitor and Cytotoxic Drug: Comparative Studies with Different Gold Metallodrugs. *Metallomics* **2019**, *11*, 533–545.

(9) Rubbiani, R.; Salassa, L.; de Almeida, A.; Casini, A.; Ott, I. Cytotoxic Gold(I) N-Heterocyclic Carbene Complexes with Phosphane Ligands as Potent Enzyme Inhibitors. *ChemMedChem* **2014**, *9*, 1205–1210.

(10) Holenya, P.; Can, S.; Rubbiani, R.; Alborzinia, H.; Jünger, A.; Cheng, X.; Ott, I.; Wölfl, S. Detailed Analysis of Pro-Apoptotic Signaling and Metabolic Adaption Triggered by a N-Heterocyclic Carbene-Gold(I) Complex. *Metallomics* **2014**, *6*, 1591–1601.

(11) Rubbiani, R.; Can, S.; Kitanovic, I.; Alborzinia, H.; Stefanopoulou, M.; Kokoschka, M.; Mönchgesang, S.; Sheldrick, W. S.; Wölfl, S.; Ott, I. Comparative in Vitro Evaluation of N-Heterocyclic Carbene Gold (I) Complexes of the Benzimidazolylidene Type. *J. Med. Chem.* **2011**, *54*, 8646–8657.

(12) Patil, S.; Deally, A.; Gleeson, B.; Müller-Bunz, H.; Paradisi, F.; Tacke, M. Novel Benzyl-Substituted N-Heterocyclic Carbene-Silver Acetate Complexes: Synthesis, Cytotoxicity

and Antibacterial Studies. *Metallomics* **2011**, *3*, 74–88.

(13) Hackenberg, F.; Müller-Bunz, H.; Smith, R.; Streciwilk, W.; Zhu, X.; Tacke, M. Novel Ruthenium(II) and Gold(I) NHC Complexes: Synthesis, Characterization, and Evaluation of Their Anticancer Properties. *Organometallics* **2013**, *32*, 5551–5560.

(14) Collado, A.; Gómez-Suárez, A.; Martin, A. R.; Slawin, A. M. Z.; Nolan, S. P. Straightforward Synthesis of [Au(NHC)X] (NHC = N-Heterocyclic Carbene, X = Cl, Br, I) Complexes. *Chem. Commun.* **2013**, *49*, 5541–5543.

(15) Muenzner, J. K.; Biersack, B.; Albrecht, A.; Rehm, T.; Lacher, U.; Milius, W.; Casini, A.; Zhang, J.; Ott, I. Ferrocenyl-Coupled N-Heterocyclic Carbene Complexes of Gold (I): A Successful Approach to Multinuclear Anticancer Drugs. *Chem. Eur. J.* **2016**, *22*, 18953–18962.

(16) Muenzner, J. K.; Biersack, B.; Albrecht, A.; Rehm, T.; Lacher, U.; Milius, W.; Casini, A.; Zhang, J. J.; Ott, I.; Brabec, V.; Stuchlikova, O.; Andronache, I. C.; Kaps, L.; Schuppan, D.; Schobert, R. Ferrocenyl-Coupled N-Heterocyclic Carbene Complexes of Gold(I): A Successful Approach to Multinuclear Anticancer Drugs. *Chem. Eur. J.* **2016**, *22*, 18953–18962.

(17) Navarro, M.; Pérez, H.; Sánchez-Delgado, R. A. Toward a Novel Metal-Based Chemotherapy against Tropical Diseases. 3. Synthesis and Antimalarial Activity in Vitro and in Vivo of the New Gold-Chloroquine Complex [Au(PPh_3)(CQ)]PF_6. *J. Med. Chem.* **1997**, *40*, 1937–1939.

(18) Vellé, A.; Cebollada, A.; Macías, R.; Iglesias, M.; Gil-Moles, M.; Sanz Miguel, P. J. From Imidazole toward Imidazolium Salts and N-Heterocyclic Carbene Ligands: Electronic and Geometrical Redistribution. *ACS Omega* **2017**, *2*, 1392–1399.

(19) Paolini, J. P. The Bond Order—Bond Length Relationship. *J. Comput. Chem.* **1990**, *11*, 1160–1163.

(20) Tacke, M.; Dada, O.; O'Beirne, C.; Zhu, X.; Müller-Bunz, H. The Non-Isomorphous Crystal Structures of NHC-Au-Cl and NHC-Au-Br (NHC Is 1,3-Dibenzyl-4,5-Diphenylimidazol-2-Ylidene). *Acta Cryst.* **2016**, *72*, 857–860.

(21) Flörke, U.; Haupt, H.-J.; Jones, P. G. Trifluoromethyl(Triphenylphosphine)Gold(I). *Acta Cryst.* **1996**, *C52*, 609–611.

(22) Barnes, N. A.; Brisdon, A. K.; William Brown, F. R.; Cross, W. I.; Crossley, I. R.; Fish, C.; Herbert, C. J.; Pritchard, R. G.; Warren, J. E. Synthesis of Gold(I) Fluoroalkyl and Fluoroalkenyl-Substituted Phosphine Complexes and Factors Affecting Their Crystal Packing. *Dalton Trans.* **2011**, *40*, 1743–1750.

(23) Schmidbaur, H.; Schier, A. Aurophilic Interactions as a Subject of Current Research: An Up-Date. *Chem. Soc. Rev.* **2012**, *41*, 370–412.

(24) Tabrizi, L.; Abyar, F. Conjugation of Gold(III) Complex with Vitamin B1 and Chlorambucil Derivatives: Anticancer Evaluation and Mechanistic Insights. *Metallomics* **2020**, *12*, 721–731.

(25) Clark, R. C.; Reid, J. S. The Analytical Calculation of Absorption in Multifaceted Crystals. *Acta Cryst.* **1995**, *A51*, 887–897.

(26) Sheldrick, G. M. A Short History of SHELX. *Acta Cryst.* **2008**, *A64*, 112–122.

(27) Yu, H. S.; He, X.; Li, S. L.; Truhlar, D. G. MN15: A Kohn-Sham Global-Hybrid Exchange-Correlation Density Functional with Broad Accuracy for Multi-Reference and Single-Reference Systems and Noncovalent Interactions. *Chem. Sci.* **2016**, *7*, 5032–5051.

(28) Frisch, M. J.; Pople, J. A.; Binkley, J. S. Self-Consistent Molecular Orbital Methods 25. Supplementary Functions for Gaussian Basis Sets. *J. Chem. Phys.* **1984**, *80*, 3265–3269.

(29) Hay, P. J.; Wadt, W. R. Ab Initio Effective Core Potentials for Molecular Calculations. Potentials for the Transition Metal Atoms Sc to Hg. *J. Chem. Phys.* **1985**, *82*, 270–283.

(30) Frisch, M. J.; Trucks, G. W.; Schlegel, H. B.; Scuseria, G. E.; Robb, M. A.; Cheeseman, J. R.; Scalmani, G.; Barone, V.; Petersson, G. A.; Nakatsuji, H.; Li, X.; Caricato, M.; Marenich, A. V.; Bloino, J.; Janesko, B. G.; Gomperts, R.; Mennucci, B.; … Fox, D. J. Gaussian 16. **2016**.

(31) Glendening, E. D.; Badenhoop, J. K.; Reed, A. E.; Carpenter, J. E.; Bohmann, J. A.; Morales, C. M.; Landis, C. R.; Weinhold, F. NBO 6.0. **2013**.

(32) Jmol: an open-source Java viewer for chemical structures in 3D. http://www.jmol.org/.

Chapter Three

NHC*-Gold(I) Complexes of Cyanides and Acetylides

Work published as:

Synthesis and Cytotoxicity Studies of Novel NHC*-Gold(I) Complexes Derived from Lepidiline A

D. Curran, O. Dada, H. Müller-Bunz, M. Rothemund, G. Sánchez-Sanz, R. Schobert, X. Zhu, M. Tacke, *Molecules*, **2018**, *23*, 2031-2048

And

Novel Anticancer NHC*-Gold(I) Complexes Inspired by Lepidiline A

D. Curran, H. Müller-Bunz, S. I. Bär, R. Schobert, X. Zhu, M. Tacke,

Molecules, **2020**, *25*, 3474-3491

3.1 Introduction

3.1.1 Overview of Gold(I) Cyanides

The use of gold cyanide for biological applications began as early as 1890 with the discovery by Robert Koch that $K[Au(CN)_2]$ was bacteriostatic against tubercle bacillus *in vitro*. This discovery laid the foundation for gold-based medicines. Later in 1982, it was observed that patients taking sodium aurothiomalate (Myocrisin) had higher blood gold concentrations if they were smokers, due to the increased presence of cyanide from the tobacco.[1] The cyanide converted the aurothiomalate into aurocyanide, which was readily taken up by red blood cells. Interestingly, cyanoaurates experience disproportionation, or ligand scrambling, in solution affording aurocyanide $[Au(CN)_2]^-$ (**Equation 3.1**).[2]

$$2[L-Au-CN] \rightleftharpoons [AuL_2]^+ + [Au(CN)_2]^- \quad (3.1)$$

Biological applications of aurocyanide include the inhibition of HIV replication.[3] The coordination of gold(I) cyanide to a stabilising ligand such as phosphines has led to complexes with significantly higher activity. $[Au(CN)(PEt_3)]$ was tested against a selection of cancer cell lines including the breast carcinoma MCF-7 and the colon carcinoma HCT-15, exhibiting high cytotoxicity (IC_{50} values: 0.45 ± 0.12 μM and 0.08 ± 0.01 μM, respectively).[4] Heterometallic complexes with bishydeten ligands and bridging cyanide groups were shown to have excellent antiproliferative effects against cervical, colon and brain cancer cells (**3.1**, **Figure 3.1**).[5] The authors associated the high activity of these complexes with the $[Au(CN)_2]^-$ moieties. However, NHC-gold cyanide complexes are rare in the literature. Raubenheimer synthesised the (1-methylimidazol-2-ylidene)gold(I) cyanide in 1996 (**3.2**).[6] Instability of the cyanometalate in solution resulted in "a homoleptic rearrangement" to form $[Au(CN)_2]^-$ and the cationic biscarbene, as seen in **Equation 3.1**. NHC-gold(I) and gold(III) cyanide complexes have been developed for their catalytic and photoluminescent properties (**3.3** and **3.4**), [7,8] however, to the best of our knowledge, there are no reports of NHC-gold cyanide complexes developed for biological evaluation.

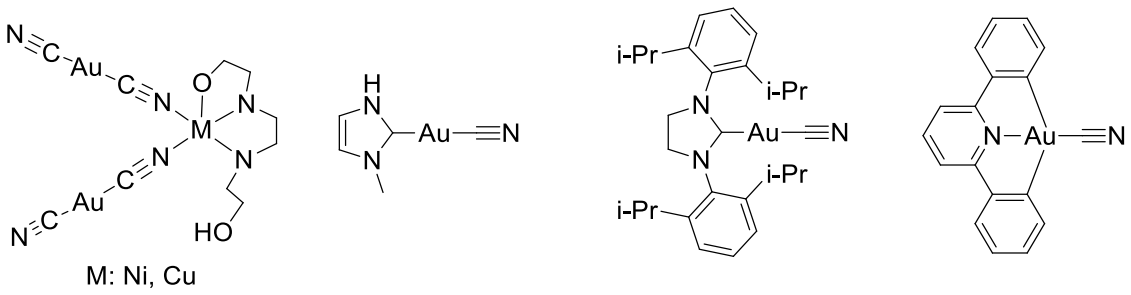

Figure 3.1 Selected examples of gold cyano complexes.

3.1.2 Overview of Gold(I) Acetylides

Alkynyl compounds are prevalent in the literature due to their versatility. They are a highly studied multifaceted ligand featuring in photoluminescence studies,[9,10] catalysis,[11,12] click-chemistry,[13,14] liquid crystallinity[15,16] and cation binding.[17,18] However, their use in biological applications has not been developed to the same extent. The incorporation of alkynes into gold(I) based drug design didn't arise until 2009, however it was another eight years before NHCs were involved.

The biological activity of gold(I) acetylides was first reported in 2009, by two different groups. Early research into these acetylide complexes involved phosphine ancillary ligands. Mohr et al. published phosphine-gold(I) acetylides with the propargyl ethers 7-chloro-(4-propargyloxy)quinolone, 1-propargyloxynaphthalene and 2-propargyloxybenzophenone.[19] The *in vitro* antimalarial activity of these compounds was tested alongside the anticancer activity on ovarian, cervical and colon cancer cell lines. The highest activity was found with the benzophenone compound (**3.5**, **Figure 3.2**) against the colon carcinoma cell line SW480 (IC_{50}: 4.5 ± 0.7 μM). In the same year, two diethynylfluorene gold(I) complexes were described with activity tested against human liver and breast cancer cell lines.[20] The dinuclear bis(acetylide) gold(I) complex **3.6** with a carbonyl moiety was found to be active against the breast carcinoma cell line MDA-MB-231 with an IC_{50} value of 5.1 ± 2.6 μM. More recently, triphenylphosphine-gold(I) complexes with a variety of phenyl derived alkynes were found to be active against colon and breast cancer cell lines.[21,22]

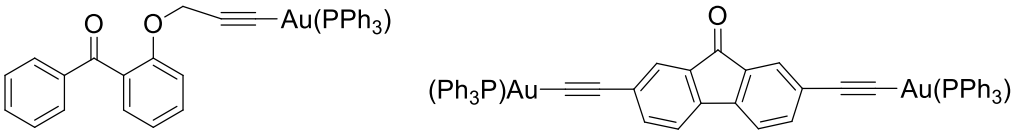

3.5 **3.6**

Figure 3.2 Examples of gold(I) acetylides studied for their biological activity.

The use of alkynes is desirable due to the strong Au-C bond formed, this strong bond is important for stabilising the gold(I) species. In the body gold is readily reduced and becomes inactive, thus stabilising ligands protect the active metal centre. As these alkynyl ligands are sufficiently stabilising there has been little research into mixed compounds with both an alkyne and a further stabilising NHC ligand. The first mixed NHC-gold(I) acetylides, studied for their luminescent properties, were developed by Gray et al. in 2009, including *tert*-butyl, naphthyl and ferrocenyl alkynes (**3.7**-**3.9**, **Figure 3.3**).[23]

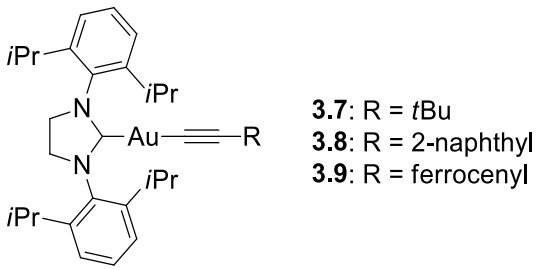

Figure 3.3 The NHC-gold(I) acetylides developed by Gray et al.

Despite the abundance of NHC-gold(I) acetylides developed since very few have been used for their biological properties. In fact, there is only a handful of NHC-gold(I) acetylides that have been tested for anticancer activity, all of which have originated in the Casini group. In 2017 Casini et al. reported the first example of a NHC-gold(I) acetylide featuring a bulky imidazole and *tert*-butylethynyl (**3.10**, **Figure 3.4**).[24] This was presented in a comparative study of NHC-gold complexes which were tested against human colon, breast and melanoma skin cancer cell lines, showing moderate activity. The highest activity was observed on the breast cancer cell line MCF-7 with an IC_{50} value of 6 ± 2 μM. Following this, Casini and co-workers[25,26] have developed more of these mixed NHC-gold acetylides. A series of xanthine based NHC-gold(I) complexes were synthesised with phenyl and pyridyl-based alkynes. These complexes were tested against the same cell lines as above, all exhibiting low cytotoxicity with compound **3.11**

displaying the highest activity against MCF-7 with an IC_{50} of 16 ± 5 μM.[25] More recently, complexes with varying NHCs were combined with phenyl, naphthyl and *tert*-butyl based alkynes. However, only two complexes were tested for antiproliferative effects, both with *tert*-butylethynyl. Compound **3.12** proved the most active with an IC_{50} value of 7.1 μM against the breast cancer cell line MCF-7.[26] As only phenyl, pyridyl and tert-butyl alkynes have been coordinated to NHC-gold(I) complexes and tested for biological properties no structure-activity relationship has been determined as of yet.

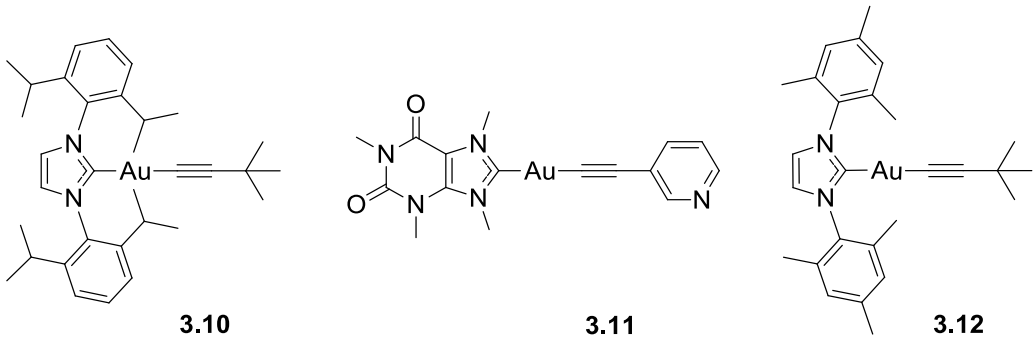

3.10 **3.11** **3.12**

Figure 3.4 NHC-gold(I) acetylides studied for their biological activity.

Chapter Proposal

The focus of this Chapter is to synthesise NHC*-gold(I) complexes with cyanides and alkynes in order to draw a structure-activity relationship. Firstly, cyanide will be compared to acetylene to assess the importance of the C-C connection. The importance of the size of the ligand can be addressed with phenylethynyl derivatives to contrast the small cyanide and acetylene compounds. Additionally, the electronic properties can be investigated by varying the phenyl substituents. These NHC*-gold(I) cyanide and acetylide complexes will be evaluated *in vitro* against human colon and breast cancer cell lines.

3.2 Synthesis

3.2.1 Synthesis of NHC*-Gold(I) Cyanide

NHC*-gold(I) cyanide (**3.13**) was synthesised via an anion exchange with NHC*-gold(I) chloride (**1.21**) and potassium cyanide in a good yield (**Scheme 3.1**). In the process of synthesising **3.13** biphasic conditions were considered. However, a EtOAC/H_2O solvent system led to the formation of the cationic imidazolium and the dicyanoaurate(I) anion (**3.14**).

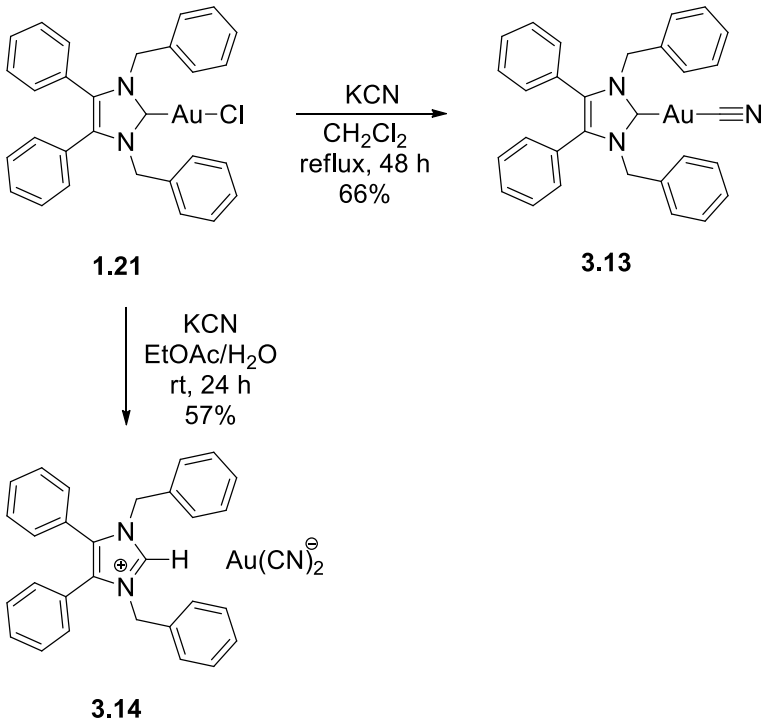

Scheme 3.1 Synthesis of NHC*-Au-CN (**3.13**) and NHC^+ $[Au(CN)_2]^-$ (**3.14**).

The ^{1}H-NMR spectra showed an upfield shift of the benzyl CH_2 signal from δ = 5.44 ppm in **1.21** to 5.37 ppm for complex **3.13** and to 5.30 ppm for **3.14**. Additionally, the protonated NHC was identified by the appearance of a ^{1}H-NMR signal at δ = 8.66 ppm, representing the imidazolium proton. The quaternary carbon of the cyanide ligand appears in the ^{13}C-NMR spectrum of **3.13** at δ = 152.6 ppm, this is consistent for coordinated cyanides.[27] Interestingly, the ^{13}C-NMR spectrum of **3.14** had a peak at δ = 110.1 ppm corresponding to the cyano carbon.[28] This was shifted significantly upfield compared to compound **3.13** as the anionic dicyanoaurate complex is more electronegative. Chemical shifts are increasingly shielded as electronegativity increases, thus complex **3.14** is the furthest upfield due to its high electronegativity and **3.13** is

more downfield. The IR spectra of complexes **3.13** and **3.14** showed bands at 2144 and 2141 cm^{-1}, respectively, denoting the C≡N stretch.[27,29]

3.2.2 Synthesis of NHC*-Gold(I) Acetylides

A series of NHC*-gold(I) acetylides were synthesised in a procedure adapted from Mohr et al. (**Scheme 3.2**).[30] It was demonstrated that ethynyltrimethylsilane (TMS-C≡CH) could be activated by fluoride ions present in solution from the addition of NaF. Due to solubility issues NaF was unsuitable for the synthesis of complexes **3.15**-**3.19**, however, tetra-*n*-butylammonium fluoride (TBAF) in THF proved effective affording the desired complexes as white powders in good to excellent yields of 60-88%. The acetylides were formed by reacting **1.21** with TMS-C≡C-R in the presence of TBAF. TBAF was added dropwise as quick addition of TBAF can result in a high concentration of fluoride ions which had been reported to impede effective synthesis.[31]

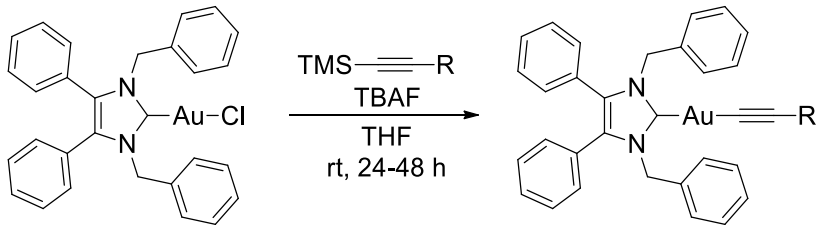

1.21

3.15: R = H; 61%
3.16: R = Ph; 83%
3.17: R = Ph-*p*-OMe; 88%
3.18: R = Ph-*p*-F; 87%
3.19: R = Ph-*p*-CF_3; 60%

Scheme 3.2 Synthesis of NHC*-Au-acetylides **3.15**-**3.19**.

The ^{1}H-NMR spectra displayed new signals for the ethynyl CH proton, for compound **3.15**, and the phenyl CH protons, for compounds **3.16**-**3.19**. A slight shift in the CH_2 peak from δ = 5.44 ppm to 5.45 and 5.49 ppm, for complexes **3.15** and **3.16**-**3.19** respectively, confirmed conjugation. ^{19}F-NMR spectroscopy proved useful as it detected the presence of the alkynyl ligand for compounds **3.18** and **3.19**. More significantly, in the ^{13}C-NMR spectra two signals for the alkyne appear: δ = 121.8-125.9 ppm and 103.9-105.3 ppm. The former signal represents the carbon bonded to the gold, the latter attached to the R group on the alkyne. The IR spectra of these compounds show the characteristic C≡C stretching at 1977 cm^{-1} for the ethynyl compound and in the 2111-2120 cm^{-1} range for the phenyl derivatives.

3.3 Structural Discussion

The molecular structures of **3.13**-**3.19** were determined by single crystal X-ray diffraction, with selected bond lengths and angles displayed in **Table 3.1**. The X-ray crystal data and structure refinement are found in **Tables 3.2** and **3.3**.

Compound **3.13** crystallised in the monoclinic space group $P2_1/m$ (#11) in the absence of any solvate molecules (**Figure 3.9**). Compound **3.14** crystallised in the triclinic space group $P\bar{1}$ (#2), in the absence of any solvate molecules (**Figure 3.6**). Compound **3.15** crystallised in the monoclinic space group $P2_1/c$ (#14) in the absence of any solvate molecules (**Figure 3.8**). Compounds **3.16**, **3.17** and **3.19** crystallised in the monoclinic space group $P2_1/n$ (#14) (**Figures 3.5** and **3.9**). Compounds **3.16** and **3.19** crystallised in the absence of solvate molecules. Compound **3.17** crystallised with two molecules of the compound and one solvate CH_2Cl_2 molecule contained in the independent unit. Compound **3.18** crystallised in the monoclinic space group I2/a (#15) with four molecules of the compound and one solvate CH_2Cl_2 molecule contained in the independent unit (**Figure 3.7**). Crystals of **3.19** were grown from the slow evaporation of a hot saturated ethanol solution at room temperature. All other crystals were grown by the slow infusion of pentane into a saturated CH_2Cl_2 solution at -18 °C.

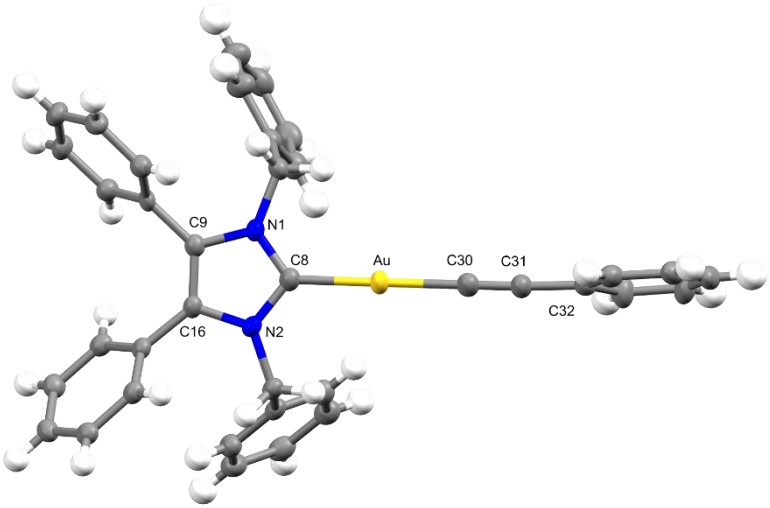

Figure 3.5 X-ray diffraction structure of complex **3.16**; thermal ellipsoids drawn on the 50% probability level.

For all complexes, the Au-C bond lengths were in good agreement with previously reported NHC-gold(I) complexes and indicated a strong bond. As seen in other NHC*-gold(I) acetylides, the bond between the gold atom and the alkynyl ligand of complexes **3.15**-**3.19** was slightly shorter than that to the carbene, however still within the margins of acceptable Au-C bond lengths.[26] The C_{30}-N_3 bond lengths of 1.113(12) Å and 1.140(5) Å, for complexes **3.13** and **3.14** respectively, were characteristic of a C-N triple bond.[32,33] The C-C bond lengths of the alkyne (C_{30}-C_{31}) in the 1.193(6)-1.217(7) Å range confirmed the presence of a triple bond.[32] Furthermore, the slightly shorter C_{31}-C_{32} single bond concurs with other reported gold(I) acetylides.[9] As expected for gold(I) complexes, complexes **3.13** and **3.15**-**3.19** displayed almost linear geometry at the gold(I) centre with bond angles of 173.24(18)-179.65(16) °. Complex **3.14** also exhibited linearity with a 180.00(15) ° angle at the gold centre.

Table 3.1 Selected bond lengths (Å) and angles (°) for complexes **3.13**-**3.19**.

	C(8)-Au	Au-C(30)	C(30)-N(3)	C(30)-C(31)	C(31)-C(32)	C(8)-Au-C(30)	Au···Au
3.13	2.031(8)	2.026(9)	1.113(12)	-	-	179.60(4)	3.2598(16)
3.14	-	1.993(4)	1.140(5)	-	-	-	-
3.15	2.018(2)	1.993(3)	-	1.198(4)	-	175.94(9)	3.5242(3)
3.16	2.028(4)	1.994(4)	-	1.196(6)	1.437(5)	179.65(16)	-
3.17	2.019(2)	1.994(2)	-	1.197(4)	1.442(3)	173.28(9)	-
3.18	2.021(4)	1.982(5)	-	1.217(7)	1.430(7)	173.24(18)	3.2077(9) 3.2666(9)
3.19	2.033(4)	1.999(4)	-	1.193(6)	1.445(6)	173.46(17)	3.3318(5)

As shown for the imidazolium salts in Chapter 2, the $Au(CN)_2^-$ anion of **3.14** is positioned near to the imidazolium proton. There are short contacts of 2.346 Å between the hydrogen atom of the imidazolium and the nitrogen atom of the cyanide. The same nitrogen atom interacts with a hydrogen atom of the CH_2 group on the NHC ligand (N···H 2.709 Å).

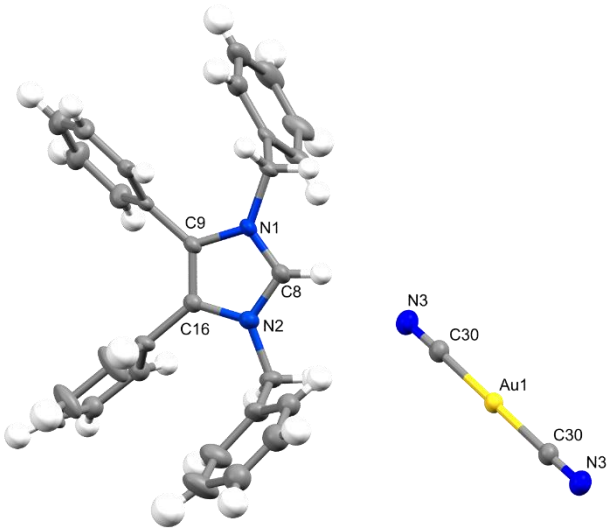

Figure 3.6 X-ray diffraction structure of complex **3.14**; thermal ellipsoids drawn on the 50% probability level. Disorder neglected.

The compact linear C≡N/C bond featured in these complexes avoids steric interactions with the bulky NHC phenyl rings. This often results in intermolecular aurophilic interactions between complexes in the solid state as there is no steric hindrance at the gold centre. These Au···Au interactions are seen in complexes **3.13**, **3.15**, **3.18** and **3.19** (**Table 3.1**).

4-Fluorophenylethynyl derivative **3.18** displayed the shortest aurophilic interactions. Two molecules presented a Au···Au distance of 3.2077(9) Å, while the distance to the next contact was 3.2666(9) Å (**Figure 3.7**). These values signify intermolecular aurophilic bonding as they are within the accepted range of 2.50-3.50 Å.[34,35] Cyano compound **3.13** and trifluoromethyl compound **3.19** exhibited aurophilic interactions with Au···Au distances of 3.2598(16) Å and 3.3318(5) Å, respectively. Lastly, ethynyl compound **3.15** had a distance of 3.5242(3) Å between gold(I) centres which is at the end of the acceptable range indicating very weak aurophilic interactions. The distance to the next gold(I) contact was 8.2461(4) Å which is well beyond the accepted range. However, the crystal packing of **3.15** does present an interesting "zig-zag" pattern with molecules alternating between the short Au···Au distance and the longer length (**Figure 3.8**).

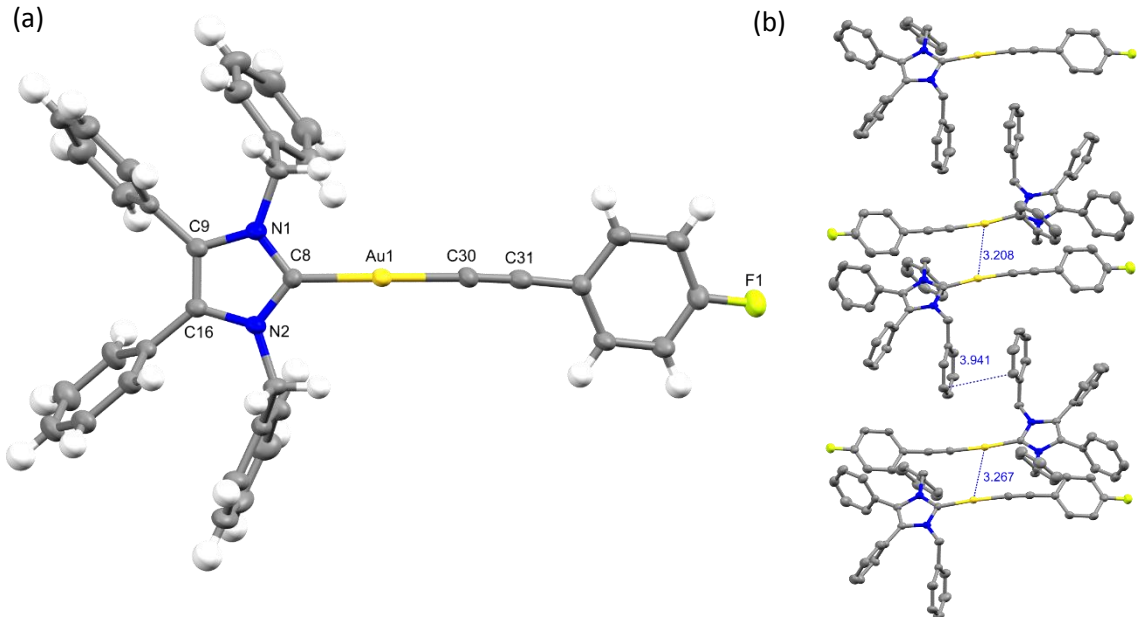

Figure 3.7 (a) X-ray diffraction structure of complex **3.18**; thermal ellipsoids drawn on the 50% probability level. Solvent molecules have been omitted for clarity. (b) A chain of molecules with the distances marked in blue between the gold atoms, and two carbon atoms in opposite phenyl rings (3.941(8) Å).

Most of the NHC*-gold(I) complexes presented interesting columnar solid state structures, whereby they were arranged either head-to-head or head-to-tail. Complexes **3.13**, **3.15**, **3.18** and **3.19** formed chains of molecules in a head-to-tail arrangement which allowed the phenyl rings of neighbouring NHCs to be positioned face-to-face. As seen in **Figure 3.8**, the phenyl rings of **3.15** overlapped along the "zig-zag" chain. However, a distance of 3.972 Å[a] was measured between the phenyl ring centroids which is outside the 3.3-3.8 Å range that is commonly accepted for π-π stacking.[36]

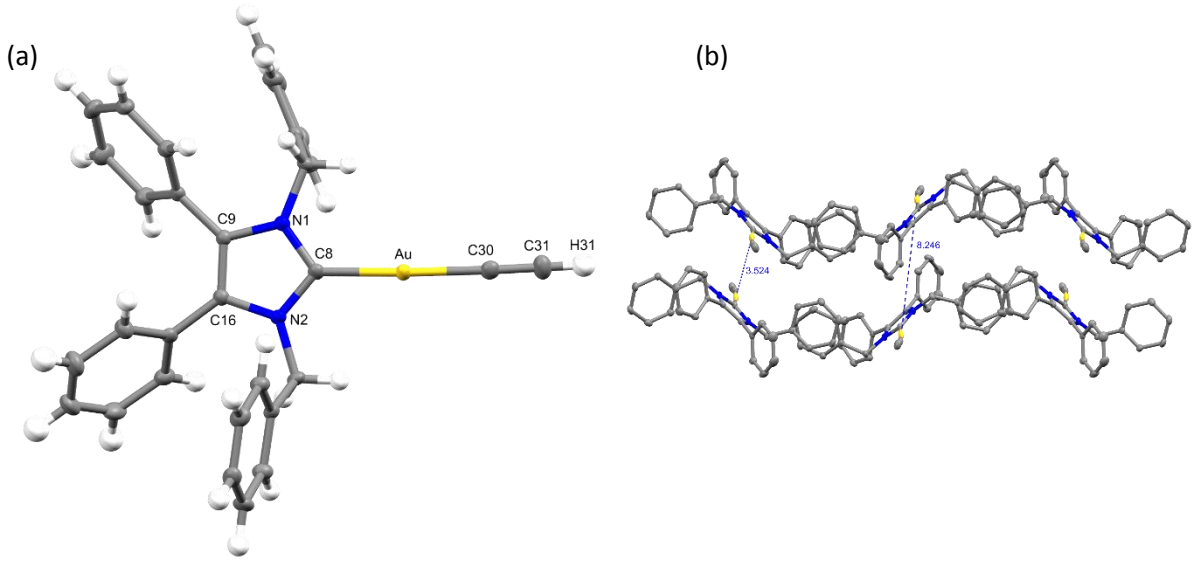

Figure 3.8 (a) X-ray diffraction structure of complex **3.15**; thermal ellipsoids drawn on the 50% probability level. (b) Crystal packing of **3.15** along the *a*-axis showing the "zig-zag" pattern. The Au···Au distances are shown between the rows marked in blue. Hydrogen atoms are omitted for clarity.

Conversely, the 4-methoxyphenylethynyl complex **3.17** showed an array of molecules assembled in a head-to-head pattern. Between the rows the phenyl rings of the NHCs are arranged face-to-face (centroid distance: 3.925 Å). The methoxy moieties are positioned towards one another, however they presented a shorter contact to a hydrogen atom of an adjacent NHC phenyl ring (O···H 2.671 Å[a]) rather than a hydrogen atom of the opposite methoxy group (O···H 4.247 Å). Solvate CH_2Cl_2 molecules are interpolated between the gold atoms, with Au···C distances of 4.057(5) Å, which prevented any aurophilic interactions.

[a] Standard uncertainties for bond lengths are not provided for distances measured between calculated ring centroids or hydrogen atoms.

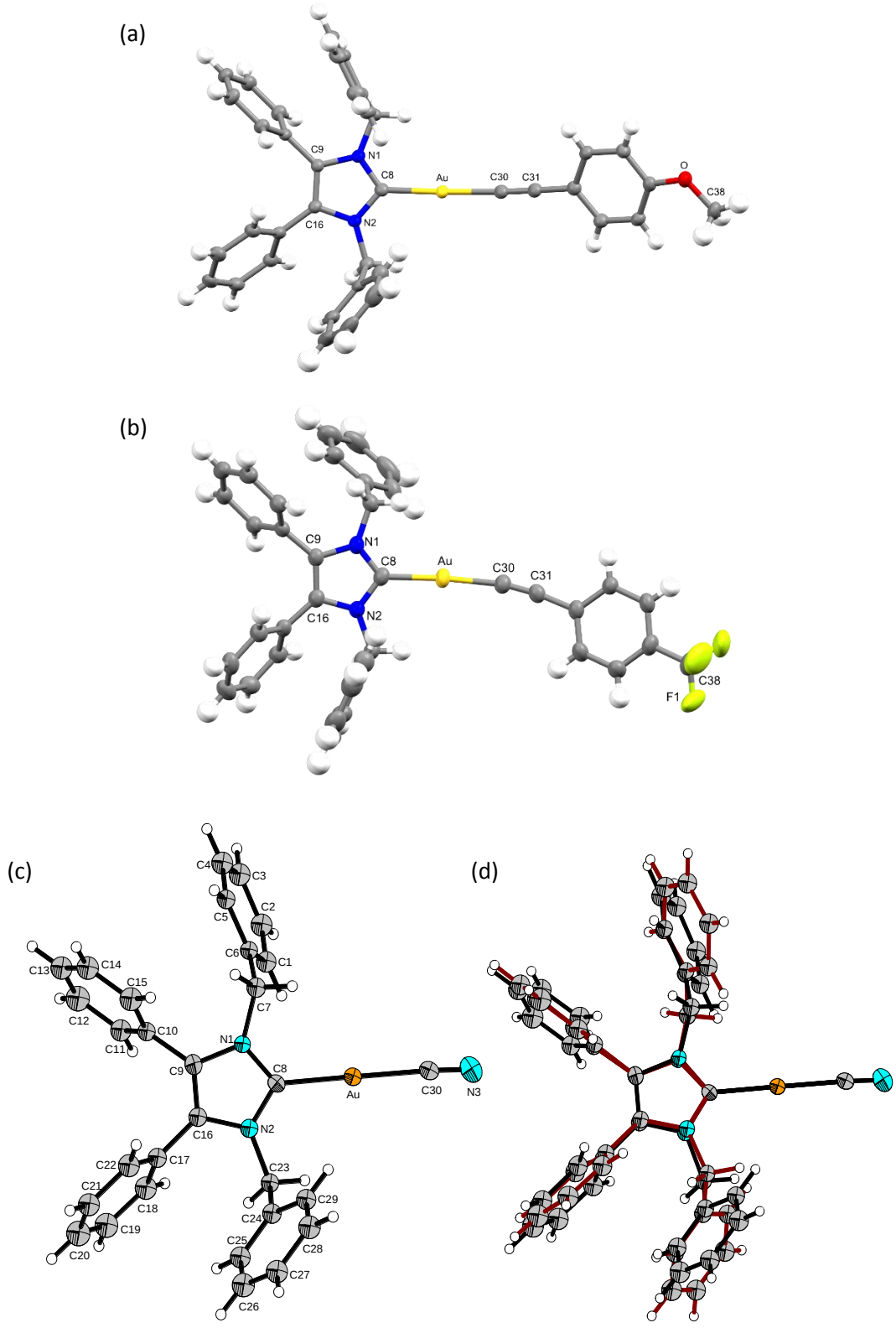

Figure 3.9 X-ray diffraction structures of complexes (a) **3.17**, (b) **3.19** and (c) **3.13**; thermal ellipsoids are drawn on the 50% probability level. (d) Disorder, shown with red bonds, due to the positioning of **3.13** along a mirror plane. Structures are generally drawn on Mercury, however due to the disorder complex **3.13** was drawn on Olex2.

CCDC 1854008 (**3.13**), CCDC 2012889 (**3.15**), CCDC 2012890 (**3.16**), CCDC 2012893 (**3.17**), CCDC 2012891 (**3.18**) and CCDC 2012892 (**3.19**) contain the supplementary crystallographic data for this Chapter, available free of charge from the Cambridge Crystallographic Data Centre via www.ccdc.cam.ac.uk/structures.

Table 3.2 X-ray crystal data and structure refinement for complexes **3.13**-**3.16**.

	3.13	**3.14**	**3.15**	**3.16**
Empirical Formula	$C_{30}H_{24}AuN_3$	$C_{31}H_{25}N_4Au$	$C_{31}H_{25}N_2Au$	$C_{37}H_{29}N_2Au$
Formula Weight ($g \cdot mol^{-1}$)	623.49	650.51	622.49	698.59
Temperature (K)	100(2)	100(2)	100(2)	100(2)
Crystal system	Monoclinic	Triclinic	Monoclinic	Monoclinic
Space group	$P2_{1/m}$ (#11)	$P\bar{1}$ (#2)	$P2_1/c$ (#14)	$P2_1/n$ (#14)
Unit cell dimensions				
a (Å)	12.8150(7)	10.0263(2)	12.3303(3)	17.3520(3)
b (Å)	6.4797(3)	10.2754(2)	18.3303(3)	10.4155(1)
c (Å)	15.6802(8)	13.8269(3)	11.0923(2)	17.6623(2)
α (°)	90	82.053(2)	90	90
β (°)	112.268(6)	77.990(2)	103.150(2)	114.610(2)
γ (°)	90	69.584(2)	90	90
Volume ($Å^3$)	1204.94(12)	1302.45(5)	2441.32(9)	2902.14(8)
Z	2	2	4	4
Density (calcd) (mg/m^3)	1.718	1.659	1.694	1.599
Absorption coefficient (mm^{-1})	11.641	10.810	6.048	9.730
F (000)	608	636	1216	1376
Crystal size (mm^3)	0.255 × 0.034 × 0.026	0.102 x 0.100 x 0.087	0.221 x 0.172 x 0.100	0.172 x 0.108 x 0.018
θ (°)	3.727 to 77.196	3.276 to 76.861	2.796 to 32.854	4.676 to 76.852
Index ranges	$-16 \le h \le 15$	$-12 \le h \le 12$	$-18 \le h \le 17$	$-21 \le h \le 20$
	$-8 \le k \le 8$	$-12 \le k \le 12$	$-27 \le k \le 27$	$-13 \le k \le 12$
	$-19 \le l \le 19$	$-17 \le l \le 17$	$-16 \le l \le 16$	$-22 \le l \le 22$
Reflections collected	24420	41725	76578	54931
Independent reflections R_{int}	2760 (0.1335)	5451 (0.0322)	8710 (0.0446)	6111 (0.0645)
Completeness to θ_{max} (%)	99.8	100.0	99.8	100.0
Absorption correction	Gaussian	Gaussian	Gaussian	Gaussian
Max and min transmission	0.788 and 0.291	0.544 and 0.434	0.601 and 0.377	0.845 and 0.363
Refinement method	Full–matrix Least–squares on F^2	Full–matrix Least–squares on F^2	Full–matrix Least–squares on F^2	Full–matrix Least–squares on F^2
Data/ restraints/ parameters	2760/0/147	5451 / 0 / 326	8710 / 0 / 307	6111 / 0 / 361
Goodness-of-fit on F2	1.139	1.089	1.081	1.031
Final R indices [$I > 2\sigma(I)$]	R1 = 0.0442	R1 = 0.0254	R1 = 0.0246	R1 = 0.0328
	wR2 = 0.0983	wR2 = 0.0595	wR2 = 0.0505	wR2 = 0.0836
R indices (all data)	R1 = 0.0464	R1 = 0.0339	R1 = 0.0331	R1 = 0.0399
	wR2 = 0.0998	wR2 = 0.0644	wR2 = 0.0535	wR2 = 0.0903
Largest diff. peak and hole	1.982 and −1.411	1.308 and −0.875	1.321 and −0.610	1.857 and −1.785

Table 3.3 X-ray crystal data and structure refinement for complexes **3.17**-**3.19**.

	3.17	**3.18**	**3.19**
Empirical Formula	C_{77} H_{64} N_4 O_2 Cl_2 Au_2	C_{149} H_{114} N_8 F_4 Cl_2 Au_4	C_{38} H_{28} F_3 N_2 Au
Formula Weight ($g \cdot mol^{-1}$)	1542.15	2951.24	766.59
Temperature (K)	100(2)	100(2)	100(2)
Crystal system	Monoclinic	Monoclinic	Monoclinic
Space group	$P2_1/n$ (#14)	I2/a (#15)	$P2_1/n$ (#14)
Unit cell dimensions			
a (Å)	15.0757(2)	31.4887(3)	14.9691(2)
b (Å)	9.14899(9)	9.06171(8)	10.91009(9)
c (Å)	23.2187(2)	42.0249(3)	19.2159(2)
α (°)	90	90	90
β (°)	93.0801(8)	98.2131(7)	90.0427(7)
γ (°)	90	90	90
Volume ($Å^3$)	3197.87(6)	11868.46(18)	3138.23(6)
Z	2	4	4
Density (calcd) (mg/m^3)	1.602	1.652	1.623
Absorption coefficient (mm^{-1})	9.665	10.007	9.199
F (000)	1524	5800	1504
Crystal size (mm^3)	0.121 x 0.066 x 0.020	0.201 x 0.047 x 0.027	0.151 x 0.108 x 0.039
θ (°)	3.413 to 76.907	3.292 to 76.873	3.742 to 76.879
Index ranges	$-18 \le h \le 18$	$-37 \le h \le 39$	$-18 \le h \le 18$
	$-11 \le k \le 11$	$-11 \le k \le 10$	$-13 \le k \le 13$
	$-29 \le l \le 29$	$-52 \le l \le 51$	$-24 \le l \le 24$
Reflections collected	34565	78037	63588
Independent reflections R_{int}	6711 (0.0383)	12388 (0.0507)	6602 (0.0516)
Completeness to θ_{max} (%)	100.0	99.9	100.0
Absorption correction	Gaussian	Gaussian	Gaussian
Max and min transmission	0.845 and 0.521	0.762 and 0.323	0.724 and 0.366
Refinement method	Full–matrix	Full–matrix	Full–matrix
	Least–squares on F^2	Least–squares on F^2	Least–squares on F^2
Data/ restraints/ parameters	6711 / 0 / 407	12388 / 0 / 753	6602 / 0 / 397
Goodness-of-fit on F2	1.029	1.055	1.033
Final R indices [$I > 2\sigma(I)$]	R1 = 0.0209	R1 = 0.0477	R1 = 0.0361
	wR2 = 0.0496	wR2 = 0.1204	wR2 = 0.0886
R indices (all data)	R1 = 0.0243	R1 = 0.0540	R1 = 0.0401
	wR2 = 0.0515	wR2 = 0.1274	wR2 = 0.0915
Largest diff. peak and hole	0.770 and –0.851	3.002 and –2.638	3.496 and –1.281

3.4 Biological Evaluation

The *in vitro* biological evaluation of the compounds synthesised in this chapter was carried out by Prof. Rainer Schobert and Sofia I. Bär at the University of Bayreuth, Germany. The anticancer activity of compounds **3.13** and **3.15**-**3.19** were tested via MTT-based proliferation assays against the human colon carcinoma cell line HCT-116^{wt} and the multidrug-resistant human breast carcinoma cell line MCF-7^{topo} (**Table 3.4**).

Table 3.4 IC_{50} values (μM) of compounds **3.13** and **3.15**-**3.19** against HCT-116^{wt} and MCF-7^{topo} cells after 72 h of incubation.

Compound	HCT-116^{wt}	MCF-7^{topo}
3.13	14.8 ± 1.9	10.8 ± 0.9
3.15	3.2 ± 0.3	7.3 ± 0.8
3.16	14.1 ± 1.3	>50
3.17	8.3 ± 0.5	>50
3.18	>50	>50
3.19	>50	>50

Against the colon carcinoma cell line HCT-116^{wt} compounds **3.15** and **3.17** showed good single-digit micromolar IC_{50} values, while compounds **3.13** and **3.16** exhibited moderate cytotoxicity with IC_{50} values of 14 μM. Compound **3.15** also presented a low IC_{50} value on the breast carcinoma cell line MCF-7^{topo}. Interestingly, compound **3.13** exhibited higher activity against the MCF-7^{topo} cell line than the HCT-116^{wt} cell line. Disappointingly, compounds **3.16**-**3.19** reported very little activity with values over 50 μM on the breast cancer cell line; activity above 50 μM was also observed on the colon cancer cell line for **3.18** and **3.19**. These high values correlate with the solubility of these alkynyl compounds, as **3.16**-**3.19** displayed poor water solubility.

Comparing the two smaller compounds, the acetylide **3.15** was considerably more active than the cyanide complex **3.13**. The cyanide's deactivating effect on the gold contributed to its low activity. Electronic properties also effect the cytotoxicity of the phenyl based complexes. Considering the colon cancer cell line results, this is evident as the methoxy derivative **3.17**

exhibited the highest activity due to its electron donating properties and fluorinated complexes **3.18** and **3.19** exhibited the lowest activity due to their deactivating substituents. Additionally, these IC_{50} values indicated that the addition of a phenyl group decreased the activity of these complexes as the small acetylide **3.15** displayed the highest activity.

Overall, the highest anticancer activity was observed for NHC*-Au-CCH (**3.15**) with low micromolar activity (IC_{50}: 3.2 ± 0.3 μM) against the colon carcinoma cell line HCT-116^{wt}. In comparison to NHC*-gold chloride (**1.21**: 22.7 μM for HCT-116^{wt} and 20.8 μM for MCF-7^{topo}) compound **3.15** showed a seven-fold increase in cytotoxicity on the HCT-116^{wt} cell line. Thus, the most active compounds, the ethynyl derivative **3.15** and 4-methoxyphenylethynyl complex **3.17** showed potential as anticancer agents, however, in comparison to complexes previously developed (**2.6**, Chapter 2) these NHC*-gold(I) acetylides are not sufficiently cytotoxic to be pursued as anticancer drug candidates. However, the complexes reported herein compare well to the gold(I) acetylides highlighted in the introduction.

3.5 Conclusion and Outlook

A series of NHC*-gold(I) cyanides and acetylides have been synthesised and characterised, including X-ray crystallography. The solid state structures of **3.13**, **3.15**, **3.18** and **3.19** displayed weak aurophilicity with Au···Au interactions in the 3.2077(9)-3.5242(3) Å range. *In vitro* cytotoxicity of compounds **3.13** and **3.15**-**3.19** were tested by our collaborators against the human colon cancer cell line HCT-116^{wt} and the multidrug-resistant human breast cancer cell line MCF-7^{topo}. Compounds **3.15** and **3.17** displayed single-digit micromolar activity, with ethynyl derivative **3.15** being the most active with IC_{50} values of 3.2 ± 0.3 μM and 7.3 ± 0.8 μM against HCT-116^{wt} and MCF-7^{topo} respectively. This research contributes to the development of a structure-activity relationship for NHC-gold(I) alkynyl complexes. To the best of our knowledge, these complexes are some of the first examples of NHC-gold(I) cyanides and acetylides that have been assessed for their antiproliferative effects. Future work will involve pursuing ethynyl compound **3.15** for azide-alkyne cycloaddition reactions in an effort to afford more complex coordinated compounds. Additionally, probing the luminescent properties of these acetylides is of interest in the future.

3.6 Experimental Section

(1,3-Dibenzyl-4,5-diphenylimidazol-2-ylidene)gold(I) cyanide (3.13)

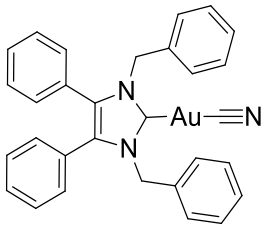

NHC*-gold(I) chloride (**1.21**) (65 mg, 0.103 mmol) and potassium cyanide (7.5 mg, 0.115 mmol) were stirred in CH_2Cl_2 (15 mL) under reflux for 48 h. The reaction was washed with deionised water (2 × 10 mL). The organic solution was extracted and dried over anhydrous $MgSO_4$. This was filtered, and the excess solvent reduced under pressure to 3 mL. Pentane (40 mL) was added to precipitate a white solid. The product was filtered, washed with pentane (15 mL), and dried *in vacuo* to give a white solid (40.8 mg, 66%). ^{1}H-NMR (400 MHz, $CDCl_3$, δ ppm): 7.32 (t, *J* = 7.4 Hz, 2H, ArCH), 7.25–7.20 (m, 10H, ArCH), 6.99 (t, *J* = 5.9 Hz, 8H, ArCH), 5.37 (s, 4H, CH_2). ^{13}C-NMR (101 MHz, $CDCl_3$, δ ppm): 182.9 (NCN), 152.6 (C≡N), 135.7 (C), 132.6 (C), 130.9 (CH), 129.7 (CH), 128.9 (CH), 128.8 (CH), 128.4 (CH), 127.6 (C), 127.2 (CH), 53.0 (CH_2). HRMS (ESI$^+$) *m*/*z*: $[M + H]^+$ calcd. 624.1714; found 624.1720. IR (ATR, cm^{-1}): 3058 (w), 3030 (w), 2143 (w) (C≡N), 1594 (w), 1488 (m), 1447 (m), 1348 (m), 1026 (m), 758 (m), 696 (s). Melting point range: 265–268 °C. Anal. calcd. for $C_{30}H_{24}N_3Au$ (623.51) in %: C, 57.79; H, 3.88; N, 6.74. Found: C, 57.14; H, 3.59; N, 6.40.

1,3-Dibenzyl-4,5-diphenylimidazolium dicyanoaurate(I) (3.14)

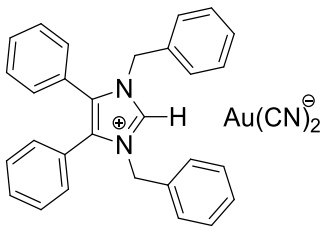

KCN (7.5 mg, 0.115 mmol) was dissolved in 5 mL H_2O and added to **1.21** (65 mg, 0.103 mmol) in 6 mL EtOAc. This stirred at rt for 24 h. The reaction was washed with deionised water (2 x 10 mL). The extracted organic solution was dried over $MgSO_4$ and filtered. The solvent was

removed under reduced pressure to approximately 2 mL. Pentane (40 mL) was added to precipitate a white solid. This was filtered, washed with pentane (15 mL) and dried *in vacuo* (38 mg, 57%). ^{1}H NMR (400 MHz, $CDCl_3$, δ ppm): 8.66 (s, 1H, $CH_{imidazole}$), 7.48-7.35 (m, 12H, ArCH) 7.31 (d, J = 6.9 Hz, 4H, ArCH), 7.14 (dd, J = 6.4, 3.0 Hz, 4H, ArCH), 5.30 (s, 4H, CH_2). ^{13}C NMR (101 MHz, $CDCl_3$, δ ppm*):* 134.6 (C), 133.5 (CH), 132.3 (C), 131.1 (CH), 130.9 (CH), 129.8 (CH), 129.7 (CH), 129.4 (CH), 128.7 (CH), 124.3 (C), 110.1 (C≡N), 52.3 (CH_2). HRMS (ESI^+) *m*/*z*: $[M - Au(CN)_2]^+$ calcd. 401.2012; found 401.2016. HRMS (ESI^-): *m*/*z* $[Au(CN)_2]^-$ calcd. 248.9727; found 248.9733. IR (ATR, cm^{-1}): 3120 (w), 3033 (w), 2141 (m) (C≡N), 1552 (m), 1489 (w), 1446 (m), 1022 (m). Anal. calcd. for $C_{31}H_{25}N_4Au$ (650.52) in %: C, 57.24; H, 3.87; N, 8.61. Found: C, 57.15; H, 3.69; N, 8.50.

(1,3-Dibenzyl-4,5-diphenylimidazol-2-ylidene)(ethynyl)gold(I) (3.15)

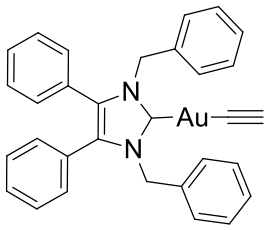

Ethynyltrimethylsilane (12 μL, 0.087 mmol, 1.1 equiv.) was added to a solution of **1.21** (50 mg, 0.079 mmol, 1.0 equiv.) in THF (10 mL). TBAF (1 M in THF- 0.87 mL, 0.087 mmol, 1.1 equiv.) was added dropwise and the reaction stirred at rt for 48 h. The solvent was removed under reduced pressure. The residue was dissolved in EtOAc (20 mL) and filtered through a short silica plug. The solvent was reduced to approximately 2 mL and pentane (40 mL) was added to precipitate the product. This was filtered, washed with pentane (15 mL) and dried *in vacuo* to give a white solid (30.1 mg, 61%). ^{1}H-NMR (400 MHz, $CDCl_3$, δ ppm): 7.29 (d, J = 7.4 Hz, 1H, ArCH) 7.20 (m, 10H, ArCH), 7.01 (dd, J = 7.4, 2.0 Hz, 4H, ArCH), 6.93 (m, 4H, ArCH), 5.45 (s, 4H, CH_2), 1.75 (s, 1H, CH). ^{13}C-NMR (101 MHz, $CDCl_3$, δ ppm): 187.1 (NCN), 136.0 (C), 132.3 (C), 130.9 (CH), 129.4 (CH), 128.7 (CH), 128.6 (CH), 128.1 (CH), 127.7 (C), 127.6 (CH), 122.2 (C≡C), 90.7 (CH), 52.8 (CH_2). HRMS (ESI^+) *m*/*z*: $[M+H]^+$ calcd. 623.1762; found 623.1749. IR (ATR, cm^{-1}): 3291 (w) (C-H), 3053 (w), 3027 (w), 1977 (w) (C≡C), 1603 (w), 1448 (m), 1407 (m), 1023 (m). Anal. calcd. for $C_{31}H_{25}N_2Au$ (622.51) in %: C, 59.81; H, 4.05; N, 4.50. Found: C, 59.28; H, 3.95; N, 4.32.

(1,3-Dibenzyl-4,5-diphenylimidazol-2-ylidene)(phenylethynyl)gold(I) (3.16)

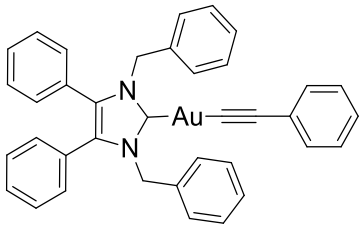

In a procedure identical to above reaction: Phenylethynyl-trimethylsilane (17.0 μL, 0.087 mmol, 1.1 equiv.), **1.21** (50 mg, 0.079 mmol, 1.0 equiv.), TBAF (1 M in THF- 0.087 mL, 0.087 mmol, 1.1 equiv.) stirred in THF (10 mL) at rt for 30 h. After workup and precipitation a white solid was formed (46.2 mg, 76%). ^{1}H-NMR (400 MHz, $CDCl_3$, δ ppm): 7.49 (d, *J* = 7.0 Hz, 2H, ArCH), 7.29 (m, 1H, ArCH), 7.19 (m, 12H, ArCH), 7.03 (d, *J* = 3.5 Hz, 4H, ArCH), 6.93 (m, 4H, ArCH), 5.49 (CH_2). ^{13}C-NMR (101 MHz, $CDCl_3$, δ ppm): 187.4 (NCN), 136.1 (C), 132.5 (CH), 132.3 (C), 130.9 (CH), 129.3 (CH), 128.7 (CH), 128.6 (CH), 128.0 (CH), 127.9 (CH), 127.7 (C), 126.4 (CH), 125.8 (C≡C), 105.3 (C≡C), 52.9 (CH_2). HRMS (ESI$^+$) *m*/*z*: $[M+H]^+$ calcd. 699.2075; found 699.2084. IR (ATR, cm^{-1}): 3055 (w), 2947 (w), 2120 (w) (C≡C), 1593 (w), 1485 (m), 1444 (m), 1021 (m). Anal. calcd. for $C_{37}H_{29}N_2Au$ (698.60) in %: C, 63.61; H, 4.18; N, 4.01. Found: C, 63.26; H, 4.04; N, 3.95.

(1,3-Dibenzyl-4,5-diphenylimidazol-2-ylidene)(4-methoxyphenylethynyl)gold(I) (3.17)

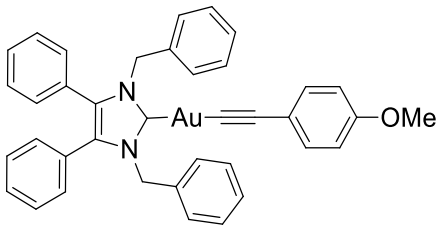

In a procedure identical to above reaction: (4-Methoxyphenylethynyl)trimethylsilane (18.5 μL, 0.087 mmol, 1.1 equiv.), **1.21** (50 mg, 0.079 mmol, 1.0 equiv.), TBAF (1 M in THF- 0.087 mL, 0.087 mmol, 1.1 equiv.) stirred in THF (10 mL) at rt for 30 h. After workup and precipitation a white solid was formed (50 mg, 88%). ^{1}H-NMR (400 MHz, $CDCl_3$, δ ppm): 7.43 (d, *J* = 8.8 Hz, 2H, ArCH), 7.28 (m, 1H, ArCH), 7.19 (m, 10H, ArCH), 7.03 (d, *J* = 3.7 Hz, 4H, ArCH), 6.93 (d, *J* = 7.1 Hz, 4H, ArCH), 6.76 (d, *J* = 8.7 Hz, 2H, ArCH), 5.49 (s, 4H, CH_2), 3.77 (s, 3H, CH_3). ^{13}C-

NMR (101 MHz, $CDCl_3$, δ ppm): 187.6 (NCN), 158.3 (C), 136.1 (C), 133.7 (CH), 132.3 (C), 130.9 (CH), 129.3 (CH), 128.6 (CH), 128.5 (CH), 128.0 (CH), 127.9 (CH), 125.9 (C≡C), 118.1 (C), 113.5 (CH), 105.1 (C≡C), 55.3 (CH_3), 52.9 (CH_2). HRMS (ESI$^+$) *m*/*z*: $[M + H]^+$ calcd. 729.2180; found 729.2171. IR (ATR, cm^{-1}): 3030 (w), 2961 (w), 2831 (w) (OCH_3), 2111 (w) (C≡C), 1601 (m), 1503 (s), 1435 (m), 1023 (m). Anal. calcd. for $C_{38}H_{31}N_2OAu$ (728.63) in %: C, 62.64; H, 4.29; N, 3.84. Found: C, 62.42; H, 3.97; N, 3.58.

(1,3-Dibenzyl-4,5-diphenylimidazol-2-ylidene)(4-fluorophenylethynyl)gold(I) (3.18)

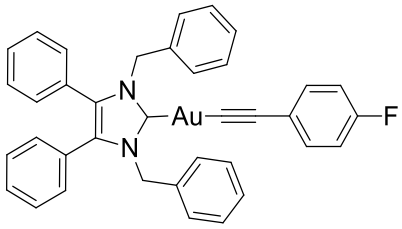

In a procedure identical to above reaction: (4-Fluorophenylethynyl)trimethylsilane (17.6 μL, 0.087 mmol, 1.1 equiv.), **1.21** (50 mg, 0.079 mmol, 1.0 equiv.), TBAF (1 M in THF- 0.087 mL, 0.087 mmol, 1.1 equiv.) stirred in THF (10 mL) at rt for 30 h. After workup and precipitation a white solid was formed (39.6 mg, 70%). ^{1}H-NMR (400 MHz, $CDCl_3$, δ ppm): 7.45 (dd, *J* = 8.7, 5.5 Hz, 2H, CH), 7.29 (m, 1H, ArCH), 7.20 (m, 10H, ArCH), 7.02 (m, 5H, ArCH), 6.92 (m, 6H, ArCH), 5.49 (s, 4H, CH_2). ^{13}C-NMR (101 MHz, $CDCl_3$, δ ppm): 187.3 (NCN), 136.1 (C), 134.1 (C), 134.0 (CH), 132.3 (C), 130.9 (CH), 129.3 (CH), 128.7 (CH), 128.6 (CH), 128.1 (CH), 127.7 (CH), 127.6 (CH), 121.8 (C≡C), 115.1 (C), 114.9 (CH), 104.1 (C≡C), 52.9 (CH_2). ^{19}F-NMR (376 MHz, $CDCl_3$, δ ppm): -114. 32. HRMS (ESI$^+$) *m*/*z*: $[M + H]^+$ calcd. 717.1980; found 717.1978. IR (ATR, cm^{-1}): 3054 (w), 2964 (w), 2113 (w) (C≡C), 1593 (w), 1497 (s), 1441 (m), 1203 (m) (C-F), 1022 (m). Anal. calcd. for $C_{37}H_{28}N_2FAu$ (716.60) in %: C, 62.01; H, 3.94; N, 3.91; F, 2.65. Found: C, 61.68; H, 3.77; N, 3.83; F, 3.04.

(1,3-Dibenzyl-4,5-diphenylimidazol-2-ylidene)[4-(trifluoromethyl)phenylethynyl]gold(I) (3.19)

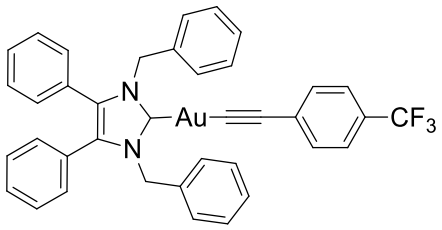

In a procedure identical to above reaction: [4-(Trifluoromethyl)phenyl] (trimethylsilyl)acetylene (20.4 μL, 0.087 mmol, 1.1 equiv.), **1.21** (50 mg, 0.079 mmol, 1.0 equiv.), TBAF (1 M in THF- 0.087 mL, 0.087 mmol, 1.1 equiv.) stirred in THF (10 mL) at rt for 24 h. After workup and precipitation a white solid was formed (37 mg, 60%). ^{1}H-NMR (400 MHz, $CDCl_3$, δ ppm): 7.56 (d, *J* = 8.0 Hz, 2H, ArCH), 7.46 (d, *J* = 8.3 Hz, 2H, ArCH), 7.29 (d, *J* = 7.5 Hz, 1H, ArCH), 7.21 (m, 10H, ArCH), 7.03 (dd, *J* = 7.2, 2.2 Hz, 4H, ArCH), 6.93 (m, 4H, ArCH), 5.49 (s, 4H, CH_2). ^{13}C-NMR (101 MHz, $CDCl_3$, δ ppm): 187.0 (NCN), 136.0 (C), 132.5 (CH), 132.4 (C), 132.1 (C), 130.9 (CH), 129.4 (CH), 128.7 (CH), 128.6 (CH), 128.1 (CH), 127.6 (CH), 127.5 (C), 124.9 (CH), 124.8 (C≡C), 103.9 (C≡C), 52.9 (CH_2). ^{19}F-NMR (376 MHz, $CDCl_3$, δ ppm): -62.52. HRMS (ESI^+) *m*/z: $[M + H]^+$ calcd. 767.1948; found 767.1922. IR (ATR, cm^{-1}): 3024 (w), 2119 (w) (C≡C), 1608 (m), 1493 (w), 1434 (m), 1113 (s) (C-F), 1063 (s). Anal. calcd. for $C_{38}H_{28}N_2F_3Au$ (766.60) in %: C, 59.54; H, 3.68; N, 3.65; F, 7.43. Found: C, 59.33; H, 3.43; N, 3.52; F, 7.09.

References

(1) Graham, G. G.; Haavisto, T. M.; McNaught, P. J.; Browne, C. D.; D, C. G. The Effect of Smoking on the Distribution of Gold in Blood. *J. Rheumatol.* **1982**, *9*, 527–531.

(2) Ahmad, S. The Chemistry of Cyano Complexes of Gold(I) with Emphasis on the Ligand Scrambling Reactions. *Coord. Chem. Rev.* **2004**, *248*, 231–243.

(3) Tepperman, K.; Zhang, Y.; Roy, P. W.; Floyd, R.; Zhao, Z.; Dorsey, J. G.; Elder, R. C. Transport of the Dicyanogold(I) Anion. *Met. Based. Drugs* **1994**, *1*, 433–443.

(4) Gandin, V.; Fernandes, A. P.; Rigobello, M. P.; Dani, B.; Sorrentino, F.; Tisato, F.; Björnstedt, M.; Bindoli, A.; Sturaro, A.; Rella, R.; Marzano, C. Cancer Cell Death

Induced by Phosphine Gold(I) Compounds Targeting Thioredoxin Reductase. *Biochem. Pharmacol.* **2010**, *79*, 90–101.

(5) Karadağ, A.; Aydın, A.; Tekin, Ş.; Akbaş, H.; Şahin, O.; Sen, F. Synthesis, Characterization and Anticancer Activity in Vitro Evaluation of Novel Dicyanoaurate (I)-Based Complexes. *Life Sci.* **2020**, *251*, 117635–117648.

(6) Raubenheimer, H. G.; Lindeque, L.; Cronje, S. Synthesis and Characterisation of Neutral and Cationic Diamino Carbene Complexes of Gold(I). *J. Organomet. Chem.* **1996**, *511*, 177–184.

(7) Celik, M. A.; Dash, C.; Adiraju, V. A. K.; Das, A.; Yousufuddin, M.; Frenking, G.; Dias, H. V. R. End-On and Side-On π-Acid Ligand Adducts of Gold(I): Carbonyl, Cyanide, Isocyanide, and Cyclooctyne Gold(I) Complexes Supported by N-Heterocyclic Carbenes and Phosphines. *Inorg. Chem.* **2013**, *52*, 729–742.

(8) Roşca, D.-A.; Fernandez-Cestau, J.; Romanov, A. S.; Bochmann, M. Synthesis, C-N Cleavage and Photoluminescence of Gold(III) Isocyanide Complexes. *J. Organomet. Chem.* **2015**, *792*, 117–122.

(9) Shakirova, J. R.; Tomashenko, O. A.; Grachova, E. V; Starova, G. L.; Sizov, V. V; Khlebnikov, A. F.; Tunik, S. P. Gold (I)– Alkynyl Complexes with an N-Donor Heterocyclic Ligand: Synthesis and Photophysical Properties. *Eur. J. Inorg. Chem.* **2017**, 4180–4186.

(10) Garg, J. A.; Blacque, O.; Heier, J.; Venkatesan, K. (Benzimidazolin-2-Ylidene)-Au(I)-Alkynyl Complexes: Syntheses, Structure, and Photophysical Properties. *Eur. J. Inorg. Chem.* **2012**, 1750–1763.

(11) Halliday, C. J. V; Lynam, J. M. Gold-Alkynyls in Catalysis: Alkyne Activation, Gold Cumulenes and Nuclearity. *Dalton Trans.* **2016**, *45*, 12611–12626.

(12) Guo, L.; Song, F.; Zhu, S.; Li, H.; Chu, L. Syn-Selective Alkylarylation of Terminal Alkynes via the Combination of Photoredox and Nickel Catalysis. *Nat. Commun.* **2018**, *9*, 4543–4550.

(13) Robilotto, T. J.; Deligonul, N.; Updegraff, J. B.; Gray, T. G. Azido, Triazolyl, and

Alkynyl Complexes of Gold(I): Syntheses, Structures, and Ligand Effects. *Inorg. Chem.* **2013**, *52*, 9659–9668.

(14) Boominathan, M.; Pugazhenthiran, N.; Nagaraj, M.; Muthusubramanian, S.; Murugesan, S.; Bhuvanesh, N. Nanoporous Titania-Supported Gold Nanoparticle-Catalyzed Green Synthesis of 1,2,3-Triazoles in Aqueous Medium. *ACS Sustain. Chem. Eng.* **2013**, *1*, 1405–1411.

(15) Wang, Y.; Burke, K. A. Phase Behavior of Main-Chain Liquid Crystalline Polymer Networks Synthesised by Alkyne-Azide Cycloaddition Chemistry. *Soft Matter* **2018**, *14*, 9885–9900.

(16) Zhou, D.; Chen, Y.; Chen, L.; Li, F.; Yao, K. Liquid Crystallinity and Enhanced Photoluminescence of Terphenyl-Containing Poly(1-Alkynes) with Tuning Spacers and Tails. *Synth. Met.* **2010**, *160*, 892–905.

(17) Mohr, F.; Puddephatt, R. J. Golden Crowns: Cation Binding by Macrocyclic Gold(I) Crown Ether Derivatives. *J. Organomet. Chem.* **2004**, *689*, 374–379.

(18) Hau, F. K.-W.; Yam, V. W.-W. Synthesis and Cation-Binding Studies of Gold(I) Complexes Bearing Oligoether Isocyanide Ligands with Ester and Amide as Linkers. *Dalton Trans.* **2016**, *45*, 300–306.

(19) Schuh, E.; Valiahdi, S. M.; Jakupec, M. A.; Keppler, B. K.; Chiba, P.; Mohr, F. Synthesis and Biological Studies of Some Gold(I) Complexes Containing Functionalised Alkynes. *Dalton Trans.* **2009**, 10841–10845.

(20) Chui, C.-H.; Wong, R. S.-M.; Gambari, R.; Cheng, G. Y.-M.; Yuen, M. C.-W.; Chan, K.-W.; Tong, S.-W.; Lau, F.-Y.; Lai, P. B.-S.; Lam, K.-H.; Ho, C.-L.; Kan, C.-W.; Leung, K. S.-Y.; Wong, W.-Y. Antitumor Activity of Diethynylfluorene Derivatives of Gold(I). *Bioorg Med. Chem.* **2009**, *17*, 7872–7877.

(21) Andermark, V.; Göke, K.; Kokoschka, M.; Abu el Maaty, M. A.; Lum, C. T.; Zou, T.; Sun, R. W.; Aguiló, E.; Oehninger, L.; Rodríguez, L.; Bunjes, H.; Wöl, S.; Che, C.; Ott, I. Alkynyl Gold (I) Phosphane Complexes : Evaluation of Structure–Activity-Relationships for the Phosphane Ligands, Effects on Key Signaling Proteins and

Preliminary in-Vivo Studies with a Nanoformulated Complex. *J. Inorg. Biochem.* **2016**, *160*, 140–148.

(22) Abas, E.; Espallargas, N.; Burbello, G.; Mesonero, J. E.; Rodriguez-Dieguez, A.; Grasa, L.; Laguna, M. Anticancer Activity of Alkynylgold(I) with $P(NMe_2)_3$ Phosphane in Mouse Colon Tumors and Human Colon Carcinoma Caco-2 Cell Line. *Inorg. Chem.* **2019**, *58*, 15536–15551.

(23) Gao, L.; Partyka, D. V; Updegraff III, J. B.; Deligonul, N.; Gray, T. G. Synthesis, Structures, and Excited-State Geometries of Alkynylgold(I) Complexes. *Eur. J. Inorg. Chem.* **2009**, *2009*, 2711–2719.

(24) Estrada-Ortiz, N.; Guarra, F.; de Graaf, I. A. M.; Marchetti, L.; de Jager, M. H.; Groothuis, G. M. M.; Gabbiani, C.; Casini, A. Anticancer Gold N -Heterocyclic Carbene Complexes : A Comparative in Vitro and Ex Vivo Study. *ChemMedChem* **2017**, *12*, 1429–1435.

(25) Meier-Menches, S. M.; Aikman, B.; Döllerer, D.; Klooster, W. T.; Coles, S. J.; Santi, N.; Luk, L.; Casini, A.; Bonsignore, R. Comparative Biological Evaluation and G-Quadruplex Interaction Studies of Two New Families of Organometallic Gold (I) Complexes Featuring N - Heterocyclic Carbene and Alkynyl Ligands. *J. Inorg. Biochem.* **2020**, *202*, 110844–110855.

(26) Oberkofler, J.; Aikman, B.; Bonsignore, R.; Pöthig, A.; Platts, J.; Casini, A.; Kühn, F. E. Exploring the Reactivity and Biological Effects of Heteroleptic N-Heterocyclic Carbene Gold (I) -Alkynyl Complexes. *Eur. J. Inorg. Chem.* **2020**, 1040–1051.

(27) Hormann, A. L.; Shaw III, C. F.; Bennett, D. W.; Reiff, W. M. Solid-State Structure and Solution Equilibria of Cyano(Triethylphosphine)Gold(I). *Inorg. Chem.* **1986**, *25*, 3957–3961.

(28) Al-Maythalony, B. A.; Wazeer, M. I. M.; Isab, A. A. Synthesis of Aurocyanide and Auricyanide Complexes of Phosphines, Phosphine Sulfides and Phosphine Selenides, and Their Characterization by IR, Far-IR, UV Solution, and Solid-State NMR Spectroscopic Methods. *J. Coodination Chem.* **2010**, *63*, 3824–3832.

(29) Mooney, Á.; Tiedt, R.; Maghoub, T.; O'Donovan, N.; Crown, J.; White, B.; Kenny, P. T. M. Structure–Activity Relationship and Mode of Action of *N* -(6-Ferrocenyl-2-Naphthoyl) Dipeptide Ethyl Esters: Novel Organometallic Anticancer Compounds. *J. Med. Chem.* **2012**, *55*, 5455–5466.

(30) Klauke, K.; Werner, S.; Mohr, F. Ethynyl Complexes of Gold (I) Formed by Transmetallation Using Tin (IV) or Silicon (IV) Compounds. *Eur. J. Inorg. Chem.* **2018**, 1053–1056.

(31) Heuft, M. A.; Collins, Shawn, K.; Yap, G. P. A.; Fallis, A. G. Synthesis of Diynes and Tetraynes from in Situ Desilylation/Dimerization of Acetylenes. *Org. Lett.* **2001**, *3*, 2883–2886.

(32) Paolini, J. P. The Bond Order—Bond Length Relationship. *J. Comput. Chem.* **1990**, *11*, 1160–1163.

(33) Al-Arfaj, A. R.; Reibenspies, J. H.; Hussain, M. S.; Darensbourg, M. Y.; Akhtar, N.; Isab, A. A. Cyano[Tri(Cyclohexyl)Phosphino]Gold(I), [Au(CN){$(C_6H_{11})_3P$}]. *Acta Cryst.* **1997**, *C53*, 1553–1555.

(34) Schmidbaur, H.; Schier, A. Aurophilic Interactions as a Subject of Current Research: An up-Date. *Chem. Soc. Rev.* **2012**, *41*, 370–412.

(35) Głodek, M.; Pawlędzio, S.; Makal, A.; Plażuk, D. The Impact of Crystal Packing and Aurophilic Interactions on the Luminescence Properties in Polymorphs and Solvate of Aroylacetylide–Gold(I) Complexes. *Chem. Eur. J.* **2019**, *25*, 13131–13145.

(36) Janiak, C. A Critical Account on π-π Stacking in Metal Complexes with Aromatic Nitrogen-Containing Ligands. *Dalton Trans.* **2000**, 3885–3896.

Chapter Four

NHC*-Gold(I) Dithiocarbamates

Work published as:

Synthesis and Cytotoxicity Studies of Novel NHC*-Gold(I) Complexes Derived from Lepidiline A

D. Curran, O. Dada, H. Müller-Bunz, M. Rothemund, G. Sánchez-Sanz, R. Schobert, X. Zhu, M. Tacke, *Molecules*, **2018**, *23*, 2031-2048

And

In vitro and *in vivo* Investigations into the Carbene-Gold Anticancer Drug Candidates NHC*-Au-SCSNMe$_2$ and NHC*-Au-S-GLUC against Advanced Prostate Cancer PC3

W. Walther, D. Althagafi, D. Curran, C. O'Beirne, C. Mc Carthy, I. Ott, U. Basu, B. Büttner, A. Sterner-Kock, H. Müller-Bunz, G. Sánchez-Sanz, X. Zhu, M. Tacke,

Anti-Cancer Drugs, **2020**, *31*, 672-683

4.1 Introduction

As discussed in the Introduction (**Section 1.2.3**), the mitochondrial enzyme thioredoxin reductase (TrxR) is the primary target for gold(I) complexes. Inhibition of the enzyme occurs when the soft gold species binds to the selenocysteine/cysteine bridge at the redox centre. However, there are other intracellular thiols that can irreversibly bind to the gold(I) complex before it arrives at the mitochondria. Coordination with thiol-containing enzymes, like serum albumin (SA) and glutathione (GSH), diminishes the bioavailability of the drug, thus reducing the efficacy.[1] Gold complexes with thiolate ligands can avoid additional interactions with intracellular thiols, thus producing gold(I) complexes that are more stable under physiological conditions.[2,3] Since the success of auranofin which featured a thiol ligand, it has been further shown that thiolates result in highly cytotoxic complexes.[4]

Dithiocarbamates were investigated for their inhibition of cisplatin-induced nephrotoxicity. Unlike other thiolates, the dithiocarbamates did not reduce the antitumoural effect whilst removing the toxic platinum(II).[5,6] Thus, they were incorporated into metal-based drugs to act as chemoprotective moieties.[7] Gold(III) complexes with *N*,*N*-dimethyl- (DMDT), *S*-methyl-*N*,*N*-dimethyl- (DMDTM) and ethylsarcosine- (ESDT) dithiocarbamates were developed to resemble the highly active cisplatin (**Figure 4.1**).[8] These gold(III) complexes are isoelectronic with platinum(II) and assume square-planar geometry with bidentate dithiocarbamate coordination. The dimethyl- and ethylsarcosinedithiocarbamato complexes reported stronger cytotoxicity than cisplatin against several tumour cell lines, in particular against the human leukaemia cell line HL60 and Burkitt lymphoma cell line Daudi.

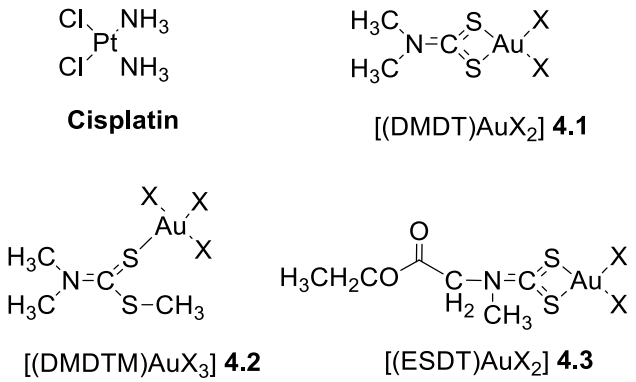

Figure 4.1 Cisplatin and gold(III) dithiocarbamato complexes (**4.1**-**4.3**; X= Cl, Br).[8]

Dithiocarbamates were also employed in gold(III) complexes in order to access their inherent stability. The stability bidentate ligands, such as dithiocarbamates, lend to metal complexes is known as the chelate effect.[3,9] A gold(III) complex was developed with the chemotherapeutic agent chlorambucil and a vitamin B1 derivative (**Figure 4.2**, **4.4**).[10] A dithiocarbamate moiety was incorporated into the vitamin B1 fragment to impart heightened stability to the gold(III) species. Complex **4.4** proved significantly more active than both cisplatin and auranofin against a series of human cancer cell lines and interestingly, less toxic towards the non-tumourigenic cell line MRC-5. The use of dithiocarbamates in gold(III) complexes has led to many potential anticancer agents due to their increased stability and chemoprotective properties.[11–13]

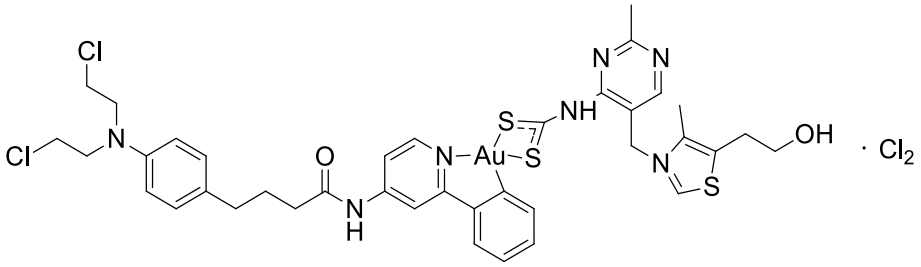

4.4

Figure 4.2 Gold(III) complex **4.4** with chlorambucil and vitamin B1 derivatives, featuring a dithiocarbamate moiety.[10]

Gold(I) dithiocarbamato complexes employ monodentate coordination and still retain their high potency. A series of [(1,1'-biphenyl-2-yl)di-*tert*-butylphosphine]gold(I) dialkylthiocarbamato complexes were developed and evaluated for their anticancer potential.[14] The diethyldithiocarbamato complex **4.5** (**Figure 4.3**) proved the most reactive against ovarian cancer cell lines, when compared to dimethyl-, diisopropyl- and diisobutyldithiocarbamates. This trend was also observed in a study conducted with carbene-gold(I) dialkyldithiocarbamates, where diethyldithiocarbamato complex **4.6** reported the highest cytotoxic response in comparison to dimethyl- and dibenzyldithiocarbamates.[15] Carbene-gold(I) pyrrolidinedithiocarbamato (PDTC) complexes, with varying nitrogen substituents on the heterocycle, were prepared and tested on several cancer cell lines.[16] Although, the mononuclear complexes displayed good activity comparable to cisplatin, the dinuclear complex **4.7** reported the best IC_{50} values.

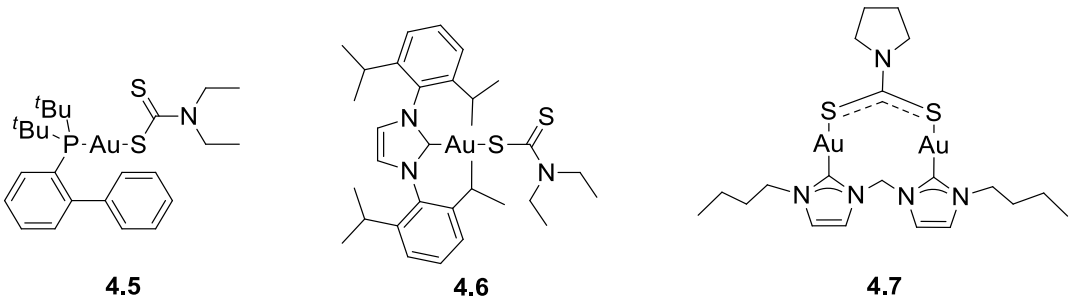

4.5 **4.6** **4.7**

Figure 4.3 Gold(I) dithiocarbamato complexes.

Chapter Proposal

The aim of this Chapter is to investigate the use of thiolate ligands in order to develop more active gold(I) complexes. Dithiocarbamates have proven successful thus the three most promising dithiocarbamate ligands will be coordinated to the NHC*-gold(I) species and subsequently tested for their chemotherapeutic properties *in vitro* and *in vivo*. As seen in the literature, it is hoped the coordination of a thiolate will improve the cytotoxicity compared to the previously used halide and alkyne ligands (Chapter 2 and 3).

4.2 Synthesis of NHC*-Gold(I) Dithiocarbamates

NHC*-gold(I) dithiocarbamato complexes **4.8**-**4.10** were prepared by reacting **1.21** with the corresponding sodium carbamate salt (**Scheme 4.1**). This was performed under biphasic conditions with ethyl acetate and water at room temperature for 48 h, with relatively good yields of 61–74%. The use of dichloromethane at reflux for 24 h afforded the products in significantly lower yields.

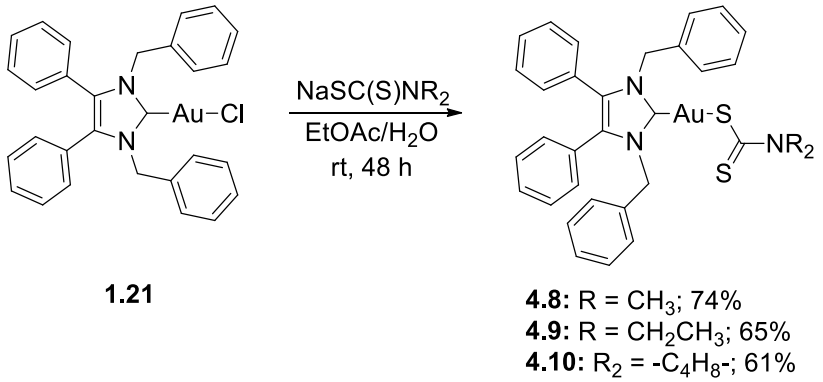

1.21

4.8: R = CH_3; 74%
4.9: R = CH_2CH_3; 65%
4.10: R_2 = -C_4H_8-; 61%

Scheme 4.1 General reaction scheme for the synthesis of NHC*-gold(I) dithiocarbamato complexes **4.8**-**4.10**.

In the ^{1}H-NMR spectra of complexes **4.8**-**4.10** the CH_2 protons of the benzyl groups shifted from δ = 5.44 ppm to δ = 5.55–5.57 ppm upon coordination to the dithiocarbamates. Additionally, the new ^{1}H-NMR singlet at δ = 3.51 ppm corresponding to the two methyl groups of the dimethyldithiocarbamato complex **4.8** confirmed its coordination to the gold(I) centre. Similarly, the CH_2 and CH_3 peaks of the diethyldithiocarbamato complex **4.9** appeared at δ = 3.96 ppm and 1.31 ppm, respectively. The pyrrolidine CH_2 peaks of **4.10** appeared at δ = 3.85 and 1.97 ppm, with a triplet and pentet distinguishing these two peaks.

The IR spectra of complexes **4.8**-**4.10** showed a medium band at 971, 910, and 949 cm^{-1}, respectively, which corresponds to the C-S stretch. Furthermore, a shift at 1020-1023 cm^{-1} was assigned to the second C-S stretch. These shifts confirmed the monodentate coordination of the dithiocarbamate to the gold(I) centre as the two C-S bonds are unsymmetrical and thus appear split.[14,17] Additionally, the IR spectra of complexes **4.8**-**4.10** displayed bands at 1447, 1411, and 1406 cm^{-1}, respectively, which corresponded to the C–N stretching of the carbamate or the "thioureide". The region of 1480-1550 cm^{-1} represents a C-N bond vibration that is between a single and double bond.[18] The thioureide moiety has been observed in other gold-based dithiocarbamate complexes and indicates that more double bond character is present in the C-N bond than the C-S bonds.[8,17] The resonant structure of these gold(I) dithiocarbamates is illustrated in **Figure 4.4**.

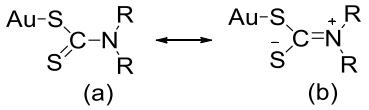

Figure 4.4 Resonance found in the gold(I) dithiocarbamato complexes.

4.3 Structural Discussion

The molecular structures of complexes **4.8**-**4.10** were determined by single crystal X-ray diffraction, with selected bond lengths displayed in **Table 4.1**. The X-ray crystal data and structure refinement are found in **Table 4.2**. Compound **4.8** and **4.9** crystallised in the monoclinic space group I2/a (#15) and C2/c (#15), respectively. Compound **4.10** crystallised in the triclinic space group $P\bar{1}$ (#2) with two molecules of the compound contained in the independent unit; the two **4.10** molecules displayed slight conformational differences (**Table 4.1**). All complexes crystallised in the absence of any solvate molecules. The crystals of **4.8** and **4.10** were formed from the slow evaporation of hot saturated ethanol solutions at room temperature (**Figures 4.5** and **4.7**), while the crystal of **4.9** was grown from the slow infusion of pentane into a saturated CH_2Cl_2 solution at −18 °C (**Figure 4.6**).

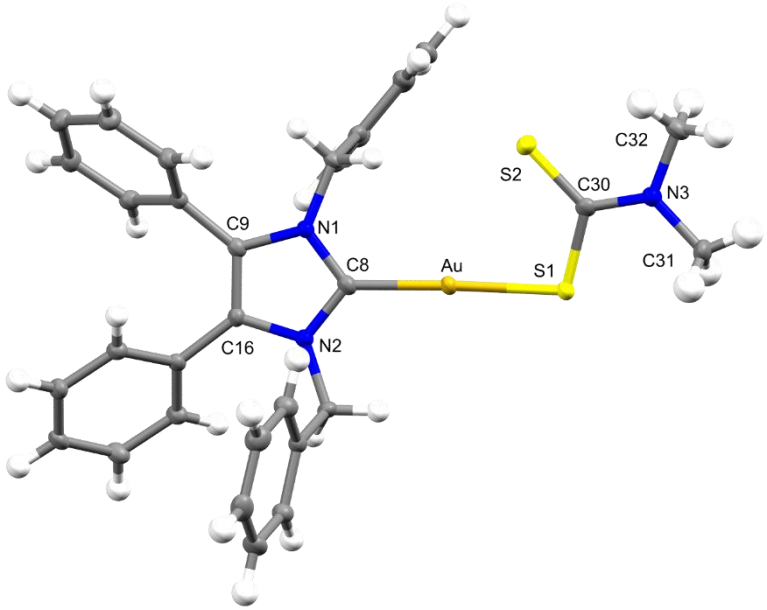

Figure 4.5 X-ray diffraction structure of **4.8**; thermal ellipsoids are drawn on the 50% probability level.

Table 4.1 Selected bond lengths (Å) for complexes **4.8**-**4.10**.

	C(8)-Au	Au-S(1)	S(1)-C(30)	S(2)-C(30)	C(30)-N(3)	N(3)-C(31)	N(3)-C(X)
4.8[a]	1.998(2)	2.3019(5)	1.759(2)	1.685(2)	1.340(3)	1.459(3)	1.465(3)
4.9[b]	2.001(2)	2.3008(6)	1.761(3)	1.689(3)	1.342(3)	1.470(3)	1.469(4)
4.10[c,d]	2.008(4)	2.2991(12)	1.750(5)	1.697(5)	1.303(10)	1.489(12)	1.463(12)
	2.003(4)	2.2969(12)	1.743(5)	1.689(5)	1.322(6)	1.478(11)	1.487(11)

[a] X= C(32). [b] X= C(33). [c] X= C(34A). [d] Two crystallographically independent molecules contained in the unit cell.

Complexes **4.8**-**4.10** reported Au-C bond lengths similar to those reported previously. Additionally, the complexes were all almost linear at the gold(I) centre with C(8)–Au–S(1) bond angles of 177.47(6), 175.91(7) and 177.38(12) ° for complexes **4.8**-**4.10,** respectively. The Au–S bond lengths of 2.2991(12)-2.3019(5) Å were within the acceptable range and comparable to other gold(I) dithiocarbamates.[14,19] In all complexes, both C-S bonds appeared between the standard single and double bond lengths of 1.81 and 1.61 Å, respectively.[20] The longer of these two C-S bonds is that of S(1) which is coordinated to the gold centre. The C(30)–S(1) bond is slightly shorter than the expected single bond and the C(30)–S(2) bond is longer than the expected double bond. Furthermore, the measured C(30)–N(3) bond exhibited more double bond character with reported bond lengths of 1.340(3), 1.342(3) and 1.303(10) Å for complexes **4.8**-**4.10** respectively (single bond: 1.47 Å, double bond: 1.27 Å).[20] These bond lengths, along with the IR data, clearly indicated that the dithiocarbamate structures exist in a resonant form as highlighted above in **Figure 4.4**.

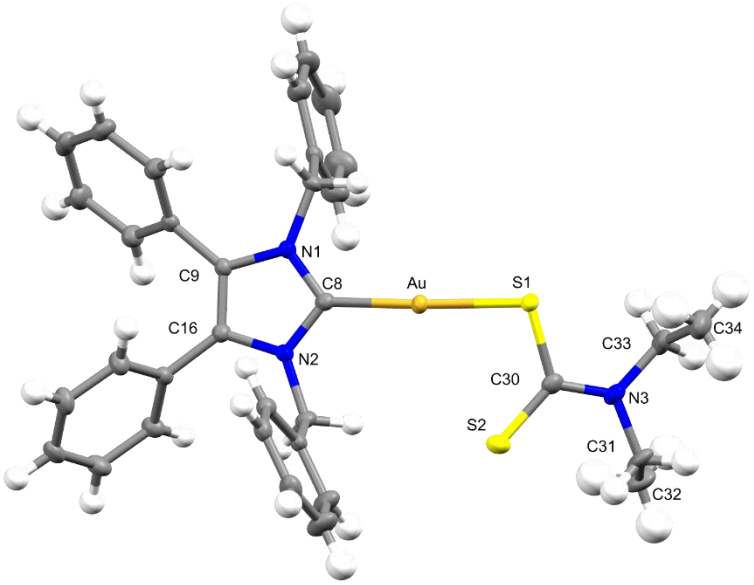

Figure 4.6. X-ray diffraction structure of **4.9**; thermal ellipsoids are drawn on the 50% probability level.

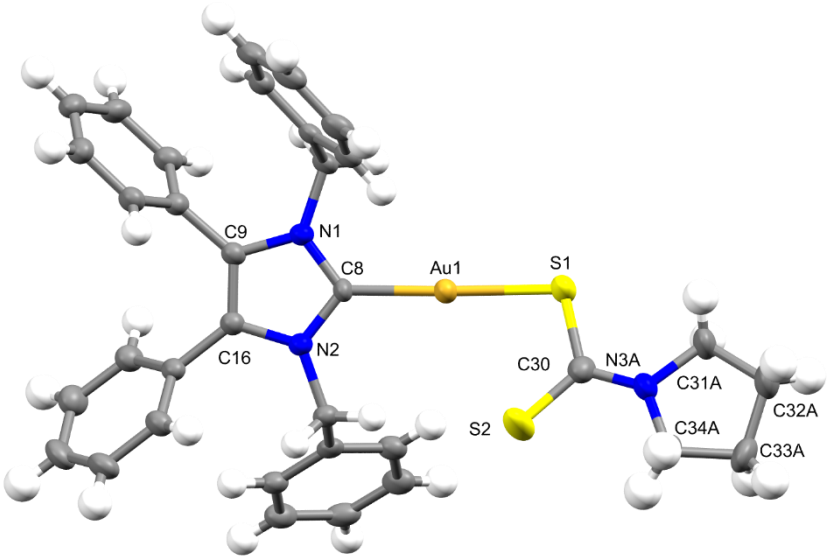

Figure 4.7 X-ray diffraction structure of **4.10**; thermal ellipsoids are drawn on the 50% probability level, disorder neglected.

Table 4.2 Crystal data and structure refinement for complexes **4.8**-**4.10.**

	4.8	**4.9**	**4.10**
Empirical Formula	C_{32} H_{30} N_3 S_2 Au	C_{34} H_{34} N_3 S_2 Au	C_{34} H_{32} N_3 S_2 Au
Formula Weight (g·mol^{-1})	717.67	745.73	743.71
Temperature (K)	100(2)	100(2)	100(2)
Crystal system	Monoclinic	Monoclinic	Triclinic
Space group	I2/a (#15)	C2/c (#15)	P$\bar{1}$ (#2)
Unit cell dimensions			
a (Å)	20.4271(2)	24.2068(6)	14.6143(2)
b (Å)	13.05968(9)	9.8159(2)	15.4593(2)
c (Å)	21.6149(2)	26.1046(6)	16.1676(2)
α (°)	90	90	67.5183(8)
β (°)	103.5937(8)	98.572(3)	84.0508(7)
γ (°)	90	90	62.4289(9)
Volume (Å^3)	5604.71(9)	6133.5(2)	2979.79(7)
Z	8	8	4
Density (calcd) (mg/m^3)	1.701	1.615	1.658
Absorption coefficient (mm^{-1})	11.455	4.961	10.798
F (000)	2832	2960	1472
Crystal size (mm^3)	0.229 x 0.123 x 0.083	0.272 x 0.218 x 0.139	0.204 x 0.139 x 0.054
θ (°)	3.986 to 76.963	3.157 to 30.996	3.425 to 76.904
Index ranges	–25 ≤ h ≤ 25	–34 ≤ h ≤ 33	–16 ≤ h ≤ 18
	–16 ≤ k ≤ 16	–14 ≤ k ≤ 14	–19 ≤ k ≤ 19
	–26 ≤ l ≤ 27	–37 ≤ l ≤ 37	–20 ≤ l ≤ 20
Reflections collected	44,165	48,954	118,093
Independent reflections R_{int}	5909 (0.0344)	9747 (0.0483)	12466 (0.0388)
Completeness to θ_{max} (%)	100.0	99.8	100.0
Absorption correction	Gaussian	Gaussian	Gaussian
Max and min transmission	0.547 and 0.211	0.558 and 0.353	0.430 and 0.087
Refinement method	Full–matrix Least–squares on F^2	Full–matrix Least–squares on F^2	Full–matrix Least–squares on F^2
Data/ restraints/ parameters	5909 / 0 / 346	9747 / 0 / 363	12466 / 0 / 759
Goodness-of-fit on F2	1.080	1.088	1.119
Final R indices [I > 2σ(I)]	R1 = 0.0185	R1 = 0.0286	R1 = 0.0317
	wR2 = 0.0442	wR2 = 0.0596	wR2 = 0.0743
R indices (all data)	R1 = 0.0210	R1 = 0.0367	R1 = 0.0358
	wR2 = 0.0456	wR2 = 0.0633	wR2 = 0.0764
Largest diff. peak and hole	0.622 and –0.722	1.437 and –0.817	1.548 and –1.464

4.4 Biological Evaluation

4.4.1 *In vitro* MTT-Based Proliferation Assays

Initially, the *in vitro* anticancer activity of complexes **4.8**-**4.10** was tested via MTT-based proliferation assays against the human colon carcinoma cell line HCT-116^{wt}, the p53 knockout mutant HCT-116$^{-/-}$ and the *mdr* human breast cancer cell line MCF-7^{topo} (**Table 4.3**). The anticancer drug cisplatin and gold(I) based cancer drug candidate auranofin have been included as positive controls,[10] alongside **1.21** as an internal group comparison. These proliferation assays were carried out by Prof. Rainer Schobert and Matthias Rothemund at the University of Bayreuth, Germany.

All complexes reached single-digit IC_{50} values in the low micromolar range against the tested cell lines after 72 h of treatment. In fact, compounds **4.8** and **4.9** exhibited sub-micromolar activity against the human breast cancer cell line MCF-7^{topo}. The dimethyldithiocarbamato complex **4.8** proved the most active, with IC_{50} values of 1.5 ± 0.1 μM against the HCT-116^{wt} and 0.28 ± 0.03 μM against the MCF-7^{topo} cells. It has been shown that dithiocarbamato complexes elicit apoptosis that is not p53 dependent.[21] Thus, to test the complexes for their dependency on fully functional p53, one activator of the apoptotic cascade, complexes **4.9** and **4.10** were tested for their toxicity against a HCT-116 p53 knockout mutant. Compounds **4.9** and **4.10** exerted a higher toxicity against the knockout mutant HCT-116$^{-/-}$ than against the wildtype HCT-116^{wt}. This indicated that p53 may not be an important factor in the apoptotic response of these NHC*-Au-SC(S)NR complexes.[22]

Selectivity towards the breast cancer cell line was observed for all three dithiocarbamato complexes. In comparison to cisplatin and auranofin, all three complexes displayed higher cytotoxicity on the MCF-7^{topo} cell line. Compound **4.8** presented higher cytotoxicity than both cisplatin and auranofin on the colon cancer cell line HCT-116^{wt}. Moreover, a significant increase in activity was found with the dithiocarbamato complexes compared to their precursor **1.21**. Overall, complexes **4.8**-**4.10** exhibited high antitumoural activity against the colon carcinoma cell line HCT-116^{wt} and the *mdr* breast cancer cell line MCF-7^{topo}.

Table 4.3 IC_{50} values (μM) of complexes **1.21** and **4.8**-**4.10** against MCF-7^{topo}, HCT-116^{wt} and HCT-116 p53$^{-/-}$ cells after 72 h of incubation.

	HCT-116^{wt}	**HCT-116 p53$^{-/-}$**	**MCF-7^{topo}**
Cisplatin[a]	5.42 ± 0.12	-	18.21 ± 0.10
Auranofin[a]	3.78 ± 0.10	-	2.89 ± 0.05
1.21	22.7 ± 1.2	-	20.8 ± 1.9
4.8	1.5 ± 0.1	-	0.28 ± 0.03
4.9	8.0 ± 0.1	3.8 ± 0.4	0.36 ± 0.03
4.10	6.2 ± 0.3	2.0 ± 0.6	1.5 ± 0.3

[a] Cisplatin and auranofin IC_{50} values against HCT-116 and MCF-7 cell lines have been included for comparative purposes.[10]

4.4.2 *In vitro* Cell Viability Tests

Next, the *in vitro* cell viability of complex **4.8** was tested on the US National Cancer Institute's 60 cancer cell panel (NCI 60). Tests were carried out against 6 leukaemia, 9 non-small cell (NSC) lung, 7 colon, 6 CNS, 9 melanoma, 7 ovarian, 8 renal, 2 prostate, and 6 breast cancer cell lines. Sulforhodamine B (SRB) assay was employed after a 48 h incubation period.

Generally, single-digit GI_{50} values in the low micromolar range were observed, with an average GI_{50} value of 1.58 μM across the 60 cell lines investigated. Complex **4.8** exhibited its highest activity against the human ovarian cancer cell line OVCAR-3 and the human NSC lung cancer cell line NCI-H522 with GI_{50} values of 0.264 and 0.385 μM, respectively. Excellent sub-micromolar activity was also observed on the human colon, prostate and breast cancer cell lines

HT29, PC-3 and T-47D with GI_{50} values of 0.506, 0.720 and 0.791 μM, respectively. The full NCI 60 cancer cell panel results can be found in the Appendix. In summary, these tests further illustrated the high potential of complex **4.8** as a chemotherapeutic agent with high cytotoxic activity against several human cancer cell lines.

4.4.3 Inhibition of Mammalian Thioredoxin Reductase

The inhibition of mammalian TrxR by complex **4.8** was evaluated. Inhibition experiments were conducted by Prof. Ingo Ott and Dr Uttara Basu at the Technical University of Braunschweig, Germany. Complex **4.8** displayed moderate activity against mammalian TrxR with an IC_{50} value of 1.2 ± 0.2 μM. Auranofin reported a heightened response to TrxR with an IC_{50} value of 0.0903 ± 0.009 μM.[23] Complexes NHC*-Au-SCN (**4.11**) and NHC*-Au-S-GLUC (**4.12**) with the same NHC* ligand (**Figure 4.8**), developed previously in the Tacke group, have shown a varied response to TrxR with IC_{50} values of 0.77 ± 0.34 and 7.4 ± 0.4 μM, respectively.[24,25] These inhibition results correlate well with other reported NHC-gold(I) complexes.[26,27]

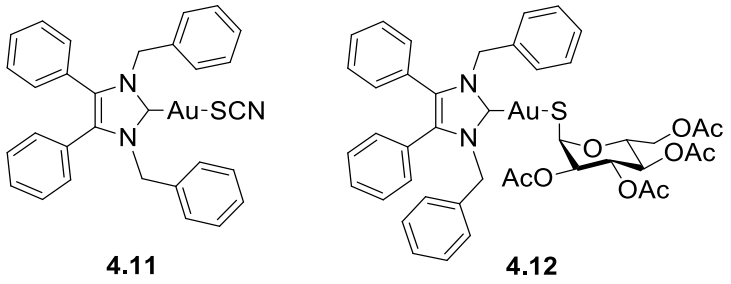

Figure 4.8 NHC*-Au-SCN (**4.11**) and NHC*-Au-S-GLUC (**4.12**).

4.4.4 *In vivo* PC-3 Xenograft Mouse Model

As a result of the encouraging *in vitro* results an *in vivo* mouse xenograft experiment was carried out with complex **4.8**. In addition, NHC*-Au-S-GLUC (**4.12**) was included in the experiment to examine the concept of targeted and non-targeted therapies. Glucose-derived complexes have a built-in delivery system as cancer cells overexpress the GLUT and sodium-dependent glucose transporters.[28,29] Complex **4.12** may demonstrate higher cellular uptake and consequently an elevated cytotoxic response. In order to test this theory we compared the *in vitro* activity of **4.12** to **4.8**, as complex **4.8** was shown in cell studies to be highly active without a "targeting" moiety. Both complexes were found to be particularly active against the human prostate cancer cell line PC-3, with complex **4.12** reporting a GI_{50} value of 0.215 μM.[25] Thus the PC-3 xenograft was chosen for the mouse model experiments. These experiments was carried out by Prof. Dr Wolfgang Walther, Prof. Dr Anja Sterner-Kock and Britta Büttner at Experimental Pharmacology & Oncology Berlin-Buch GmbH (EPO), Germany.

First, the maximum tolerated dose (MTD) was determined for complexes **4.8** and **4.12**. Male NMRI:nu/nu mice were treated daily for 5 days with complex **4.8** or **4.12** in doses of 2.5 to 20 mg/kg. In general, both compounds were tolerated well by the mice. Doses of up to 20 mg/kg were tolerated without body weight loss and without generation of other obvious side effects. Since such high doses were tolerated well by the mice, further dose progressions to find the MTD were not performed. Thus, doses of 10 and 20 mg/kg were defined as acceptable doses for further therapeutic experiments.

For the PC-3 xenograft experiment 5 groups of 5 mice each were treated on days 6-10, 12-16 and 19-20 intraperitoneally with the solvent DMSO (group A), the dithiocarbamato compound **4.8** (groups B and C) or the α-thioglucoside compound **4.12** (group D and E). An overview of the experiment including dosing schedules and results is presented in **Table 4.4**. The body weight development of all groups during the experiment is shown in **Figure 4.9**, while the tumour growth development is shown in **Figure 4.10** and **Table 4.5**.

Table 4.4 Overview of the PC-3 mouse xenograft experiment with NHC-Au-SCSNMe$_2$ (**4.8**) and NHC-Au-S-GLUC (**4.12**).

Group	Number of mice	Substance	Treatment [on day]	Dose (mg/kg)	Optimal T/C [on day]	Deaths [on day]
A	5	DMSO	6-10, 12-16, 19-20	-	-	0/5
B	5	NHC-Au-SCSNMe$_2$	6-10, 12-16, 19-20	10	0.45 [13]	0/5
C	5	NHC-Au-SCSNMe$_2$	6-10, 12-16, 19-20	20	0.31 [13]	0/5
D	5	NHC-Au-S-GLUC	6-10, 12-16, 19-20	10	0.44 [19]	0/5
E	5	NHC-Au-S-GLUC	6-10, 12-16, 19-20	20	0.44 [16]	1/5 [19]

The treated mice from groups B to D showed no significant body weight loss when compared to the mice of the untreated group A. In the high dosage group E only one animal showed loss in body weight of 22%. When exposed to 12 treatments of complex **4.8** or **4.12** at dosages of 10 or 20 mg/kg, only one mouse in the group E cohort (**4.12**) died on day 19.

Figure 4.9 The effect of NHC-Au-SCSNMe$_2$ (**4.8**) and NHC-Au-S-GLUC (**4.12**) on the mean body weight (g) over time (d) in comparison to the vehicle control group A.

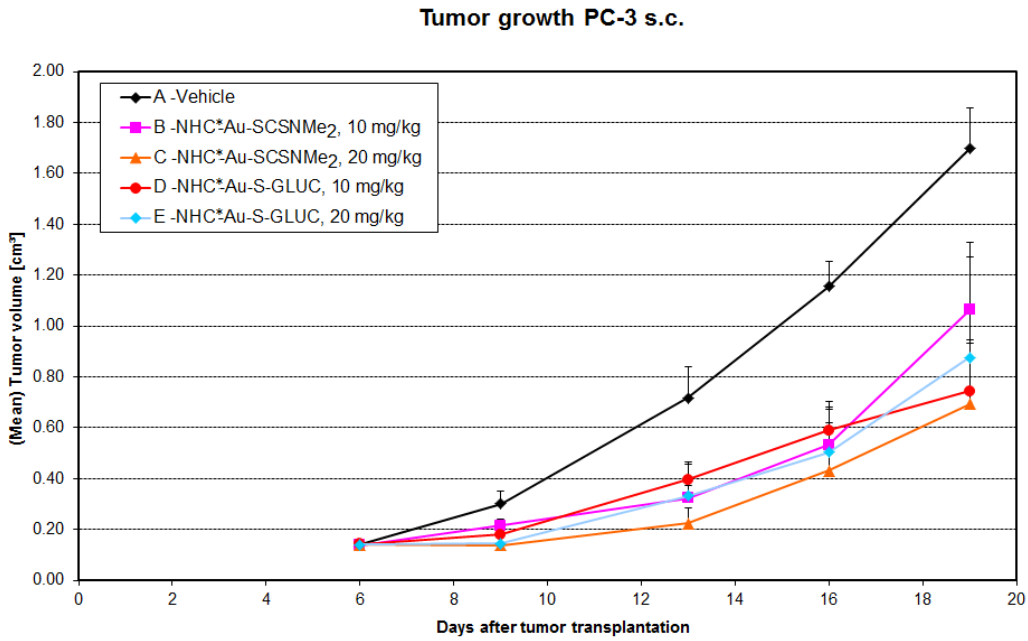

Figure 4.10 The effect of NHC-Au-SCSNMe$_2$ (**4.8**) and NHC-Au-S-GLUC (**4.12**) on the mean tumour volume (cm^3) over time (d) in comparison to the vehicle control group A.

All groups started with a tumour volume of 0.140 cm^3 on day 6. After the first treatments the two low dosage groups B and D showed a modest tumour increase, while the tumour volume of the higher dosage groups C and E remained constant. The control group A monitored the continued tumour growth without interference and thus had the highest tumour weight. During (day 13) and after (day 16) the second treatment period groups B and C which were treated with complex **4.8** grew less than those treated by **4.12**. As expected, the higher dosage groups C and E resulted in less tumour growth than the lower dosage groups B and D. The final measurements were taken on day 19 during the third treatment. Interestingly, group B had a significant increase in tumour weight on day 19, as did group E, to a lesser extent. Overall, the highest tumour growth was found with the low dose group B, followed by the high dose group E. The lowest tumour growth was found with the high dose group C, which was treated with complex **4.8**. Interestingly, the low dose group D which was treated with complex **4.12** exhibited less tumour growth than its high dose counterpart group E.

Table 4.5 Mean tumour growth development (cm^3) of groups A-E (days 6, 9, 13, 16 and 19) and the mean tumour weight (g).

Group	Day 6	Day 9	Day 13	Day 16	Day 19	Mean tumour weight
A	0.140	0.300	0.717	1.155	1.697	1.252
B	0.140	0.216	0.322	0.533	1.063	0.876
C	0.140	0.139	0.224	0.430	0.693	0.733
D	0.140	0.174	0.395	0.589	0.744	0.697
E	0.140	0.145	0.331	0.503	0.876	0.920

The therapeutic efficacy is further supported by the comparison of the mean tumour weights of the respective groups. As shown in **Table 4.5**, groups C and D reported both the lowest tumour volumes and tumour weights. Whereas, group E had the highest tumour weight despite not having the largest tumour volume. As expected, the mean tumour weight of group A was the highest.

Optimal treated to control (T/C) values for each group were reported revealing that group C had the best treatment with the higher dose of 20 mg/kg of complex **4.8** (**Table 4.4**). Optimal T/C values for treatment with both doses of complex **4.8** were on day 13 in comparison to the T/C values for treatment with complex **4.12** which were on days 19 (10 mg/kg) and 16 (20 mg/kg). These values suggest that complex **4.8** might be more successful for shorter treatment periods while complex **4.12** proved efficacious until days 16-19.

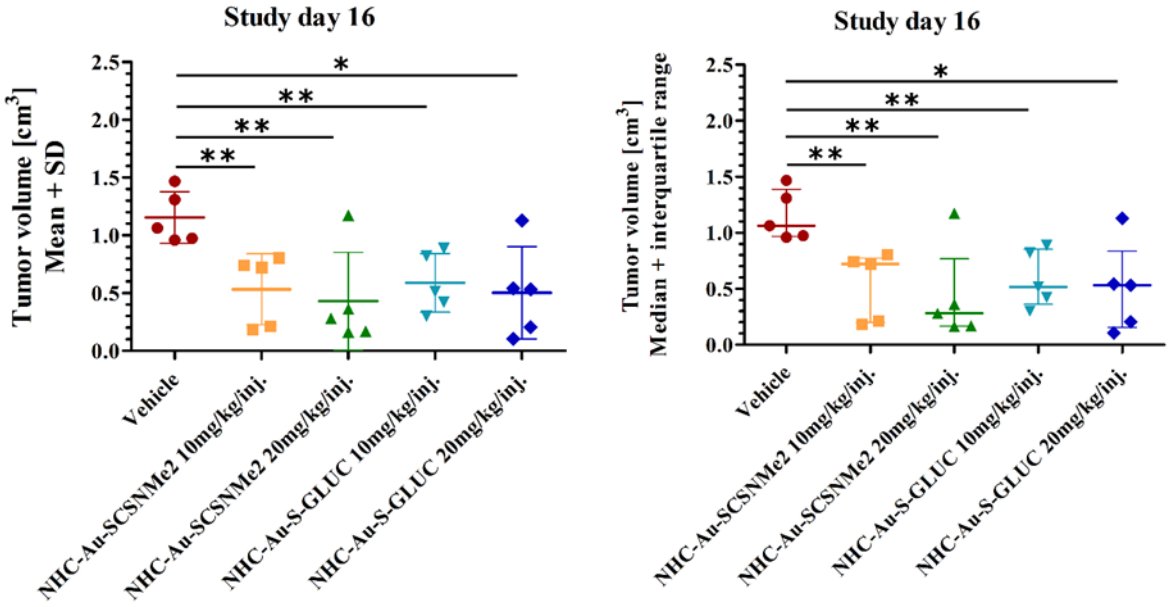

Figure 4.11 Statistical analysis for antitumoural effects of NHC-Au-SCSNMe$_2$ (**4.8**) and NHC-Au-S-GLUC (**4.12**) on tumour volume on study day 16 at doses of 10 and 20 kg/mg (groups B-E) and the vehicle control (group A).

The statistical analysis, as shown in **Figure 4.11**, revealed in more detail that particularly on study day 16, there were significant differences between the tumour volumes of the vehicle control group and group B, treated with 10 mg/kg of complex **4.8** (P<0.01), as well as between the vehicle control and group D, treated with 10 mg/kg of complex **4.12** (P<0.01). With the exception of one outlier in each group there is also a clear difference between the tumour volume of the vehicle control group and both groups C and E which were treated with 20 mg/kg of complex **4.8** (P<0.05) and **4.12** (P<0.05), respectively. Regarding potential dose dependency of these antitumoural effects, only on study day 9 were significant differences determined for complex **4.8** with 10 mg/kg versus 20 mg/kg.

4.4.5 Ki67 Immunohistochemistry

The nuclear protein Ki67 acts as an indicator for cell proliferation thus, semi-quantitative analysis of Ki67 stained control and treated tumour tissues was carried out to monitor the drug-mediated reduction of Ki67. As seen in **Figure 4.12**, both drugs were able to reduce Ki67 in the tumours, indicating their inhibitory impact on cell proliferation in this PC-3 tumour mouse model. Untreated tumour tissue had a high Ki67 score (+++), while a reduced medium Ki67 score (++) was observed in both dosage groups of complex **4.12**; treatment with complex **4.8** showed a medium Ki67 score with the 10 mg/kg dose and a low Ki67 score (+) with 20 mg/kg. Complex **4.8** exhibited a dose-dependent reduction of Ki67 underlining its superior antitumoural effect when compared to complex **4.12**.

Vehicle control (Ki67 score: +++)

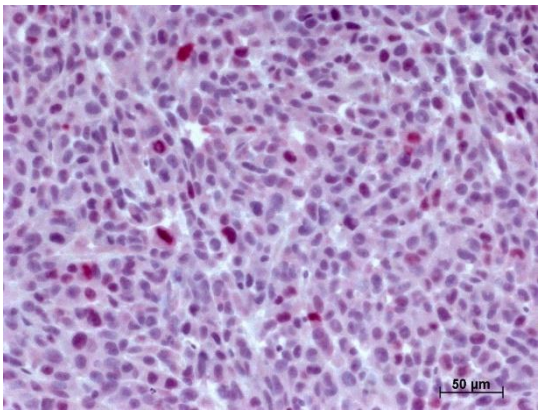

4.8, 10 mg/kg (Ki67 score: ++)

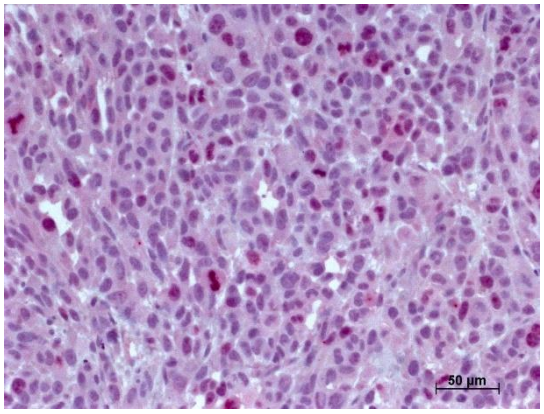

4.8, 20 mg/kg (Ki67 score: +)

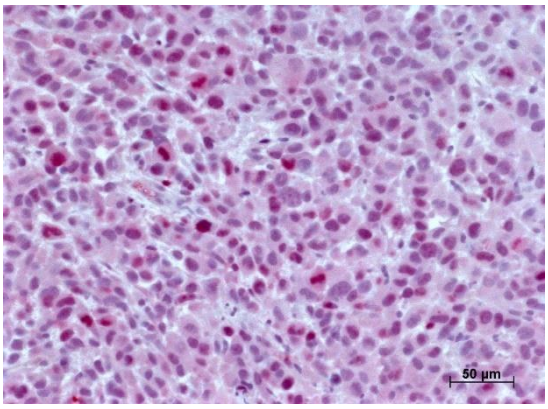

4.12, 10 mg/kg (Ki67 score: ++)

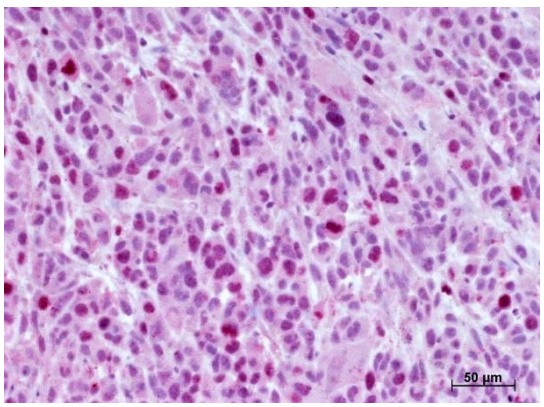

4.12, 20 mg/kg (Ki67 score: ++)

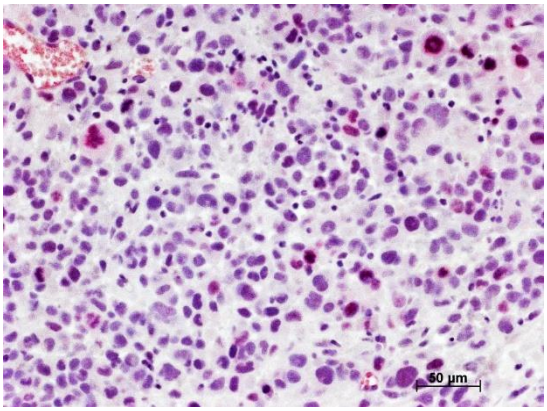

Figure 4.12 Ki67 immunohistochemical images of the vehicle control and of NHC-Au-SCSNMe$_2$ (**4.8**) and NHC-Au-S-GLUC (**4.12**) treated PC-3 tumours. The red stained cell nuclei indicate Ki67 positivity. A scale from 0 to +++ is used (0 = absent; + = less than 10 Ki67-positive cells /high power field (HPF); ++ = 10–20 Ki67-positive cells /HPF; +++ = more than 20 Ki67-positive cells /HPF.

4.5 Conclusion and Outlook

In summary, three novel NHC*-gold(I) dithiocarbamates (**4.8**-**4.10**) were synthesised in good yields. The X-ray crystal structures were obtained and revealed for all three complexes, a shorter C-N bond with double bond characteristics and slightly longer C-S bonds indicating that a resonant form is present. *In vitro* cytotoxicity studies conducted against the human colon carcinoma cell lines HCT-116^{wt} and HCT-116 p53$^{-/-}$, and the *mdr* human breast cancer cell line MCF-7^{topo}, showed low micromolar and even sub-micromolar activity. Compound **4.8** exhibited the best activity with IC_{50} values of 1.5 ± 0.1 μM and 0.28 ± 0.03 μM, against HCT-116^{wt} and MCF-7^{topo} cell lines, respectively. Cell viability tests against the NCI 60 cell panel found compound **4.8** to have an average GI_{50} value of 1.58 μM across the 60 cell lines investigated. It proved exceptionally active with sub-micromolar GI_{50} values against the human colon, prostate and breast cancer cell lines HT29, PC-3 and T-47D. Additionally, compound **4.8** exerted moderate inhibition against mammalian TrxR.

In vivo MTD and xenograft mouse model experiments were carried out with complexes **4.8** and α-thioglucoside **4.12** for comparison. The MTD experiment was halted after it was noted that the high dose of 20 mg/kg of either complex **4.8** or **4.12** was tolerated well by the mice. Thus, the PC-3 xenograft experiment was conducted with doses of 10 and 20 mg/kg of either complex **4.8** or **4.12**. Groups B-D reacted well to the treatments, however group E experienced body weight reduction of 22% and one mouse died on day 19 following the three high dose treatments of complex **4.12**. Group C was quite successful as it presented the lowest tumour growth with treatment of 20 mg/kg of complex **4.8** and an optimal T/C value of 0.31 on day 13. Furthermore, the Ki67 immunohistochemical analysis of the treated tumour tissues reported a dose-dependent reduction with complex **4.8**. Consequently, complex **4.8** demonstrated its strong potential as a chemotherapeutic agent. Future work will focus on further investigation into the potential of complex **4.8** as an anticancer drug by means of additional *in vivo* experiments and mechanistic studies.

4.6 Experimental Section

4.6.1 Synthesis

(1,3-Dibenzyl-4,5-diphenylimidazol-2-ylidene)gold(I) dimethyldithiocarbamate (4.8)

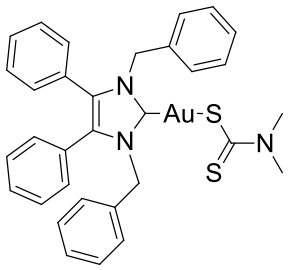

NHC*-gold(I) chloride (**1.21**) (155 mg, 0.244 mmol, 1.0 equiv.) and $NaSC(S)N(CH_3)_2.H_2O$ (42 mg, 0.293 mmol, 1.2 equiv.) were stirred in EtOAc/H_2O (1:1, 14 mL) at rt for 48 h. The reaction mixture was washed with water (2 × 10 mL) and brine (10 mL). The combined organic phase was dried over anhydrous $MgSO_4$, filtered, and reduced to approximately 2 mL under reduced pressure. Pentane (40 mL) was added to precipitate a solid. The product was filtered, washed with pentane (15 mL) and dried *in vacuo* to give a white solid (129 mg, 74%). ^{1}H-NMR (300 MHz, $CDCl_3$, δ ppm): 7.32–7.27 (m, 2H, ArCH), 7.24–7.16 (m, 10H, ArCH), 7.10–7.04 (m, 4H, ArCH), 6.95 (d, J = 7.1 Hz, 4H, ArCH), 5.55 (s, 4H, CH_2), 3.51 (s, 6H, CH_3). ^{13}C-NMR (101 MHz, $CDCl_3$, δ ppm): 207.6 (SCS), 179.8 (NCN), 136.9 (C), 132.4 (C), 131.2 (CH), 131.1 (CH), 129.6 (CH), 129.1 (CH), 128.9 (CH), 128.3 (CH), 127.1 (C), 53.0 (CH_2), 45.4 (CH_3). HRMS (ESI$^+$) *m*/*z*: [M + H]$^+$ calcd. 718.1625; found 718.1640. IR (ATR, cm^{-1}): 3025 (w), 2910 (w), 1603 (w), 1496 (m), 1447 (m), 1248 (m), 1140 (m), 1023 (m), 971 (m), 726 (m), 695 (s). Melting point range: 186–187 °C. Anal. calcd. for $C_{32}H_{30}N_3S_2Au$ (717.71) in %: C, 53.55; H, 4.21; N, 5.85; S, 8.94. Found: C, 53.50; H, 4.17; N, 5.77; S, 8.64.

1,3-Dibenzyl-4,5-diphenylimidazol-2-ylidene)gold(I) diethyldithiocarbamate (4.9)

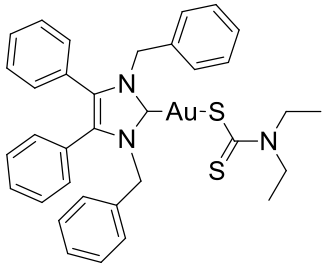

In a procedure identical to above reaction: **1.21** (65 mg, 0.103 mmol, 1.0 equiv.), $NaSC(S)N(C_2H_5)_2.3H_2O$ (28 mg, 0.124 mmol, 1.2 equiv.) and EtOAc-H_2O (1:1, 15 mL). After workup and precipitation a pale yellow solid was formed (49 mg, 65%). ^{1}H-NMR (300 MHz, $CDCl_3$, δ ppm): 7.27 (t, *J* = 7.3 Hz, 2H, ArCH), 7.25–7.14 (m, 15H, ArCH), 7.08–7.04 (m, 3H, ArCH), 6.93 (d, *J* = 7.2 Hz, 3H, ArCH), 5.57 (s, 4H, $CH_{2\text{-Bz}}$), 3.96 (q, *J* = 7.1 Hz, 4H, $CH_{2\text{-Et}}$), 1.31 (t, *J* = 7.0 Hz, 6H, CH_3). ^{13}C-NMR (101 MHz, $CDCl_3$, δ ppm): 205.8 (SCS), 180.1 (NCN), 136.3 (C), 132.1 (C), 130.9 (CH), 129.2 (CH), 128.6 (CH), 128.5 (CH), 127.9 (CH), 127.8 (C), 53.1 ($CH_{2\text{-Bz}}$), 49.3 ($CH_{2\text{-Et}}$), 12.4 (CH_3). HRMS (ESI$^+$) *m*/*z*: $[M + H]^+$ calcd. 746.1938; found 746.1937. IR (ATR, cm^{-1}): 3025 (w), 2925 (w), 1603 (w), 1495 (w), 1411 (m), 1260 (m), 1133 (m), 1020 (m), 981 (m), 910 (m), 733 (s), 694 (s). Melting point range: 187–188 °C. Anal. calcd. for $C_{34}H_{34}N_3S_2Au$ (745.75) in %: C, 54.76; H, 4.60; N, 5.63; S, 8.60. Found: C, 54.58; H, 4.52; N, 5.53; S, 8.72.

(1,3-Dibenzyl-4,5-diphenylimidazol-2-ylidene)gold(I) pyrrolidinedithiocarbamate (4.10)

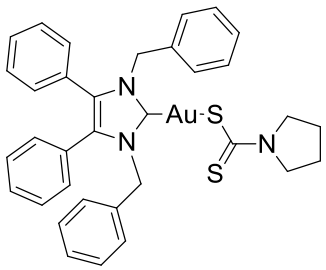

In a procedure identical to above reaction: **1.21** (66 mg, 0.105 mmol, 1.0 equiv.), $NaSC(S)N(C_2H_5)$ (21 mg, 0.126 mmol, 1.2 equiv.) and EtOAc-H_2O (1:1, 15 mL). After workup and precipitation a yellow solid was formed (48 mg, 61%). ^{1}H-NMR (300 MHz, $CDCl_3$, δ ppm): 7.29 (d, *J* = 7.5 Hz, 1H, ArCH), 7.24–7.14 (m, 10H, ArCH), 7.12–7.03 (m, 4H, ArCH), 6.95 (d, *J* = 7.0 Hz, 4H, ArCH), 5.56 (s, 4H, $CH_{2\text{-Bz}}$), 3.85 (t, 4H, CH_2), 1.97 (p, 4H, CH_2). ^{13}C-NMR (101 MHz, $CDCl_3$, δ ppm): 202.8 (SCS), 180.2 (NCN), 136.3 (C), 132.1 (C), 130.9 (CH), 129.3 (CH), 128.6 (CH), 128.5 (CH), 128.0 (CH), 127.9 (CH), 127.8 (C), 54.4 (CH_2), 53.1 ($CH_{2\text{-Bz}}$), 26.3 (CH_2). HRMS (ESI$^+$) *m*/*z*: $[M + H]^+$ calcd. 744.1782; found 744.1753. IR (ATR, cm^{-1}): 3027 (w), 2961 (w), 1602 (w), 1494 (w), 1406 (m), 1165 (m), 1021 (m), 949 (m), 733 (m), 695 (s). Melting point range: 188–189 °C. Anal. calcd. for $C_{34}H_{32}N_3S_2Au$ (743.73) in %: C, 54.91; H, 4.34; N, 5.65; S, 8.63. Found: C, 54.48; H, 4.26; N, 5.52; S, 8.85.

4.6.2 NCI 60 Cell Viability Tests

The cell viability tests were performed on the US National Cancer Institute's 60 cancer cell panel (NCI 60) at Frederick, Maryland, USA. Compound **4.8** was formulated in a DMSO and glycerol mixture (9:1) and given to the cells at concentrations ranging from 10 nM to 10 μM and incubated for 48 h. The sulforhodamine B assay was used to measure drug-induced cytotoxicity.[30]

4.6.3 Inhibition of Mammalian Thioredoxin Reductase

The inhibition experiments were carried out by Prof. Ingo Ott and Dr Uttara Basu at the Technical University of Braunschweig, Germany. To determine the inhibition of mammalian TrxR, an established microplate reader-based assay was performed. For this purpose, commercially available rat liver TrxR (Sigma-Aldrich) was used and diluted with distilled water to achieve a concentration of 2.5 μM. The compounds **4.8** and **4.12** were freshly dissolved as stock solutions in DMF. The enzyme solution (25 μL) was added to a solution of potassium phosphate buffer (25 μL; pH 7.0) containing the compounds in graded concentrations. A buffer solution containing only DMF (0.5% V/V) was prepared as the positive control. The resulting solutions were incubated with moderate shaking for 75 min at 37 °C in a 96-well plate. After incubation, 225 μL of warm reaction mixture was added to each well [1 mL reaction mixture consists of 500 μL potassium phosphate buffer (pH 7.0), 80 μL ethylene diamine tetraacetate (EDTA) solution (100 mM; pH 7.5), 20 μL BSA solution (0.2%), 100 μL of NADP solution (20 mM) and 300 μL distilled water]. The reaction started immediately by the addition of 25 μL of an ethanolic solution of 5,5′-dithio-bis-[2-nitrobenzoic acid](DTNB) (20 mM). The formation of 5-TNB was monitored with a microplate reader at 37 °C at 405 nm for about 6 min (10 times in 35 seconds intervals). The increase in 5-TNB concentration over time followed a linear trend ($r2 \geq 0.990$), and the enzymatic activities were calculated as the slopes (increase in absorbance per second) thereof. For each tested compound, the non-interference with the assay components was confirmed by a negative control experiment using an enzyme-free test solution. The IC_{50} values were calculated as the concentration of compound decreasing the enzymatic activity of the untreated control by 50% and are given as the means and error of three repeated experiments.

4.6.4 *In vivo* PC-3 Xenograft Mouse Model

The PC-3 xenograft mouse model experiment, including the Ki67 immunohistochemistry and statistical analysis, was carried out by Prof. Dr Wolfgang Walther, Prof. Dr Anja Sterner-Kock and Britta Büttner at Experimental Pharmacology & Oncology Berlin-Buch GmbH (EPO), Germany in a single study. All animals were received from Janvier Labs; housing and animal care were in accordance to all legal and ethical regulations. The animal experiments were performed according to the German Animal Protection Law and with approval from the responsible local authorities (LaGeSo Berlin, Germany). The *in vivo* procedures were consistent and in compliance with the United Kingdom Co-ordinating Committee on Cancer Research (UKCCCR) guidelines.[31]

In the first animal experiment, the MTD of complexes **4.8** and **4.12** was determined in male NMRI:nu/nu mice. Both compounds were dissolved in DMSO (final concentration 10%) and further diluted with 5% Tween 80 in saline. Male NMRI:nu/nu mice (n = 2 mice per group) were administered with 2.5, 5, 10, and 20 mg/kg of complex **4.8** or **4.12** intraperitoneally (i.p.) in single injections of 0.1 mL in order to determine the approximate MTD. In this experiment, maximum body weight loss and side effects were documented.

In the second *in vivo* experiment, 1×10^6 PC-3 cells (expanded *in vitro* in RPMI medium + 10% fetal bovine serum) were injected subcutaneously (s.c.) in a volume of 0.1 mL to male NMRI:nu/nu mice (n = 5 mice per group) on day 0. When tumours were grown to a palpable size of around 0.1 cm^3 mice were randomized and treatment was initiated on day 6. For groups B and C, complex **4.8** and for groups D and E complex **4.12** were injected into mice i.p. at doses of 10 mg/kg (groups B and D) or 20 mg/kg (groups C and E) on 12 days during the experiment, while the control group (group A) of mice was treated with the solvent only. Tumour volumes were measured with a caliper instrument at indicated time points and calculated using the formula: tumour volume = $(\text{width}^2 \times \text{length})/2$. Tumour volumes, relative tumour volumes (relative to the first treatment day), and treated to control (T/C) values were calculated. Body weight and health conditions of the mice were determined continuously during the experiments to estimate tolerability of the drug. Mice were sacrificed on day 20 after their last treatment and necropsy was performed for evaluation of side effects.

4.6.5 Ki67 Immunohistochemistry

The 3 μm thick sections from formalin-fixed paraffin-embedded PC-3 tumours were fixed with 3.7% paraformaldehyde. For the staining of the Ki67 protein, slides were incubated with the primary mouse anti-human Ki67 antibody (Abcam, ab 155801), and the detection system Super Vision Red-2 (DCS Diagnostics) was used. For evaluation of Ki67 expression images of each tumour were taken and the number of positive versus negative cells was counted in 10 high power fields (HPFs). The results include independent blinded histological analysis of the Ki67 expression using a semi-quantitative method. When discrepancies occurred (defined as a greater than two point difference in a given score), a final consensus was reached. A scale from 0 to +++ is used (0 = absent; + = less than 10 Ki67-positive cells/HPF; ++ = 10-20 Ki67- positive cells/HPF; +++ = more than 20 Ki67- positive cells/HPF). Final mean histological scores were assigned through analysis of 10 HPFs.

4.6.6 Statistical Analysis

Statistical evaluation of all experiments was performed using the One-way ANOVA test and Bonferroni-correction. Statistical significance for the *in vivo* testing of the compounds was determined by the unpaired *t*-test. The level of statistical significance was defined with a *P* value of $P \leq 0.05$.

References

(1) Schmidt, C.; Albrecht, L.; Balasupramaniam, S.; Misgeld, R.; Karge, B.; Brönstrup, M.; Prokop, A.; Baumann, K.; Reichl, S.; Ott, I. A Gold(I) Biscarbene Complex with Improved Activity as a TrxR Inhibitor and Cytotoxic Drug: Comparative Studies with Different Gold Metallodrugs. *Metallomics* **2019**, *11*, 533–545.

(2) Zou, T.; Lum, C. T.; Lok, C.-N.; Zhang, J.-J.; Che, C.-M. Chemical Biology of Anticancer Gold(III) and Gold(I) Complexes. *Chem. Soc. Rev.* **2015**, *44*, 8786–8801.

(3) Cattaruzza, L.; Fregona, D.; Mongiat, M.; Ronconi, L.; Fassina, A.; Colombatti, A.; Aldinucci, D. Antitumor Activity of Gold(III)-Dithiocarbamato Derivatives on Prostate Cancer Cells and Xenografts. *Int. J. Cancer* **2010**, *128*, 206–215.

(4) Tiekink, E. R. T. Phosphinegold(I) Thiolates- Pharmacological Use and Potential.

Bioinorg. Chem. Appl. **2003**, *1*, 53–67.

(5) Bodenner, D. L.; Dedon, P. C.; Keng, P. C.; Borch, R. F. Effect of Diethyldithiocarbamate on Cis-Diamminedichloroplatinum(II)-Induced Cytotoxicity, DNA Cross-Linking, and Ɣ-Glutamyl Transpeptidase Inhibition. *Cancer Res.* **1986**, *46*, 2745–2750.

(6) Basinger, M. A.; Jones, M. M.; Gilbreath IV, S. G.; Walker Jr., E. M.; Fody, E. P.; Mayhue, M. A. Dithiocarbamate-Induced Biliary Platinum Excretion and the Control of Cis-Platinum Nephrotoxicity. *Toxicol. Appl. Pharmacol.* **1989**, *97*, 279–288.

(7) Hogarth, G. Metal-Dithiocarbamate Complexes: Chemistry and Biological Activity. *Mini-Rev. Med. Chem.* **2012**, *12*, 1202–1215.

(8) Ronconi, L.; Giovagnini, L.; Marzano, C.; Bettìo, F.; Graziani, R.; Pilloni, G.; Fregona, D. Gold Dithiocarbamate Derivatives as Potential Antineoplastic Agents: Design, Spectroscopic Properties, and in Vitro Antitumor Activity. *Inorg. Chem.* **2005**, *44*, 1867–1881.

(9) Adeyemi, J. O.; Onwudiwe, D. C. The Mechanisms of Action Involving Dithiocarbamate Complexes in Biological Systems. *Inorg. Chim. Acta* **2020**, *511*, 119809–119819.

(10) Tabrizi, L.; Abyar, F. Conjugation of Gold(III) Complex with Vitamin B1 and Chlorambucil Derivatives: Anticancer Evaluation and Mechanistic Insights. *Metallomics* **2020**, *12*, 721–731.

(11) Kouodom, M. N.; Boscutti, G.; Celegato, M.; Crisma, M.; Sitran, S.; Aldinucci, D.; Formaggio, F.; Ronconi, L.; Fregona, D. Rational Design of Gold(III)-Dithiocarbamato Peptidomimetics for the Targeted Anticancer Chemotherapy. *J. Inorg. Biochem.* **2012**, *117*, 248–260.

(12) Boscutti, G.; Feltrin, L.; Lorenzon, D.; Sitran, S.; Aldinucci, D.; Ronconi, L.; Fregona, D. T-Butylsarcosinedithiocarbamato Gold(III)-Based Anticancer Agents: Design, in Vitro Biological Evaluation and Interaction with Model Biomolecules. *Inorg. Chim. Acta* **2012**, *393*, 304–317.

(13) Williams, M. R. M.; Bertrand, B.; Hughes, D. L.; Waller, Z. A. E.; Schmidt, C.; Ott, I.; O'Connell, M.; Searcey, M.; Bochmann, M. Cyclometallated Au(III) Dithiocarbamate Complexes: Synthesis, Anticancer Evaluation and Mechanistic Studies. *Metallomics* **2018**, *10*, 1655–1666.

(14) Le, H. Van; Babak, M. V.; Ehsan, M. A.; Altaf, M.; Reichert, L.; Gushchin, A. L.; Ang, W.

H.; Isab, A. A. Highly Cytotoxic Gold(I)-Phosphane Dithiocarbamate Complexes Trigger an ER Stress-Dependent Immune Response in Ovarian Cancer Cells. *Dalton Trans.* **2020**, *49*, 7355–7363.

(15) Altaf, M.; Monim-ul-Mehboob, M.; Seliman, A. A. A.; Isab, A. A.; Dhuna, V.; Bhatia, G.; Dhuna, K. Synthesis, X-Ray Structures, Spectroscopic Analysis and Anticancer Activity of Novel Gold(I) Carbene Complexes. *J. Organomet. Chem.* **2014**, *765*, 68–79.

(16) Sun, R. W.-Y.; Zhang, M.; Li, D.; Zhang, Z.-F.; Cai, H.; Li, M.; Xian, Y.-J.; Ng, S. W.; Wong, A. S.-T. Dinuclear Gold(I) Pyrrolidinedithiocarbamato Complex: Cytotoxic and Antimigratory Activities on Cancer Cells and the Use of Metal-Organic Framework. *Chem. Eur. J.* **2015**, *21*, 18534–18538.

(17) Altaf, M.; Monim-ul-Mehboob, M.; Seliman, A. A. A.; Sohail, M.; Wazeer, M. I. M.; Isab, A. A.; Li, L.; Dhuna, V.; Bhatia, G.; Dhuna, K. Synthesis, Characterization and Anticancer Activity of Gold(I) Complexes That Contain Tri-Tert-Butylphosphine and Dialkyl Dithiocarbamate Ligands. *Eur. J. Med. Chem.* **2015**, *95*, 464–472.

(18) Sathyanarayana, D. N. *Vibrational Spectroscopy: Theory and Applications*, First.; New Age International (P) Ltd.: New Delhi, 2004.

(19) Ho, S. Y.; Tiekink, E. R. T. Crystal Structure of (Diethyldithiocarbamato)(Triethylphosphine)Gold(I), $Au[P(C_2H_5)_3][S_2CN(C_2H_5)_2]$. *Zeitschrift für Krist. - New Cryst. Struct.* **2005**, *220*, 342–344.

(20) Paolini, J. P. The Bond Order—Bond Length Relationship. *J. Comput. Chem.* **1990**, *11*, 1160–1163.

(21) Altaf, M.; Monim-ul-Mehboob, M.; Kawde, A.-N.; Corona, G.; Larcher, R.; Ogasawara, M.; Casagrande, N.; Celegato, M.; Borghese, C.; Siddik, Z. H.; Aldinucci, D.; Isab, A. A. New Bipyridine Gold(III) Dithiocarbamate-Containing Complexes Exerted a Potent Anticancer Activity against Cisplatin-Resistant Cancer Cells Independent of P53 Status. *Oncotarget* **2017**, *8*, 490–505.

(22) Boyer, J.; McLean, E. G.; Aroori, S.; Wilson, P.; McCulla, A.; Carey, P. D.; Longley, D. B.; Johnston, P. G. Characterisation of P53 Wild-Type and Null Isogenic Colorectal Cancer Cell Lines Resistant to 5-Fluorouracil, Oxaliplatin, and Irinotecan. *Clin. Cancer Res.* **2004**, *10*, 2158–2167.

(23) Schmidt, C.; Karge, B.; Misgeld, R.; Prokop, A.; Brönstrup, M.; Ott, I. Biscarbene Gold(I)

Complexes: Structure-Activity-Relationships Regarding Antibacterial Effects, Cytotoxicity, TrxR Inhibition and Cellular Bioavailability. *MedChemComm* **2017**, *8*, 1681–1689.

(24) Walther, W.; Dada, O.; Ott, I.; Prochnicka, A.; Büttner, B.; Zhu, X.; Tacke, M. In Vivo Investigations into the Carbene Gold Anticancer Drug Candidates NHC*-Au-SCN and NHC*-Au-Scyclo. *Trends Cancer Res.* **2018**, *13*, 63–70.

(25) Dada, O.; Sánchez-Sanz, G.; Tacke, M.; Zhu, X. Synthesis and Anticancer Activity of Novel NHC-Gold(I)-Sugar Complexes. *Tetrahedron Lett.* **2018**, *59*, 2904–2908.

(26) Rubbiani, R.; Schuh, E.; Meyer, A.; Lemke, J.; Wimberg, J.; Metzler-Nolte, N.; Meyer, F.; Mohr, F.; Ott, I. TrxR Inhibition and Antiproliferative Activities of Structurally Diverse Gold N-Heterocyclic Carbene Complexes. *MedChemComm* **2013**, *4*, 942–948.

(27) Gandin, V.; Fernandes, A. P.; Rigobello, M. P.; Dani, B.; Sorrentino, F.; Tisato, F.; Björnstedt, M.; Bindoli, A.; Sturaro, A.; Rella, R.; Marzano, C. Cancer Cell Death Induced by Phosphine Gold(I) Compounds Targeting Thioredoxin Reductase. *Biochem. Pharmacol.* **2010**, *79*, 90–101.

(28) Szablewski, L. Expression of Glucose Transporters in Cancers. *Biochem. Biophys. Acta - Rev. Cancer* **2013**, *1835*, 164–169.

(29) Brown, R. S.; Wahl, R. L. Overexpression of Glut-1 Glucose Transporter in Human Breast Cancer. An Immunohistochemical Study. *Cancer* **1993**, *72*, 2979–2985.

(30) Skehan, P.; Storeng, R.; Scudiero, D.; Monks, A.; McMahon, J.; Vistica, D.; Warren, J. T.; Bokesch, H.; Kenney, S.; Boyd, M. R. New Colorimetric Cytotoxicity Assay for Anticancer-Drug Screening. *J. Natl. Cancer Inst.* **1990**, *82*, 1107–1112.

(31) United Kingdom Co-Ordinating Committee on Cancer Research (UKCCCR) Guidelines for the Welfare of Animals in Experimental Neoplasia (Second Edition). *Br. J. Cancer* **1998**, *77*, 1–10.

Chapter Five

Synthesis of NHC*-Gold(I) Amino Acid and Peptide Conjugates

5.1 Introduction

Cancer cells differ from normal healthy cells in several ways, one of which is their uptake of nutrients. Cancer cells require an increased input of amino acids in order to continue their rapid cell proliferation. These amino acids have key roles in the TCA cycle, redox regulation and glutamine transporters.[1] As a result, cancer cells over-express amino acid transporters.[2,3] There is a particular demand for essential amino acids, which enter the cell via solute carriers (SLC). Both the L-type amino acid transporters (LAT1-4) and the alanine-serine-cysteine transporter 2 (ASCT2) serve as important routes for amino acid entry into the cell.[4,5] Cancer cell specificity can be achieved by utilising the over-expression of amino acid transporters on tumour cells. The concept of combining a metal complex and a biomolecule for heightened cell selectivity and cytotoxicity is very promising.[6,7] However, NHC-gold complexes conjugated to amino acids and peptides remain quite scarce. Approaches to incorporate amino acids to NHC-gold complexes include coordination to the nitrogen atom of the imidazole,[8] to the gold atom via the sulfur atom of cysteine[9] or a thiolated non-proteinogenic amino acid, or via the sulfur atom of a thiolate ligand that is capable of further functionalisation.

Metzler-Nolte et al. first reported the conjugation of a NHC-gold(I) complex to *N*-Boc protected cysteine methyl ester (Boc-Cys-OMe) and *N*-Boc protected leucine-cysteine ethyl ester (Boc-Leu-Cys-OEt; **5.1**, **Figure 5.1**).[10] The amino acid and dipeptide were coordinated to the metal centre via the thiol of the amino acid cysteine. NHC-gold(I) halide complexes were also synthesised with a phenylalanine derivative attached to the nitrogen atom of the imidazole

(**1.44**). Interestingly, when tested for their antitumoural properties significantly higher activity was observed when the amino acid was coordinated directly to the gold.

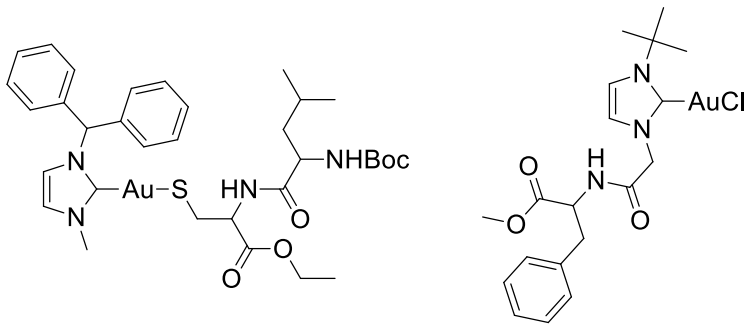

5.1 **1.44**

Figure 5.1 Amino acid derived NHC-gold(I) complexes developed by Metzler-Nolte et al.[10]

Gimeno et al. designed complexes with mercaptonicotinic acid to provide a site for further functionalisation.[11] The mercaptonicotinic acid enabled the gold-sulfur bond to be formed, whilst the carboxylic acid allowed functionalisation to occur with amino acids and peptides. This technique led to the synthesis of phosphine gold(I) complexes with glycine, alanine, phenylalanine, valine, methionine and proline methyl esters (**5.3**, **Figure 5.2**). The group progressed on to develop a series of phosphine gold(I) complexes with cysteine-containing dipeptides, which coordinated directly to the gold atom (**5.4**, **Figure 5.2**).[12] The latter complexes displayed significantly more activity than cisplatin and proved more active than their nicotinic derivatives. Furthermore, increased activity was observed when the dipeptide included a glycine or proline amino acid.

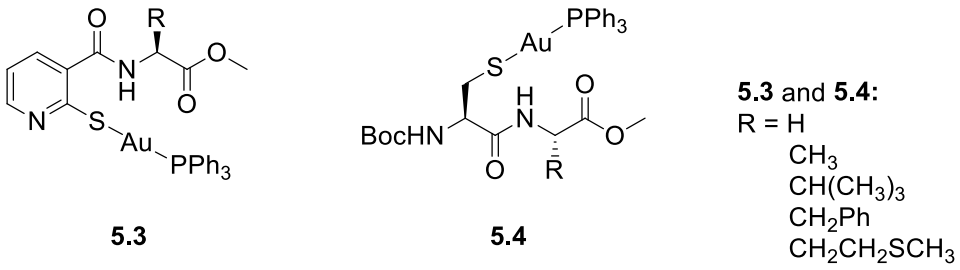

5.3 **5.4**

Figure 5.2 Phosphine gold(I) complexes with amino acids and peptides.

In light of this discovery, gold(I) complexes with 4-mercaptoproline were developed.[13] Thiolation of commercially available 4-hydroxyproline aminoester chlorohydrate led to phosphine-gold(I) complexes with triphenylphosphine (**5.5**, **Figure 5.3**) and 2-pyridyl diphenylphosphine. From these compounds the dinuclear analogues were also synthesised. As elucidated in previous work, the presence of the amino acid glycine increased the cytotoxicity of the compounds. Thus, glycine was incorporated via the carboxylic acid of the proline to give gold(I)-dipeptide complex **5.6**. While all complexes exhibited higher activity than cisplatin, the proline carboxylic acid displayed the lowest activity. Both the methyl ester and dipeptide complex showed excellent cytotoxicity.

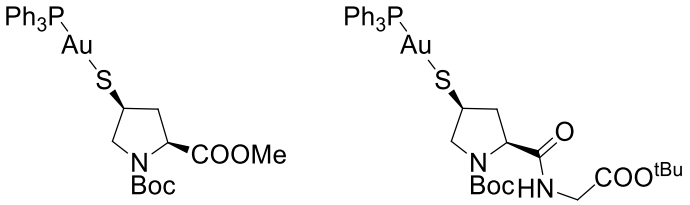

5.5 **5.6**

Figure 5.3 *N*-Protected 4-thioproline gold(I) complexes.

Previous work in the Tacke group has incorporated *N*-acetyl-L-cysteine (NAC) derivatives to produce more biocompatible complexes (**5.7**-**5.9**, **Figure 5.4**).[14] NHC*-Au-NAC and the methyl and ethyl ester derivatives displayed low single-digit micromolar activity against the human colon cancer cell line HCT-116 and the multidrug-resistant breast cancer cell line MCF-7^{topo}. It was noted that the ester derivatives displayed higher cytotoxicity than the free carboxylic acid complex. In the best case, an eight-fold increase in activity was observed when compared to the precursor complex **1.21**. This could be as a result of the amino acid cysteine acting as a drug transporter.

This concept of involving a biomolecule to enhance the cell targeting properties of a drug has also been addressed previously in our group with the conjugation of thioglucosides. A series of NHC*-gold(I) complexes with α- and β-thioglucosides were tested for their antiproliferative properties.[15] Cell testing on the National Cancer Institute (NCI) 60 cancer cell panel reported low micromolar and even sub-micromolar GI_{50} values against several human cancer cell lines. As demonstrated in Chapter 4, the α-thioglucoside **4.12** (**Figure 5.4**) displayed very high activity against the human prostate cancer PC-3. Its β-thioglucoside analogue reported an IC_{50} value of 6.1 μM[16] against the MCF-7 breast cancer cell line which is comparable to the IC_{50} values reported by the NAC-based complexes.

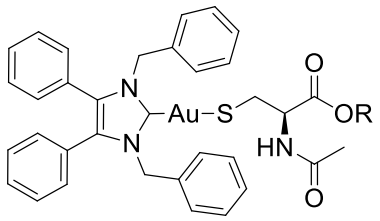

5.7: R = H; IC_{50} 7.1 μM
5.8: R = CH_3; IC_{50} 6.3 μM
5.9: R = CH_2CH_3; IC_{50} 5.4 μM

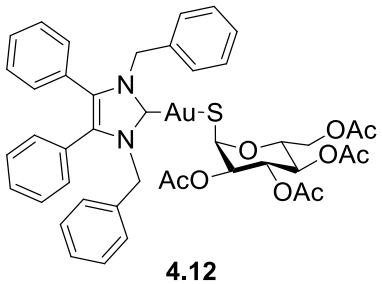

4.12

Figure 5.4 NHC*-gold(I) NAC derivatives with IC_{50} values reported against the MCF-7 cell line.

Chapter Proposal

In this Chapter, we seek to build on the success of the NHC*-gold(I) dithiocarbamate complexes developed in Chapter 4 by further modification of the NHC-gold complex with a thiolate ligand. As previously shown with the dimethyldithiocarbamato complex **4.8** the presence of a thiolate ligand can increase the cytotoxicity significantly. Drawing inspiration from the NAC compounds **5.7**-**5.9** and the α-thioglucoside **4.12**, amino acids and dipeptides will be conjugated to the NHC*-gold(I) complex. The aim is to enhance the cell targeting properties of the gold complex in an effort to develop more potent anticancer drug candidates.

5.2 Synthesis

5.2.1 Solid-Phase Dipeptide Synthesis

In order to investigate the potential of NHC-gold(I) complexes with dipeptides we first prepared a series of cysteine-based dipeptide compounds with L-alanine, L-tyrosine and L-phenylalanine. The dipeptide compounds were synthesised via solid-phase peptide synthesis (**Scheme 5.1**). Starting from Fmoc-Rink Amide aminomethyl-polystyrene resin, Fmoc cleavage with piperidine/DMF gave the free amine which was subsequently coupled to the first Fmoc-protected amino acid (i, **Scheme 5.1**). Two successive coupling reactions with OxymaPure/DIC (ii) and PyBOP/DIPEA (iii) ensured full coordination of the Fmoc-protected amino acid to the resin. Next, the Fmoc group on the amino acid was removed to allow the amino group to attach to the carboxylic acid of the second amino acid with the same coupling conditions as before. After the final Fmoc cleavage the free amine was acetylated by treatment with acetic anhydride/DIPEA (iv) and the products were released from the resin with 95% TFA (v). After workup the compounds **5.10**-**5.14** were confirmed with ^{1}H-NMR spectroscopy.

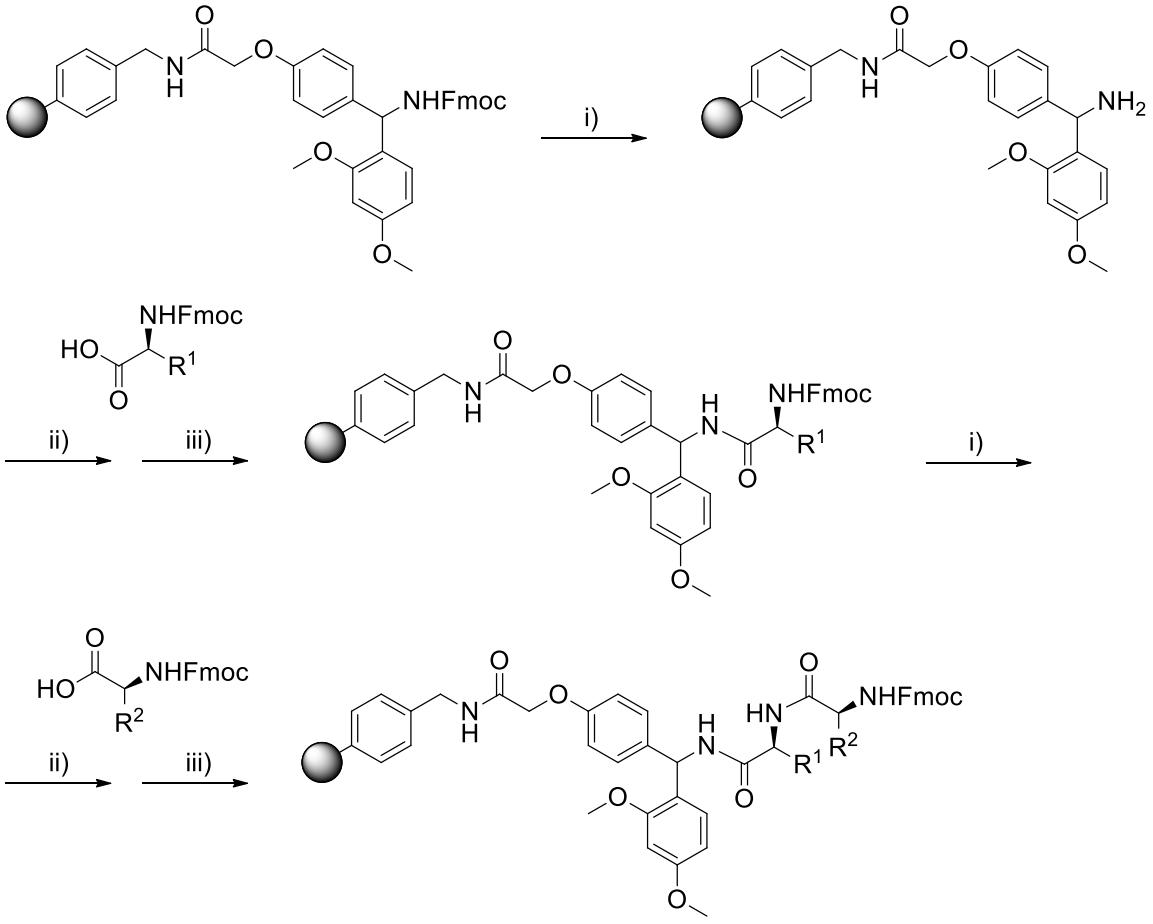

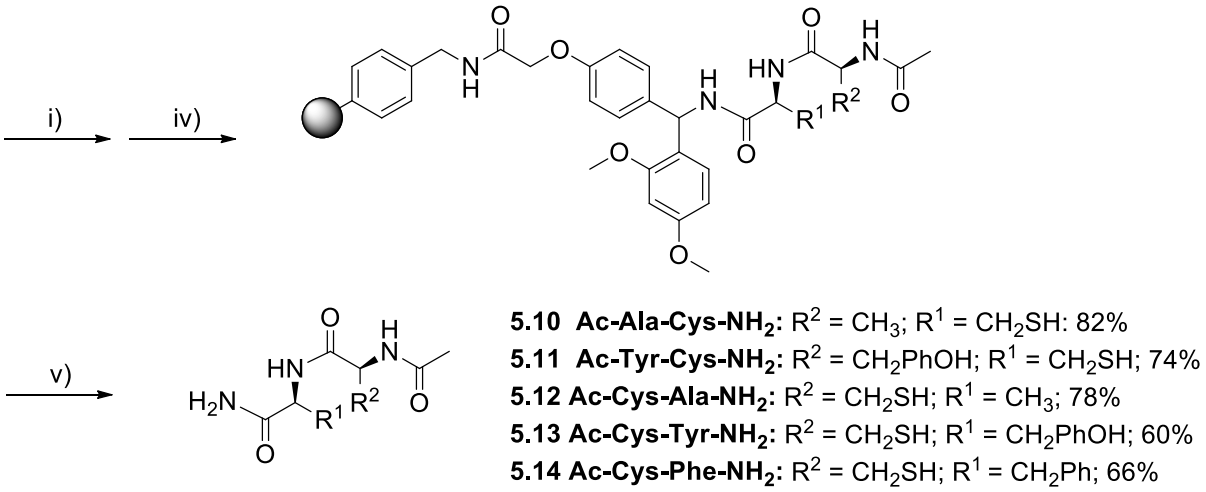

Scheme 5.1 Synthesis of the dipeptides **5.10**-**5.14**. i) 1. 40% piperidine in DMF, 10 min. 2. 20% piperidine in DMF, 10 min ii) Fmoc-aa, OxymaPure, DIC, DMF, 60 min, iii) Fmoc-aa, PyBOP, DIPEA, DMF, 1 h, iv) 30% acetic anhydride, 5% DIPEA, DMF, 15 min, v) 95% TFA, 2.5% Et_3Si, H_2O, 4 h.

5.2.2 Synthesis of NHC*-Gold(I) Dipeptide Complexes

Originally, the NHC*-gold(I) NAC derivatives (**5.7**-**5.9**) were prepared using an excess of potassium carbonate in a biphasic medium of EtOAc/H_2O.[14] We established a procedure with stoichiometric amounts of potassium *tert*-butoxide in THF at -30 °C. This method was tested by reacting **1.21** with NAC (**5.15**) and its methyl and ethyl ester derivatives **5.16** and **5.17** (**Scheme 5.2**). The condition afforded compounds **5.7**-**5.9** in greater yields and higher purities. Additionally, the reaction time was reduced significantly from 24 h to 3 h.

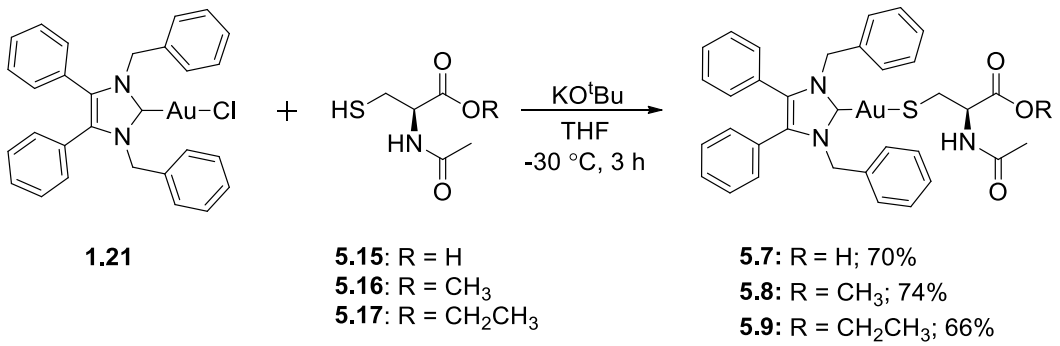

Scheme 5.2 Synthesis of NHC*-gold(I) NAC compounds **5.7**-**5.9**.

This method was applied to the conjugation of the prepared dipeptides **5.10**-**5.14** to the NHC*-gold(I) complex. However, these reactions were not successful and led to a mixture of products. Reacting Ac-Ala-Cys-NH_2 (**5.10**) and **1.21** according to the conditions applied above (**Scheme 5.2**) resulted in only 37% formation of **5.18** (percentage conversion is based on ^{1}H-NMR integration). Interestingly, the major product formed appeared at δ = 5.21 ppm in the ^{1}H-NMR spectra, which corresponds to the dimeric $[NHC^*_2Au]^+$ complex, as seen in Chapter 2. However, when the reaction proceeded for 24 h, as opposed to 3 h, the conversion increased to give **5.18** as the major component (85%, **Table 5.1**). Thus, we allowed the conjugation of dipeptides **5.11**-**5.13** to **1.21** to occur over 24 h. Unfortunately, complexes **5.19**-**5.21** were also formed in mixtures.

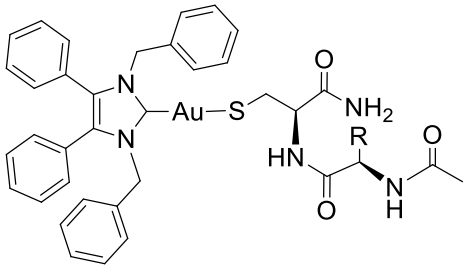

5.18: R = CH_3 (Ala-Cys)
5.19: R = CH_2PhOH (Tyr-Cys)

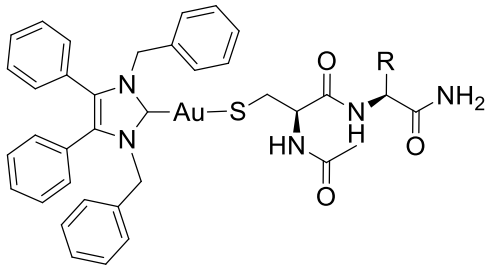

5.20: R = CH_3 (Cys-Ala)
5.21: R = CH_2PhOH (Cys-Tyr)
5.22: R = CH_2Ph (Cys-Phe)

Figure 5.3 NHC*-gold(I) dipeptide complexes **5.18**-**5.22**.

Table 5.1 details the best results obtained for the synthesis of complexes **5.18**-**5.22**. In all cases, the formation of the dimeric complex was observed in their respective ^{1}H-NMR spectra at δ = 5.21-5.23 ppm but for **5.21** and **5.22** a third species appeared at δ = 5.15-5.16 ppm. In addition, some reactions led to the formation of the imidazolium salts, which were detected by the presence of the imidazolium proton on the ^{1}H-NMR spectra in the region of δ = 8-11 ppm.

Table 5.1 Formation of gold(I) dipeptide compounds **5.18**-**5.22**.

Dipeptide	Gold-Dipeptide	Conversion (%)	Ratio (a:b:c)*
5.10	**5.18**	85	**5.7** : 1
5.11	**5.19**	62	**1.6** : 1
5.12	**5.20**	77	**3.4** : 1
5.13	**5.21**	37	**1.6** : 1.7 : 1
5.14	**5.22**	27	**1.3** : 2.4 : 1

* a= 5.46 ppm, b= 5.21 ppm, c= 5.16 ppm.

The ratios of product formed were determined with ^{1}H-NMR integration. As highlighted in Chapter 2, the CH_2 group on the NHC ligand acts as an important diagnostic tool to detect the presence of the NHC species. It has been useful to differentiate between the imidazolium salts, the monocarbene complexes and the biscarbene complexes as upon modification the singlet shifts. Considering compound **5.21**, the region of δ = 4.7-5.8 ppm in the ^{1}H-NMR spectra presents three distinct peaks at δ = 5.15, 5.21 and 5.46 ppm (**Figure 5.6**). The latter is the desired peak of the gold dipeptide complex which can be identified as the quartet. These peaks represent the four protons of the two CH_2 groups on the NHC. Although for the determination of the ratios the integration of the smallest peak has been set to one. Therefore, we can deduce the percentage of our desired product.

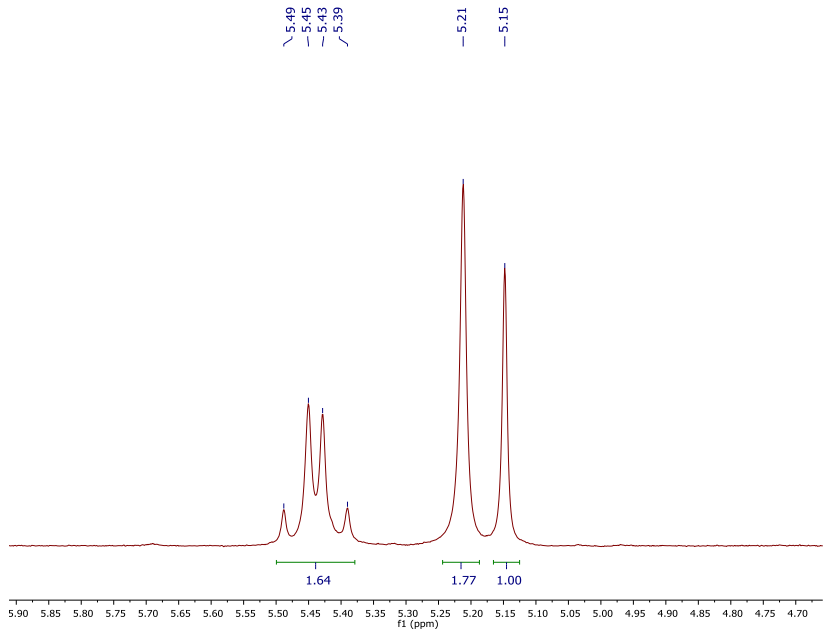

Figure 5.6 ^{1}H-NMR spectra of **5.21** in the region of δ = 4.7-5.8 ppm.

Unfortunately, the NHC-gold dipeptide complexes **5.18**-**5.22** were unable to be isolated from their mixtures. Purification via column chromatography isolated the starting material and dimeric product. While an attempt at recrystallisation resulted in the formation of a cationic trimeric NHC*-gold(I) species with a proposed sulfur centre. The quality of the crystal was poor and thus was not refined. **Figure 5.7** displays the most probable structure of the cationic species formed as a result of the disproportionation reaction in **Equation 5.1**.

$$2SR^{-} \longrightarrow S^{2-} + R\text{-}R + \tfrac{1}{8}S_8 \qquad \text{(Equation 5.1)}$$

The desulfurization of the cysteine-based dipeptide revealed how instable these complexes are.[17] Disappointedly, attempts at purification led to the degradation of the product as it rapidly underwent ligand scrambling to form the highly stable dimeric product.

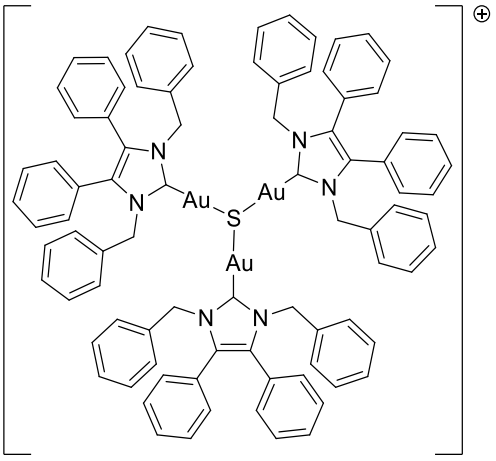

Figure 5.7 Proposed structure of $[(NHC^*Au)_3S]^+$.

Although complexes **5.18**-**5.22** could not be isolated from their impurities, the complexes were confirmed with ^1H and ^{13}C-NMR spectroscopy. The ^1H-NMR spectra showed the appearance of new peaks corresponding to the dipeptide compounds. The disappearance of the thiol triplet seen in the ^1H-NMR of the dipeptides at δ = 2.19-2.26 ppm confirmed the coordination of the sulfur to the gold. Furthermore, the CH_2 peak of the NHC benzyl group was shifted from a singlet at δ =5.44 ppm to a quartet at δ = 5.44-5.48 ppm. The presence of the chiral dipeptide caused the CH_2 peak to shift from a symmetrical singlet to a quartet. In addition, ESI mass spectrometry confirmed the formation of the complexes. High resolution MS detected the $[M + H]^+$ ions of compounds **5.18** and **5.22**, while the $[M + K]^+$ ions of compounds **5.19** and **5.21** were confirmed with low resolution MS.

5.2.3 Reaction Optimisation

Reaction optimisation was conducted in an attempt to design a procedure capable of forming stable NHC*-gold(I) dipeptide complexes. Commercially available L-cysteine methyl ester hydrochloride was selected for the reaction. Methanol was added initially to aid the solubility of L-cysteine methyl ester. As shown in **Table 5.2**, switching from THF to CH_2Cl_2 improved the formation of **5.24** drastically (entry 1 and 2). Entries 2-6 reported equally high percentages of **5.24** formed, despite the modification of both the temperature and reaction time. Interestingly, there was no difference in the percentage of product converted when reacted at -30 °C and allowed to warm for 4 h (entry 3) or when reacted at room temperature for 1 h (entry 6).

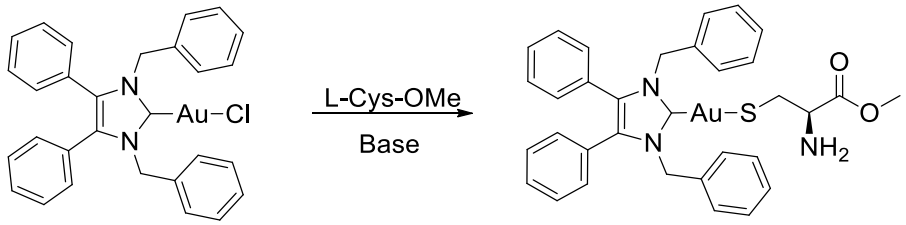

1.21 **5.24**

Entry	Base (equiv.)	Solvent	Temp (°C)	Time (h)	Conversion (%)
1	KO^{t}Bu (1)	THF-MeOH	-30[a]	24	47
2	KO^{t}Bu (1)	CH_2Cl_2-MeOH	-30[a]	24	93
3	KO^{t}Bu (1)	CH_2Cl_2-MeOH	-30[a]	4	98
4	KO^{t}Bu (1)	CH_2Cl_2-MeOH	rt	24	90
5	KO^{t}Bu (1)	CH_2Cl_2-MeOH	rt	4	96
6	KO^{t}Bu (1)	CH_2Cl_2-MeOH	rt	1	98
7	Cs_2CO_3 (1)	CH_2Cl_2-MeOH	rt	4	4.9
8	KOH (10)	CH_2Cl_2-MeOH	rt	4	16
9	K_2CO_3 (2)	Acetone	rt	24	92
10	Et_3N (5)	CH_2Cl_2	rt	48	55
11	Et_3N (5)	CH_2Cl_2	rt	72	46

Table 5.2 NHC*-Au-Cys-OMe (**5.24**) reaction optimisation. Percentage conversions were determined by ^{1}H-NMR spectroscopic analysis of the crude products. [a] Reaction began at -30 °C and was allowed to warm.

The highest conversions of **5.24** were achieved with potassium *tert*-butoxide. Low conversions of product were observed with caesium carbonate (entry 7), potassium hydroxide (entry 8) and triethylamine (entry 10 and 11). Using the conditions reported by Gimeno et al.,[12] excess potassium carbonate in acetone resulted in high conversions of **5.24** (entry 9). As seen in the synthesis of the dipeptide complexes, the formation of the dimeric $[NHC^*_2Au]^+$ complex was apparent. The use of triethylamine and caesium carbonate led to multiple species.

Fortunately, the reaction optimisation led to the successful synthesis of NHC*-Au-Cys (**5.23**) and the methyl ester complex **5.24** (**Scheme 5.3**). Compounds **5.23** and **5.24** were of interest as they would help elucidate the effect of the protecting groups on the carboxylic acid and amine moieties. Compounds **5.23** and **5.24** were prepared by reacting **1.21** with the corresponding cysteine compound and potassium *tert*-butoxide at room temperature for an 1 h (entry 6, **Table 5.2**). Both compounds were achieved in high yields of 76% and 73%, respectively. The ^{1}H-NMR spectra of the compounds showed the appearance of new signals corresponding to the CH_2, CH and in the case of **5.24** the CH_3 moieties of the cysteine derivatives. Also, both compounds were confirmed with ESI mass spectrometry and IR spectroscopy.

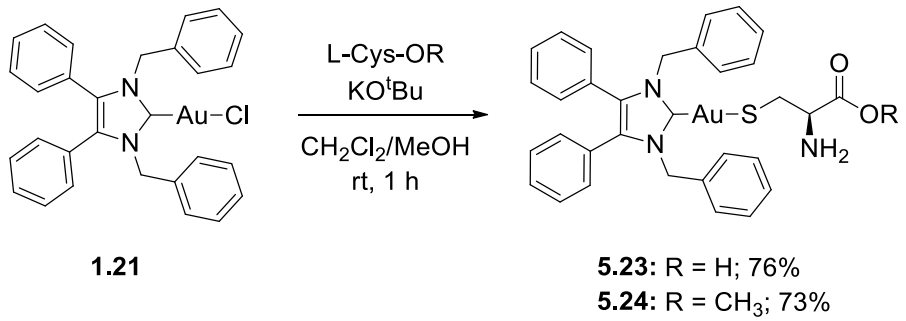

1.21

5.23: R = H; 76%
5.24: R = CH_3; 73%

Scheme 5.3 Synthesis of NHC*-Au-Cys (**5.23**) and NHC*-Au-Cys-OMe (**5.24**).

After considering the results of the reaction optimisation, it was decided to perform the coordination of dipeptides to the gold complex under conditions used in entries 6 and 9. The data would suggest a shorter reaction time would avoid the generation of the dimeric complex. Firstly, dipeptide **5.12** was reacted with potassium *tert*-butoxide and **1.21** at room temperature for 45 min. Unfortunately, the ^{1}H-NMR spectra of the crude product revealed only the starting material **1.21** and a small amount of the dimer. This indicated that the formation of the dimer began before the dipeptide complex, as opposed to as a result of the degradation of the fully formed gold-dipeptide complex. To investigate this theory further, a reaction was conducted

at room temperature for 4 h instead of the shorter 45 min. The ^{1}H-NMR spectra of the crude product showed the CH_2 peaks for the starting material **1.21** at δ = 5.44 ppm, the dimer at δ = 5.22 pm, and the desired dipeptide complex at δ = 5.47 ppm. As predicted, more of the dimeric compound had been made than the dipeptide compound. At this stage we proposed that the issue lay with the base potassium *tert*-butoxide. Thus, **5.14** was reacted with **1.21** and an excess of potassium carbonate in acetone at room temperature (entry 9). However, after 24 h the ^{1}H-NMR spectra of the crude product revealed the same result. The major component found was the dimer at δ = 5.21 pm, while the impurity at δ = 5.16 ppm was present also. Unfortunately, screening the choice of base, base equivalents, dipeptide equivalents, choice of solvent, under wet or dried schlenk conditions, temperature and time of the reaction has been extensively investigated to no avail.

5.3 Conclusion and Outlook

This Chapter investigated the synthesis of NHC-gold(I) complexes with amino acids and peptides. These compounds were achieved through a novel approach using potassium *tert*-butoxide. The successful synthesis of previously reported NHC*-gold(I) NAC derivatives **5.7**-**5.9** acted as proof of concept. Cysteine-based dipeptides with alanine, tyrosine and phenylalanine (**5.10**-**5.14**) were synthesised via solid-phase peptide synthesis in high yields. Unfortunately, the above method towards the synthesis of NHC*-gold(I) complexes with cysteine-based dipeptides was unsuccessful. NHC*-gold(I) dipeptides **5.18**-**5.22** were formed alongside the dimeric $[NHC^*_2Au]^+$ complex and proved inseparable. Purification and isolation led to degradation of the complexes. Reaction optimisation led to the synthesis and characterisation of NHC*-gold(I) cysteine (**5.23**) and NHC*-gold(I) cysteine methyl ester (**5.24**). After consideration, the NHC-gold bioconjugates were not sent for biological assessment due to their instability in solution. These complexes were designed with cell specificity in mind. It was intended that their dipeptide moieties would provide transport for the drug directly to the TrxR redox centre, thus increasing their efficacy. However, these complexes do not warrant further investigation as potential drug candidates as they are too fugacious. Future work will concentrate on establishing a reliable synthesis to stable NHC-gold(I) dipeptide complexes.

5.4 Experimental Section

General Procedure for the Solid-Phase Synthesis of the Dipeptides:

***N*-Acetyl-L-alanyl-L-cysteine amide (Ac-Ala-Cys-NH_2) (5.10)**

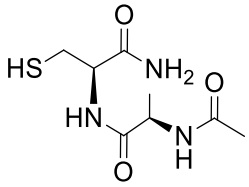

The Fmoc-Rink Amide aminomethyl-polystyrene resin (300 mg, 0.22 mmol; 100-200 mesh; Iris Biotech GMBH) was added to the reactor. The Fmoc protecting group was removed by treating the resin with 40% piperidine in DMF (3 mL). This was stirred for 10 min on a mechanical stirrer, followed by washing with DMF (3 mL x 3 times). A solution of 20% piperidine in DMF (3 mL) was added and stirred for 10 min, followed by washing with DMF (3 mL x 3). The first Fmoc-protected amino acid (0.89 mmol, 4 equiv.), Fmoc-Cys-OH, was coupled to the Rink Amide resin with ethyl-2-cyano-2-(hydroxyimino)acetate (OxymaPure, 0.89 mmol, 4 equiv.) and *N*,*N*′-diisopropylcarbodiimide (DIC, 1.78 mmol, 8 equiv.) in DMF (4 mL) and stirred for 60 min. After washing with DMF (3 mL x 3), the Rink Amide resin was treated to a second coupling of the Fmoc-protected amino acid with the addition of benzotriazole-1-yl-oxy-tris-pyrrolidino-phosponium hexaflourophosphate (PyBOP, 0.89 mmol, 4 equiv.) and *N*-*N*′-diisopropylethylamine (DIPEA, 1.78 mmol, 8 equiv.) in DMF (4 mL) and stirred for 1 h. After washing with DMF (3 mL x 3), the Fmoc group was removed with the addition of both 40% piperidine and 20% piperidine in DMF (3 mL) as described above. The second Fmoc-protected amino acid (0.89 mmol, 4 equiv.), Fmoc-Ala-OH, was coupled to the resin firstly, by the procedure above with OxymaPure and DIC and subsequently, with PyBOP and DIPEA. After washing with DMF (3 mL x 3), the Fmoc group was removed with both 40% piperidine and 20% piperidine in DMF (3 mL) as detailed above. After the standard washing procedure the resin was acetylated with 30% acetic anhydride and 5% DIPEA solution in DMF (4 mL). This was stirred for 15 min and then washed with DMF (3 mL x 3), MeOH (4 mL x 3) and Et_2O (4 mL). The dipeptide was cleaved from the resin with the addition of 95% trifluoroacetic acid (TFA) and 2.5% triethylsilane in water (3 mL) and stirred for 4 h. The resin was rinsed with TFA (2 mL). The excess solvent was removed by N_2 purging. Et_2O (10 mL) was added to

precipitate the product and was washed with 10% acetonitrile in water (5 mL x 3). The final product was isolated in the aqueous phase and was lyophilised to give **5.8** as a white powder (42.7 mg, 82%). ^{1}H-NMR (500 MHz, D_2O, δ ppm): 4.51 (dd, *J* = 7.2, 5.4 Hz, 1H, CH), 4.32 (q, *J* = 7.2 Hz, 1H, CH), 3.01-2.90 (m, 2H, CH_2), 2.24 (s, 1H, SH), 2.04 (s, 3H, CH_3), 1.41 (dd, *J* = 7.2 Hz, 3H, $CH_{3\text{-Ala}}$). ^{13}C-NMR (101 MHz, D_2O, δ ppm): 175.4 (C=O), 174.2 (C=O), 55.2 (CH), 49.8 (CH), 25.1 (CH_2), 21.5 (CH_3), 16.3 (CH_3).

The following dipeptides were synthesised according to the peptide synthesis procedure described above.

***N*-Acetyl-L-tyrosinyl-L-cysteine amide (5.11)**

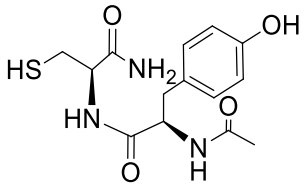

A white powder was afforded (53.6 mg, 74%). ^{1}H-NMR (400 MHz, d^6-DMSO, δ ppm): 9.15 (s, 1H, NH), 8.04 (dd, *J* = 12.6, 8.1 Hz, 2H, ArCH), 7.33-7.12 (m/q, 2H, ArCH), 4.39 (td, *J* = 9.4, 4.6 Hz, 1H, CH), 4.28 (td, *J* = 7.3, 5.1 Hz, 1H, CH), 2.93-2.85 (m, 2H, CH_2), 2.69-2.56 (m, 2H, CH_2), 2.19 (t, *J* = 8.3 Hz, 1H, SH), 1.76 (s, 3H, CH_3). ^{13}C-NMR (101 MHz, d^6-DMSO, δ ppm): 171.6 (C=O), 171.3 (C=O), 169.4 (C=O), 155.7 (C), 130.0 (CH), 127.9 (C), 114.8 (CH), 54.7 (CH), 52.9 (CH), 36.4 (CH_2), 30.7 (CH_2), 22.5 (CH_3).

***N*-Acetyl-L-cysteinyl-L-alanine amide (5.12)**

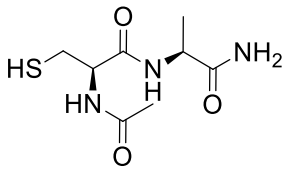

A white powder was afforded (40.5 mg, 78%). ^{1}H-NMR (300 MHz, D_2O, δ ppm): 4.57 (td, *J* = 7.5, 5.5 Hz, 1H, CH), 4.39 (q, *J* = 7.2 Hz, 1H, CH), 2.98 (ddd, *J* = 13.8, 8.5, 5.5 Hz, 1H, CH_2), 2.86 (dt, *J* = 13.5, 7.9 Hz, 1H, CH_2), 2.61 (t, *J* = 8.4 Hz, 1H, SH), 2.08 (s, 3H, CH_3), 1.43 (d, *J* = 7.3 Hz, 3H,

$CH_{3\text{-Ala}}$). ^{13}C-NMR (101 MHz, D_2O, δ ppm): 177.3 (C=O), 172.8 (C=O), 55.3 (CH), 51.4 (CH), 25.8 (CH_2), 21.4 (CH_3), 17.2 (CH_3).

_N_-Acetyl-L-cysteinyl-L-tyrosine amide (5.13)

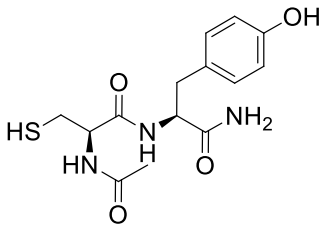

A white powder was afforded (43.4 mg, 60%). ^{1}H-NMR (400 MHz, d^6-DMSO, δ ppm): 9.15 (s, 1H, NH), 8.04 (d, *J* = 7.8 Hz, 2H, ArCH), 7.88 (d, *J* = 8.2 Hz, 2H, ArCH), 4.36-4.27 (m, 1H, CH), 3.38 (q, *J* = 7.0 Hz, 1H, CH), 2.89 (dd, *J* = 13.8, 4.8 Hz, 1H, CH_2), 2.75-5.66 (m, 2H, CH_2), 2.59 (dt, *J* = 13.4, 7.9 Hz, 1H, CH_2), 2.26 (t, *J* = 8.4 Hz, 1H, SH), 1.84 (s, 3H, CH_3). ^{13}C-NMR (101 MHz, d^6-DMSO, δ ppm): 172.8 (C=O), 169.6 (C=O), 169.5 (C=O), 155.7 (C), 130.1 (CH), 127.8 (C), 114.8 (CH), 55.1 (CH), 51.2 (CH), 36.5 (CH_2), 30.7 (CH_2), 22.5 (CH_3).

_N_-Acetyl-L-cysteine methyl ester (5.16)

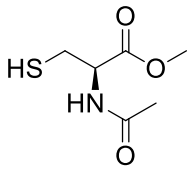

Using modified literature conditions,[18] *N*-acetyl-L-cysteine (**5.15**) (1.0 g, 6.13 mmol) was dissolved in MeOH (30 mL) with 1 drop of concentrated H_2SO_4 and refluxed at 90 °C for 24 h. The solvent was removed under reduced pressure to give a clear oil. The crude oil was purified by column chromatography (*c*-Hex/EtOAc; 1:1) to yield a clear oil, which gradually solidified as a white solid (413.5 mg, 38%). ^{1}H-NMR (300 MHz, $CDCl_3$, δ ppm): 6.76 (d, *J* = 6.0 Hz, 1H, NH), 4.82 (dt, *J* = 8.1, 4.4 Hz, 1H, CH), 3.72 (s, 3H, OCH_3), 2.93 (dd, *J* = 8.9, 4.4 Hz, 2H, CH_2), 2.01 (s, 3H, CH_3), 1.39 (t, *J* = 8.9 Hz, 1H, SH). ^{13}C-NMR (101 MHz, $CDCl_3$, δ ppm): 170.7 (C=O), 169.9 (C=O), 53.7 (CH), 52.9 (OCH_3), 27.0 (CH_2), 23.3 (CH_3). Data is consistent with that reported in the literature.[19]

***N*-Acetyl-L-cysteine ethyl ester (5.17)**

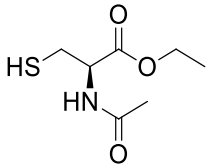

In a procedure identical to the above reaction: **5.15** (1.0 g, 6.13 mmol) stirred in EtOH (30 mL) with H_2SO_4 (1 drop) at reflux for 24 h. After purification by column chromatography (*c*-Hex/EtOAc; 1:1) a white solid was obtained (527 mg, 45%). ^{1}H-NMR (300 MHz, $CDCl_3$, δ ppm): 6.75 (d, *J* = 6.3 Hz, 1H, NH), 4.79 (dt, *J* = 8.0, 4.4 Hz, 1H, CH), 4.18 (dd, *J* = 7.1, 3.2 Hz, 2H, OCH_2), 2.93 (dd, *J* = 8.9, 4.4 Hz, 2H, CH_2), 2.01 (s, 3H, CH_3), 1.36 (t, *J* = 8.9 Hz, 1H, SH), 1.24 (t, *J* = 7.2 Hz, 3H, CH_2CH_3). ^{13}C-NMR (101 MHz, $CDCl_3$, δ ppm): 172.3 (C=O), 170.0 (C=O), 70.1 (OCH_2), 54.9 (CH), 51.9 (CH_2CH_3), 26.2 (CH_2), 23.1 (CH_3). Data is consistent with that reported in the literature.[20]

(1,3-Dibenzyl-4,5-diphenylimidazol-2-ylidene)gold(I) *N*-acetyl-L-cysteine (5.7)

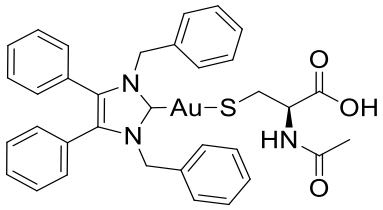

KO^{t}Bu (8.9 mg, 0.079 mmol, 1.0 equiv.) was added to a solution of **5.15** (14 mg, 0.087 mmol, 1.1 equiv.) in THF (5 mL) at -30 °C. NHC*-gold(I) chloride (**1.21**) (50 mg, 0.079 mmol, 1.0 equiv.) in THF (5 mL) was added to the reaction and stirred for 3 h warming gradually to rt. The reaction was monitored by TLC (*c*-Hex/EtOAC; 1:1). The solvent was removed under reduced pressure. The residue was dissolved in CH_2Cl_2 (20 mL) and filtered through sintered glass. The solvent was reduced to approximately 2 mL and pentane (40 mL) was added to precipitate the product. This was filtered, washed with pentane (15 mL) and dried *in vacuo* to give a white solid (41.9 mg, 70%). ^{1}H-NMR (400 MHz, $CDCl_3$, δ ppm): 7.33-7.27 (m, 3H, ArCH), 7.25-7.17 (m, 11H, ArCH), 7.06-6.95 (dd, *J* = 11.1, 5.9 Hz, 8H, ArCH), 6.81 (d, *J* = 6.5 Hz, 1H, NH), 5.42 (s, 4H, $CH_{2\text{-}Bz}$), 4.86 (s, 1H, CH), 3.48-3.40 (m, 1H, CH_2), 3.04 (m, 1H, CH_2), 1.99 (s, 3H, CH_3). ^{13}C-NMR (101 MHz, $CDCl_3$, δ ppm): 175.6 (C=O), 171.2 (C=O), 136.7 (C), 132.3 (C), 131.2 (CH), 129.6 (C), 129.0 (CH), 128.9 (CH), 128.3 (CH), 127.9 (CH), 127.8 (CH), 58.0 (CH), 53.0 ($CH_{2\text{-}Bz}$), 30.1 (CH_2), 26.0 (CH_3). Data is consistent with that reported in the literature.[14]

(1,3-Dibenzyl-4,5-diphenylimidazol-2-ylidene)gold(I) *N*-acetyl-L-cysteine methyl ester (5.8)

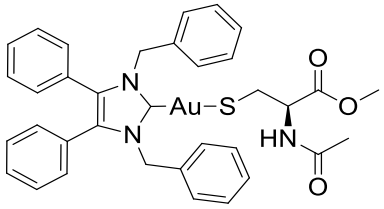

In a procedure identical to the above reaction: **1.21** (50 mg, 0.079 mmol, 1 equiv.), **5.16** (14 mg, 0.087 mmol, 1.1 equiv.), KO^{t}Bu (8.9 mg, 0.079 mmol, 1 equiv.) and THF (2 x 5 mL). White solid (45.5 mg, 74%). ^{1}H-NMR (400 MHz, $CDCl_3$, δ ppm): 7.30 (t, *J* = 7.4 Hz, 3H, ArCH), 7.24-7.19 (m, 10H, ArCH), 7.03 (dd, *J* = 6.5, 2.8 Hz, 6H, ArCH), 6.99-6.95 (m, 6H, ArCH), 5.44 (s, 4H, $CH_{2\text{-Bz}}$), 4.73 (dt, *J* = 7.3, 4.9 Hz, 1H, CH), 3.66 (s, 3H, OCH_3), 3.37 (dd, *J* = 13.1, 5.3 Hz, 1H, CH_2), 3.24 (dd, *J* = 13.2, 4.6 Hz, 1H, CH_2), 1.96 (s, 3H, CH_3). ^{13}C-NMR (101 MHz, $CDCl_3$, δ ppm): 172.1 (C=O), 170.8 (C=O), 136.2 (C), 132.4 (C), 130.5 (CH), 129.4 (CH), 129.0 (CH), 128.6 (CH), 128.4 (CH), 128.0 (CH), 126.8 (C), 55.4 (CH), 53.0 ($CH_{2\text{-Bz}}$), 51.8 (OCH_3), 31.1 (CH_2), 23.6 (CH_3). Data is consistent with that reported in the literature.[14]

(1,3-Dibenzyl-4,5-diphenylimidazol-2-ylidene)gold(I) *N*-acetyl-L-cysteine ethyl ester (5.9)

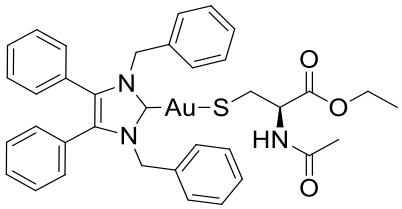

In a procedure identical to the above reaction: **1.21** (50 mg, 0.079 mmol, 1 equiv.), **5.17** (14 mg, 0.087 mmol, 1.1 equiv.), KO^{t}Bu (8.9 mg, 0.079 mmol, 1 equiv.) and THF (2 x 5 mL). White solid (40.4 mg, 66%). ^{1}H-NMR (400 MHz, $CDCl_3$, δ ppm): 7.38 (t, *J* = 7.5 Hz, 2H, ArCH), 7.29 (d, *J* = 7.9 Hz, 4H, ArCH), 7.27-7.20 (m, 10H, ArCH), 7.19-7.14 (m, 4H, ArCH), 7.09-7.06 (m, 4H, ArCH), 5.44 (s, 4H, $CH_{2\text{-Bz}}$), 4.85 (dt, *J* = 7.5, 5.2 Hz, 1H, CH), 4.23 (dd, *J* = 7.2, 2.0 Hz, 1H, CH_2), 3.22 (dd, *J* = 8.0, 5,2 Hz, 1H, CH_2), 1.95 (s, 3H, CH_3), 1.22 (t, *J* = 7.2 Hz, 3H, CH_2CH_3). ^{13}C-NMR (101 MHz, $CDCl_3$, δ ppm): 183.1 (NCN), 170.5 (C=O), 170.2 (C=O), 136.1 (C), 132.1 (C), 131.0 (CH), 130.8 (CH), 129.1 (CH), 129.0 (C), 128.7 (CH), 128.4 (CH), 127.5 (CH), 62.2 (OCH_2), 52.7 (CH), 52.0 ($CH_{2\text{-Bz}}$), 41.0 (CH_2), 23.2 (CH_3), 14.2 (CH_2CH_3).

The following NHC*-gold dipeptide complexes were afforded in inseparable mixtures thus IR and elemental analysis were not performed.

(1,3-Dibenzyl-4,5-diphenylimidazol-2-ylidene)gold(I) *N*-acetyl-L-alanyl-L-cysteine amide (5.18)

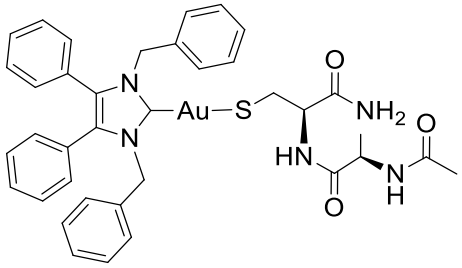

KO^{t}Bu (0.079 mL, 0.079 mmol, 1.0 equiv.) was added to a solution of **5.10** (20.2 mg, 0.087 mmol, 1.1 equiv.) in THF (2.5 mL) at -30 °C. **1.21** (50 mg, 0.079 mmol, 1.0 equiv.) in THF (2.5 mL) was added to the reaction and stirred for 24 h warming gradually to rt. The reaction was monitored by TLC (*c*-Hex/EtOAC; 1:1). The solvent was removed under reduced pressure. The residue was dissolved in CH_2Cl_2 (20 mL) and filtered. The solvent was reduced to approximately 2 mL and pentane (40 mL) was added to precipitate the product. This was filtered, washed with pentane (15 mL) and dried *in vacuo* to give a white solid (50.9 mg, 78%). ^{1}H-NMR (500 MHz, $CDCl_3$, δ ppm): 7.24-7.15 (m, 13H, ArCH), 7.04 (s, 4H, ArCH), 6.97 (d, *J* = 7.1 Hz, 5H, ArCH), 6.87 (d, *J* = 6.9 Hz, 1H, NH), 5.47 (q, *J* = 15.2 Hz, 4H, CH_2), 4.43 (td, *J* = 7.2, 3.4 Hz, 1H, CH_{cys}), 4.34 (p, *J* = 7.0 Hz, 1H, CH_{ala}), 3.53 (dd, *J* = 13.0, 3.5 Hz, 1H, CH_2), 3.03 (dd, *J* = 12.6, 7.6 Hz, 1H, CH_2), 1.98 (s, 3H, $CH_{3\text{-}NAC}$), 1.40 (d, *J* = 7.1 Hz, 3H, $CH_{3\text{-}Ala}$). ^{13}C-NMR (101 MHz, $CDCl_3$, δ ppm): 173.5 (C=O), 171.6 (C=O), 170.8 (C=O), 136.4 (C), 132.1 (C), 130.8 (CH), 129.4 (CH), 128.8 (CH), 128.7 (CH), 128.0 (CH), 127.5 (CH), 126.7 (C), 55.7 (CH_{cys}), 52.7 ($CH_{2\text{-}Bz}$), 50.3 (CH_{ala}), 29.8 (CH_2), 23.3 ($CH_{3\text{-}NAC}$), 18.4 ($CH_{3\text{-}Ala}$). HRMS (ESI$^+$) *m/z*: $[M + H]^+$ calcd. 830.2434; found 830.2433. Anal. Calc for $C_{37}H_{38}N_5O_3SAu$ (829.76) in %: C, 53.56; H, 4.62; N, 8.44; S, 3.86. Found: C, 53.69; H, 4.38; N, 7.08 (-1.36); S, 3.39 (-0.47). Although these elemental results are outside the acceptable range to establish purity, they demonstrate the best results yet obtained.

(1,3-Dibenzyl-4,5-diphenylimidazol-2-ylidene)gold(I) *N*-acetyl-L-tyrosinyl-L-cysteine amide (5.19)

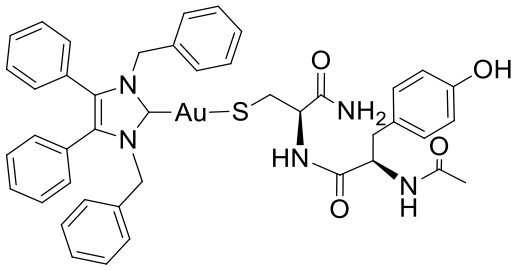

In a procedure identical to the above reaction: KO^{t}Bu (0.079 mL, 0.079 mmol, 1.0 equiv.) was added to a solution of **5.11** (38.5 mg, 0.118 mmol, 1.5 equiv.) in THF (2.5 mL) at -30 °C. **1.21** (50 mg, 0.079 mmol, 1.0 equiv.) in THF (2.5 mL) was added to the reaction and stirred for 24 h warming gradually to rt. After workup and precipitation a white solid was formed (44.6 mg, 61%). ^{1}H-NMR (500 MHz, d^6-DMSO, δ ppm): 8.04 (d, *J* = 8.0 Hz, 2H, ArCH$_{tyr}$), 7.86 (d, *J* = 7.8, 2H, ArCH$_{tyr}$), 7.36-7.12 (m, 12H, ArCH), 7.02 (d, *J* = 8.3 Hz, 3H, ArCH), 7.00-6.98 (m, 6H, ArCH), 6.87 (d, *J* = 6.7 Hz, 1H, NH), 5.48 (q, *J* = 15.7 Hz, 4H, CH$_{2\text{-}Bz}$), 4.39 (td, *J* = 9.1, 8.6, 4.2 Hz, 1H, CH), 4.19 (q, *J* = 6.1 Hz, 1H, CH), 2.98 (d, *J* = 5.9 Hz, 2H, CH$_2$), 2.92 (dd, *J* = 13.9, 4.1 Hz, 1H, CH$_2$), 2.63 (dd, *J* = 13.6, 10.4 Hz, 1H, CH$_2$), 1.72 (s, 3H, CH$_3$). ^{13}C-NMR (101 MHz, d^6-DMSO, δ ppm): 183.3 (NCN), 172.7 (C=O), 171.0 (C=O), 169.5 (C=O), 155.7 (C), 136.4 (C), 132.4 (C), 131.4 (CH), 130.7 (CH), 130.1 (CH), 129.2 (CH), 128.5 (CH), 127.7 (C), 127.3 (C) 126.9 (CH), 126.5 (CH), 114.8 (CH), 56.9 (CH), 54.9 (CH), 51.8 (CH$_{2\text{-}Bz}$), 36.6 (CH$_2$), 30.7 (CH$_2$), 22.5 (CH$_3$). LRMS (ESI$^+$) *m*/*z*: found 924.4 [M + 3H]$^+$; found 961.4 [M + K]$^+$.

(1,3-Dibenzyl-4,5-diphenylimidazol-2-ylidene)gold(I) *N*-acetyl-L-cysteinyl-L-alanine amide (5.20)

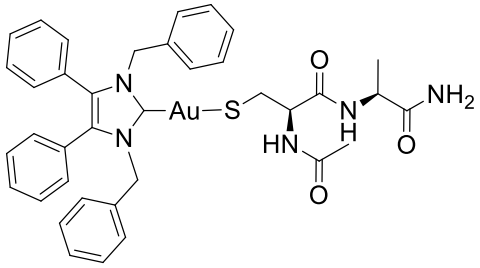

In a procedure identical to the above reaction: KO^{t}Bu (0.079 mL, 0.079 mmol, 1.0 equiv.) was added to a solution of **5.12** (20.3 mg, 0.089 mmol, 1.1 equiv.) in THF (2.5 mL) at -30 °C. **1.21** (50 mg, 0.079 mmol, 1.0 equiv.) in THF (2.5 mL) was added to the reaction and stirred for 24 h warming gradually to rt. After workup and precipitation a white solid was formed. ^{1}H-NMR (300 MHz, $CDCl_3$, δ ppm): 7.24-7.14 (m, 12H, ArCH), 7.12-6.94 (m, 7H, ArCH), 6.86 (dd, *J* = 14.8, 6.6 Hz, 3H, ArCH), 5.46 (d, *J* = 2.7 Hz, 4H, $CH_{2\text{-Bz}}$), 4.49 (dt, *J* = 12.8, 6.2 Hz, 1H, CH), 4.42-4.35 (m, 1H, CH), 3.28 (dd, *J* = 12.5, 4.7 Hz, 1H, CH_2), 3.00 (dd, *J* = 12.5, 9.3 Hz, 1H, CH_2), 1.99 (s, 3H, CH_3), 1.34 (d, *J* = 7.3 Hz, 3H, $CH_{3\text{-Ala}}$). ^{13}C-NMR (101 MHz, $CDCl_3$, δ ppm): 184.6 (NCN), 179.3 (C=O), 136.4 (C), 135.9 (C), 131.9 (CH), 130.8 (CH), 129.5 (C), 128.9 (CH), 128.7 (CH), 127.7 (CH), 126.7 (CH), 55.6 ($CH_{\text{-Cys}}$), 52.7 ($CH_{2\text{-Bz}}$), 52.5 ($CH_{\text{-Ala}}$), 29.6 (CH_2), 23.5 ($CH_{3\text{-NAC}}$), 17.9 ($CH_{3\text{-Ala}}$).

(1,3-Dibenzyl-4,5-diphenylimidazol-2-ylidene)gold(I) *N*-acetyl-L-cysteinyl-L-tyrosine amide (5.21)

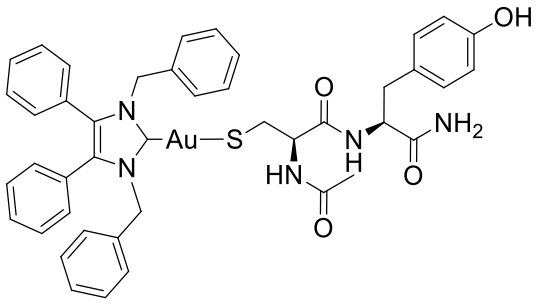

In a procedure identical to the above reaction: KO^{t}Bu (0.079 mL, 0.079 mmol, 1.0 equiv.) was added to a solution of **5.13** (38.5 mg, 0.118 mmol, 1.5 equiv.) in THF (2.5 mL) at -30 °C. **1.21** (50 mg, 0.079 mmol, 1.0 equiv.) in THF (2.5 mL) was added to the reaction and stirred for 24 h warming gradually to rt. After workup and precipitation a white solid was formed. ^{1}H-NMR (400 MHz, $CDCl_3$, δ ppm): 7.23-7.14 (m, 9H, ArCH), 7.08 (t, *J* = 7.5 Hz, 5H, ArCH), 7.04-6.93 (m, 8H, ArCH), 6.84 (dd, *J* = 14.2, 7.0 Hz, 4H, ArCH), 5.44 (q, *J* = 8.7 Hz, 4H, $CH_{2\text{-Bz}}$), 4.56 (t, *J* = 5.1 Hz, 1H, CH) 4.29 (t, *J* = 5.7, 1H, CH), 3.32 (dd, *J* = 13.0, 5.0 Hz, 1H, CH_2), 3.25 (dd, *J* = 13.8, 4.1 Hz, 1H, CH_2), 3.09 (dd, *J* = 13.0, 6.6 Hz, 1H, CH_2), 2.70 (dd, *J* = 13.7, 5.9 Hz, 1H, CH_2), 1.84 (s, 3H, CH_3). ^{13}C-NMR (101 MHz, $CDCl_3$, δ ppm): 184.5 (NCN), 179.3 (C=O), 171.5 (C=O), 151.4 (C), 136.4 (CH), 132.9 (C), 131.9 (C), 130.9 (CH), 130.7 (CH), 129.5 (C) 128.9 (CH), 128.7 (CH), 128.1

(C), 127.7 (CH), 126.6 (CH), 117.1 (CH), 57.7 (CH), 53.4 (CH), 52.6 ($CH_{2\text{-Bz}}$), 31.3 (CH_2), 29.8 (CH_2), 23.0 (CH_3). LRMS (ESI^+) *m*/*z*: found 960.8 $[M + K]^+$.

(1,3-Dibenzyl-4,5-diphenylimidazol-2-ylidene)gold(I) *N*-acetyl-L-cysteinyl-L-phenylalanine amide (5.22)

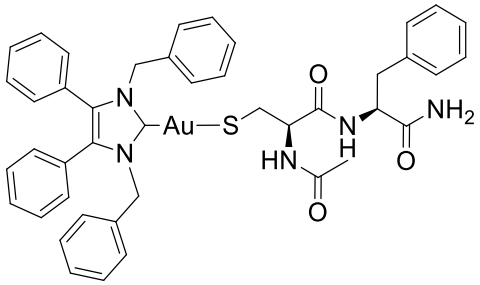

K_2CO_3 (16.2 mg, 0.117 mmol, 2.0 equiv.) and **5.14** (18.1 mg, 0.058 mmol, 1.0 equiv.) stirred in acetone (5 mL) at room temperature for 5 min. **1.21** (37.0 mg, 0.058 mmol, 1.0 equiv.) in acetone (5 mL) was added and the reaction continued for 24 h. The solvent was removed under reduced pressure. The residue was dissolved in CH_2Cl_2 (20 mL) and filtered. The solvent was reduced to afford a solid. ^{1}H-NMR (500 MHz, $CDCl_3$, δ ppm): 8.04 (d, *J* = 8.4 Hz, 2H, $ArCH_{phe}$), 7.56 (t, *J* = 7.5 Hz, 1H, $ArCH_{phe}$) 7.44 (t, *J* = 7.7 Hz, 2H, $ArCH_{phe}$) 7.32-7.27 (m, 3H, ArCH), 7.23-7.15 (m, 9H, ArCH), 7.08 (t, *J* = 7.7 Hz, 6H, ArCH), 6.91-6.80 (m, 5H, ArCH), 5.52-5.41 (m, 4H, $CH_{2\text{-Bz}}$), 4.62 (q, *J* = 6.7 Hz, 1H, CH), 4.44 (td, *J* = 7.1, 3.2 Hz, 1H, CH), 3.51 (dd, *J* = 13.0, 3.2 Hz, 1H, CH_2), 3.13 (dd, *J* = 13.7, 6.4 Hz, 1H, CH_2), 3.04 (dd, *J* = 14.1, 7.5 Hz, 1H, CH_2), 2.97 (dd, *J* = 12.9, 7.2 Hz, 1H, CH), 1.85 (s, 3H, CH_3). ^{13}C-NMR (101 MHz, $CDCl_3$, δ ppm): 179.3 (C=O), 167.8 (C=O), 136.3 (C), 135.9 (CH), 133.0 (C), 131.9 (CH), 130.7 (CH), 129.6 (C), 128.9 (CH), 128.7 (CH), 128.6 (CH), 128.2 (CH), 127.7 (CH), 127.1 (C), 126.6 (CH), 52.6 ($CH_{2\text{-Bz}}$), 52.4 (CH), 38.1 (CH_2), 36.0 (CH_2), 17.8 (CH_3). HRMS (ESI^+) *m*/*z* $[M + H]^+$ calcd. 906.2747; found 906.2743.

(1,3-Dibenzyl-4,5-diphenylimidazol-2-ylidene)gold(I) cysteine (5.23)

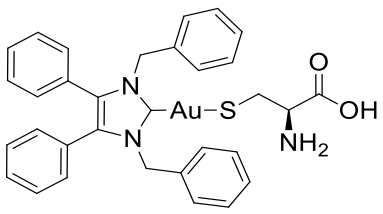

1.21 (63.3 mg, 0.10 mmol, 1.0 equiv.) in CH_2Cl_2 (5 mL) was added to a solution of L-cysteine (13.3 mg, 0.11 mmol, 1.1 equiv.) and KO^{t}Bu (12.3 mg, 0.11 mmol, 1.1 equiv.) in MeOH (5 mL) and stirred at rt for 1 h. The solvent was removed under reduced pressure. The residue was dissolved in CH_2Cl_2 (20 mL) and filtered through sintered glass. The solvent was reduced to approximately 2 mL and pentane (40 mL) was added to precipitate the product. This was filtered, washed with pentane (15 mL) and dried *in vacuo* to give a white solid (54.8 mg, 76%). ^{1}H-NMR (400 MHz, $CDCl_3$, δ ppm): 7.18 (m, 2H, ArCH), 7.12 (m, 11H, ArCH), 6.96 (m, 9H, ArCH), 5.39 (s, 4H, CH_2), 3.53 (dd, *J* = 9.7, 3.7 Hz, 1H, CH_2), 3.42 (d, *J* = 11.4 Hz, 1H, CH_2), 3.13 (t, *J* = 10.1 Hz, 1H, CH). ^{13}C-NMR (101 MHz, $CDCl_3$, δ ppm): 184.9 (NCN), 173.9 (C=O), 136.6 (C), 131.9 (C), 130.9 (CH), 129.1 (CH), 128.6 (CH), 128.5 (CH), 127.8 (CH), 127.6 (CH), 126.7 (C), 59.6 (CH), 52.8 ($CH_{2\text{-}Bz}$), 29.8 (CH_2). HRMS (ESI$^+$) *m*/*z*: $[M + H]^+$ calcd. 718.1797; found 718.1801. IR (ATR, cm^{-1}): 3324 (w) (NH), 3028 (w), 2918 (w), 1584 (s), 1487 (m), 1447 (m), 1020 (m). Anal. calcd. for $C_{32}H_{30}N_3SO_2Au$ (717.63) in %: C, 53.56; H, 4.21; N, 5.86; S, 4.47. Found: C, 50.18 (-3.38); H, 4.05; N, 5.25 (-0.61); S, 4.63. Although these elemental results are outside the acceptable range to establish purity, they demonstrate the best results yet obtained.

(1,3-Dibenzyl-4,5-diphenylimidazol-2-ylidene)gold(I) cysteine methyl ester (5.24)

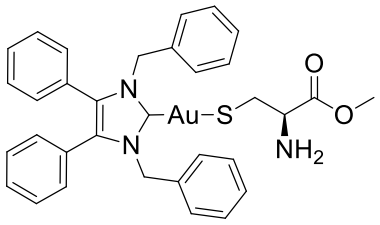

In a procedure identical to above reaction: **1.21** (63.3 mg, 0.10 mmol, 1.0 equiv.) in CH_2Cl_2 (5 mL) was added to a solution of L-cysteine methyl ester hydrochloride (18.8 mg, 0.11 mmol, 1.1 equiv.) and KOtBu (12.3 mg, 0.11 mmol, 1.1 equiv.) in MeOH (5 mL) and stirred at rt for 1 h. After workup and precipitation a white solid was formed (53.6 mg, 73%). ^{1}H-NMR (400 MHz, $CDCl_3$, δ ppm): 7.29 (t, *J* = 7.5 Hz, 3H, ArCH), 7.22 (m, 10H, ArCH), 7.04 (dd, *J* = 6.4, 2.8 Hz, 4H, ArCH), 6.97 (d, *J* = 7.3 Hz, 4H, ArCH), 5.46 (s, 4H, CH_2), 3.67 (s, 3H, CH_3), 3.56 (dd, *J* = 7.8, 3.8 Hz, 1H, CH), 3.28 (dd, *J* = 12.8, 3.8 Hz, 1H, CH_2), 3.05 (dd, *J* = 12.8, 7.8 Hz, 1H, CH_2). ^{13}C-NMR (101 MHz, $CDCl_3$, δ ppm): 183.6 (NCN), 175.0 (C=O), 136.2 (C), 132.0 (C), 130.8 (CH), 129.4

(CH), 128.7 (CH), 128.1 (CH), 127.6 (CH), 127.5 (CH), 126.7 (C), 58.7 (CH), 52.7 ($CH_{2\text{-}Bz}$), 51.9 (CH_3), 33.8 (CH_2). HRMS (ESI^+) *m*/*z*: $[M + H]^+$ calcd. 732.1954; found 732.1960. IR (ATR, cm^{-1}): 3355 (w) (NH), 3029 (w), 2922 (w), 1733 (s) (COOMe), 1496 (m), 1447 (s), 1022 (m). Anal. calcd. for $C_{33}H_{32}N_3SO_2Au$ (731.66) in %: C, 54.17; H, 4.41; N, 5.74; S, 4.38. Found: C, 49.27 (-4.9); H, 4.15; N, 5.18 (-0.56); S, 4.52 (+0.14). Although these elemental results are outside the acceptable range to establish purity, they demonstrate the best results yet obtained.

References

(1) Jin, L.; Aleshi, G.; Kang, S. Glutaminolysis as a Target for Cancer Therapy. *Oncogene* **2016**, *35*, 3619–3625.

(2) Liu, Y.; Pak, J. K.; Schmutz, P.; Bauwens, M.; Mertens, J.; Knight, H.; Alberto, R. Amino Acids Labeled with [99m $Tc(CO)_3]^+$ and Recognized by the L-Type Amino Acid Transporter LAT1. *J. Am. Chem. Soc.* **2006**, *128*, 15996–15997.

(3) Lieu, E. L.; Nguyen, T.; Rhyne, S.; Kim, J. Amino Acids in Cancer. *Exp. Mol. Med.* **2020**, *52*, 15–30.

(4) Häfliger, P.; Charles, R.-P. The L-Type Amino Acid Transporter LAT1-An Emerging Target in Cancer. *Int. J. Mol. Sci.* **2019**, *20*, 2428.

(5) Schulte, M. L.; Fu, A.; Zhao, P.; Li, J.; Geng, L.; Smith, S. T.; Kondo, J.; Coffey, R. J.; Johnson, M. O.; Rathmell, J. C.; Sharick, J. T.; Skala, M. C.; Smith, J. A.; Berlin, J.; Washington, M. K.; Nickels, M. L.; Manning, H. C. Pharmacological Blockade of ASCT2-Dependent Glutamine Transport Leads to Antitumor Efficacy in Preclinical Models. *Nat. Med.* **2018**, *24*, 194–202.

(6) Soler, M.; Feliu, L.; Planas, M.; Ribas, X.; Costas, M. Peptide-Mediated Vectorization of Metal Complexes: Conjugation Strategies and Biomedical Applications. *Dalton Trans.* **2016**, *45*, 12970–12982.

(7) Meier-Menches, S. M.; Casini, A. Design Strategies and Medicinal Applications of Metal-Peptidic Bioconjugates. *Bioconjug. Chem.* **2020**, *31*, 1279–1288.

(8) Diehl, T.; Krause, M. T. S.; Ueberlein, S.; Becker, S.; Trommer, A.; Schnakenburg, G.;

Engeser, M. Synthesis of Hydroxyl-Functionalized N-Heterocyclic Carbene Gold(I) Complexes and Peptide Conjugates. *Dalton Trans.* **2017**, *46*, 2988–2997.

(9) Gutiérrez, A.; Gimeno, M. C.; Marzo, I.; Metzler-Nolte, N. Synthesis, Characterization, and Cytotoxic Activity of AuI N,S-Heterocyclic Carbenes Derived from Peptides Containing L-Thiazolylalanine. *Eur. J. Inorg. Chem.* **2014**, 2512–2519.

(10) Lemke, J.; Pinto, A.; Niehoff, P.; Vasylyeva, V.; Metzler-Nolte, N. Synthesis, Structural Characterisation and Anti-Proliferative Activity of NHC Gold Amino Acid and Peptide Conjugates. *Dalton Trans.* **2009**, 7063–7070.

(11) Gutiérrez, A.; Bernal, J.; Villacampa, M. D.; Cativiela, C.; Laguna, A.; Gimeno, M. C. Synthesis of New Gold(I) Thiolates Containing Amino Acid Moieties with Potential Biological Interest. *Inorg. Chem.* **2013**, *52*, 6473–6480.

(12) Gutiérrez, A.; Marzo, I.; Cativiela, C.; Laguna, A.; Gimeno, M. C. Highly Cytotoxic Bioconjugated Gold(I) Complexes with Cysteine-Containing Dipeptides. *Chem. Eur. J.* **2015**, *21*, 11088–11095.

(13) Gutiérrez, A.; Cativiela, C.; Laguna, A.; Gimeno, M. C. Bioactive Gold(I) Complexes with 4-Mercaptoproline Derivatives. *Dalton Trans.* **2016**, *45*, 13483–13490.

(14) Curran, D.; Dada, O.; Müller-Bunz, H.; Rothemund, M.; Sánchez-Sanz, G.; Schobert, R.; Zhu, X.; Tacke, M. Synthesis and Cytotoxicity Studies of Novel NHC∗-Gold(I) Complexes Derived from Lepidiline A. *Molecules* **2018**, *23*, 2031–2048.

(15) Dada, O.; Sánchez-Sanz, G.; Tacke, M.; Zhu, X. Synthesis and Anticancer Activity of Novel NHC-Gold(I)-Sugar Complexes. *Tetrahedron Lett.* **2018**, *59*, 2904–2908.

(16) Hackenberg, F.; Müller-Bunz, H.; Smith, R.; Streciwilk, W.; Zhu, X.; Tacke, M. Novel Ruthenium(II) and Gold(I) NHC Complexes: Synthesis, Characterization, and Evaluation of Their Anticancer Properties. *Organometallics* **2013**, *32*, 5551–5560.

(17) Wang, Z.; Rejtar, T.; Zhou, Z. S.; Karger, B. L. Desulfurization of Cysteine-Containing Peptides Resulting from Sample Preparation for Protein Characterization by Mass Spectrometry. *Rapid Commun. Mass Spectrom.* **2010**, *24*, 267–275.

(18) Novoa, A.; Eierhoff, T.; Topin, J.; Varrot, A.; Barluenga, S.; Imberty, A.; Roemer, W.;

Winssinger, N. A LecA Ligand Identified from a Galactoside-Conjugate Array Inhibits Host Cell Invasion by Pseudomonas Aeruginosa. *Angew. Chem. Int. Ed.* **2014**, *53*, 8885–8889.

(19) Bernardes, G. J. L.; Grayson, E. J.; Thompson, S.; Chalker, J. M.; Errey, J. C.; El Oualid, F.; Claridge, T. D. W.; Davis, B. G. From Disulfide-to Thioether-Linked Glycoproteins. *Angew. Chem. Int. Ed.* **2008**, *47*, 2244–2247.

(20) Uhrig, R. K.; Picard, M. A.; Beyreuther, K.; Wiessler, M. Synthesis of Antioxidative and Anti-Inflammatory Drugs Glucoconjugates. *Carbohydr. Res.* **2000**, *325*, 72–80.

Chapter Six

Conclusion and Outlook

N-Heterocyclic carbene gold(I) complexes have rapidly become an important class of anticancer drugs. In 2011, the Tacke group observed higher cytotoxic activity with gold(I) complexes over their silver(I) counterparts. This encouraged further research into developing gold(I)-based NHCs, which resulted in several biologically active complexes. The NHC*-gold(I) chloride complex **1.21**, featuring a 1,3-dibenzyl-4,5-diphenylimidazol-2-ylidene ligand, was especially of interest as it reported strong antiproliferative properties and due to the lability of the chloride acted as the precursor for the majority of gold(I)-based complexes developed since in the Tacke group. The objective of this project was to create a structure-activity-relationship for these NHC-gold(I) complexes by modifying the ligand trans to the NHC-gold(I) species, thus it is essential to conduct a comparison of all of the complexes developed in this work. The results in this thesis are very promising and suggest that some of these complexes have high potential as anticancer agents.

Monomeric neutral complexes of the type NHC-Au-L and cationic complexes of the type $[NHC\text{-}Au\text{-}L]^+$ were synthesised featuring halide, carbene, phosphine, cyanide, alkyne, dithiocarbamate, amino acid and dipeptide ligands. These ligands were chosen to represent a broad scope of ligand classes. In the synthesis of the cationic $[NHC^*\text{-}Au\text{-}PPh_3]^+$ complexes it was noted that homoleptic rearrangement was favoured and if left in solution would result in biscarbene formation. Fortunately, a short reaction time enabled complexes **2.14** and **2.15** to be isolated, however this was not the case for the attempted $[NHC^*\text{-}Au\text{-}PTA]^+$ complexes. This was also observed in Chapter 5 when synthesising the NHC*-gold(I) dipeptide complexes. NHC*-gold(I) dipeptides **5.16**-**5.20** were formed in mixtures, with one of the impurities identified as the biscarbene. Unfortunately, the dipeptide complexes were not isolable from the mixture, however the formation of the desired complexes was confirmed with ^{1}H-NMR spectroscopy and mass spectrometry. Further work could be focussed on preparing the PTA and peptide complexes as both ligand classes have produced biologically active complexes so

it would be of interest to assess them in our group. This could be performed with either ligand modifications that increased the stability of the peptide and PTA ligand itself or modifications to the NHC ligand to prevent the favourable ligand scrambling.

X-ray crystallography allowed us to observe aurophilic interactions in the solid state structures of the halide and acetylide complexes. These complexes featured small, linear ligands which posed no steric hindrance, thus allowing the gold-gold interactions to appear. The measured Au···Au distances were in the range of 3.2077(9)-3.5850(3) Å, which indicated that weak aurophilicity was present. Often aurophilic interactions are coupled with luminescence which could prove a useful tool in developing chemotherapeutics. The luminescent properties of these complexes could be probed to determine if these complexes have a role in cellular imaging applications. Overall, the X-ray crystal structures of the presented complexes exhibited very similar C-Au bond lengths [1.998-2.033 Å] and C-Au-L bond angles [173.24-179.65 °] despite the changing ligands. It is worth noting that a correlation was drawn between the length of the newly formed Au-L bond and the cytotoxicity of the complex, where L=ligand. The bond lengths increased in the following trend: alkyne< carbene< cyanide< phosphine< dithiocarbamate< bromide< iodide.

Considering the IC_{50} values obtained on the colon carcinoma cell line HCT-116, the cytotoxicity of the complexes followed the trend of increasing bond lengths with two exceptions. Generally, the longer the bond length the lower the cytotoxicity, this was found to be true for the following ligands: carbene< phosphine< dithiocarbamate< bromide. However, the acetylide, cyanide and iodide complexes reacted inversely. The acetylide and cyanide complexes presented the shortest bonds and poor cytotoxicity, while the iodido derivative displayed the longest bond and extremely high cytotoxicity. Good antiproliferation was observed for the majority of the novel NHC-gold(I) complexes. Of the complexes evaluated only two reported less activity than their precursor NHC*-gold(I) chloride, thus the complexes can be considered as improved anticancer drug candidates. In particular, the iodido derivative **2.6**, which reached sub-micromolar activity against the colon cancer cell line; the biscarbenes **2.10** and **2.11** with sub-micromolar activity against both cell lines; and the dimethyl- and diethyldithiocarbamato complexes **4.8** and **4.9** which reported sub-micromolar activity on the breast cancer cell line.

These findings suggest that these NHC-gold(I) complexes have significant potential as anticancer agents, in particular for the treatment of colon, breast and prostate cancer.

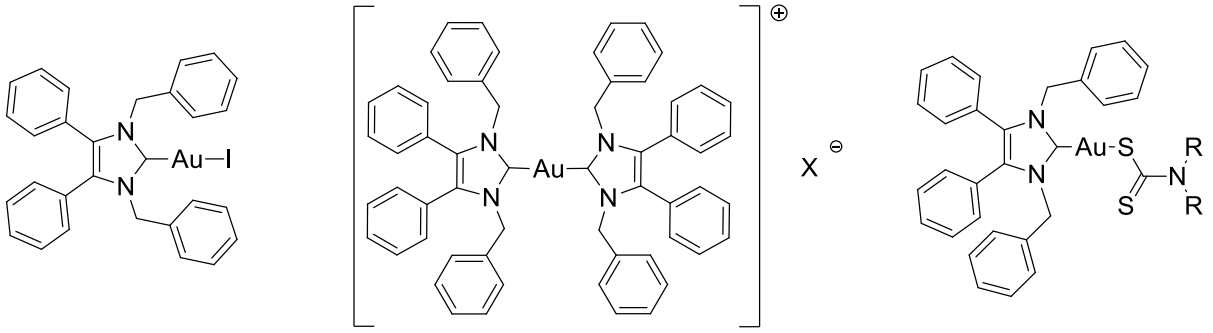

2.6
0.64 ± 0.01 μM
1.1 ± 0.2 μM

2.10-2.11
0.29 - 0.41 μM
0.7 - 0.8 μM

4.8-4.9
1.5 - 8.0 μM
0.28 - 0.36 μM

Figure 6.1 The most promising complexes developed in this work, with reported IC_{50} values against HCT-116 (top) and MCF-7 (bottom).

To further develop these NHC-gold(I) drug candidates testing the complexes on non-tumorigenic cell lines could indicate a degree of cell selectivity. In light of the successful *in vivo* xenograft mouse model experiment with dithiocarbamate **4.8**, it would be interesting to conduct further *in vivo* experiments with the biscarbene complexes, as these candidates exhibited higher cytotoxicity than the dithiocarbamates on the colon cancer cell line. Cellular uptake studies could also be performed to investigate whether the biscarbene complexes have a higher bioavailability than the neutral complexes. Although mechanistic studies have already been performed with NHC gold(I) complexes it could be beneficial to confirm our complexes initiate cell death through the proposed TrxR inhibition route. These recommendations could result in an optimised NHC-gold(I) complex being entered into clinical trials as a chemotherapeutic agent.

Appendix

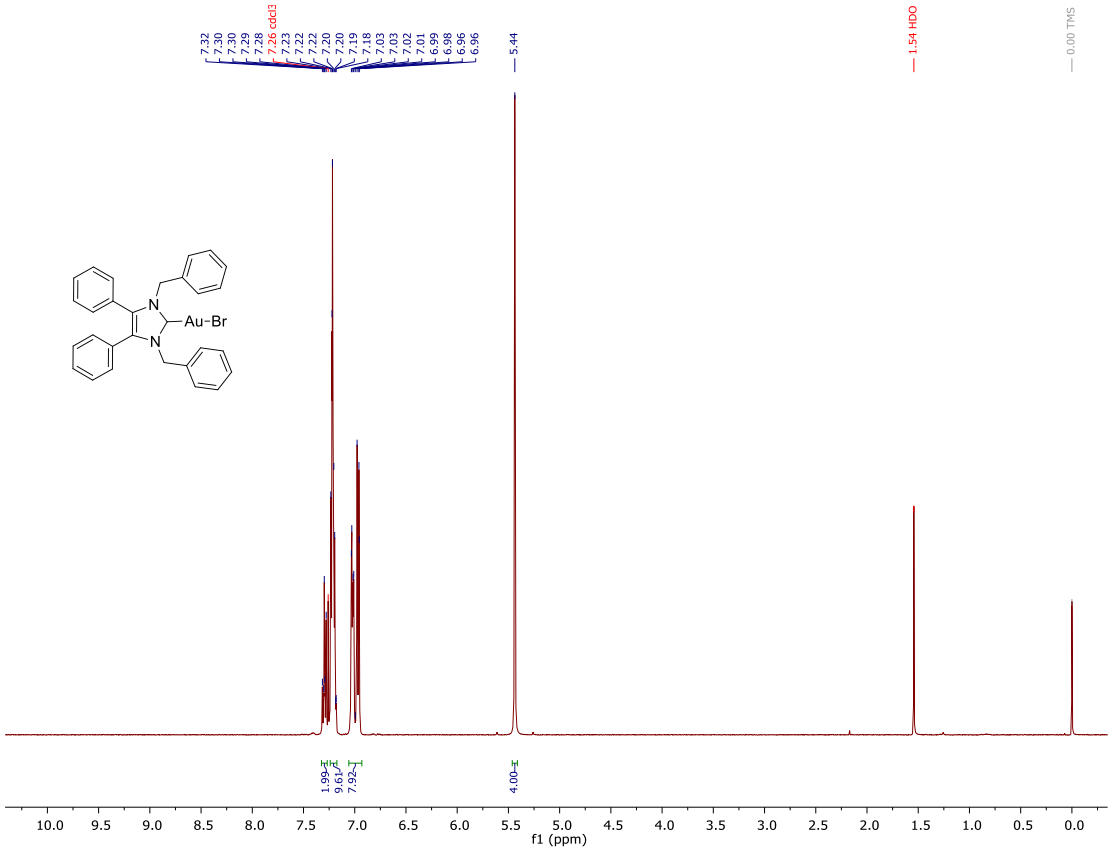

Figure S1. [1]H-NMR spectra of **2.5** in $CDCl_3$.

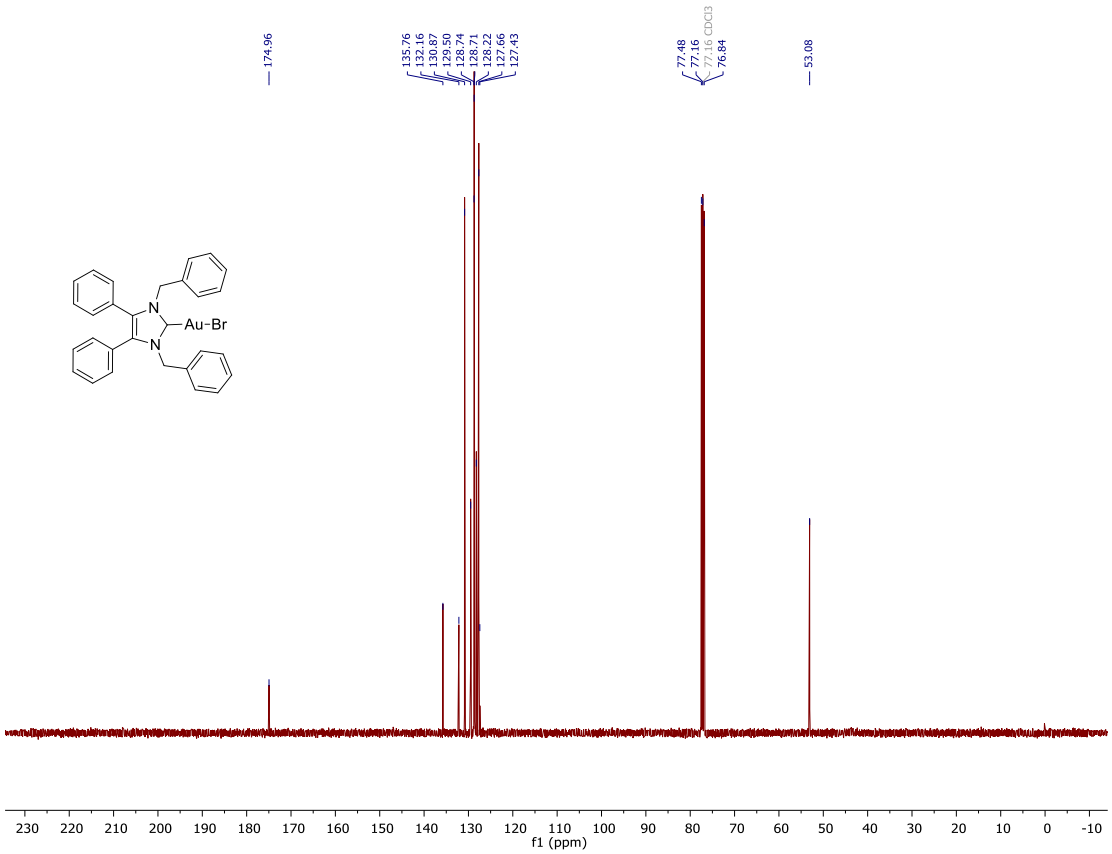

Figure S2. [13]C-NMR spectra of **2.5** in $CDCl_3$.

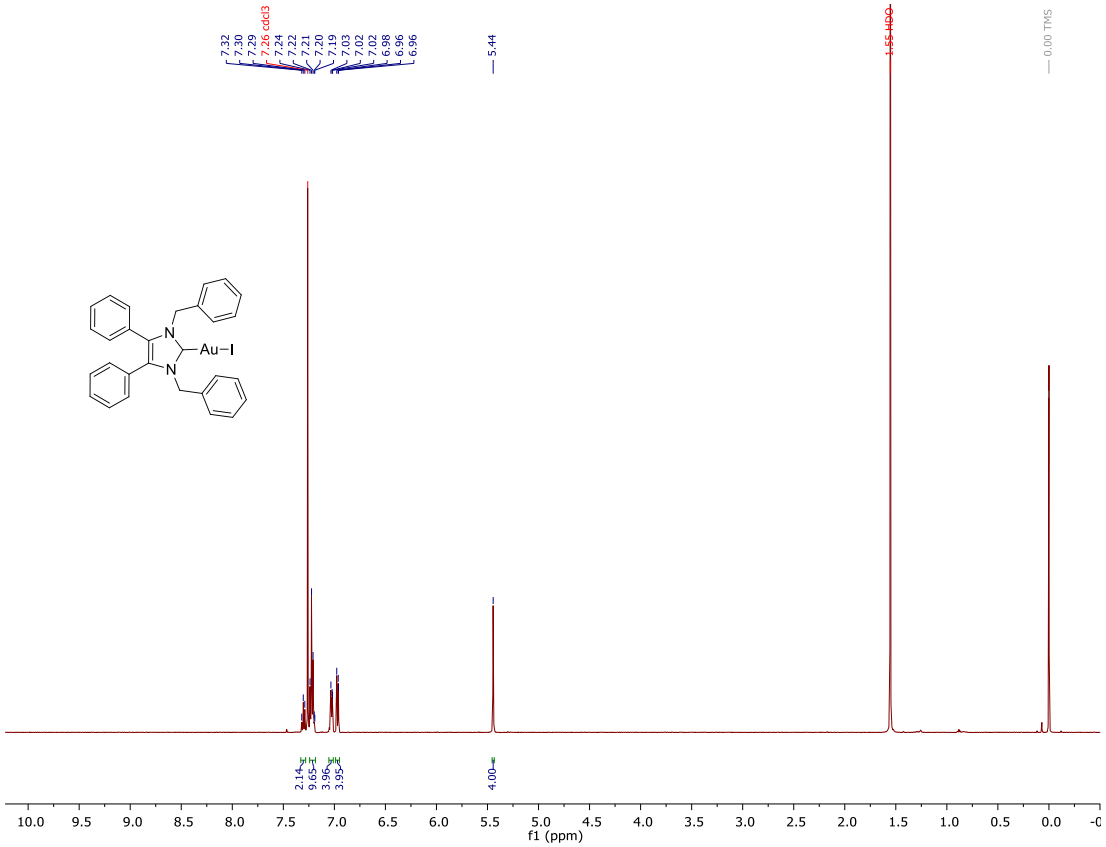

Figure S3. ^{1}H-NMR spectra of **2.6** in $CDCl_3$.

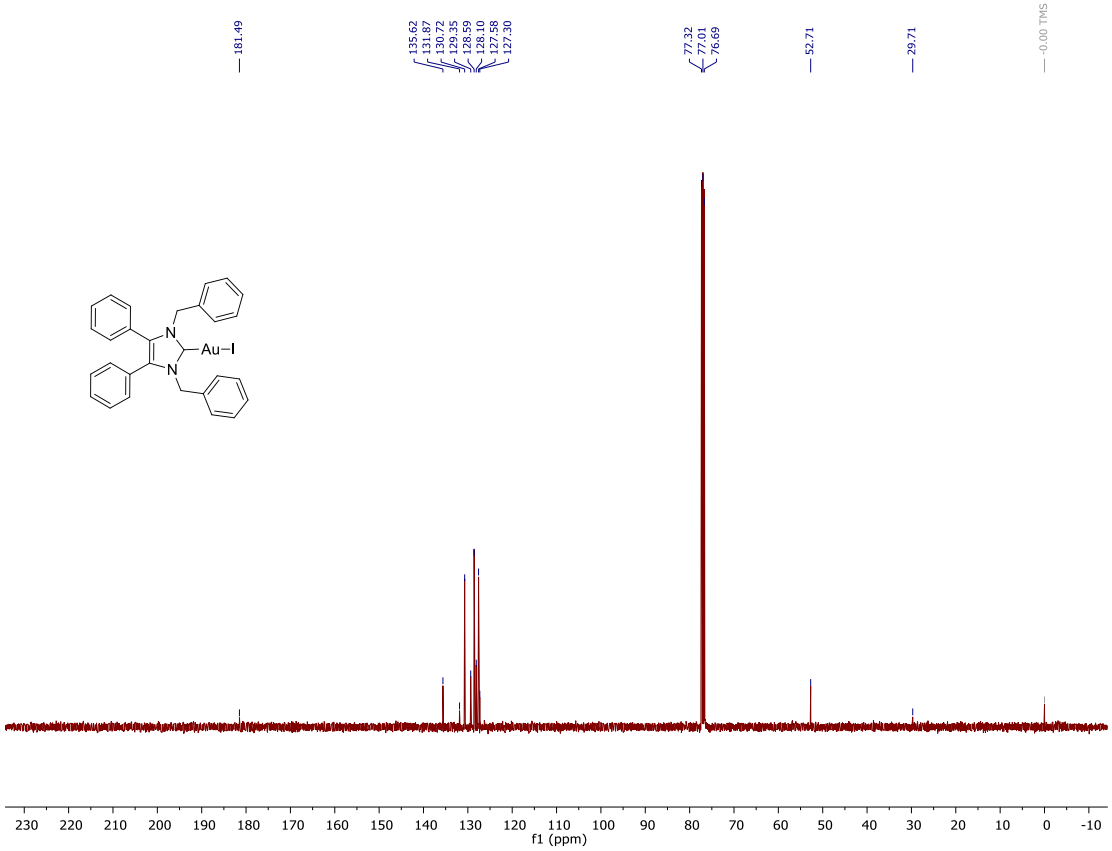

Figure S4. ^{13}C-NMR spectra of **2.6** in $CDCl_3$.

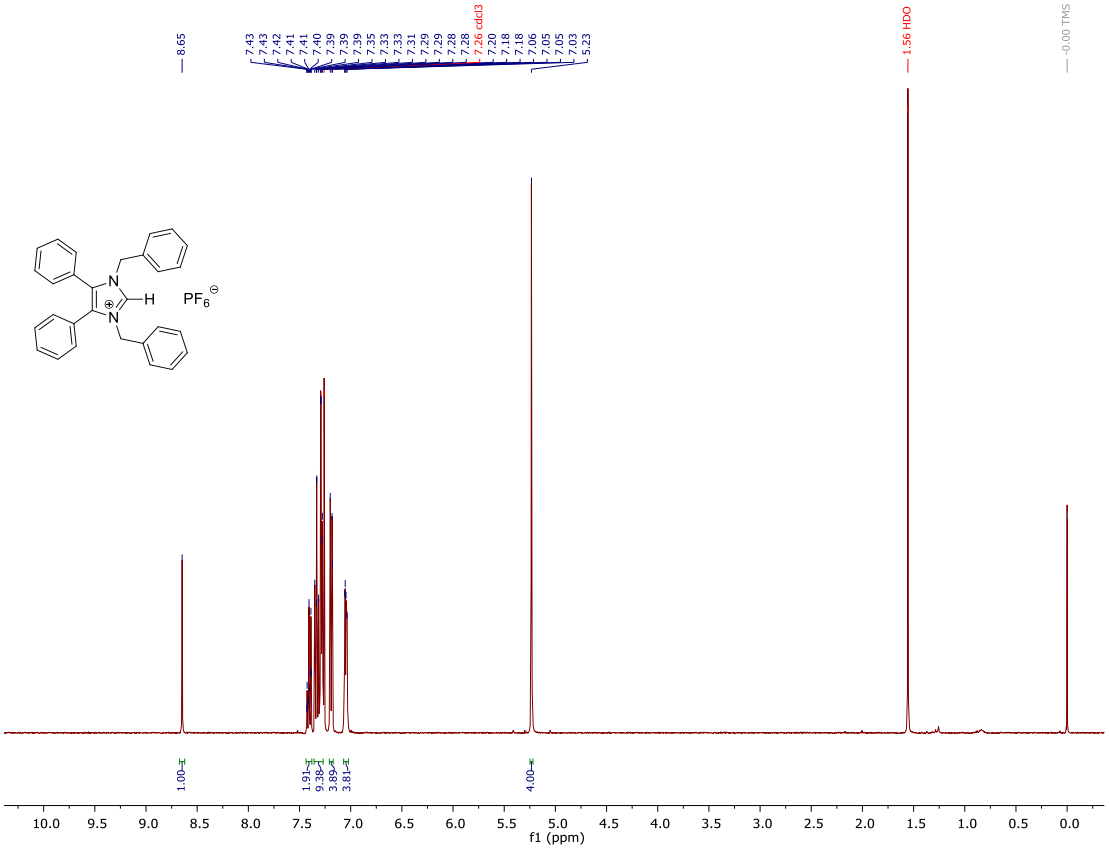

Figure S5. [1]H-NMR spectra of **2.7** in $CDCl_3$.

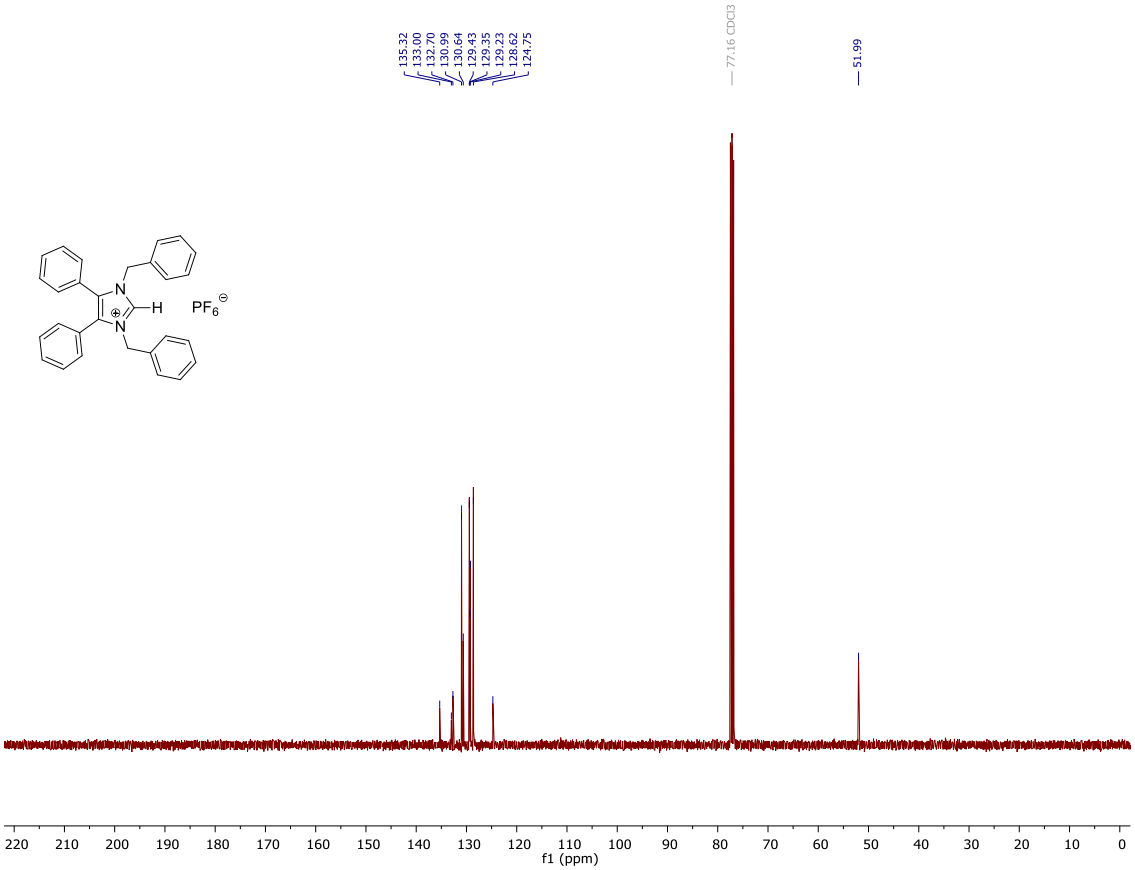

Figure S6. [13]C-NMR spectra of **2.7** in $CDCl_3$.

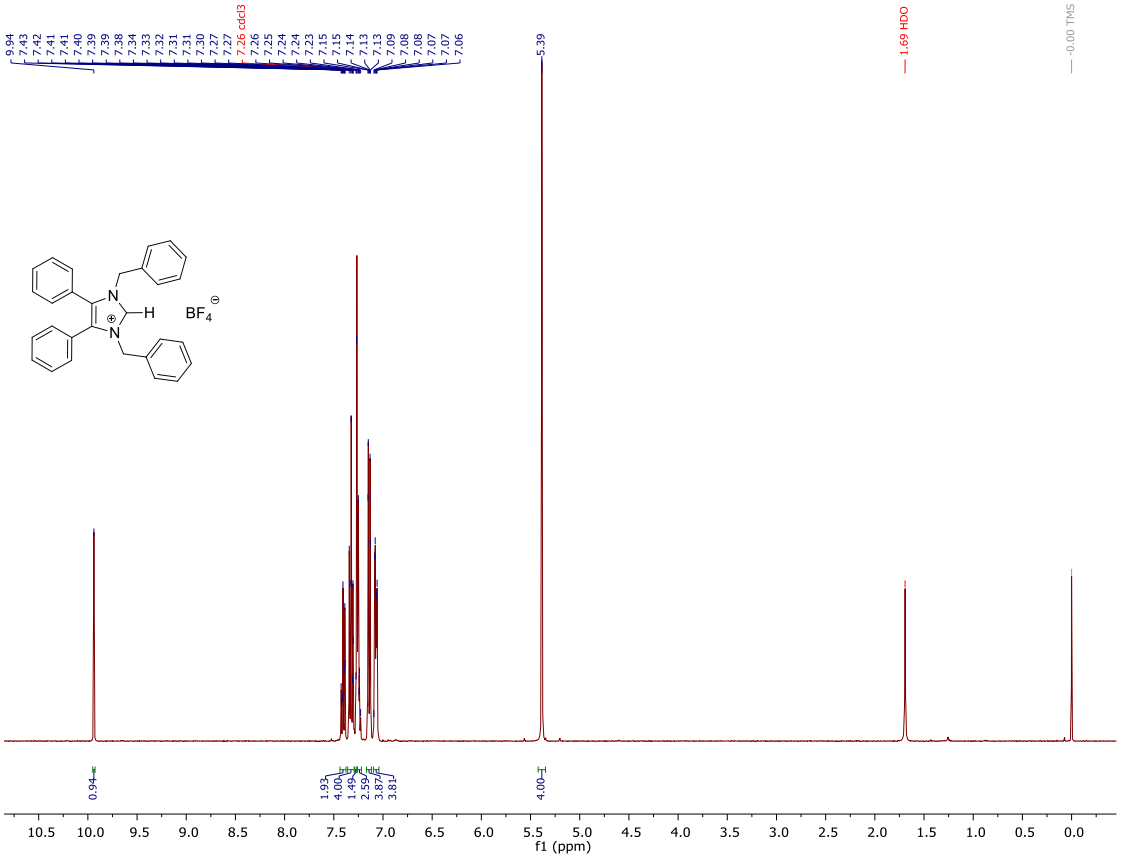

Figure S7. ^{1}H-NMR spectra of **2.8** in $CDCl_3$.

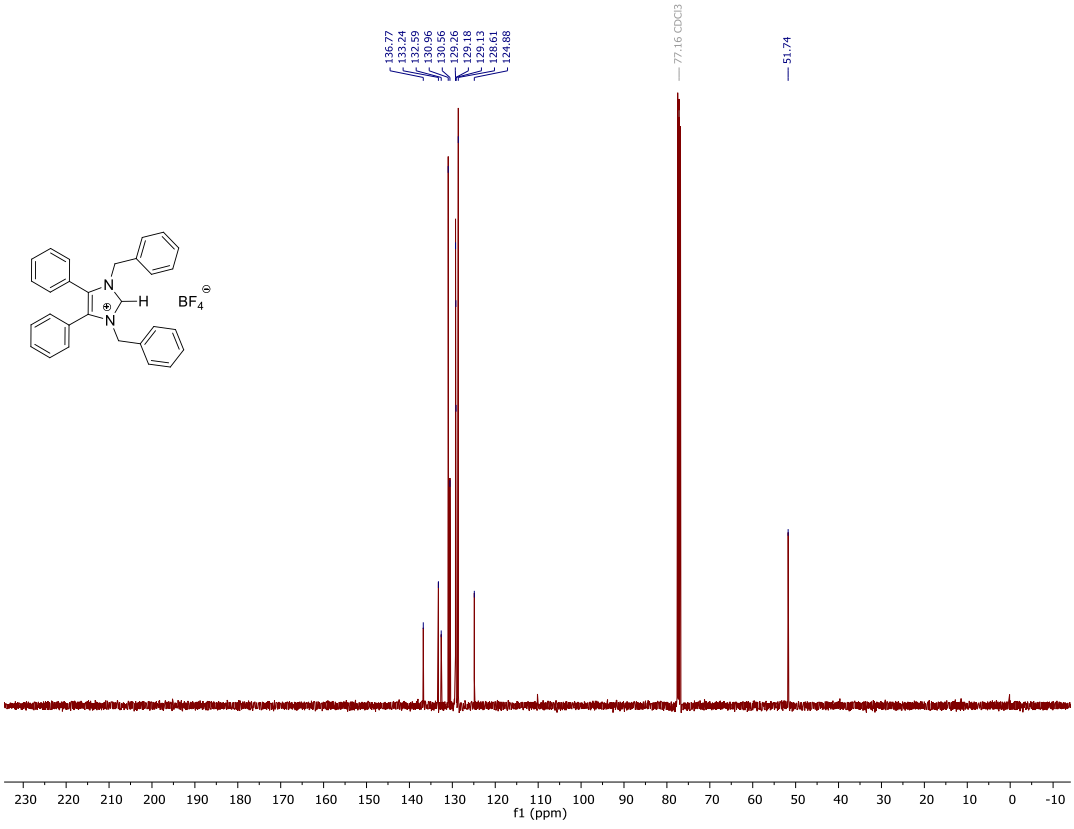

Figure S8. ^{13}C-NMR spectra of **2.8** in $CDCl_3$.

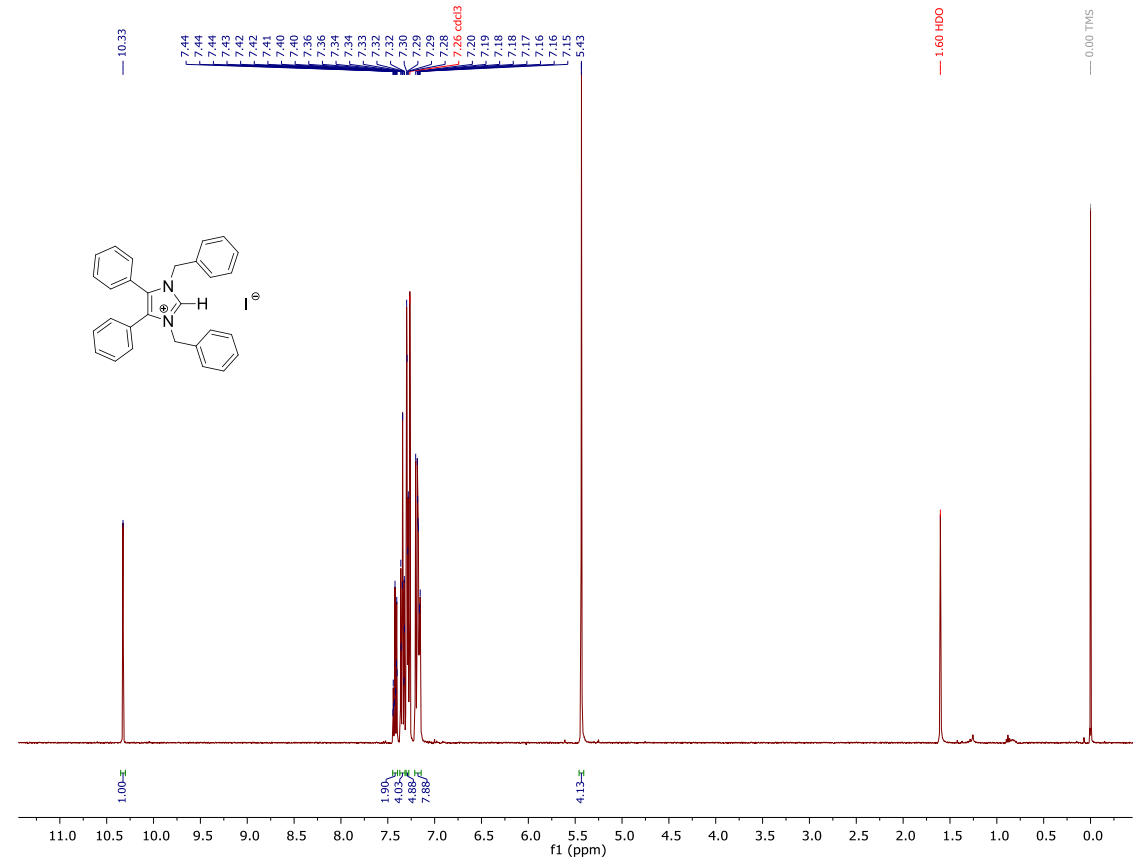

Figure S9. ^{1}H-NMR spectra of **2.9** in $CDCl_3$.

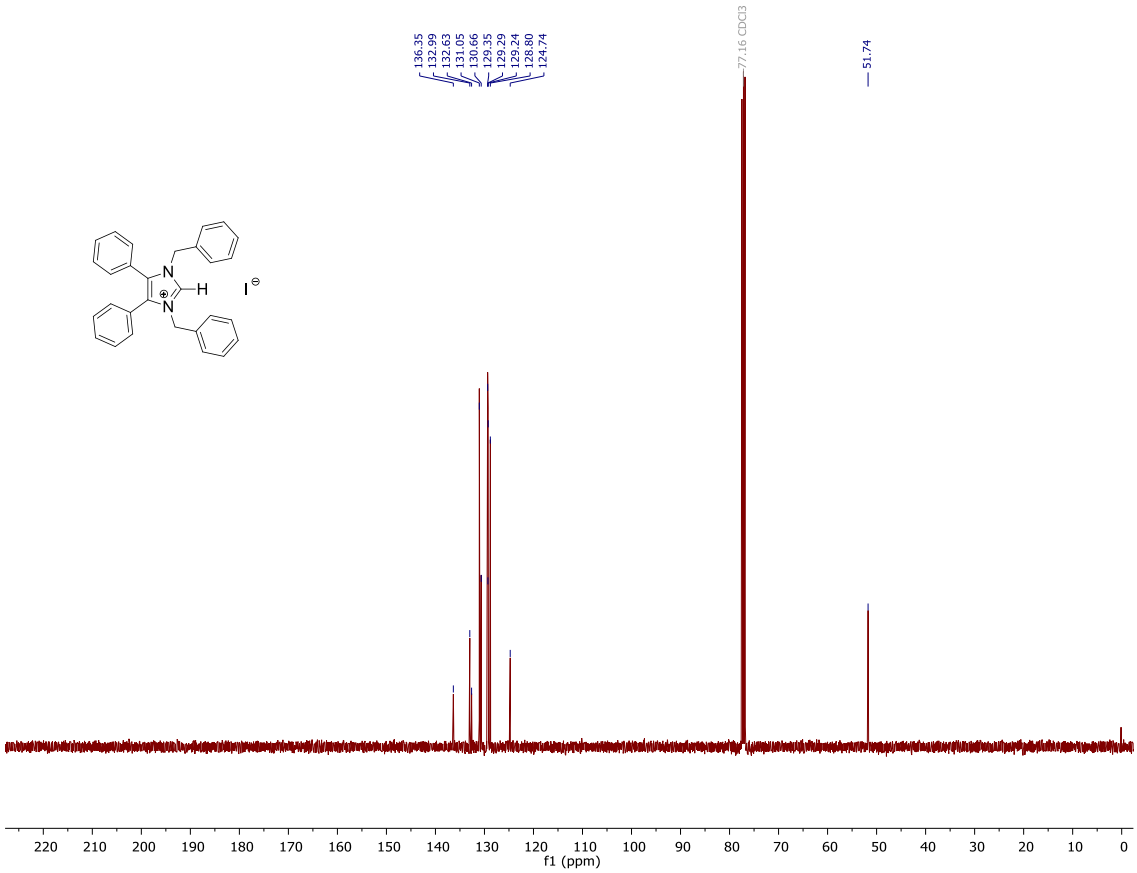

Figure S10. ^{13}C-NMR spectra of **2.9** in $CDCl_3$.

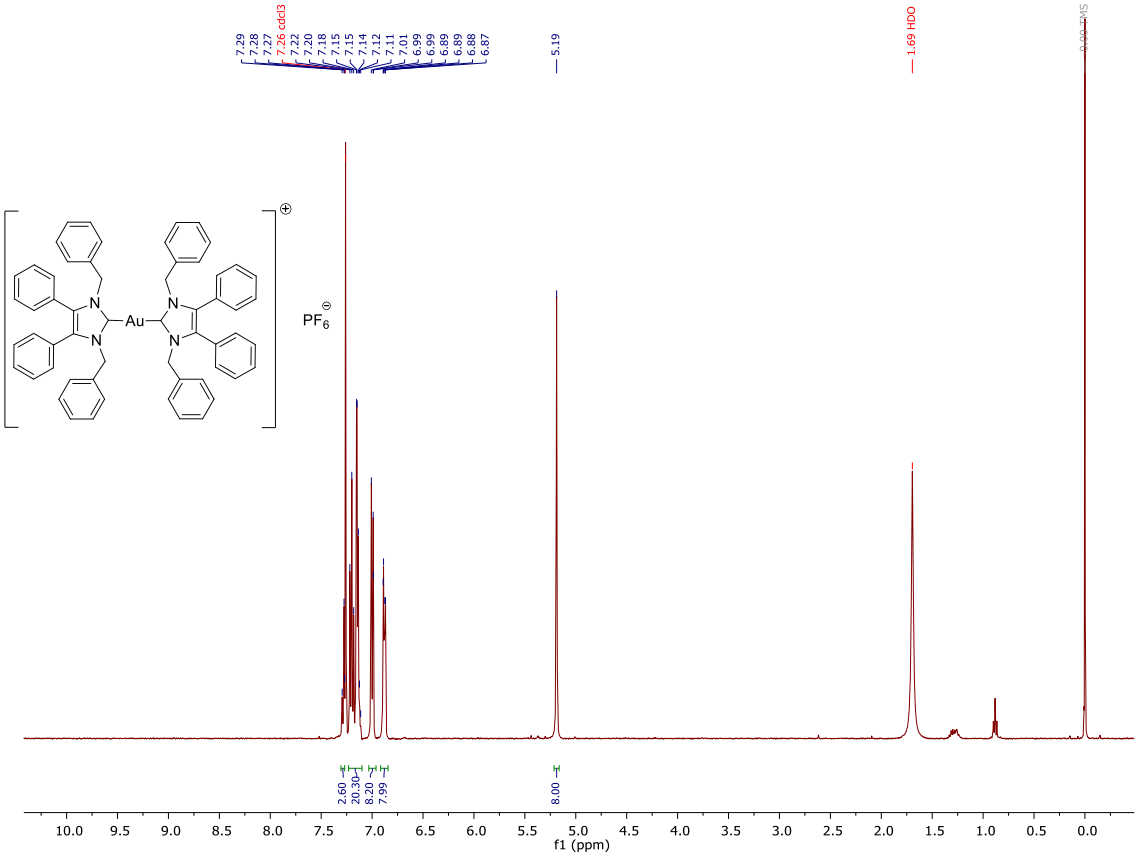

Figure S11. ^{1}H-NMR spectra of **2.10** in $CDCl_3$.

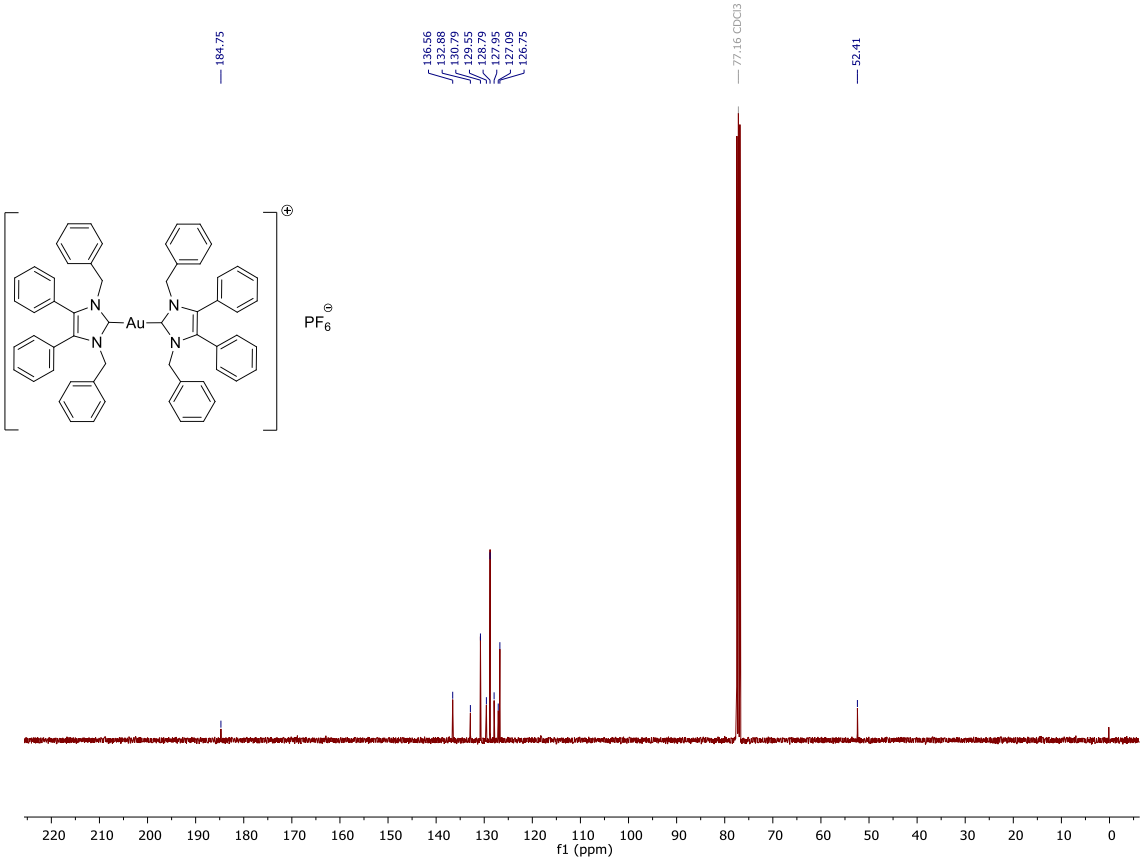

Figure S12. ^{13}C-NMR spectra of **2.10** in $CDCl_3$.

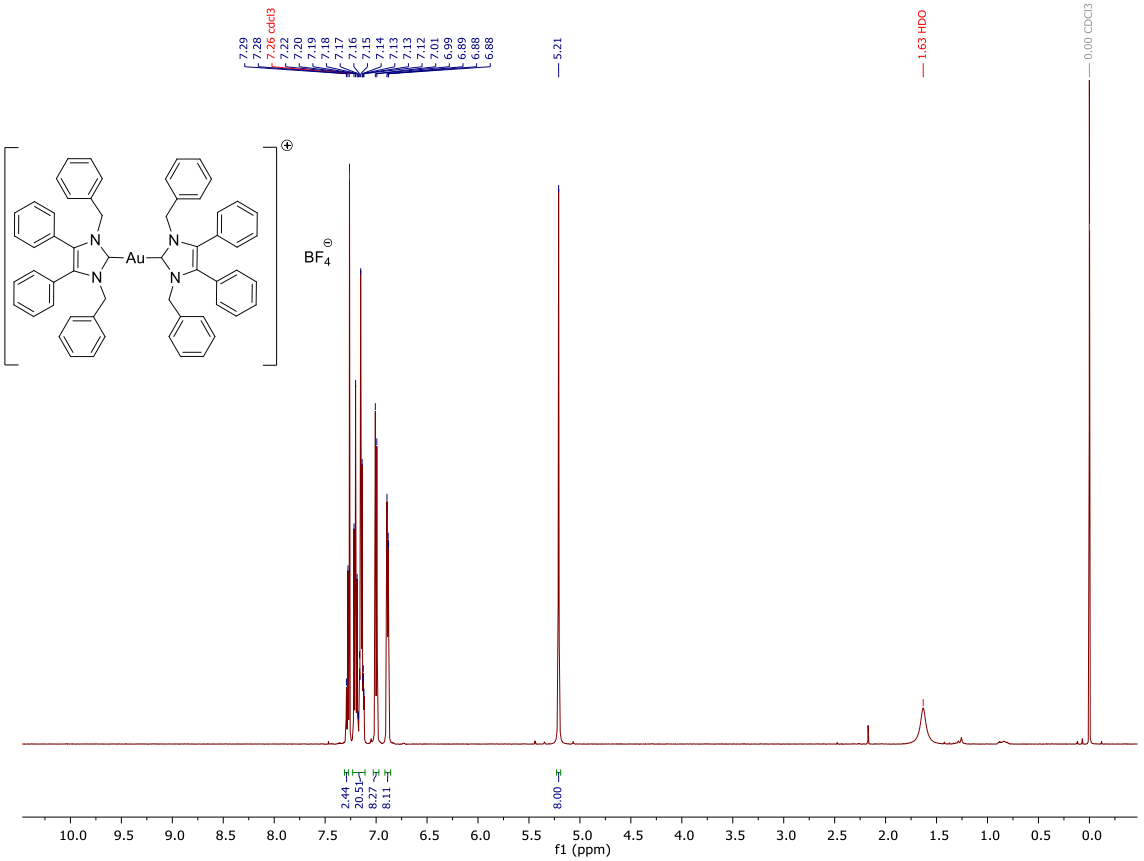

Figure S13. ^{1}H-NMR spectra of **2.11** in $CDCl_3$.

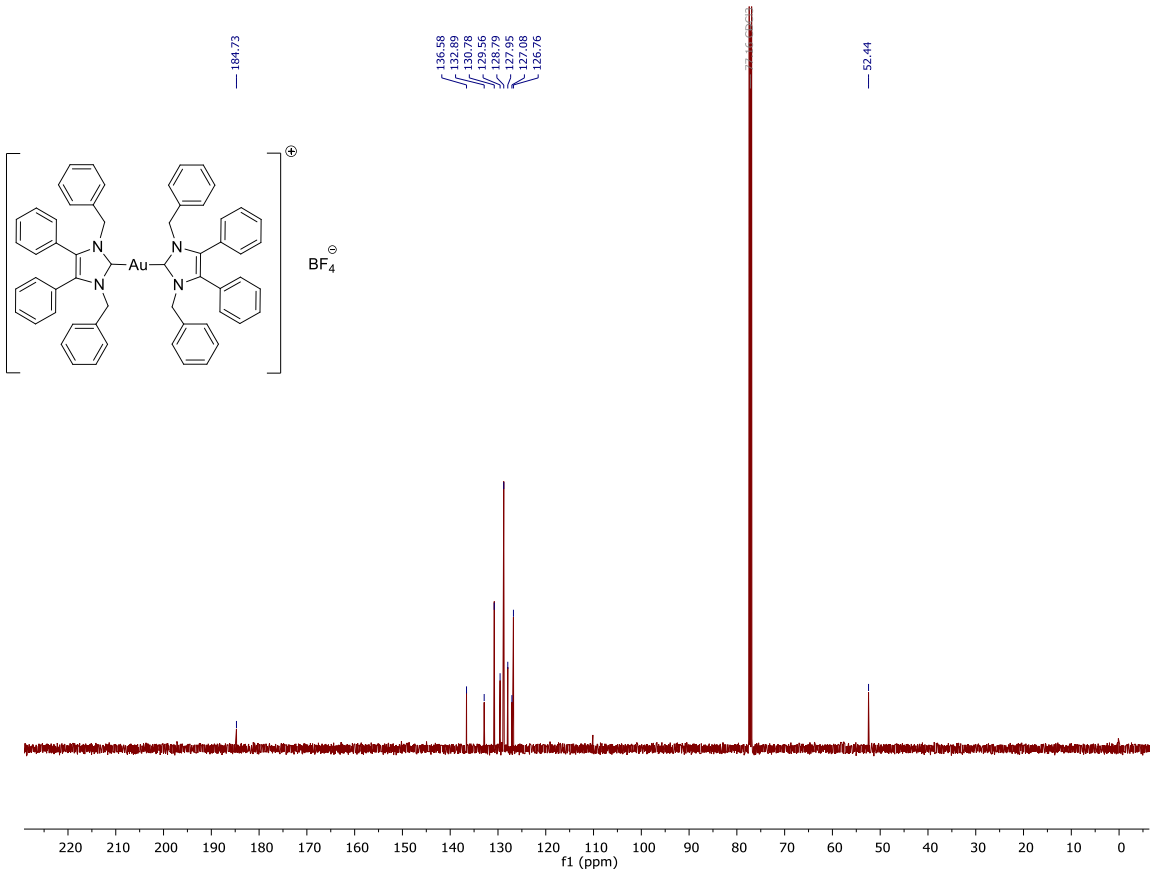

Figure S14. ^{13}C-NMR spectra of **2.11** in $CDCl_3$.

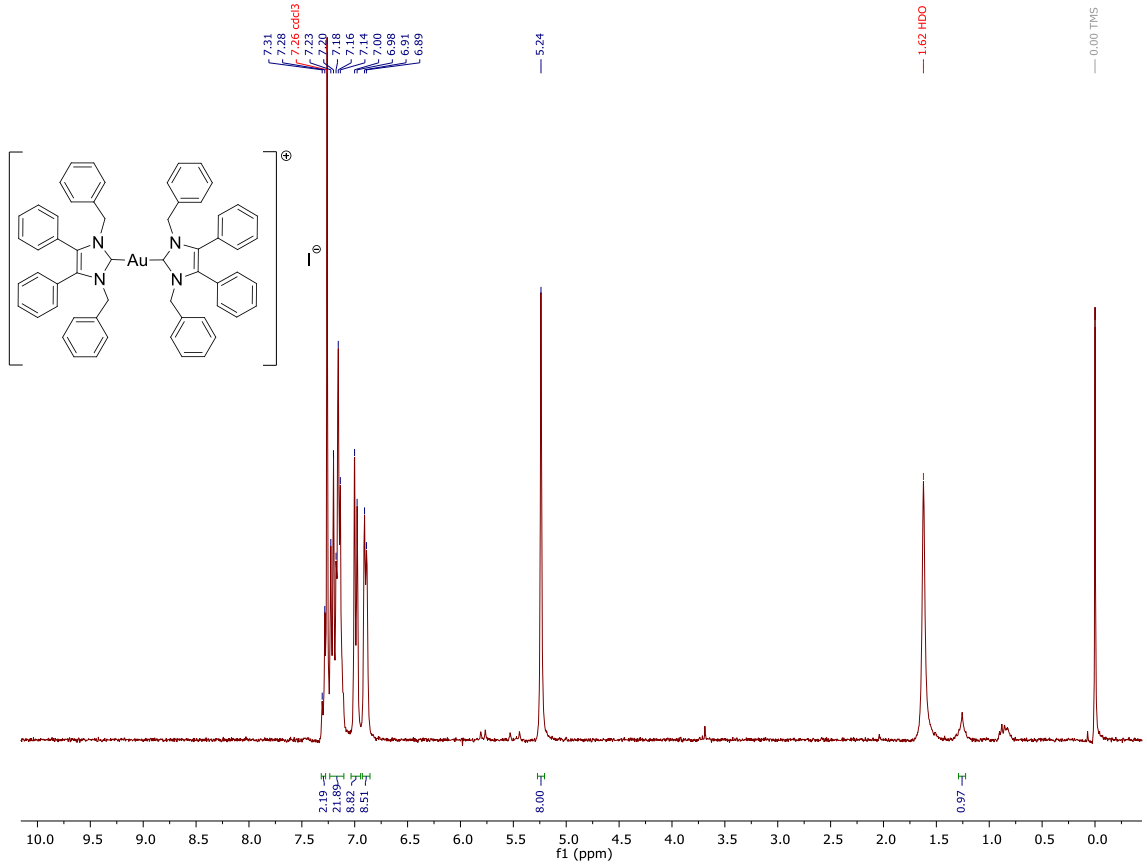

Figure S15. ^{1}H-NMR spectra of **2.13** in $CDCl_3$.

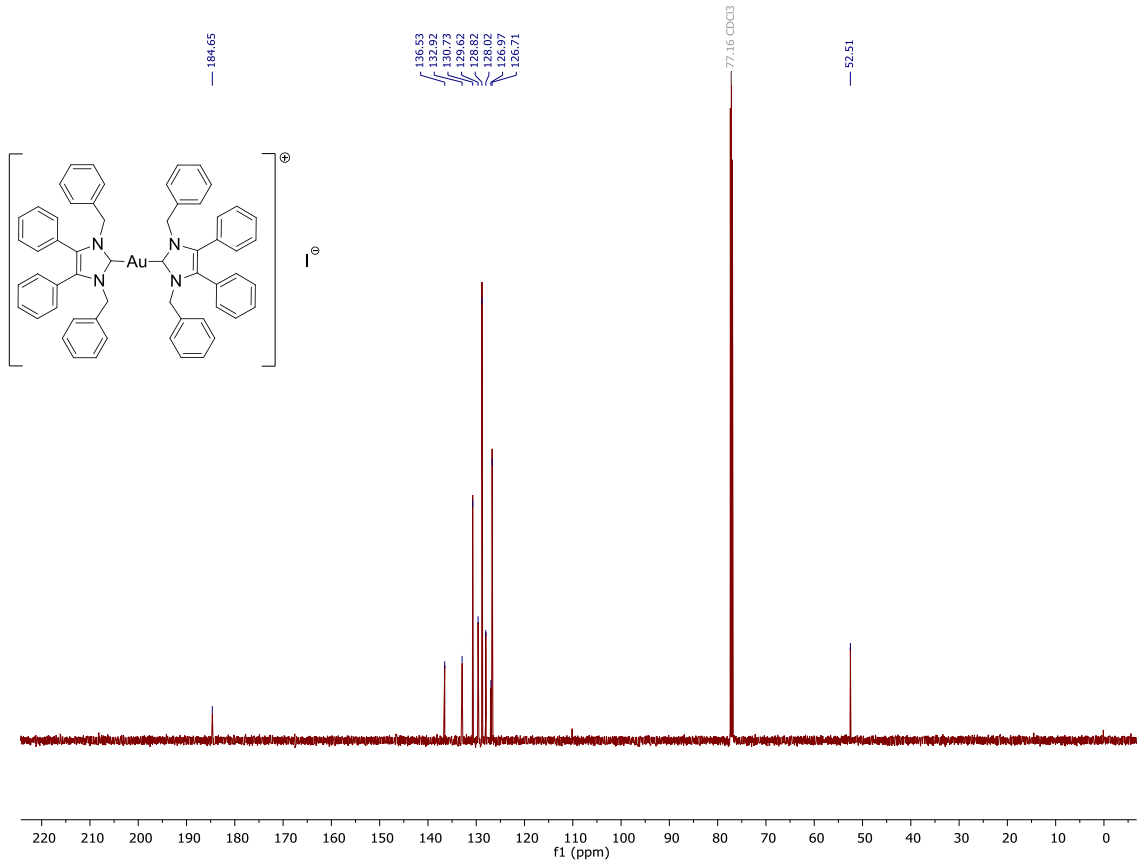

Figure S16. ^{13}C-NMR spectra of **2.13** in $CDCl_3$.

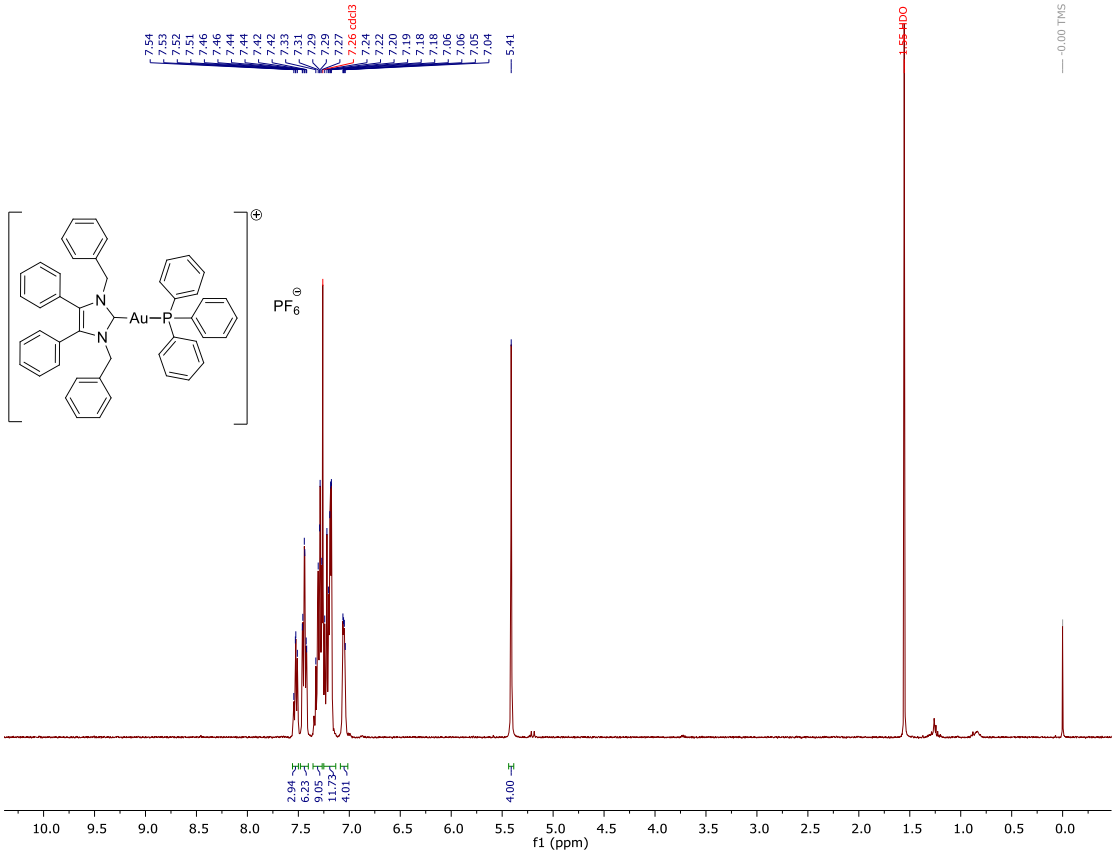

Figure S17. ^{1}H-NMR spectra of **2.14** in $CDCl_3$.

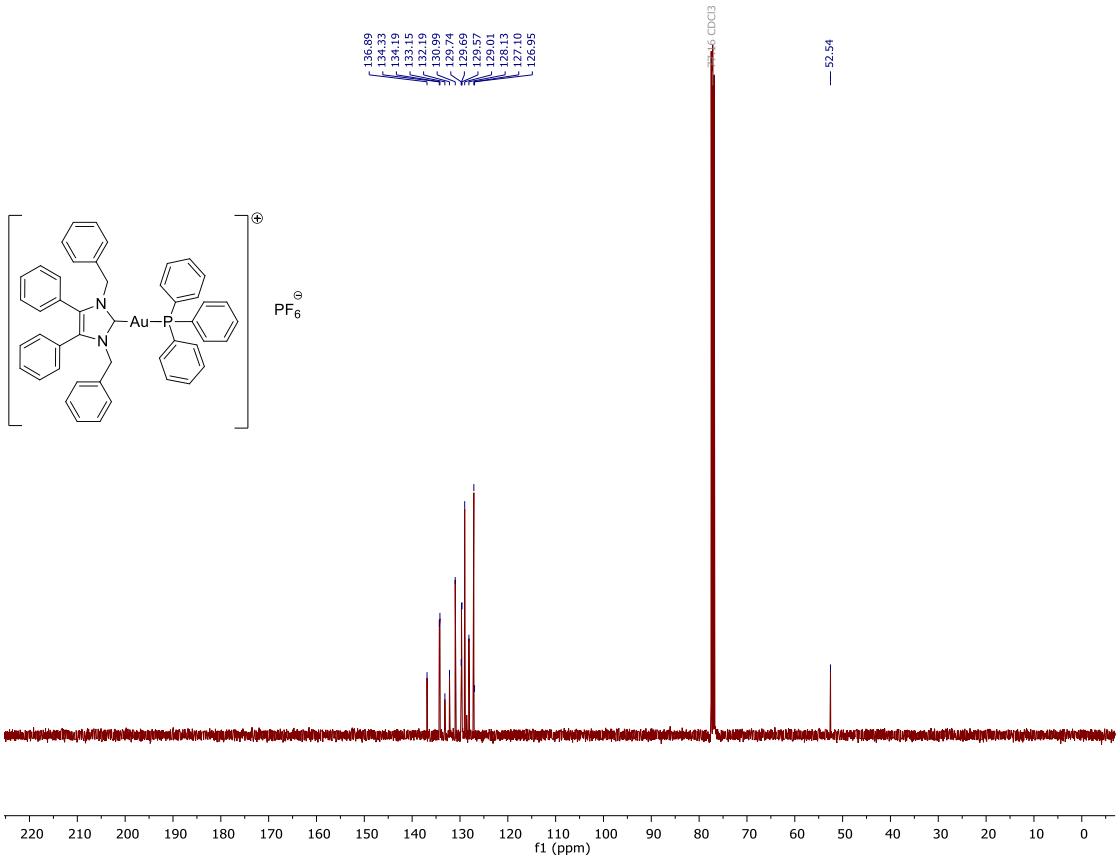

Figure S18. ^{13}C-NMR spectra of **2.14** in $CDCl_3$.

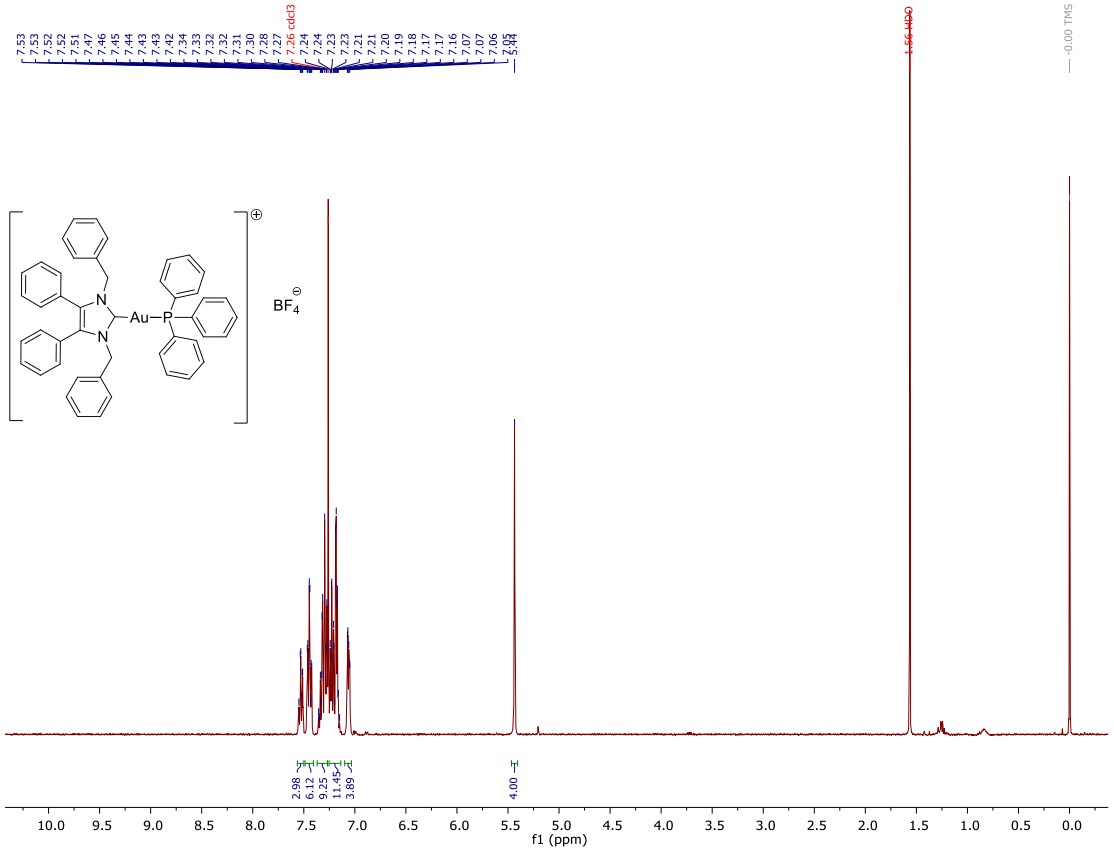

Figure S19. [1]H-NMR spectra of **2.15** in $CDCl_3$.

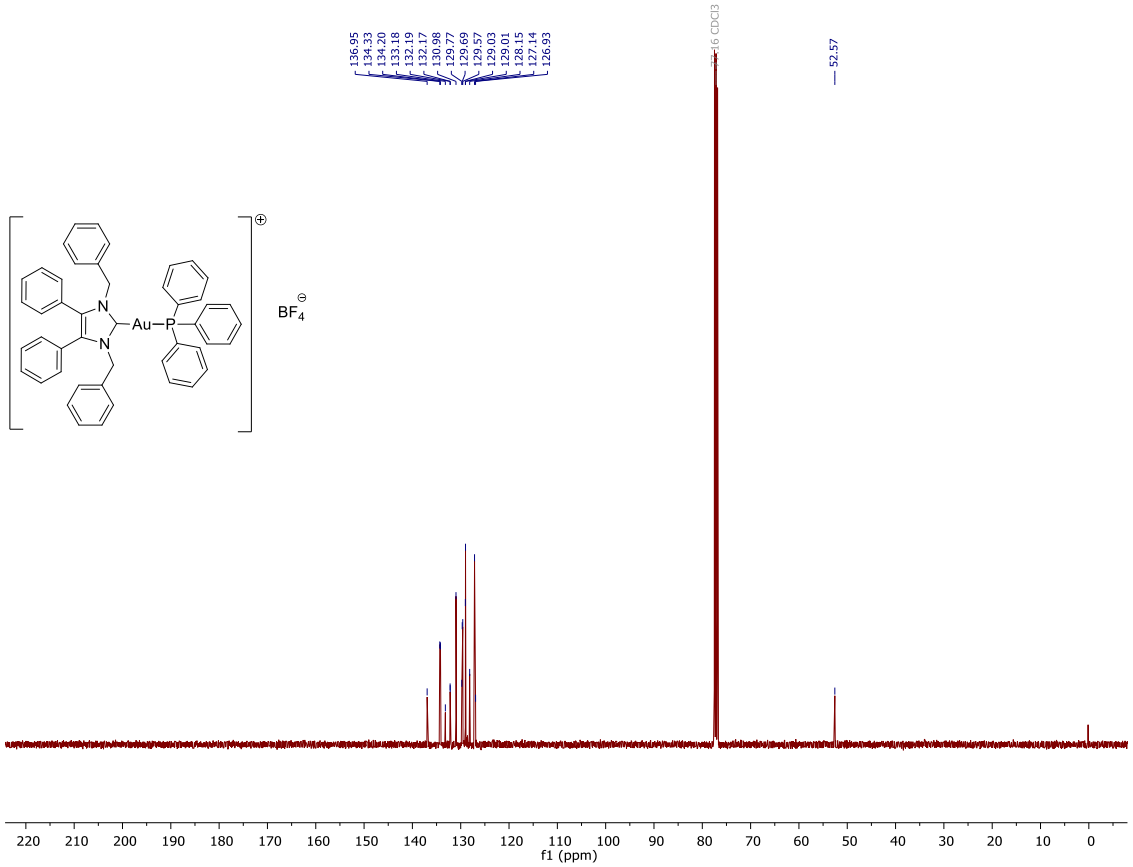

Figure S20. [13]C-NMR spectra of **2.15** in $CDCl_3$.

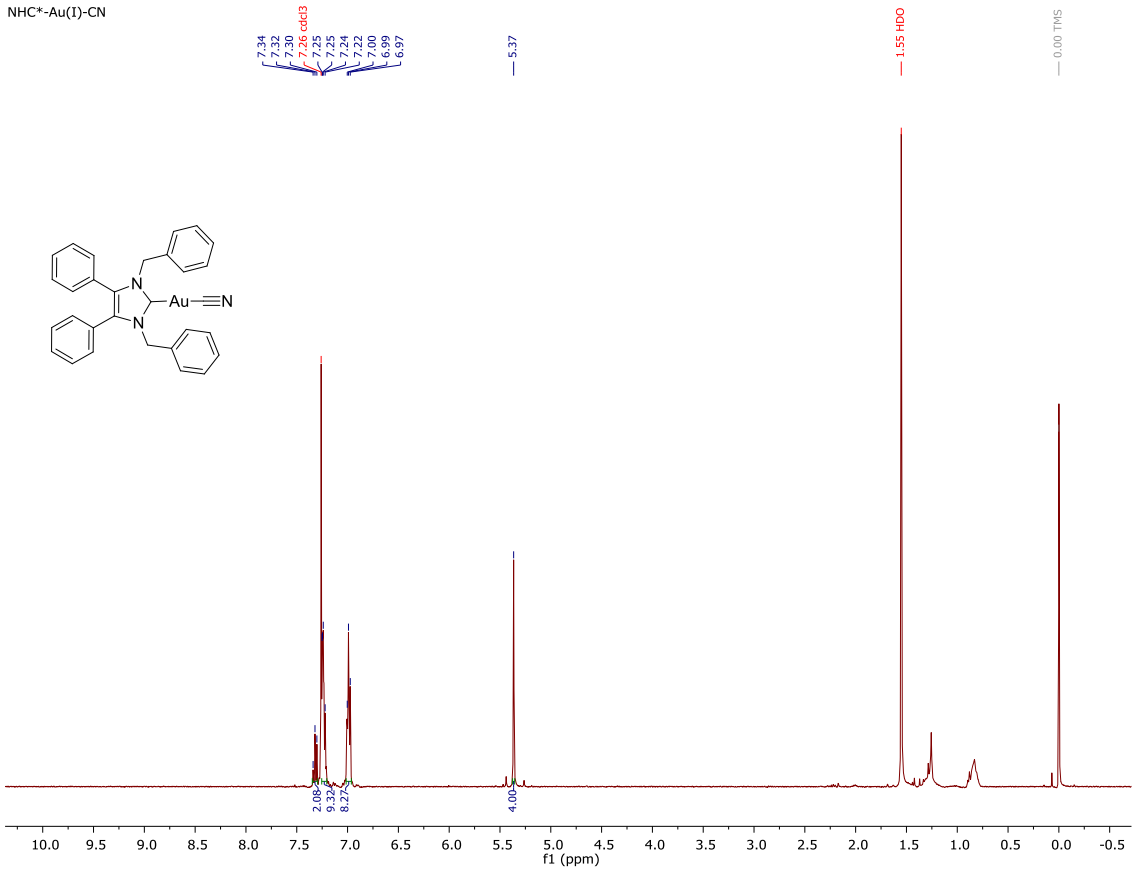

Figure S21. ^{1}H-NMR spectra of **3.13** in $CDCl_3$.

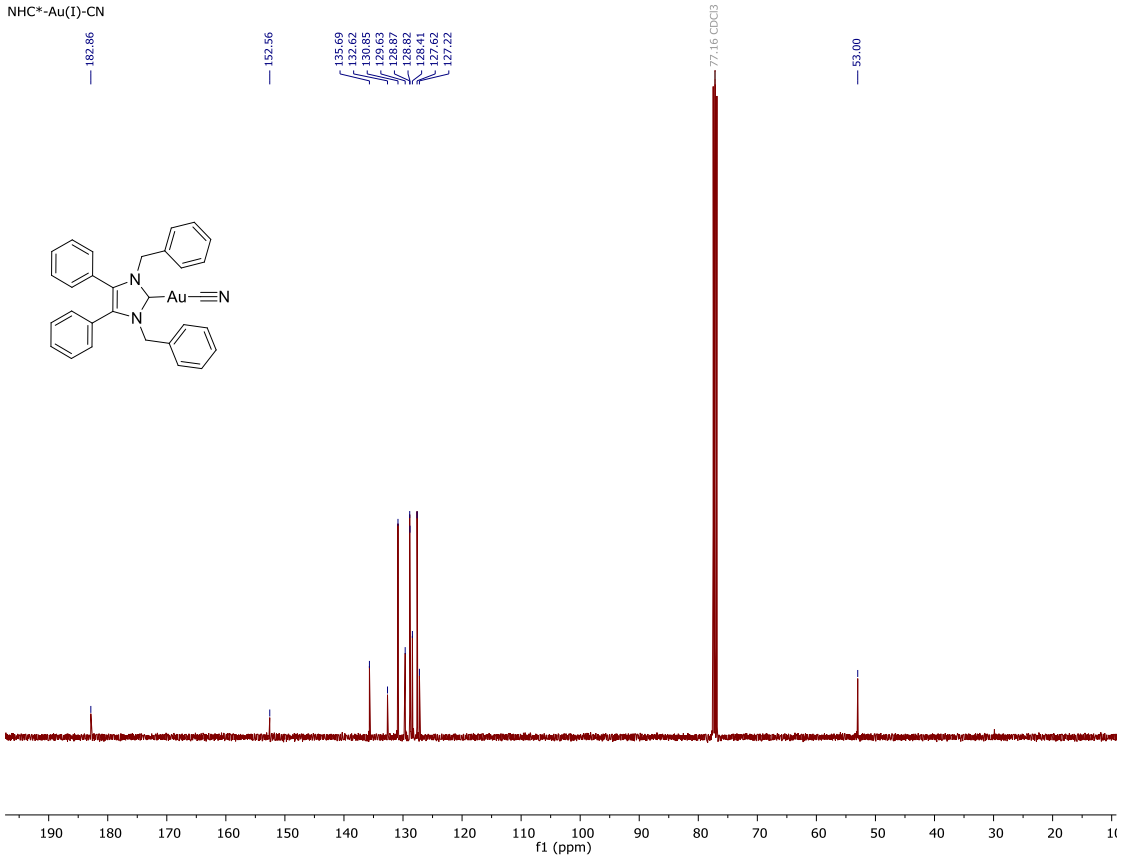

Figure S22. ^{13}C-NMR spectra of **3.13** in $CDCl_3$.

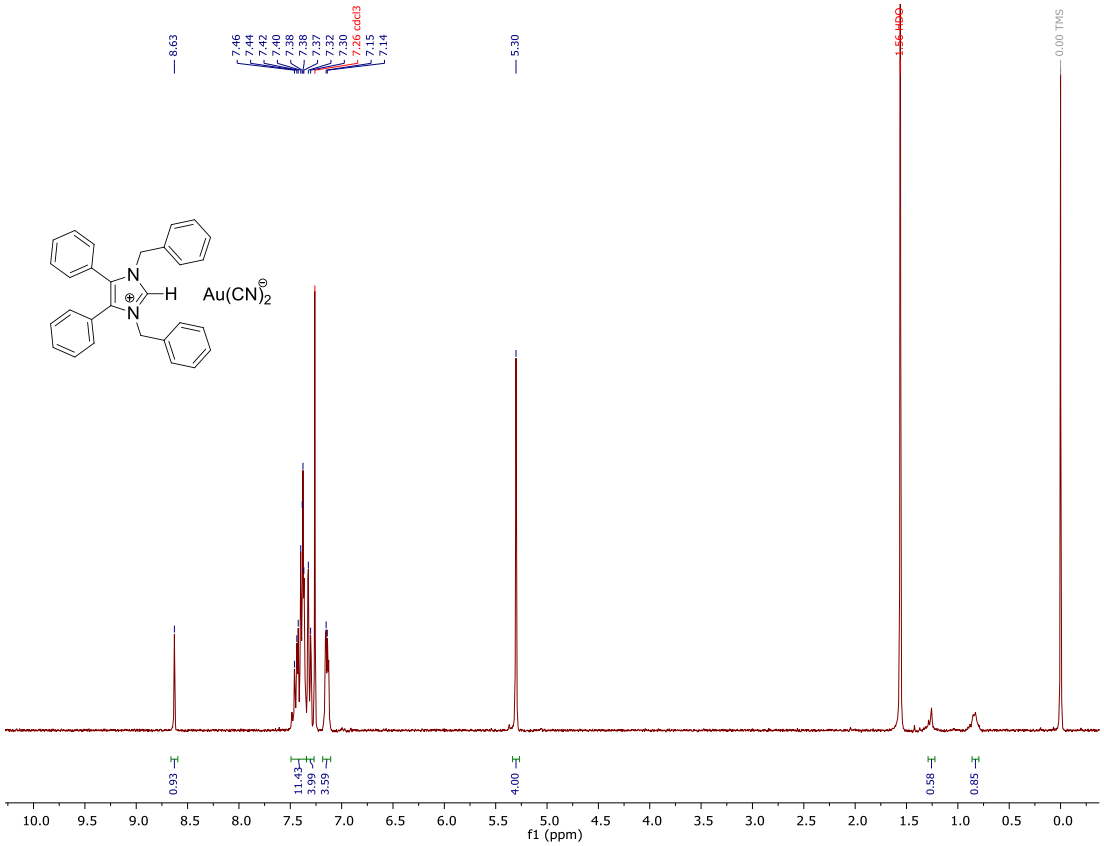

Figure S23. ^{1}H-NMR spectra of **3.14** in $CDCl_3$.

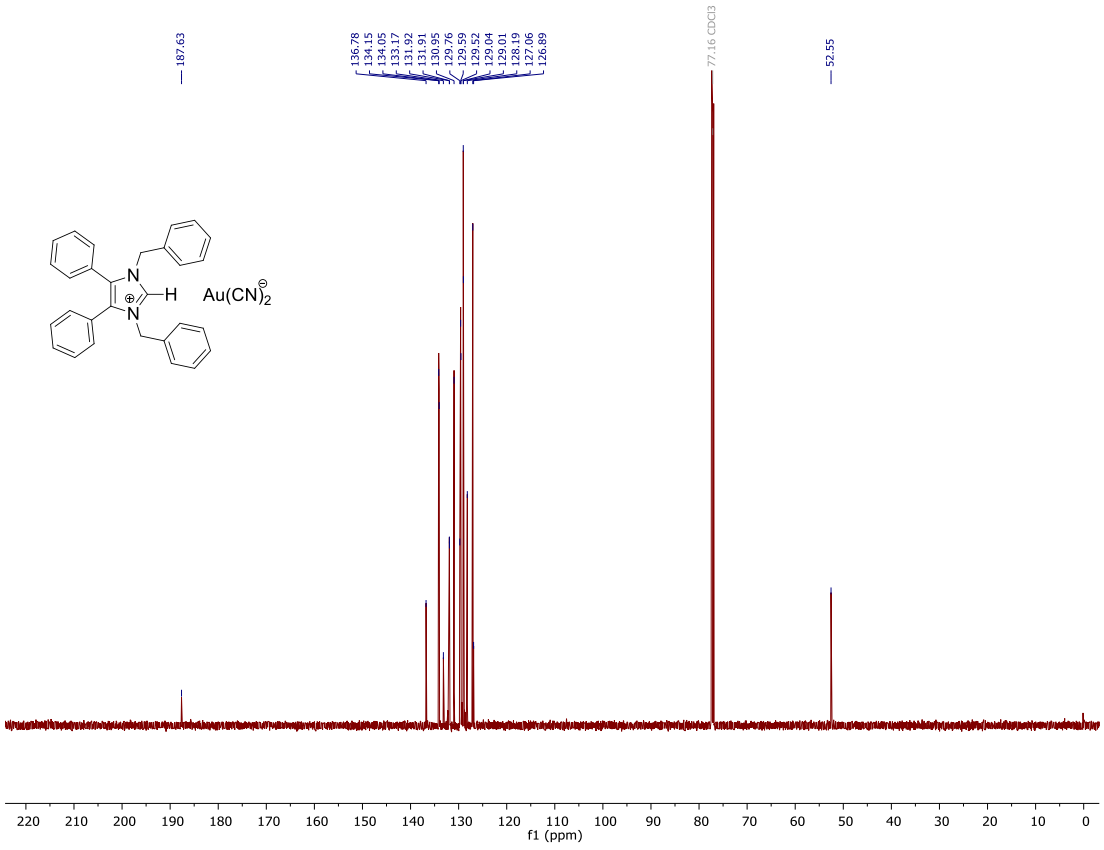

Figure S24. ^{13}C-NMR spectra of **3.14** in $CDCl_3$.

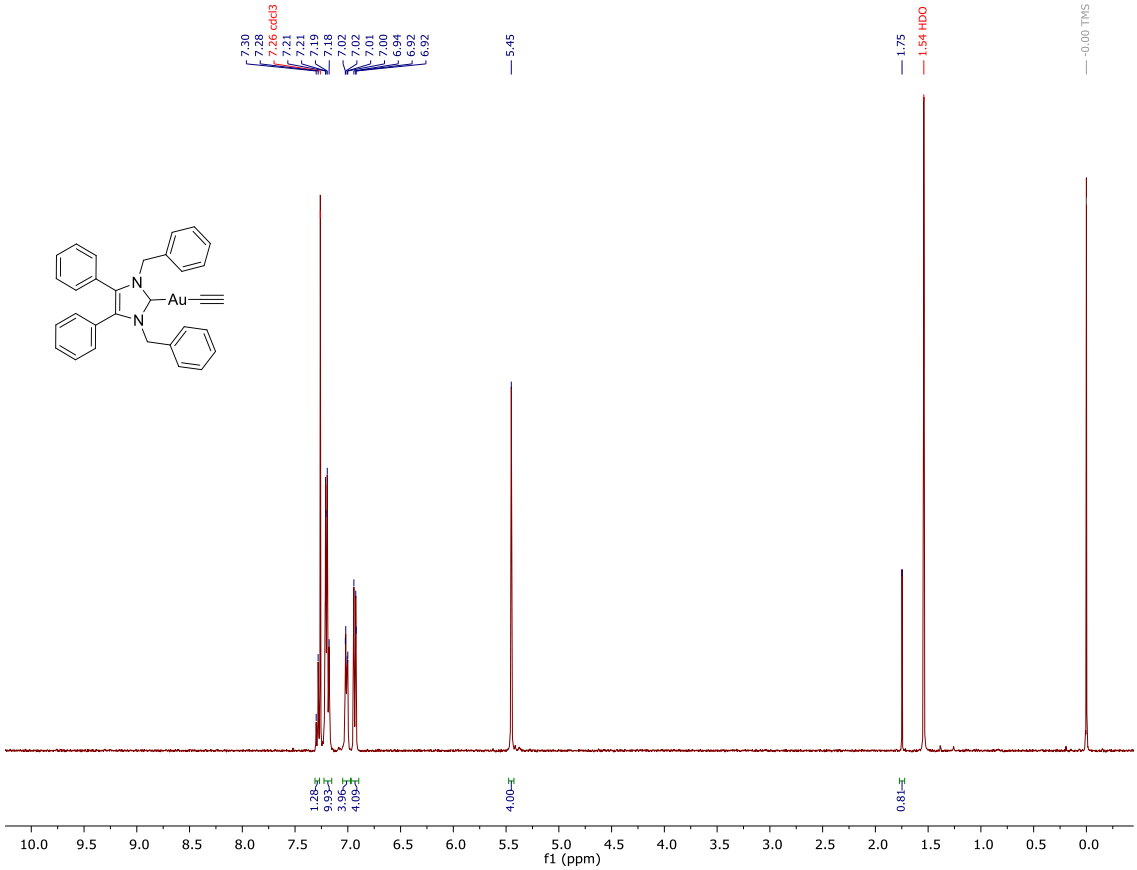

Figure S25. [1]H-NMR spectra of **3.15** in $CDCl_3$.

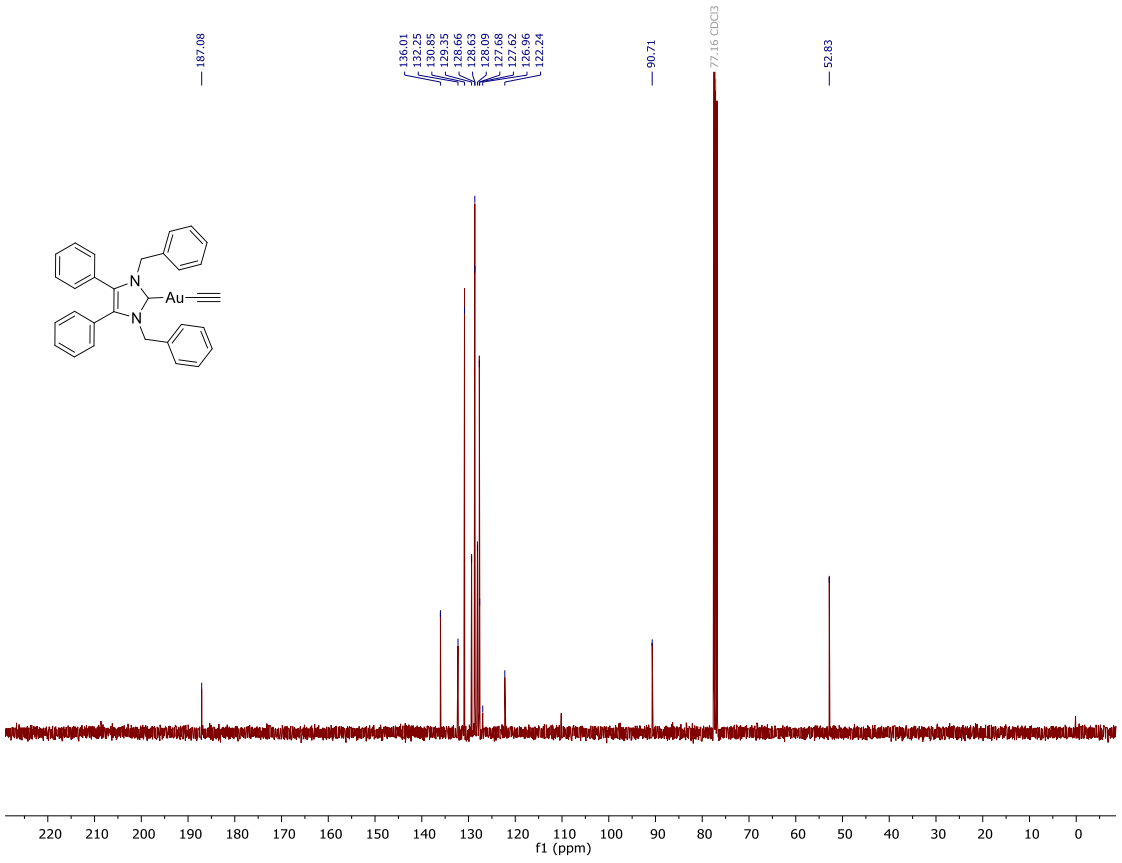

Figure S26. [13]C-NMR spectra of **3.15** in $CDCl_3$.

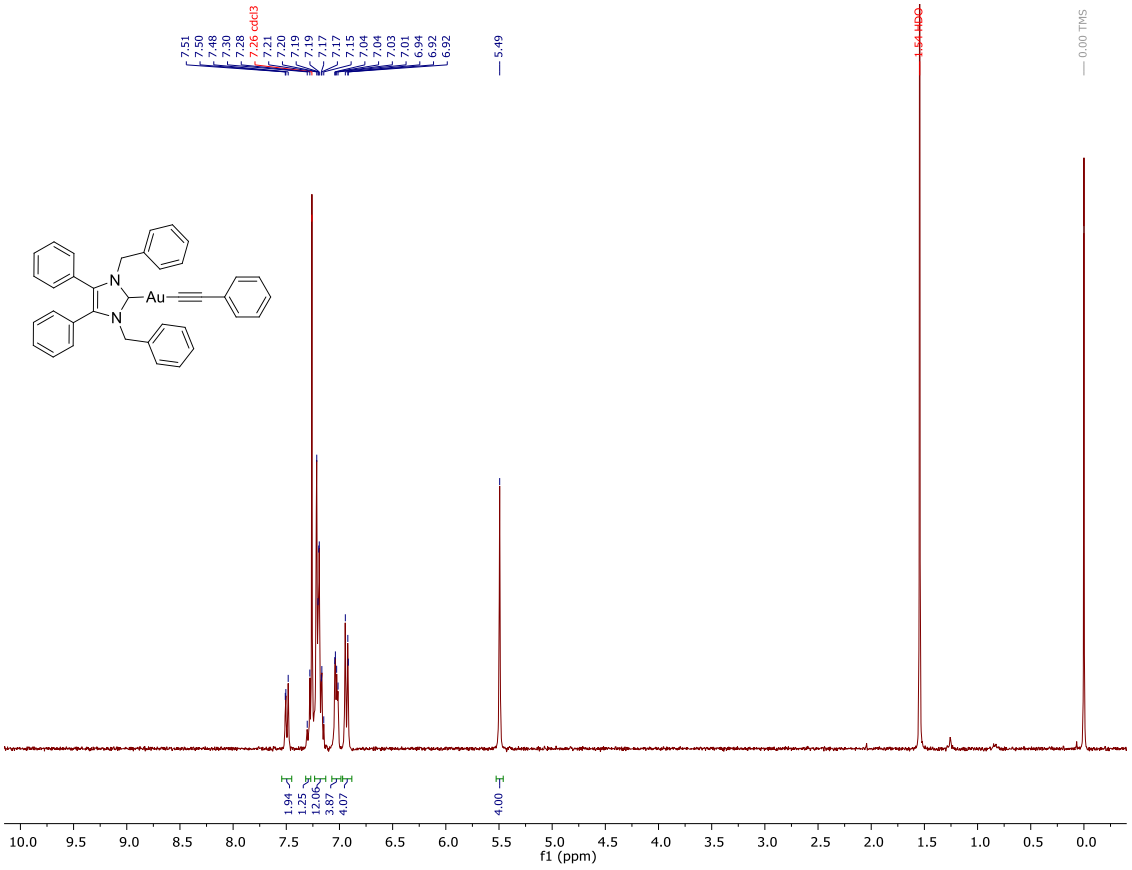

Figure S27. [1]H-NMR spectra of **3.16** in $CDCl_3$.

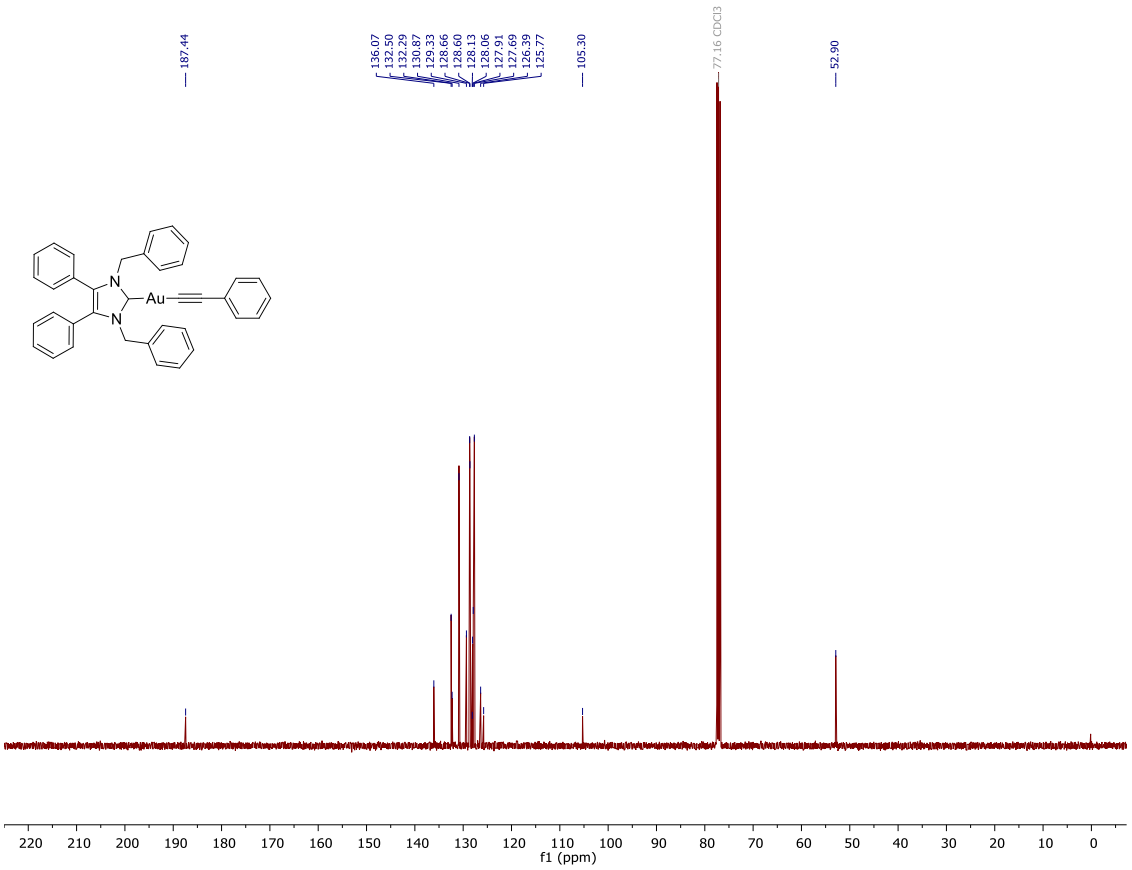

Figure S28. [13]C-NMR spectra of **3.16** in $CDCl_3$.

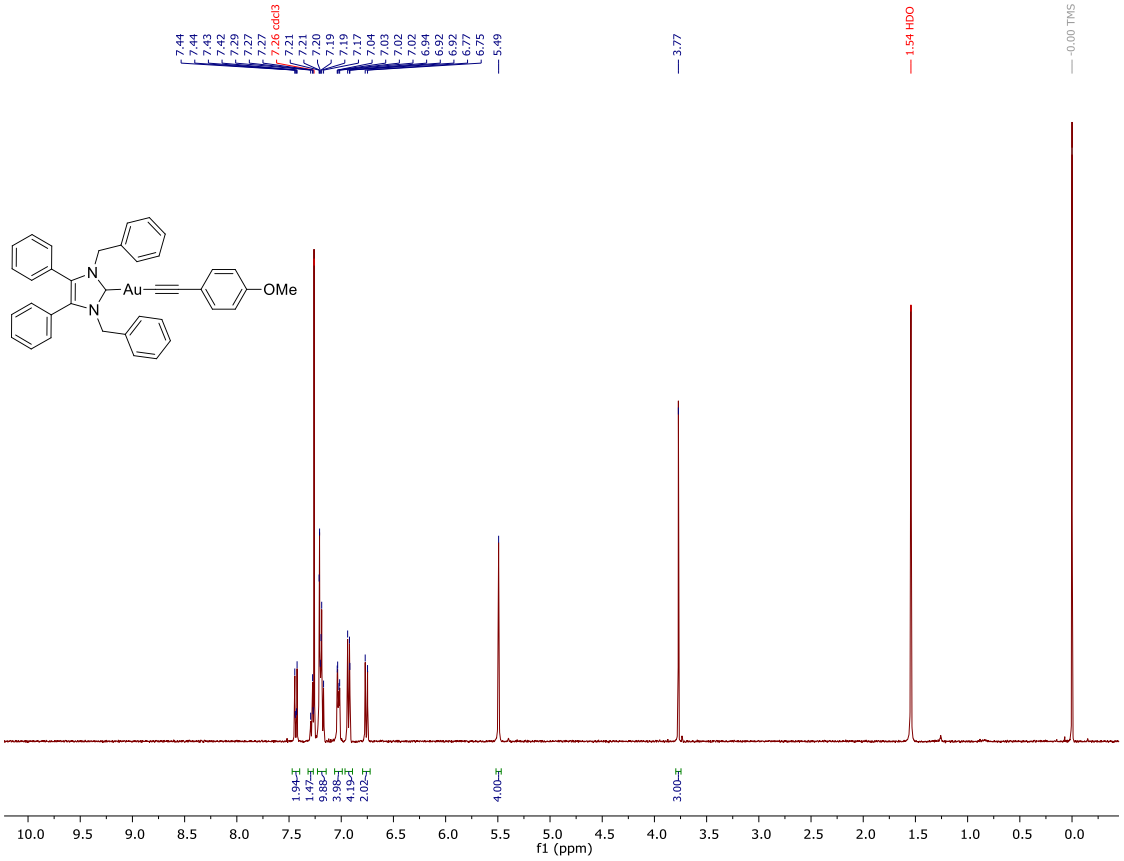

Figure S29. ^{1}H-NMR spectra of **3.17** in $CDCl_3$.

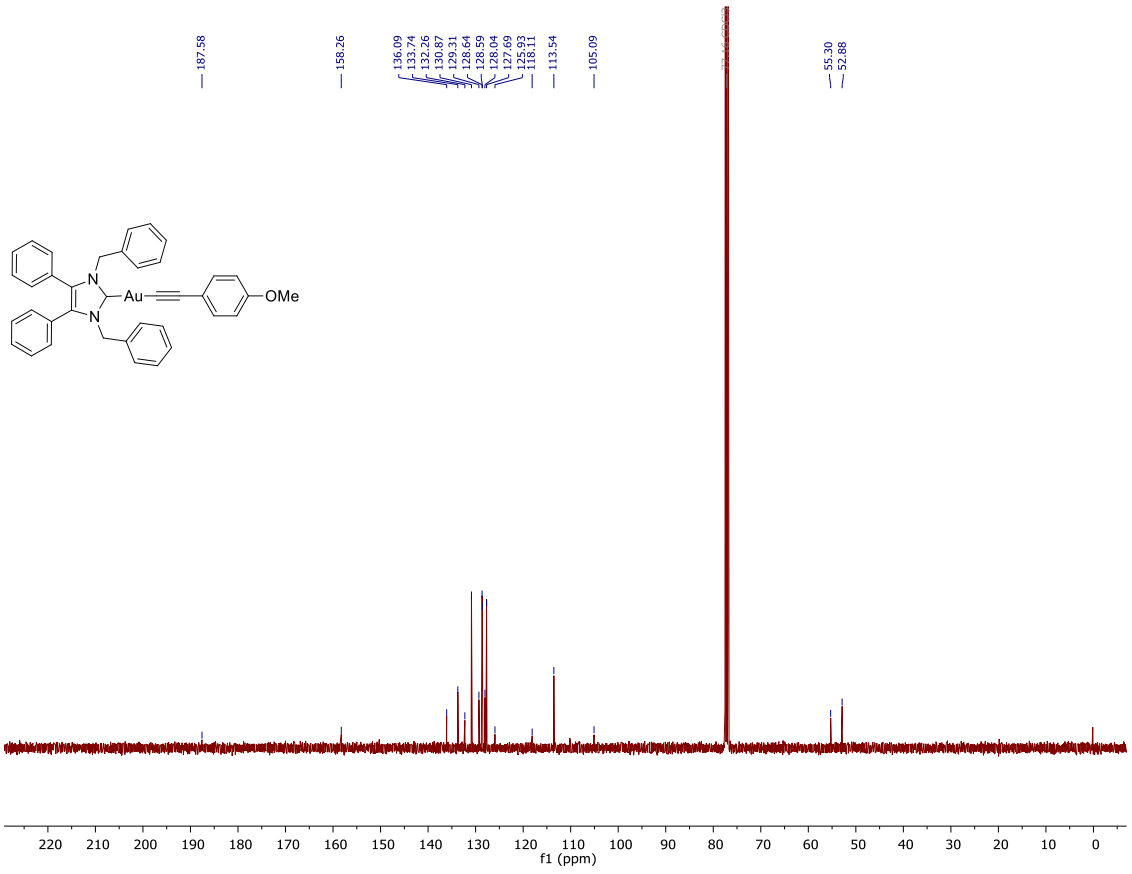

Figure S30. ^{13}C-NMR spectra of **3.17** in $CDCl_3$.

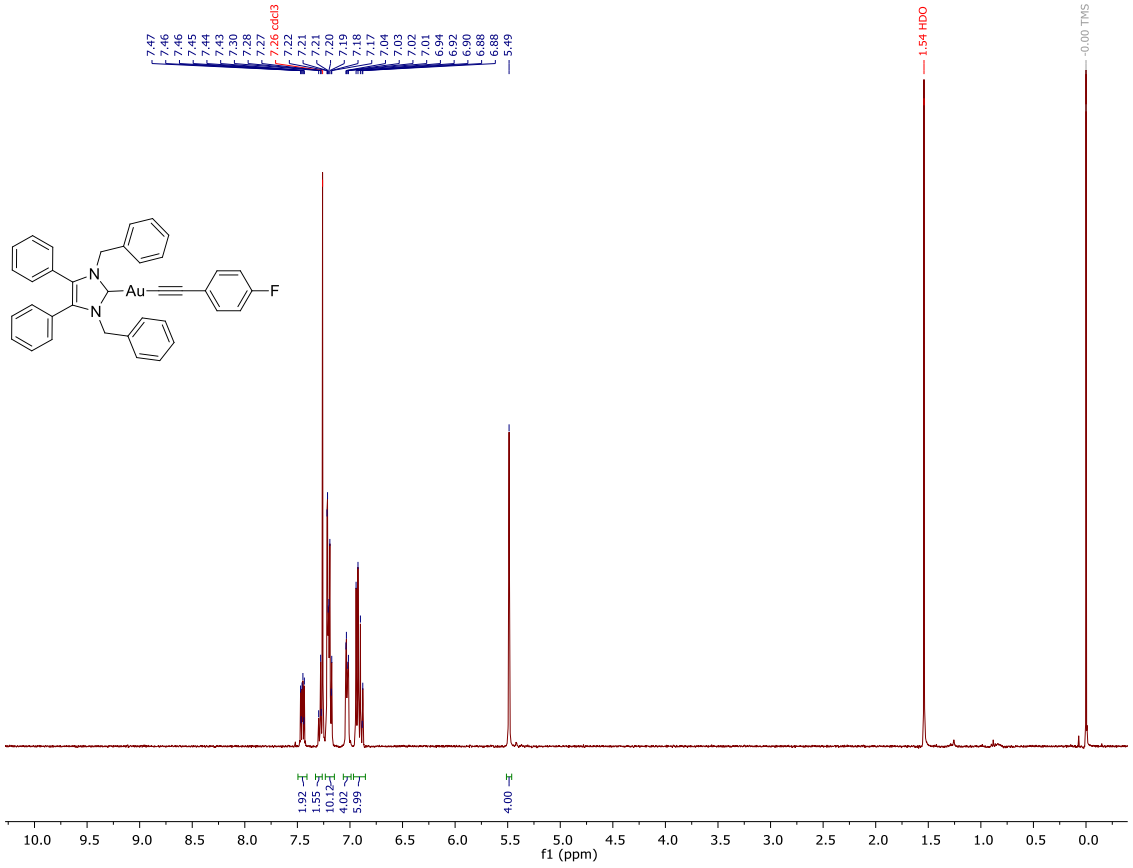

Figure S31. [1]H-NMR spectra of **3.18** in $CDCl_3$.

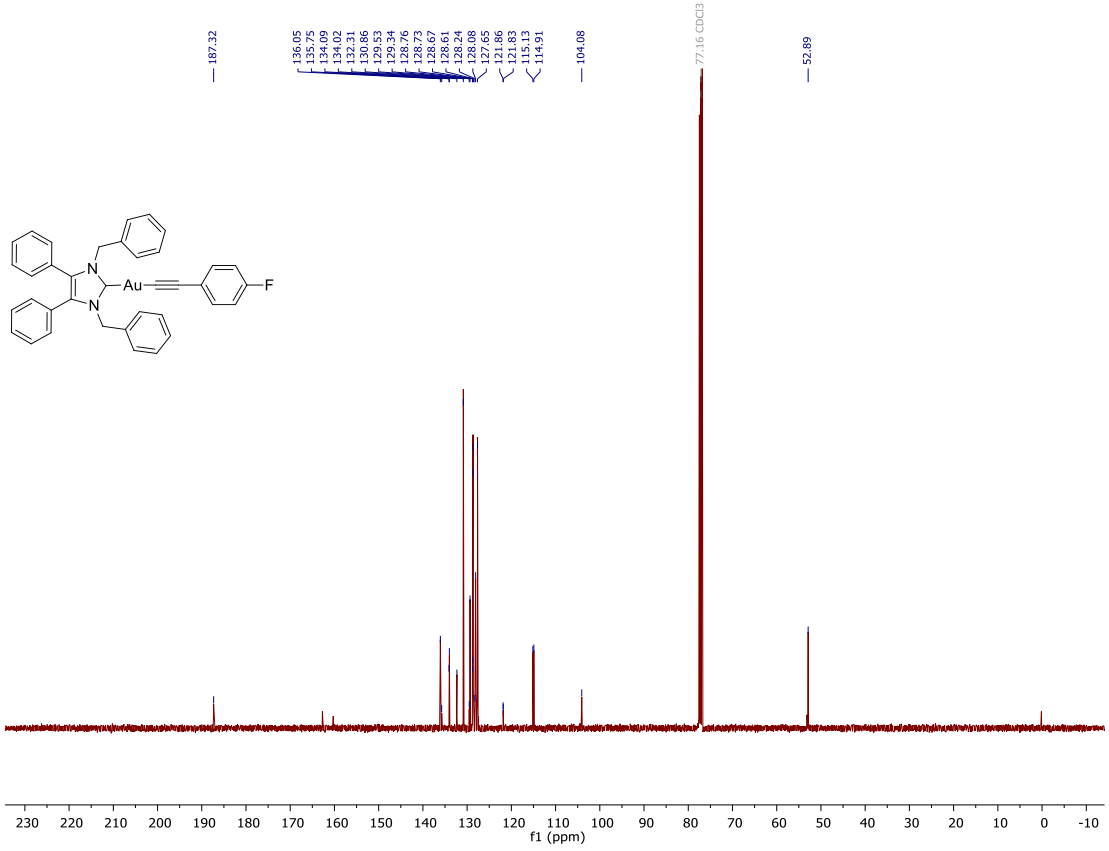

Figure S32. [13]C-NMR spectra of **3.18** in $CDCl_3$.

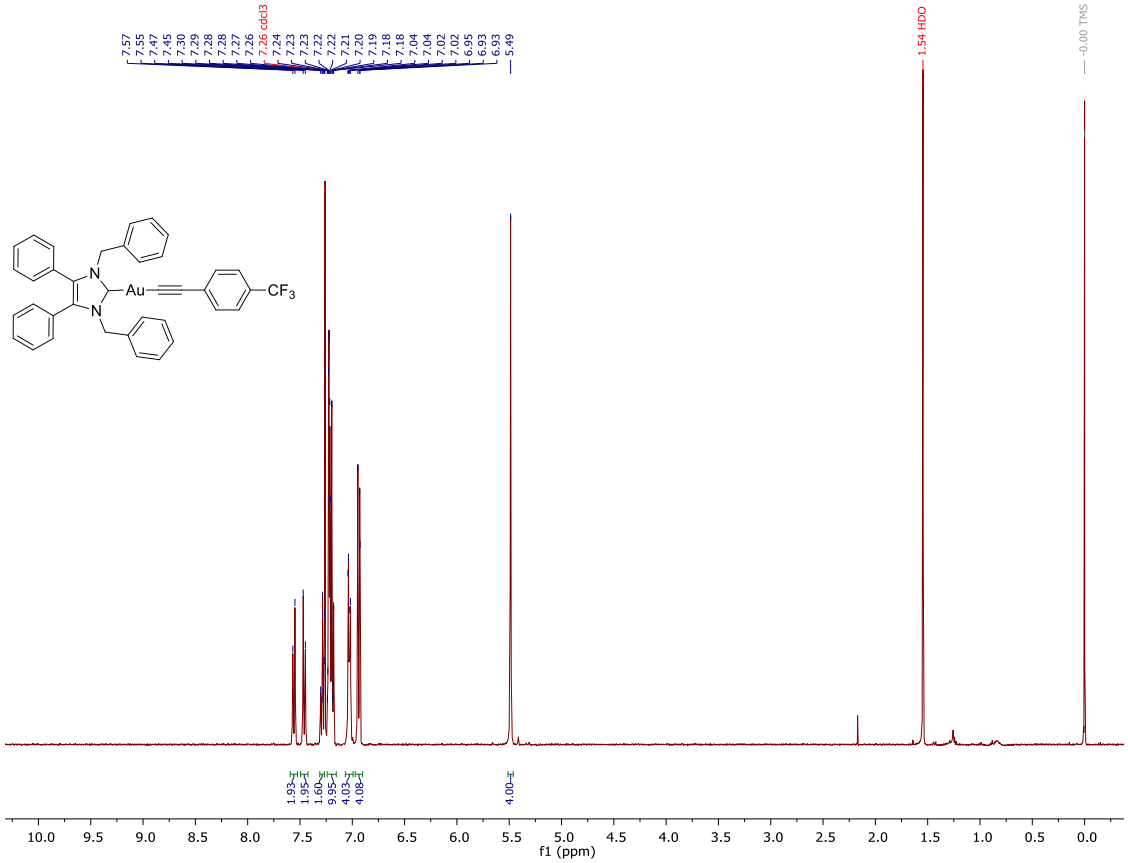

Figure S33. ^{1}H-NMR spectra of **3.19** in $CDCl_3$.

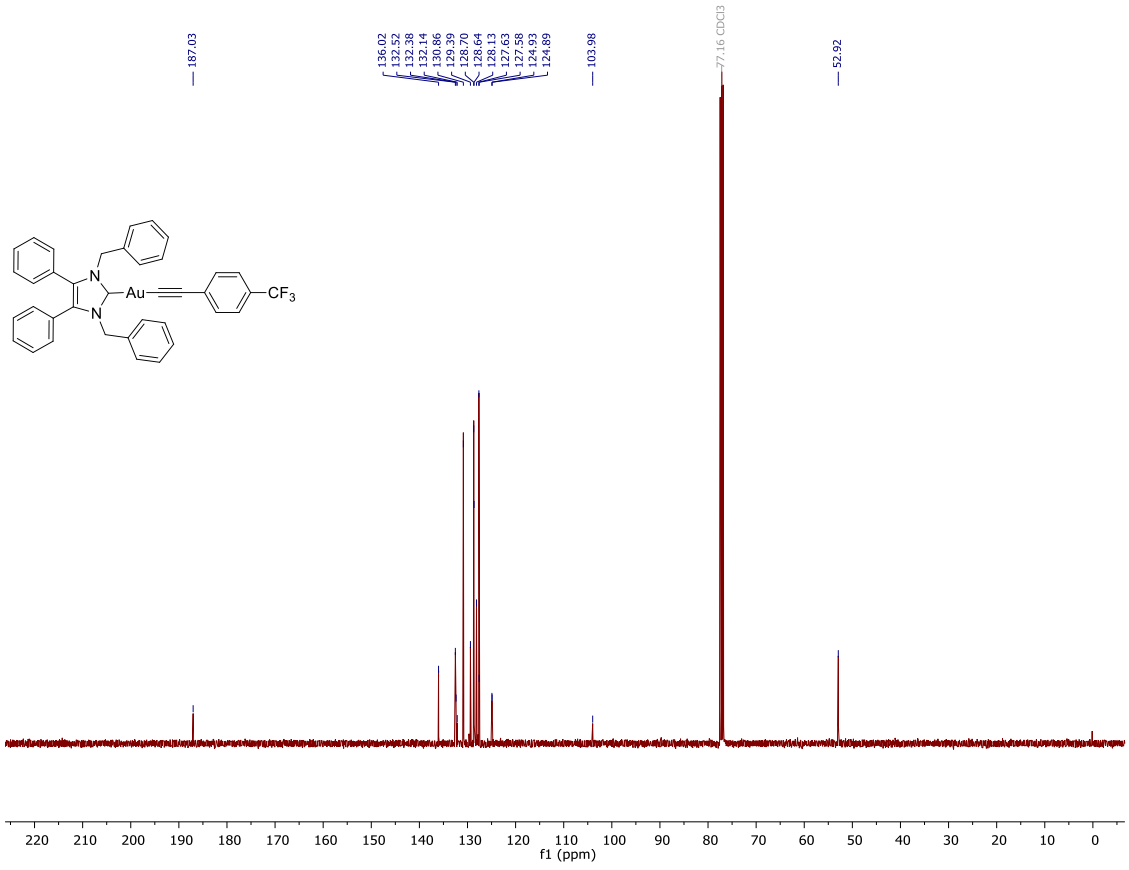

Figure S34. ^{13}C-NMR spectra of **3.19** in $CDCl_3$.

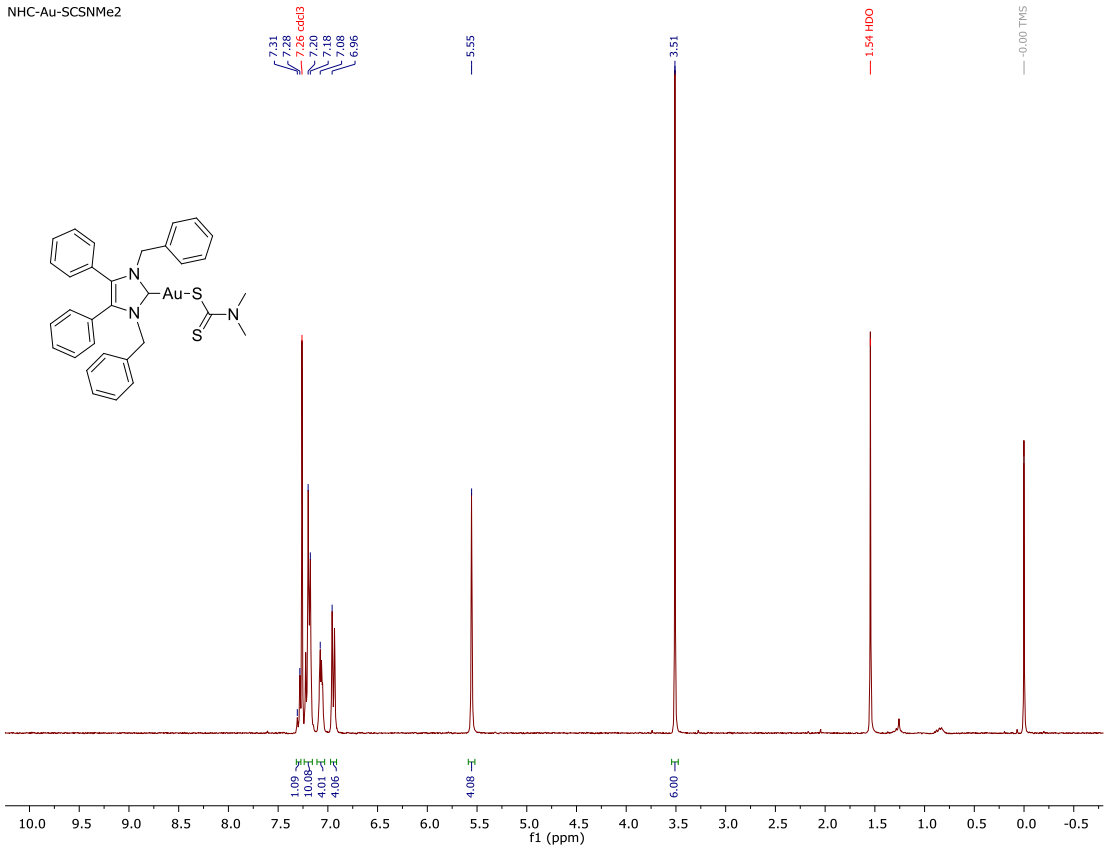

Figure S35. ^{1}H-NMR spectra of **4.8** in $CDCl_3$.

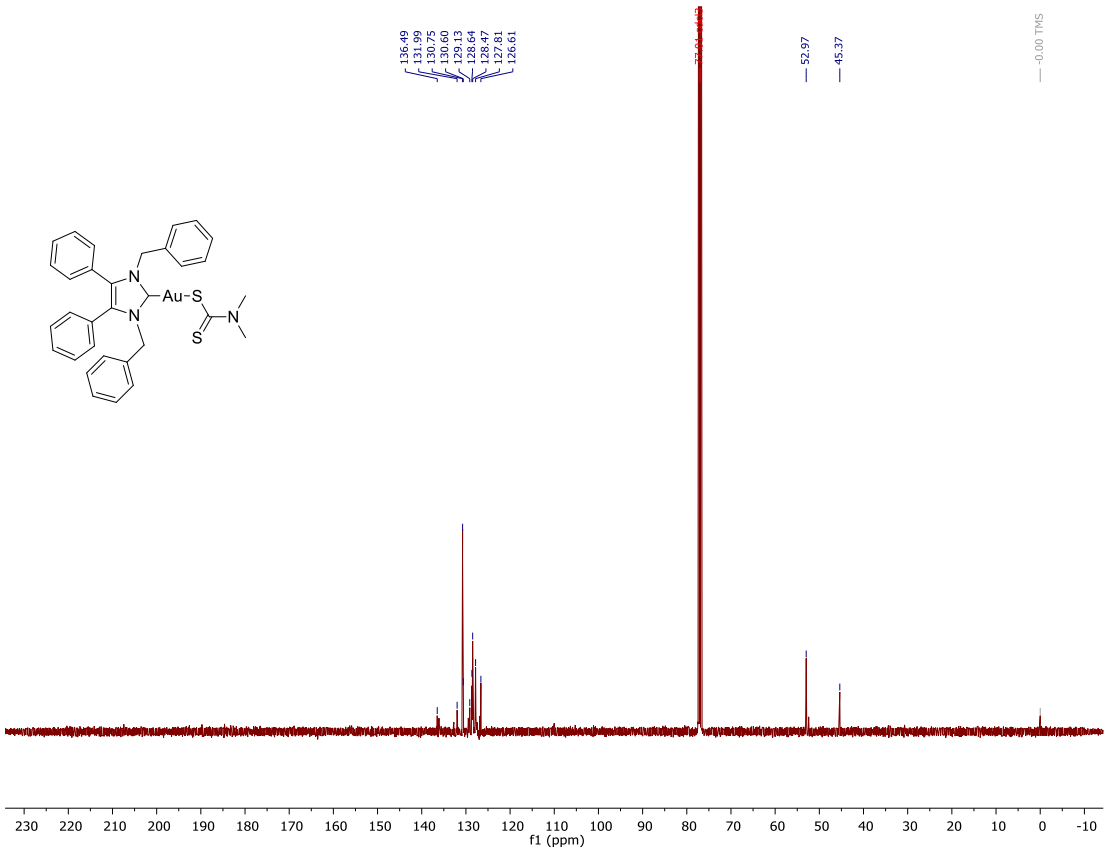

Figure S36. ^{13}C-NMR spectra of **4.8** in $CDCl_3$.

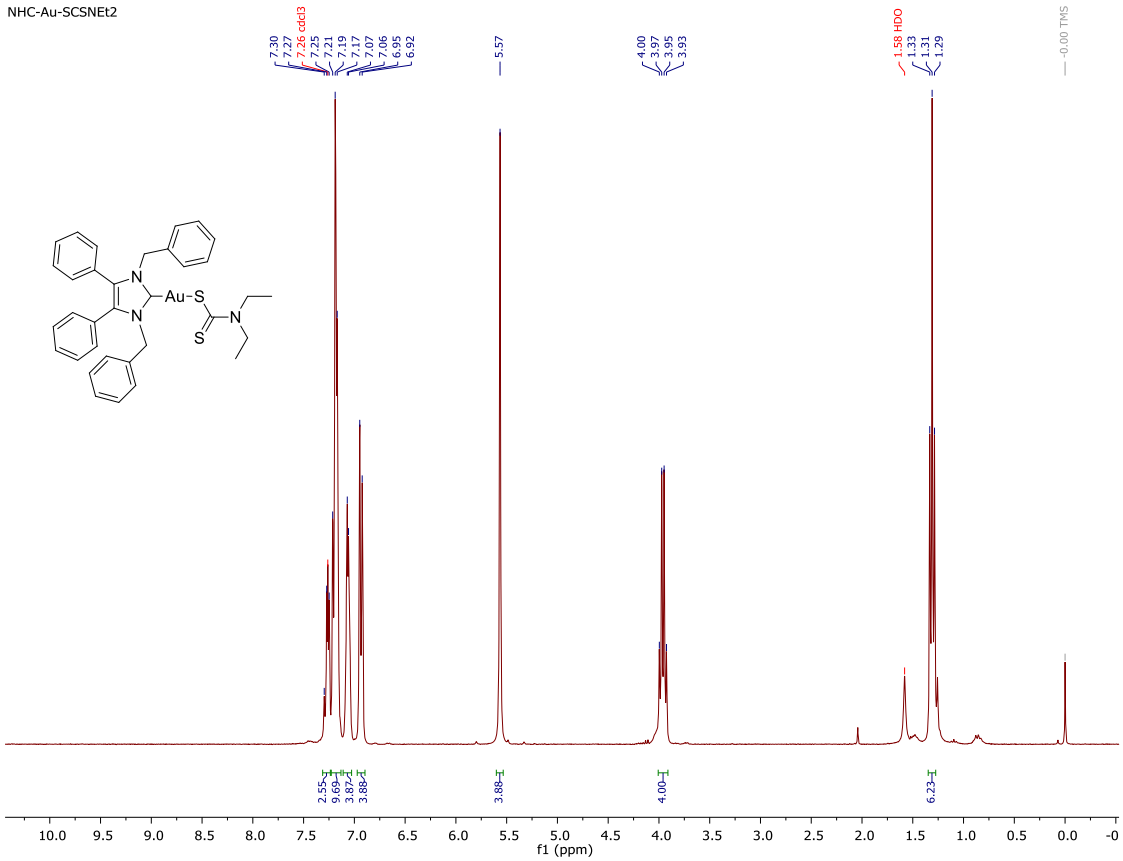

Figure S37. ^{1}H-NMR spectra of **4.9** in $CDCl_3$.

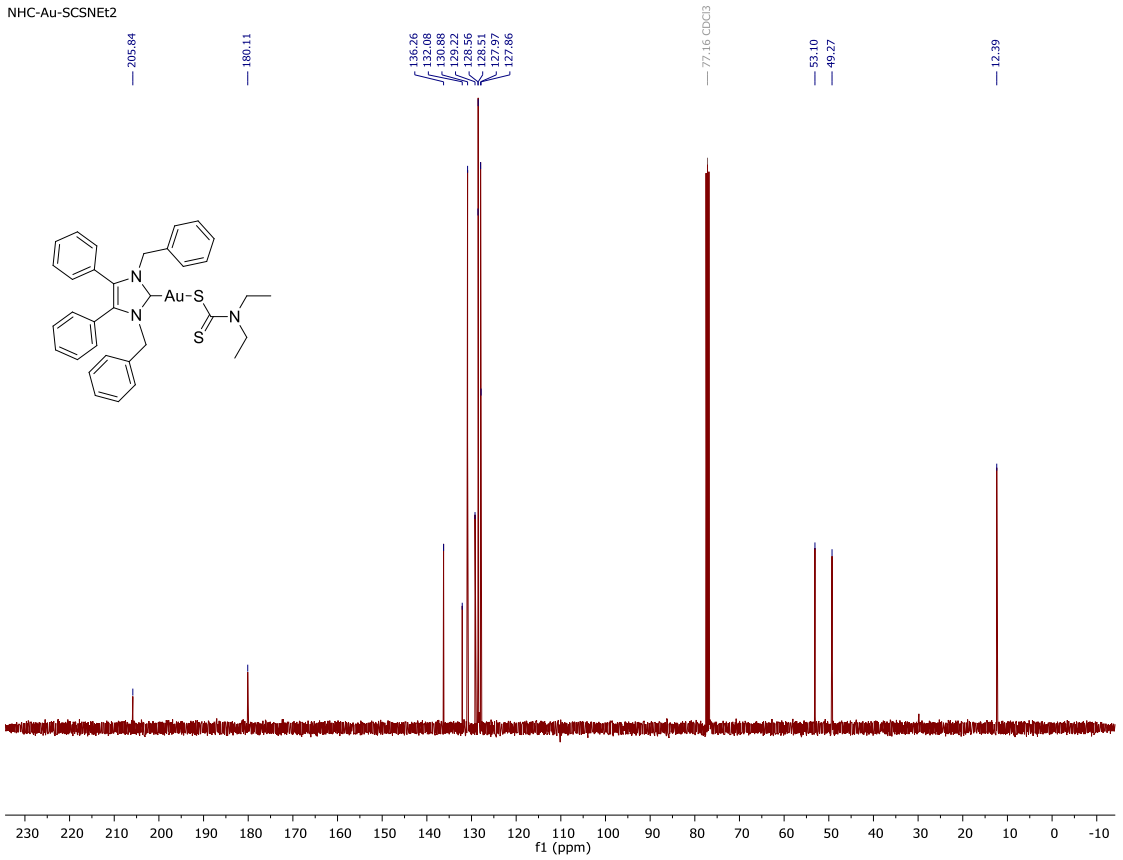

Figure S38. ^{13}C-NMR spectra of **4.9** in $CDCl_3$.

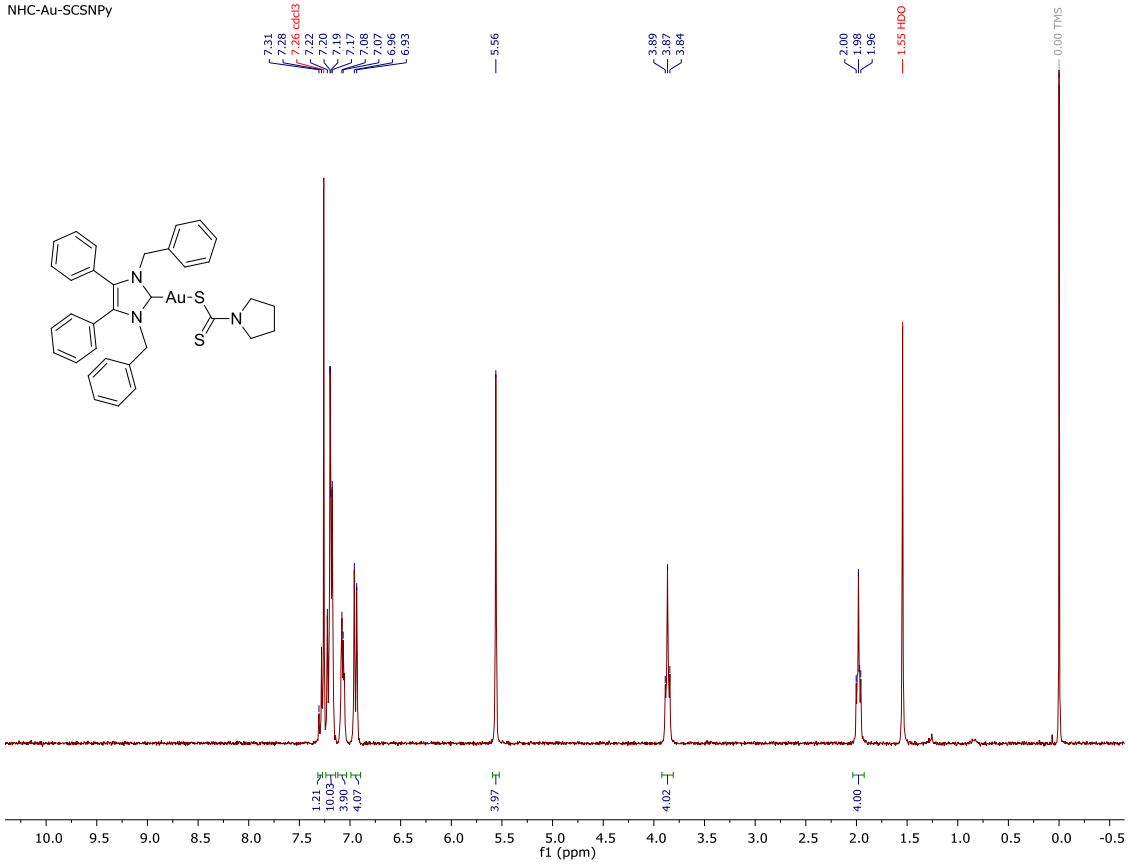

Figure S39. ^{1}H-NMR spectra of **4.10** in $CDCl_3$.

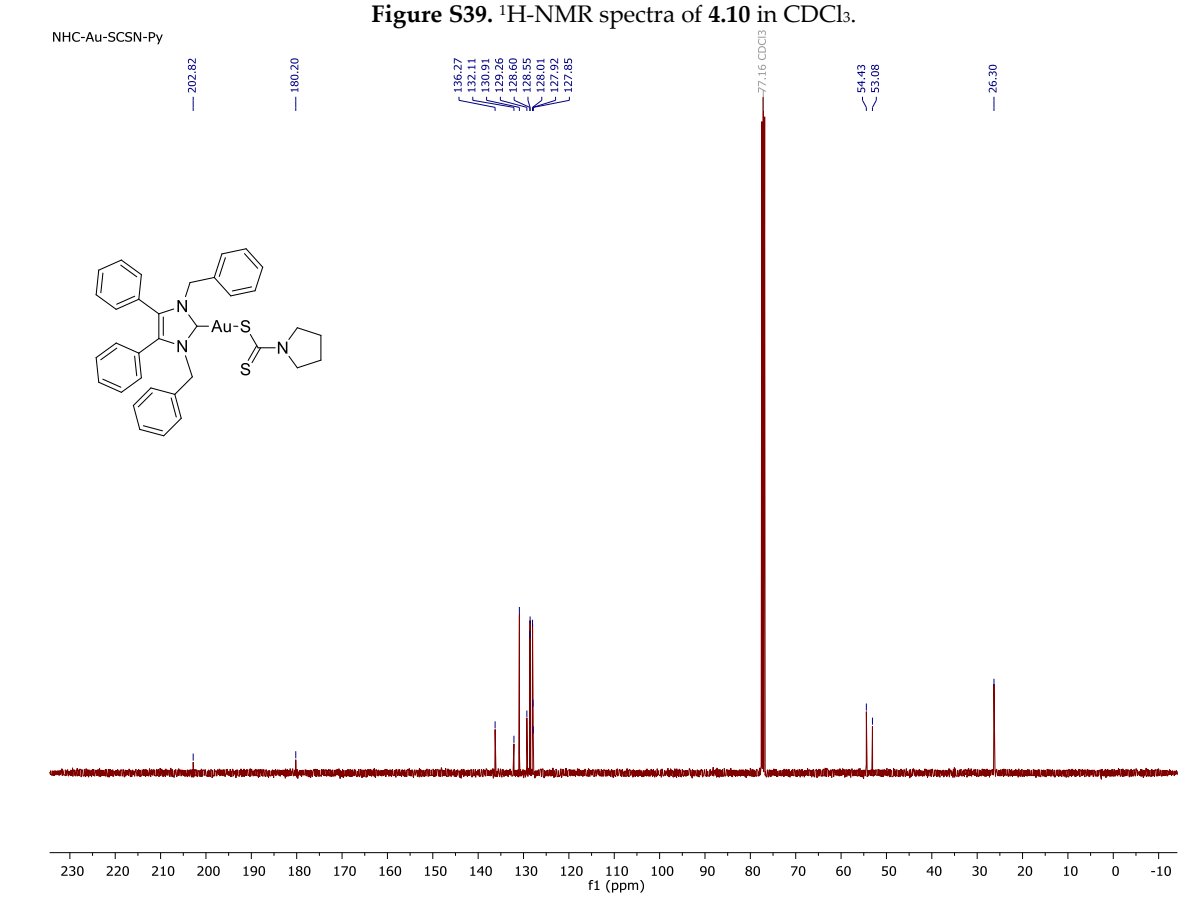

Figure S40. ^{13}C-NMR spectra of **4.10** in $CDCl_3$.

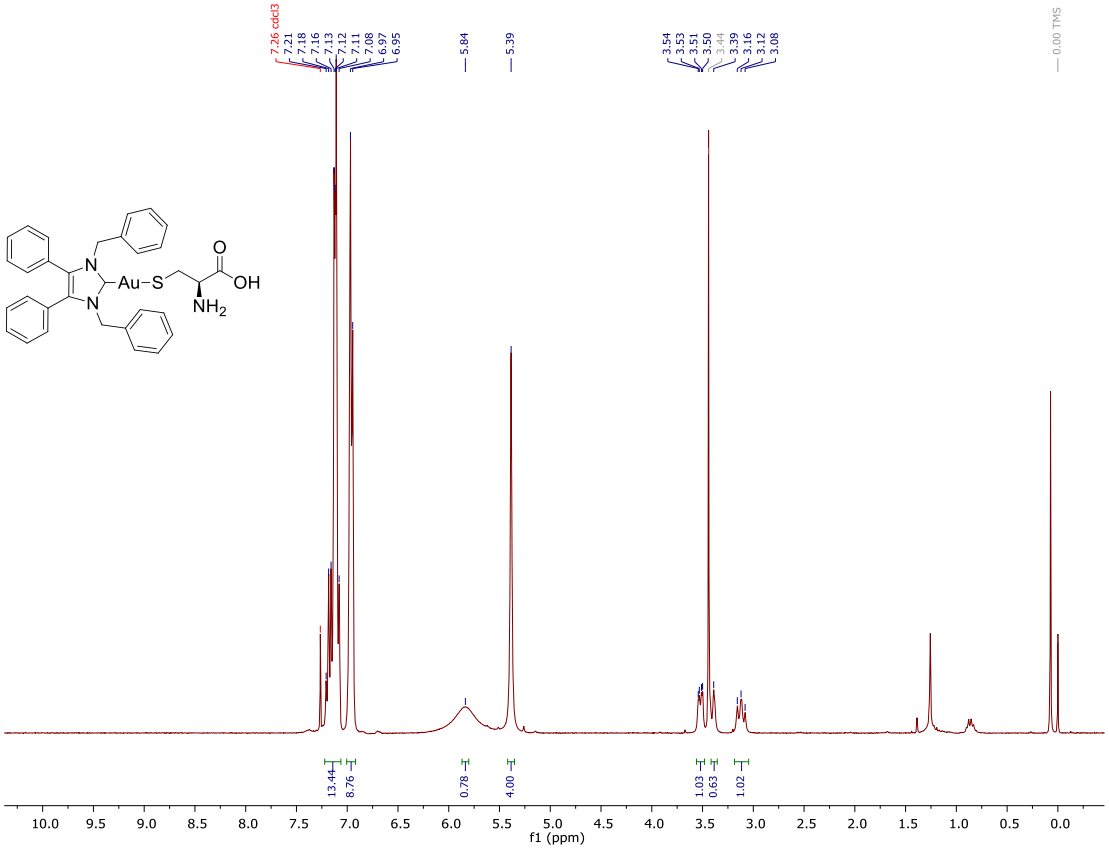

Figure S41. ^{1}H-NMR spectra of **5.21** in $CDCl_3$.

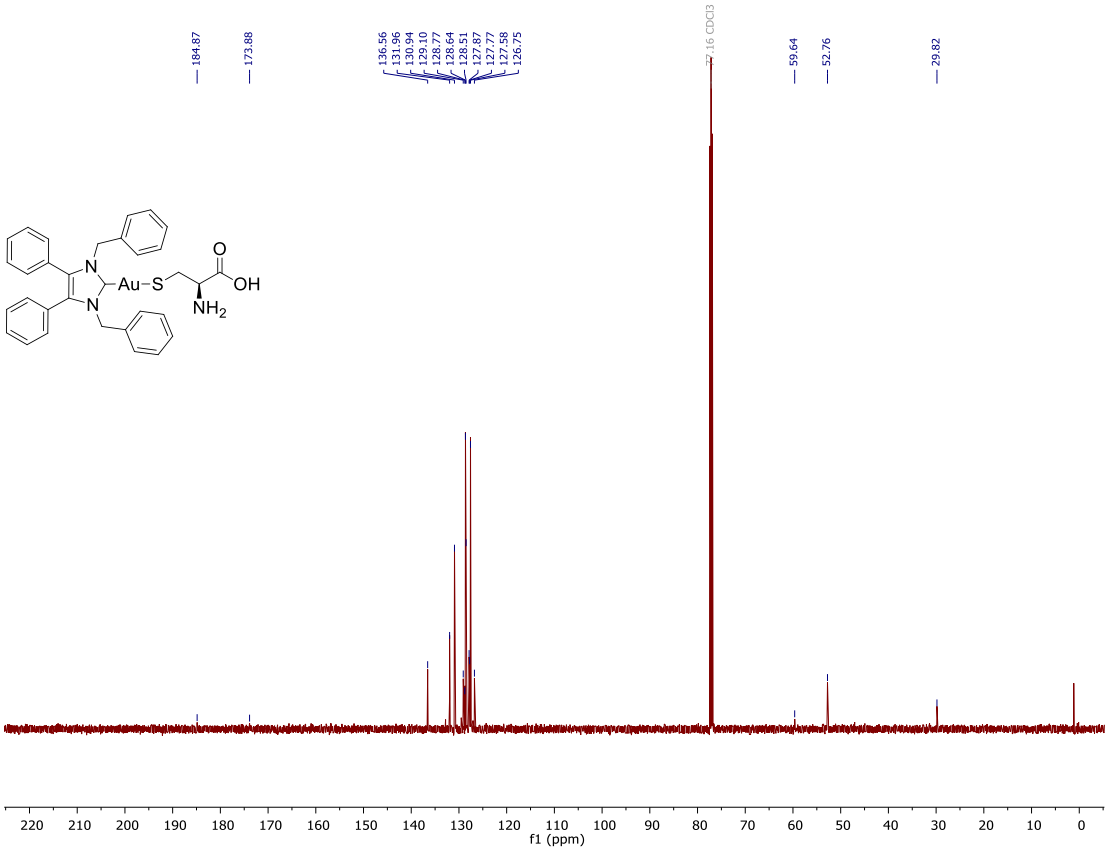

Figure S42. ^{13}C-NMR spectra of **5.21** in $CDCl_3$.

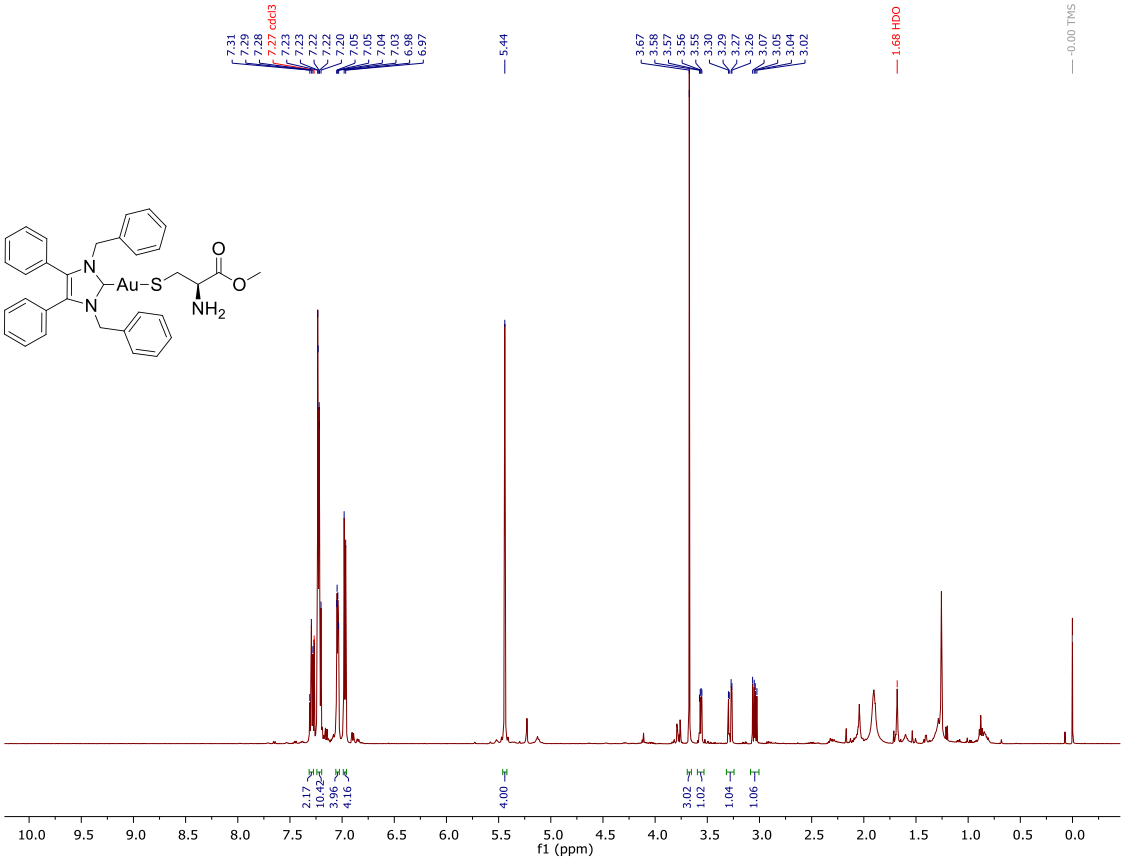

Figure S43. ^{1}H-NMR spectra of **5.22** in $CDCl_3$.

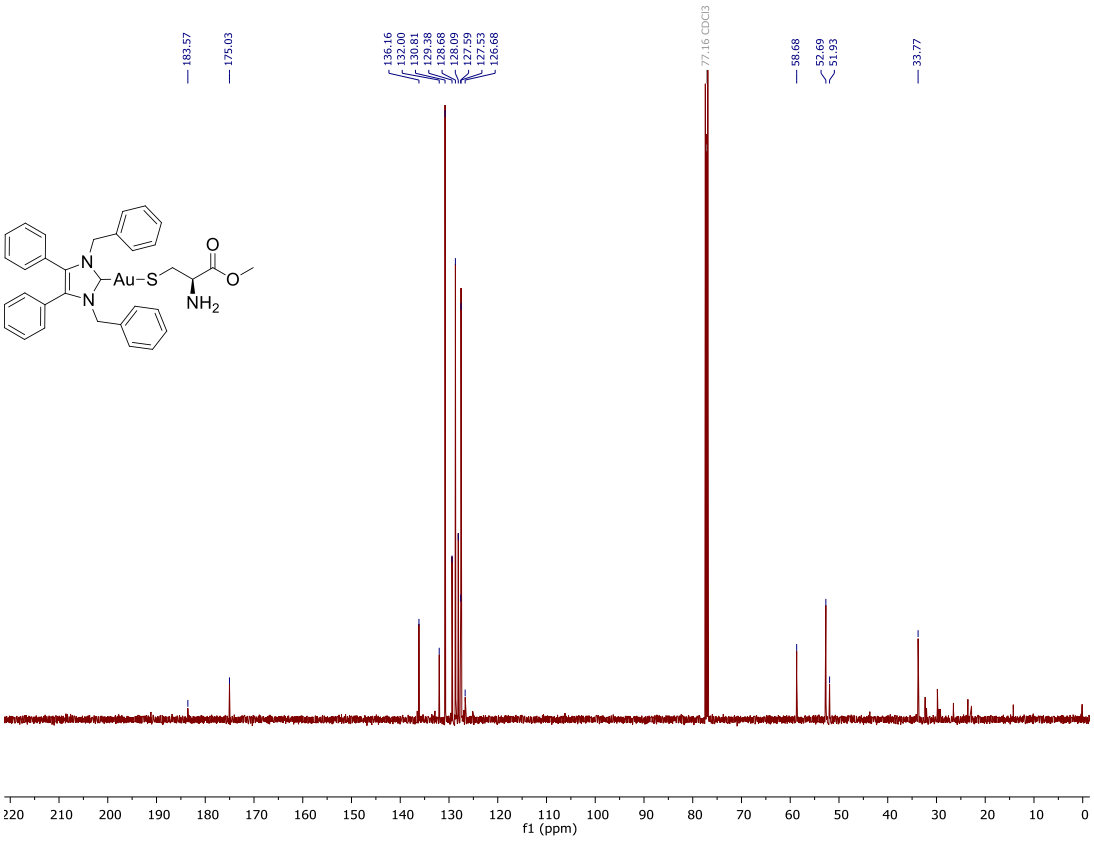

Figure S44. ^{13}C-NMR spectra of **5.22** in $CDCl_3$.

Table S4. Crystal data and structure refinement for **2.12**: 3[(NHC*$_2$Au)(AgBr$_2$)] and (NHC*$_2$Au)Br.

	2.12
Empirical Formula	C_{58} H_{48} N_4 $Br_{1.75}$ $Ag_{0.75}Au$
Formula Weight (g·mol^{-1})	1218.71
Temperature (K)	100(2)
Crystal system	Triclinic
Space group	$P\bar{1}$ (#2)
Unit cell dimensions	
a (Å)	15.4733(2)
b (Å)	15.5896(1)
c (Å)	21.7679(2)
α (°)	80.2752(6)
β (°)	70.3983(7)
γ (°)	77.4026(6)
Volume (Å^3)	4801.27(9)
Z	4
Density (calcd) (mg/m^3)	1.686
Absorption coefficient (mm^{-1})	10.175
F (000)	2398
Crystal size (mm^3)	0.112 x 0.084 x 0.048
θ (°)	3.451 to 76.951
Index ranges	$-19 \leq h \leq 19$ $-19 \leq k \leq 19$ $-27 \leq l \leq 27$
Reflections collected	128910
Independent reflections R_{int}	20109 (0.0454)
Completeness to θ_{max} (%)	100.0
Absorption correction	Gaussian
Max and min transmission	0.676 and 0.419
Refinement method	Full–matrix Least–squares on F^2
Data/ restraints/ parameters	20109 / 0 / 1191
Goodness-of-fit on F2	1.012
Final R indices [$I > 2\sigma(I)$]	R1 = 0.0324 wR2 = 0.0823
R indices (all data)	R1 = 0.0390 wR2 = 0.0861
Largest diff. peak and hole	2.525 and –1.792

Developmental Therapeutics Program

One Dose Mean Graph

NSC: D-817050 / 1	**Conc:** 1.00E-5 Molar	**Test Date:** Jul 15, 2019
Experiment ID: 1907OS39		**Report Date:** Jul 31, 2019

Panel/Cell Line	Growth Percent
Leukemia	
CCRF-CEM	15.02
HL-60(TB)	-9.22
K-562	4.34
MOLT-4	9.13
SR	10.37
Non-Small Cell Lung Cancer	
A549/ATCC	15.70
EKVX	21.43
HOP-62	26.44
HOP-92	-22.48
NCI-H23	-1.54
NCI-H322M	41.68
NCI-H460	0.62
Colon Cancer	
COLO 205	-54.28
HCC-2998	21.07
HCT-116	2.68
HCT-15	0.29
HT29	4.54
KM12	11.72
SW-620	-55.71
CNS Cancer	
SF-268	3.92
SF-295	13.34
SF-539	32.15
SNB-19	18.19
SNB-75	-5.65
U251	-2.47
Melanoma	
LOX IMVI	-34.08
MALME-3M	-19.56
M14	16.56
MDA-MB-435	1.32
SK-MEL-2	1.43
SK-MEL-28	24.42
SK-MEL-5	-18.64
UACC-257	-0.69
UACC-62	8.59
Ovarian Cancer	
IGROV1	-20.20
OVCAR-3	-95.76
OVCAR-4	11.35
OVCAR-5	36.06
OVCAR-8	18.72
NCI/ADR-RES	80.77
Renal Cancer	
786-0	1.04
A498	-4.93
ACHN	4.54
CAKI-1	-34.91
RXF 393	-28.97
SN12C	5.14
UO-31	-5.77
Prostate Cancer	
PC-3	7.73
DU-145	3.46
Breast Cancer	
MCF7	-20.84
MDA-MB-231/ATCC	-24.53
HS 578T	14.43
BT-549	25.30
MDA-MB-468	-20.83
Mean	.60
Delta	96.36
Range	176.53

Mean Growth Percent - Growth Percent

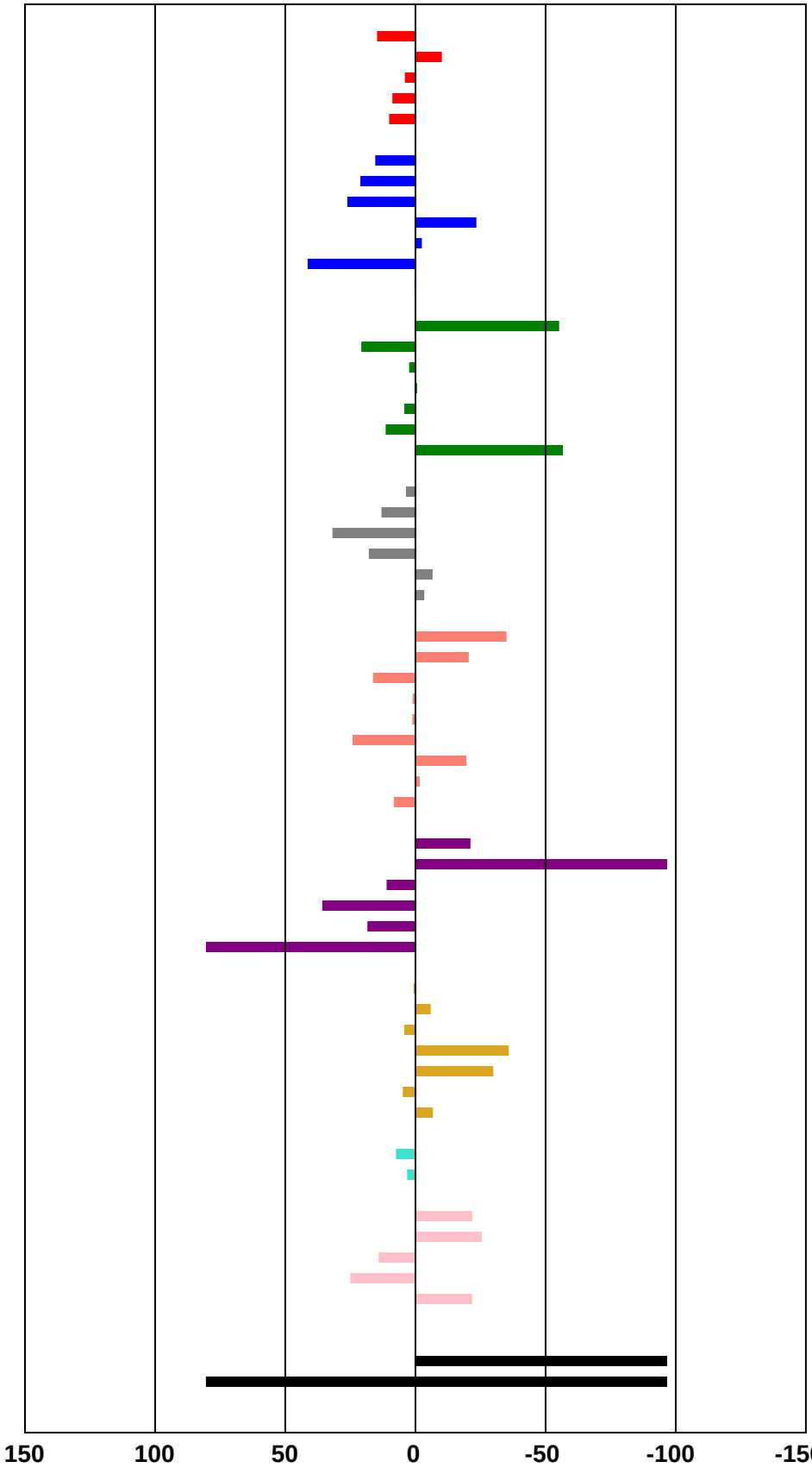

National Cancer Institute Developmental Therapeutics Program
Dose Response Curves

NSC: D - 817050 / 1	SSPL: 0Y9T	EXP. ID: 1909NS63
Report Date: October 29, 2019	Test Date: September 16, 2019	

Leukemia

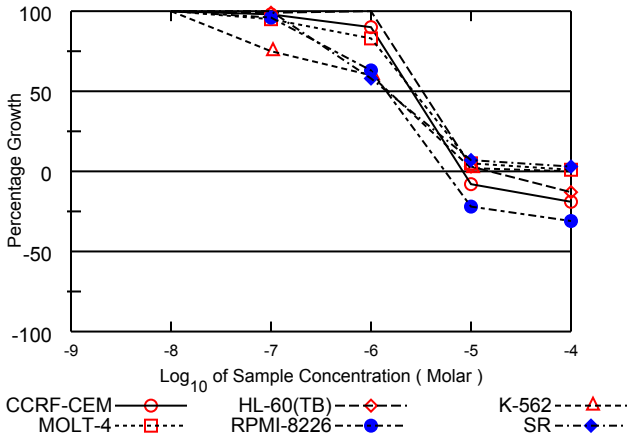

Non-Small Cell Lung Cancer

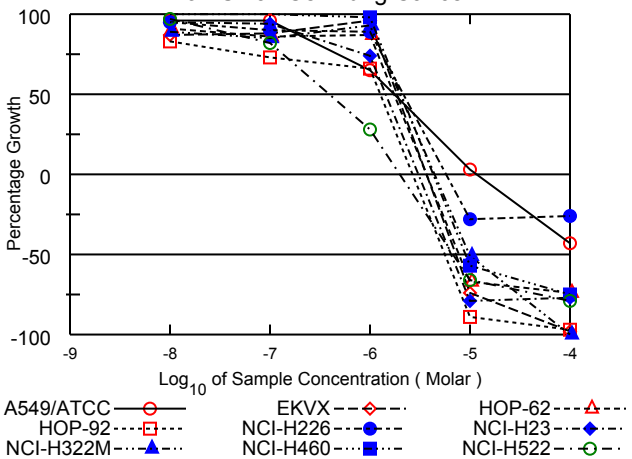

Colon Cancer

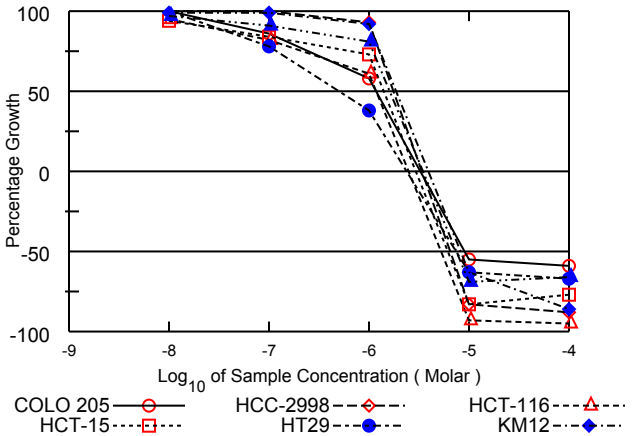

CNS Cancer

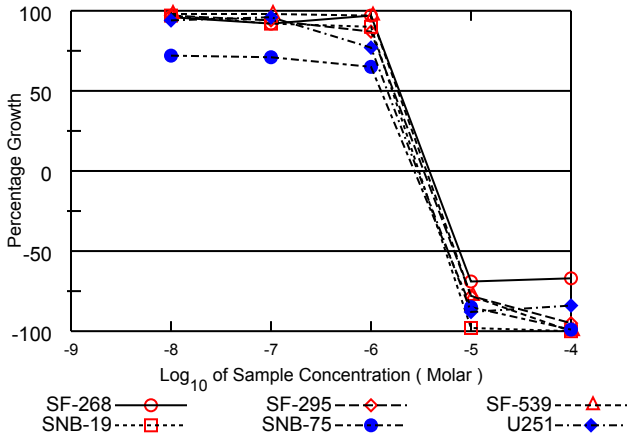

Melanoma

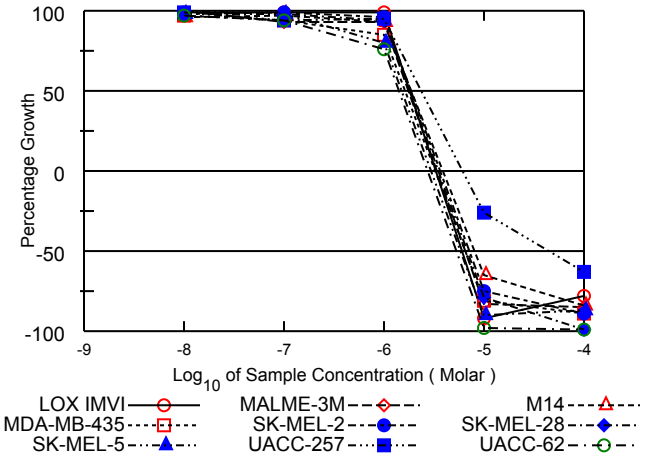

Ovarian Cancer

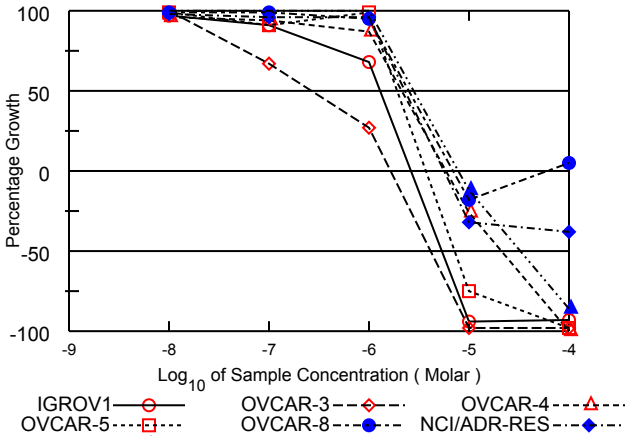

Renal Cancer

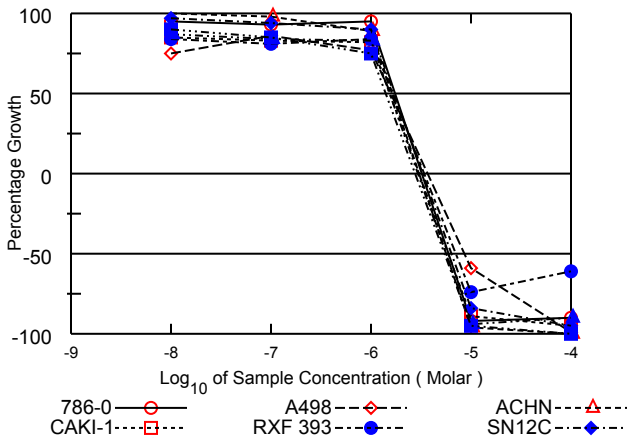

Prostate Cancer

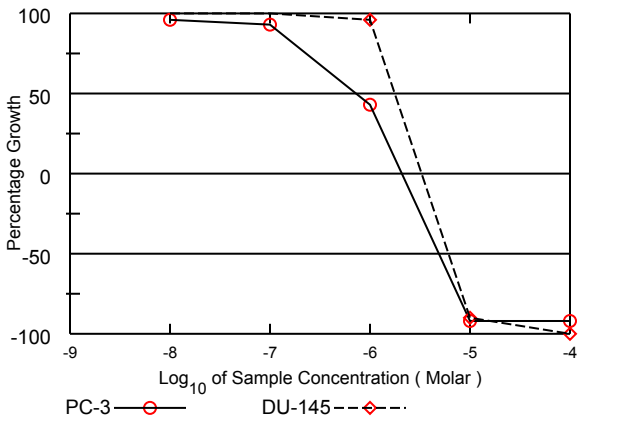

Breast Cancer

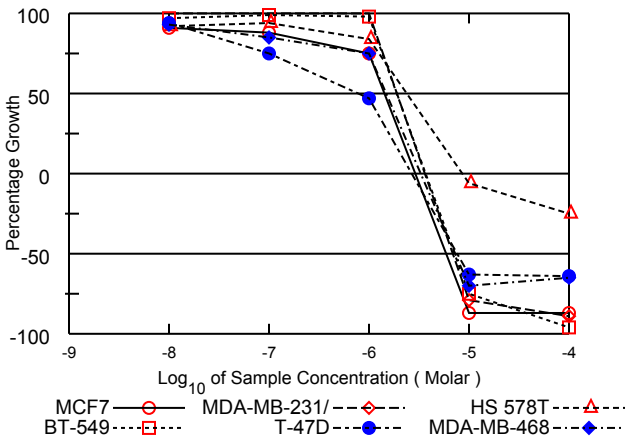

National Cancer Institute Developmental Therapeutics Program
In-Vitro Testing Results

NSC : D - 817050 / 1	Experiment ID : 1909NS63	Test Type : 08	Units : Molar
Report Date : October 29, 2019	Test Date : September 16, 2019	QNS :	MC :
COMI : NHC-Au-SCS-NMe2	Stain Reagent : SRB Dual-Pass Related	SSPL : 0Y9T	

			Log10 Concentration												
	Time		Mean Optical Densities					Percent Growth							
Panel/Cell Line	Zero	Ctrl	-8.0	-7.0	-6.0	-5.0	-4.0	-8.0	-7.0	-6.0	-5.0	-4.0	GI50	TGI	LC50
Leukemia															
CCRF-CEM	1.188	3.186	3.197	3.144	2.984	1.092	0.961	101	98	90	-8	-19	2.55E-6	8.26E-6	> 1.00E-4
HL-60(TB)	0.883	3.089	3.084	3.071	3.079	0.942	0.769	100	99	100	3	-13	3.25E-6	1.48E-5	> 1.00E-4
K-562	0.077	1.795	1.974	1.362	1.114	0.113	0.085	110	75	60	2	.	1.50E-6	> 1.00E-4	> 1.00E-4
MOLT-4	0.388	2.658	2.687	2.543	2.280	0.512	0.410	101	95	83	5	1	2.68E-6	> 1.00E-4	> 1.00E-4
RPMI-8226	0.809	2.741	2.743	2.672	2.018	0.633	0.560	100	96	63	-22	-31	1.41E-6	5.52E-6	> 1.00E-4
SR	0.265	2.080	2.142	2.109	1.310	0.384	0.316	103	102	58	7	3	1.41E-6	> 1.00E-4	> 1.00E-4
Non-Small Cell Lung Cancer															
A549/ATCC	0.310	2.061	1.984	1.997	1.453	0.355	0.176	96	96	65	3	-43	1.75E-6	1.14E-5	> 1.00E-4
EKVX	0.952	1.997	1.861	1.876	1.954	0.249	0.016	87	88	96	-74	-98	1.86E-6	3.67E-6	7.23E-6
HOP-62	0.758	2.400	2.259	2.176	2.187	0.247	0.194	91	86	87	-67	-74	1.74E-6	3.66E-6	7.71E-6
HOP-92	1.427	1.907	1.825	1.776	1.744	0.152	0.040	83	73	66	-89	-97	1.27E-6	2.66E-6	5.58E-6
NCI-H226	0.872	2.451	2.371	2.298	2.285	0.627	0.648	95	90	89	-28	-26	2.17E-6	5.77E-6	> 1.00E-4
NCI-H23	0.502	1.766	1.701	1.696	1.440	0.104	0.114	95	94	74	-79	-77	1.44E-6	3.04E-6	6.44E-6
NCI-H322M	1.587	3.048	2.887	2.831	2.940	0.783	0.002	89	85	93	-51	-100	1.98E-6	4.43E-6	9.89E-6
NCI-H460	0.612	3.353	3.355	3.366	3.310	0.266	0.155	100	100	98	-57	-75	2.05E-6	4.31E-6	9.06E-6
NCI-H522	0.943	2.740	2.682	2.408	1.441	0.319	0.194	97	82	28	-66	-79	3.85E-7	1.97E-6	6.73E-6
Colon Cancer															
COLO 205	0.484	2.204	2.206	1.967	1.485	0.220	0.197	100	86	58	-55	-59	1.18E-6	3.28E-6	9.11E-6
HCC-2998	0.929	3.085	3.157	3.085	2.945	0.158	0.108	103	100	93	-83	-88	1.76E-6	3.39E-6	6.50E-6
HCT-116	0.329	2.309	2.211	1.949	1.535	0.023	0.015	95	82	61	-93	-95	1.18E-6	2.49E-6	5.25E-6
HCT-15	0.341	2.239	2.125	1.939	1.736	0.057	0.077	94	84	73	-83	-77	1.41E-6	2.94E-6	6.12E-6
HT29	0.230	1.795	1.815	1.449	0.829	0.086	0.076	101	78	38	-63	-67	5.06E-7	2.39E-6	7.47E-6
KM12	0.662	3.143	3.119	3.113	2.956	0.244	0.090	99	99	92	-63	-86	1.87E-6	3.93E-6	8.22E-6
SW-620	0.348	2.251	2.198	2.087	1.880	0.109	0.118	97	91	81	-69	-66	1.60E-6	3.46E-6	7.50E-6
CNS Cancer															
SF-268	0.871	2.371	2.304	2.256	2.322	0.271	0.290	96	92	97	-69	-67	1.92E-6	3.84E-6	7.69E-6
SF-295	1.115	3.249	3.186	3.125	2.969	0.248	0.055	97	94	87	-78	-95	1.67E-6	3.37E-6	6.78E-6
SF-539	1.275	2.977	2.936	2.942	2.933	0.278	0.003	98	98	97	-78	-100	1.86E-6	3.59E-6	6.91E-6
SNB-19	0.855	2.635	2.579	2.498	2.465	0.021	-0.001	97	92	90	-98	-100	1.64E-6	3.03E-6	5.58E-6
SNB-75	1.325	2.074	1.862	1.856	1.809	0.203	0.009	72	71	65	-85	-99	1.25E-6	2.71E-6	5.85E-6
U251	0.496	2.441	2.330	2.357	1.991	0.062	0.079	94	96	77	-88	-84	1.46E-6	2.93E-6	5.91E-6
Melanoma															
LOX IMVI	0.746	3.344	3.320	3.320	3.326	0.061	0.162	99	99	99	-92	-78	1.81E-6	3.31E-6	6.04E-6
MALME-3M	1.155	2.545	2.552	2.449	2.451	0.196	0.170	100	93	93	-83	-85	1.76E-6	3.38E-6	6.50E-6
M14	1.405	3.283	3.210	3.225	3.155	0.496	0.223	96	97	93	-65	-84	1.88E-6	3.89E-6	8.07E-6
MDA-MB-435	0.555	2.703	2.637	2.572	2.389	0.105	0.061	97	94	85	-81	-89	1.63E-6	3.26E-6	6.51E-6
SK-MEL-2	1.374	3.110	3.080	3.095	3.041	0.342	0.153	98	99	96	-75	-89	1.86E-6	3.64E-6	7.13E-6
SK-MEL-28	1.243	2.939	2.938	2.897	2.836	0.264	0.018	100	98	94	-79	-99	1.80E-6	3.50E-6	6.81E-6
SK-MEL-5	0.782	3.186	3.131	3.132	2.698	0.075	0.099	98	98	80	-90	-87	1.49E-6	2.94E-6	5.79E-6
UACC-257	1.427	3.072	3.052	2.971	2.988	1.050	0.528	99	94	95	-26	-63	2.34E-6	6.05E-6	4.41E-5
UACC-62	0.828	2.901	2.836	2.783	2.406	0.021	0.007	97	94	76	-98	-99	1.41E-6	2.74E-6	5.32E-6
Ovarian Cancer															
IGROV1	0.574	2.200	2.159	2.050	1.674	0.034	0.041	97	91	68	-94	-93	1.29E-6	2.62E-6	5.34E-6
OVCAR-3	0.466	1.627	1.659	1.242	0.779	0.007	0.010	103	67	27	-98	-98	2.64E-7	1.64E-6	4.11E-6
OVCAR-4	1.192	2.702	2.639	2.605	2.503	0.886	.	96	94	87	-26	-100	2.12E-6	5.91E-6	2.12E-5
OVCAR-5	0.776	1.618	1.606	1.542	1.613	0.195	0.013	99	91	99	-75	-98	1.92E-6	3.72E-6	7.20E-6
OVCAR-8	0.859	3.229	3.197	3.204	3.105	0.703	0.983	99	99	95	-18	5	2.49E-6	.	> 1.00E-4
NCI/ADR-RES	0.658	2.389	2.356	2.320	2.318	0.451	0.411	98	96	96	-32	-38	2.29E-6	5.66E-6	> 1.00E-4
SK-OV-3	2.179	2.712	2.790	2.751	2.810	1.927	0.315	115	107	118	-12	-86	3.36E-6	8.14E-6	3.31E-5
Renal Cancer															
786-0	0.843	2.806	2.707	2.670	2.704	0.066	0.087	95	93	95	-92	-90	1.74E-6	3.21E-6	5.95E-6
A498	2.140	2.941	2.744	2.828	2.758	0.877	0.019	75	86	77	-59	-99	1.58E-6	3.69E-6	8.58E-6
ACHN	0.540	2.170	2.180	2.144	1.991	0.024	-0.005	101	98	89	-96	-100	1.63E-6	3.04E-6	5.66E-6
CAKI-1	1.046	2.765	2.513	2.478	2.451	0.118	0.054	85	83	82	-89	-95	1.53E-6	3.02E-6	5.93E-6
RXF 393	1.250	1.831	1.737	1.723	1.739	0.330	0.492	84	81	84	-74	-61	1.65E-6	3.41E-6	7.08E-6
SN12C	0.821	2.913	2.853	2.789	2.709	0.130	0.041	97	94	90	-84	-95	1.70E-6	3.29E-6	6.37E-6
TK-10	0.643	1.536	1.424	1.397	1.384	0.036	0.066	87	84	83	-94	-90	1.53E-6	2.93E-6	5.61E-6
UO-31	1.063	2.546	2.394	2.325	2.175	0.052	0.002	90	85	75	-95	-100	1.40E-6	2.76E-6	5.43E-6
Prostate Cancer															
PC-3	0.566	2.011	1.959	1.905	1.186	0.047	0.043	96	93	43	-92	-92	7.20E-7	2.08E-6	4.90E-6
DU-145	0.697	2.342	2.421	2.349	2.283	0.070	-0.003	105	100	96	-90	-100	1.77E-6	3.29E-6	6.10E-6
Breast Cancer															
MCF7	0.855	3.050	2.842	2.794	2.497	0.114	0.108	91	88	75	-87	-87	1.42E-6	2.90E-6	5.92E-6
MDA-MB-231/ATCC	0.902	2.004	2.052	2.019	2.022	0.186	0.102	104	101	102	-79	-89	1.93E-6	3.64E-6	6.88E-6
HS 578T	1.654	2.764	2.672	2.693	2.588	1.554	1.240	92	94	84	-6	-25	2.39E-6	8.57E-6	> 1.00E-4
BT-549	1.574	3.193	3.150	3.171	3.155	0.391	0.061	97	99	98	-75	-96	1.89E-6	3.67E-6	7.15E-6
T-47D	0.899	1.946	1.879	1.687	1.393	0.329	0.323	94	75	47	-63	-64	7.91E-7	2.67E-6	7.56E-6
MDA-MB-468	0.921	2.271	2.180	2.068	1.934	0.280	0.319	93	85	75	-70	-65	1.49E-6	3.30E-6	7.32E-6

National Cancer Institute Developmental Therapeutics Program

Mean Graphs

NSC : D - 817050/1 | Units :Molar | SSPL :0Y9T | EXP. ID :1909NS63

Report Date :October 29, 2019 | Test Date :September 16, 2019

Panel/Cell Line	Log_{10}GI50	GI50	Log_{10}TGI	TGI	Log_{10}LC50	LC50
Leukemia						
CCRF-CEM	-5.59		-5.08		> -4.00	
HL-60(TB)	-5.49		-4.83		> -4.00	
K-562	-5.82		> -4.00		> -4.00	
MOLT-4	-5.57		> -4.00		> -4.00	
RPMI-8226	-5.85		-5.26		> -4.00	
SR	-5.85		> -4.00		> -4.00	
Non-Small Cell Lung Cancer						
A549/ATCC	-5.76		-4.94		> -4.00	
EKVX	-5.73		-5.44		-5.14	
HOP-62	-5.76		-5.44		-5.11	
HOP-92	-5.90		-5.57		-5.25	
NCI-H226	-5.66		-5.24		> -4.00	
NCI-H23	-5.84		-5.52		-5.19	
NCI-H322M	-5.70		-5.35		-5.00	
NCI-H460	-5.69		-5.37		-5.04	
NCI-H522	-6.41		-5.70		-5.17	
Colon Cancer						
COLO 205	-5.93		-5.48		-5.04	
HCC-2998	-5.75		-5.47		-5.19	
HCT-116	-5.93		-5.60		-5.28	
HCT-15	-5.85		-5.53		-5.21	
HT29	-6.30		-5.62		-5.13	
KM12	-5.73		-5.41		-5.08	
SW-620	-5.80		-5.46		-5.13	
CNS Cancer						
SF-268	-5.72		-5.42		-5.11	
SF-295	-5.78		-5.47		-5.17	
SF-539	-5.73		-5.45		-5.16	
SNB-19	-5.79		-5.52		-5.25	
SNB-75	-5.90		-5.57		-5.23	
U251	-5.84		-5.53		-5.23	
Melanoma						
LOX IMVI	-5.74		-5.48		-5.22	
MALME-3M	-5.75		-5.47		-5.19	
M14	-5.73		-5.41		-5.09	
MDA-MB-435	-5.79		-5.49		-5.19	
SK-MEL-2	-5.73		-5.44		-5.15	
SK-MEL-28	-5.75		-5.46		-5.17	
SK-MEL-5	-5.83		-5.53		-5.24	
UACC-257	-5.63		-5.22		-4.36	
UACC-62	-5.85		-5.56		-5.27	
Ovarian Cancer						
IGROV1	-5.89		-5.58		-5.27	
OVCAR-3	-6.58		-5.79		-5.39	
OVCAR-4	-5.67		-5.23		-4.67	
OVCAR-5	-5.72		-5.43		-5.14	
OVCAR-8	-5.60				> -4.00	
NCI/ADR-RES	-5.64		-5.25		> -4.00	
SK-OV-3	-5.47		-5.09		-4.48	
Renal Cancer						
786-0	-5.76		-5.49		-5.23	
A498	-5.80		-5.43		-5.07	
ACHN	-5.79		-5.52		-5.25	
CAKI-1	-5.81		-5.52		-5.23	
RXF 393	-5.78		-5.47		-5.15	
SN12C	-5.77		-5.48		-5.20	
TK-10	-5.81		-5.53		-5.25	
UO-31	-5.85		-5.56		-5.27	
Prostate Cancer						
PC-3	-6.14		-5.68		-5.31	
DU-145	-5.75		-5.48		-5.21	
Breast Cancer						
MCF7	-5.85		-5.54		-5.23	
MDA-MB-231/ATCC	-5.72		-5.44		-5.16	
HS 578T	-5.62		-5.07		> -4.00	
BT-549	-5.72		-5.43		-5.15	
T-47D	-6.10		-5.57		-5.12	
MDA-MB-468	-5.83		-5.48		-5.14	
_MID	-5.8		-5.36		-4.93	
Delta	0.78		0.43		0.46	
Range	1.11		1.79		1.39	

National Cancer Institute Developmental Therapeutics Program Dose Response Curves	NSC : D - 817050/1	SSPL:0Y9T	EXP. ID:1909NS63
	Report Date:October 29, 2019	Test Date:September 16, 2019